UNIVERSIDADE D
COIMBRA

Cândida Marília das Neves Dias

DYNAMIC CHANGES OF AEROBIC BRAIN OXIDATIVE METABOLISM REVEALED BY LACTATE AND THE REDOX MODULATION BY NITRITE

Tese no âmbito do Doutoramento em Ciências Farmacêuticas, área de especialização em Bioquímica, orientada pelos Professores Doutores João António Nave Laranjinha e Ana Margarida da Cruz Ledo e apresentada à Faculdade de Farmácia da Universidade de Coimbra.

Dezembro de 2021

Faculdade de Farmácia da Universidade de Coimbra

Dynamic Changes of Aerobic Brain Oxidative Metabolism Revealed by Lactate and the Redox Modulation by Nitrite

Cândida Marília das Neves Dias

Tese no âmbito do Doutoramento em Ciências Farmacêuticas, área de especialização em Bioquímica, orientada pelos Professores Doutores João António Nave Laranjinha e Ana Margarida da Cruz Ledo e apresentada à Faculdade de Farmácia da Universidade de Coimbra.

Dezembro de 2021

Este trabalho foi realizado no Centro de Neurociências e Biologia Celular e na Faculdade de Farmácia da Universidade de Coimbra sob orientação científica dos Professores Doutores João António Nave Laranjinha e Ana Margarida da Cruz Ledo.

This work was financed by the FCT – Fundação para a Ciência e a Tecnologia – through the Medical Biochemistry and Biophysics Doctoral Programme with the fellowship PD/BD/114371/2016 and by the European Regional Development Fund (ERDF), through the COMPETE 2020 - Operational Programme for Competitiveness and Internationalisation and Portuguese national funds via FCT under projects POCI-01-0145-FEDER-029099, POCI-01-0145-FEDER-028261, and UIDB/04539/2020.

Agradecimentos

Quero agradecer a todos aqueles que me apoiaram de uma forma ou de outra no percurso que levou à concretização deste trabalho. Foi um tempo muito enriquecedor, que com os seus altos e baixos me permitiu crescer imensamente a nível científico, profissional e pessoal.

Em primeiro lugar, gostaria de agradecer aos meus orientadores Professor Doutor João Laranjinha e Professora Doutora Ana Ledo pelas oportunidades, pelos ensinamentos, incentivos e toda a ajuda e apoio dado, sem os quais o desenvolvimento e conclusão deste trabalho não teriam sido possíveis. Não poderia também deixar de agradecer ao Professor Doutor Rui Barbosa, por toda a ajuda dada neste processo.

Aos meus colegas, Cátia, Carla, João, Eliana e Bárbara, agradeço toda a ajuda que me deram e a vossa boa companhia. Foram muitos os momentos em que o vosso suporte foi essencial, tanto a nível de trabalho, como a nível pessoal. Também não poderia deixar de agradecer à Catarina e à Inês, pela sua amizade e apoio durante este tempo. Obrigada a todos por me acompanharem nesta jornada e por tornarem este tempo mais fácil no geral.

Uma palavra de agradecimento a todas as outras pessoas do Centro de Neurociências e Biologia Celular e da Faculdade de Farmácia que de alguma forma contribuíram para o desenvolvimento deste trabalho.

Por último, mas não menos importante, gostaria de expressar o meu agradecimento à minha família. Obrigada, Ricardo, por todo o apoio excecional que deste, com as tuas palavras sempre encorajadoras e a tua compreensão e ajuda nos dias mais longos. Aos meus pais, agradeço todo o suporte que me deram ao longo da minha vida, incentivando sempre que progredisse no meu percurso académico que culmina com esta tese e apoiando-me nas minhas decisões. À minha irmã pela sua amizade e ajuda em tudo o que fosse necessário.

Para além de dedicar este trabalho a todas as pessoas mencionadas, dedico-o também à Carolina que já só esteve presente na reta final, mas que é já uma parte tão importante da minha vida.

Resumo

O cérebro humano é um órgão metabolicamente muito ativo que requer um suprimento substancial de glicose e oxigénio, combinando o elevado consumo destes substratos energéticos com uma reduzida capacidade de armazenamento de glicogénio. Embora a glucose seja considerada o principal substrato energético para as células cerebrais, estudos recentes sugerem que o lactato pode desempenhar uma função importante no metabolismo energético cerebral. Os fluxos ("shuttling") de lactato são provavelmente um componente importante no complexo mecanismo que envolve a interação entre astrócitos e neurónios e que permite uma resposta mais eficaz ao aumento da necessidade energética imposta pela atividade sináptica. No entanto, a função do lactato neste processo, o acoplamento neurometabólico, tem sido suportado por vários estudos que, por regra, são não apenas inconclusivos como controversos.

A alta necessidade energética do cérebro sugere que alterações no suprimento de substratos ao tecido cerebral tem consequências disfuncionais severas. Um exemplo notório é o deficiente aporte de oxigénio e glucose a uma região cerebral durante um acidente vascular cerebral (AVC). Paradoxalmente, a reoxigenação origina uma cascata tóxica em que intervêm como componentes críticos radicais e oxidantes (espécies reativas de oxigénio, ROS) com origem predominantemente na mitocôndria. Neste contexto, o nitrito tem sido apontado como uma substância moduladora do metabolismo oxidativo, com efeitos positivos em modelos de AVC.

Assim, o objetivo principal deste trabalho é estudar a modulação do metabolismo energético cerebral pelo lactato num contexto fisiológico e pelo nitrito num contexto patológico, nomeadamente num modelo de AVC, numa estrutura cerebral específica, o hipocampo. Para este fim, dada a necessidade do desenvolvimento de novas metodologias para o estudo da ação moduladora de lactato e de nitrito no metabolismo cerebral, foram desenvolvidos (a) um protocolo para medições de taxas de consumo de oxigénio em tecido cerebral como meio de avaliação do metabolismo oxidativo, com base na produção de um suporte adaptável ao equipamento de alta resolução, mantendo o tecido íntegro ao longo do período experimental e (b) um microbiossensor de lactato para monitorizar dinâmicas de lactato em fatias de tecido cerebral. Os microbiosensores consistem em microelétrodos de fibra de carbono platinizados com a enzima lactato oxidase imobilizada e uma membrana de permeabilidade seletiva para obter um dispositivo capaz de medir lactato com elevada sensibilidade e seletividade, baixo limite de deteção e estabilidade operacional, representando assim uma boa opção para medições dinâmicas de lactato extracelular em tecido cerebral.

Relativamente à ação do lactato no acoplamento neurometabólico, os resultados mostraram que a concentração de glucose no meio extracelular, além de influenciar o consumo de oxigénio pelo tecido, determina a concentração extracelular de lactato, que se manteve dentro de um intervalo

limitado para um intervalo fisiológico de glucose. Este aumento da concentração de lactato em resposta a um aumento da concentração de glucose suporta a noção de que o lactato é o produto final da glicólise aeróbica e que é libertado no espaço extracelular. Além disso, o lactato adicionado exogenamente aumentou a taxa de respiração do tecido de uma forma independente da concentração de glucose. Também foi demonstrado que os neurónios captam lactato do espaço extracelular com aumento do metabolismo oxidativo tanto em condições basais como em atividade, permitindo uma resposta mais eficaz às necessidades energéticas impostas pela estimulação.

Por último, foi demonstrado que o nitrito modula o metabolismo oxidativo em fatias de hipocampo num modelo *in vitro* de isquemia/reperfusão (I/R), utilizado como modelo para reproduzir as condições de AVC. Foi observado um aumento significativo do metabolismo oxidativo imediatamente após a I/R, o qual pode estar associado a um aumento de espécies reativas de oxigénio envolvidas nos danos provocados por I/R. O nitrito, numa concentração que pode ser obtida *in vivo*, diminui este aumento oxidativo, provavelmente por alteração da atividade de complexos respiratórios, nomeadamente a inibição da respiração ligada ao complexo I.

Concluindo, o trabalho desenvolvido nesta tese, para além do desenvolvimento de novas metodologias para estudar metabolismo oxidativo em tecido cerebral, revelou aspetos mecanísticos relacionados com a ação de lactato e nitrito no metabolismo cerebral, quer do ponto de vista fisiológico quer fisiopatológico, abrindo caminho para a sua potencial utilização na modulação de disfunções metabólicas relacionadas com doença do cérebro.

Palavras-chave: metabolismo oxidativo, consumo de oxigénio, hipocampo, lactato, microbiossensores, nitrito, isquemia, reperfusão

Abstract

The brain is a highly active organ with high energetic needs. The main energy substrate in the brain is glucose, but lactate has also been suggested to play an important role involving a rather complex mechanism that allows for a rapid supply of energy substrates to respond to the increased energy needs during activity. Mounting evidence supports a role for lactate in such neurometabolic coupling, but the underlying mechanisms are still under debate and need further clarification.

Disruption in substrate supply to the brain has profound metabolic and physiological consequences. For instance, a decrease in glucose and oxygen supply due to a compromised cerebral blood flow results in stroke. Improving the outcome of this deadly disease can increase survivability and quality of life for patients. One possible strategy for this involves the modulation of mitochondrial oxidative metabolism by nitrite, a substance that may act as a metabolic precursor of nitric oxide, in particular at low *p*H and in the presence of reductants such as ascorbic acid.

The main purpose of this work was to study the role of lactate and nitrite in brain energy metabolism under a physiological and pathophysiology viewpoint in the hippocampus. In order to address the modulation of neurometabolism by lactate and nitrite there was the need to design and develop two new methodologies, namely (a) a protocol allowing for the monitoring of whole hippocampal tissue oxidative metabolism through measurements of oxygen consumption rates based on the design of a sample holder to fit a respirometry system that maintains the tissue integrity throughout the experiment duration and (b) a lactate microbiosensor with the purpose of monitoring lactate dynamics in brain tissue slices. The lactate microbiosensors consisted of platinized carbon fiber microelectrodes with lactate oxidase immobilized and a permselective membrane to increase selectivity. They were proven to produce reliable lactate measurements, with high sensitivity and selectivity, low limit of detection, and extended operational stability, representing a good resource for studies of lactate concentration dynamics in brain tissue preparations.

Regarding the role of lactate in neurometabolic coupling, the data supports that glucose concentration modulates both the rate of tissue oxygen consumption as well as extracellular lactate concentration, which is maintained within a limited range for physiologically relevant glucose concentrations. The increase of lactate in response to glucose supports the notion that lactate is produced during aerobic glycolysis and released into the extracellular space. Interestingly, exogenously added lactate can also increase the rate of tissue respiration at rest independently of glucose concentration. It was also demonstrated that neurons uptake lactate from the extracellular space to fuel oxidative metabolism both under resting conditions and in response

to neural activation, providing a means to better respond to the metabolic demands imposed by stimulation.

Finally, this work supports nitrite as a modulator of hippocampal slice oxidative metabolism in an *in vitro* model of ischemia/reperfusion (I/R). An oxidative burst was observed immediately after I/R, presumably associated with increased reactive oxygen species production that mediate a part of the damage from I/R. Nitrite, in a concentration attainable *in vivo*, decreased the oxidative burst, and the underlying mechanism, although not clearly discerned, might be related with the modulation of mitochondrial respiration, in particular via inhibition of complex I linked respiration.

In conclusion, the work developed in this thesis presented new methodologies that can be used to study neurometabolism in brain tissue and allowed to probe into the mechanistic of the role of lactate as a substrate and nitrite as a modulator in brain oxidative metabolism, under both physiological and pathophysiological conditions, suggesting new strategies to modulate disease-related neural energetic metabolism.

Keywords: oxidative metabolism, oxygen consumption, hippocampus, lactate, microbiosensors, nitrite, ischemia, reperfusion

Table of contents

Index of figures

Index of tables

Abbreviations and symbols

3xTgAD	Triple transgenic mouse model of Alzheimer's disease
4-CIN	α-cyano-4-hydroxycinnamic acid
A/R	Anoxia and reoxygenation
aCSF	Artificial cerebrospinal fluid
ADP	Adenosine 5′-diphosphate
Ama	Antimycin A
AMP	Adenosine 5′-monophosphate
AMPA	α-amino-3-hydroxy-5-methyl-4-isoxazolepropionic acid
ANLS	Astrocyte-neuron lactate shuttle
ANT	Adenine nucleotide translocase
ATP	Adenosine 5′-triphosphate
Azd	Azide
BBB	Blood brain barrier
BIOPS	Biopsy preservation solution
Cat	Carboxyatractyloside
CcO	Cytochrome *c* oxidase
CFM	Carbon fiber microelectrodes
CFM/Pt	Platinized carbon fiber microelectrodes
cGMP	Cyclic guanosine monophosphate
CMR_{glc}	Cerebral metabolic rate of glucose
CMR_{O2}	Cerebral metabolic rate of oxygen
CoA	Coenzyme A
CSF	Cerebrospinal fluid
Cyt *c*	Cytochrome *c*
ECS	Extracellular space
EPR	Electron paramagnetic resonance
ET	Electron transfer
ETC	Electron transport chain
ETS	Electron transfer system
$F2,6P_2$	Fructose-2,6-bisphosphate
FAD	Flavin adenine dinucleotide
$FADH_2$	Reduced flavin adenine dinucleotide
FC	Fluorocitrate
FCR	Flux control ratio

FMN	Flavin mononucleotide
FRET	Förster Resonance Energy Transfer
GLUT	Glucose transporter
HIF-1	Transcription factor hypoxia-inducible factor-1
I/R	Ischemia and reperfusion
I_{max}	Maximal current
KA	Kainic acid
K_M	Michelis constant
LDH	Lactate dehydrogenase
LOD	Limit of detection
LOx	Lactate oxidase
MCAO	Middle cerebral artery occlusion
MCT	Monocarboxylate transporters
MiR05	Mitochondrial respiration medium 05
m-PD	1,3-phenylenediamine
MRS	Magnetic resonance microscopy
NAD^+	Nicotinamide adenine dinucleotide
NADH	Reduced nicotinamide adenine dinucleotide
NADPH	Nicotinamide adenine dinucleotide phosphate
NMDA	*N*-methyl-D-aspartate
NOS	Nitric oxide synthase
NTg	Nontransgenic mice
OGD	Oxygen and glucose deprivation
PBS	Phosphate buffer saline
PD	Phenylenediamine
PDH	Pyruvate dehydrogenase
PFK	Phosphofructokinase
P_i	Inorganic phosphate
PI	Propidium iodide
PMG	Pyruvate + malate + glutamate
PU	Polyurethane
Q	Ubiquinone
QH_2	Ubiquinol
RET	Reverse electron transport
ROI	Region of interest
ROS	Reactive oxygen species

Rot	Rotenone
ROX	Residual oxygen consumption
SDH	Succinate dehydrogenase
SEM	Scanning electron microscopy
Succ	Succinate
SUIT	Substrate-uncoupler-inhibitor-titration
TCA	Tricarboxylic acid
wt	Wet tissue
α-KG	α-ketoglutarate

1. General Introduction

1.1. Fundamentals of energy metabolism

The brain is an organ with high index of metabolic activity and although it comprises only 2% of the human body mass, its oxygen (O_2) and glucose requirements amount to 20% and 25% of the total body consumption, respectively (Magistretti et al. 1999). This high energy demand is mostly due to the activity of neurons (Harris et al. 2012) and the energy expenditure results mainly from the maintenance and restoration of ion gradients, generation of action potentials and neurotransmitter uptake (Attwell and Laughlin 2001). The highest energy consumption occurs at synapses, where the changes in postsynaptic membrane potential due to Na^+ and K^+ fluxes require the maintenance of their respective electrochemical gradients through the activity of the Na^+/K^+ ATPase, which accounts for roughly 40% of total neuronal ATP consumption.

Maximal ATP production is achieved when glucose is fully oxidized through oxidative metabolism to carbon dioxide (CO_2) and water (H_2O) to produce 32-36 ATP molecules per glucose molecule (Sokoloff 1981). Glucose enters neural cells through specific glucose transporters (GLUT) and is phosphorylated to glucose 6-phosphate by hexokinase. Then, glucose-6-phosphate can be metabolized via different pathways: glycolysis, the pentose phosphate pathway, and glycogenesis, the latter of which occurs exclusively in astrocytes. Via glycolysis, glucose is converted to two molecules of pyruvate and the energy output consists in 2 molecules of ATP and 2 molecules of NADH (Nelson et al. 2008; Mor et al. 2011; Shestov et al. 2014). Pyruvate is transported into mitochondria across both the outer and inner mitochondrial membranes where it is converted by pyruvate dehydrogenase (PDH) to acetyl coenzyme A (acetyl CoA), which then fuels the tricarboxylic acid (TCA) cycle (**Fig. 1.1**), a central pathway of cell metabolism with various possible substrates.

The reduced coenzymes NADH and $FADH_2$ produced during glycolysis and the TCA cycle (as well as during fatty acid oxidation, not discussed here) donate electrons to the electron transport chain (ETC) where a series of redox reactions, which end with the reduction of O_2, power transmembrane pumping of protons to the intermembrane space. The electrochemical gradient generated during electron transfer is used by ATP synthase to phosphorylate ADP, yielding ATP (Nelson et al. 2008) – **Fig. 1.1 -** a process coined oxidative phosphorylation.

The electron carriers of the ETC consist of membrane-embedded supramolecular complexes as well as a small protein (cytochrome *c*) and ubiquinol (Vonck and Schäfer 2009). Complex I, also called NADH:ubiquinone oxidoreductase or NADH dehydrogenase, catalyzes the oxidation of NADH and reduces ubiquinone (Q) to ubiquinol (QH_2), while pumping 4 protons across the inner mitochondrial membrane (Nelson et al. 2008; Hirst 2013). The net equation for the reaction processed by this complex is

$$NADH + 5H^{+}_{matrix} + Q \rightarrow NAD^{+} + QH_2 + 4H^{+}_{intermembrane} \quad (1)$$

Ubiquinol acts as a mobile electron and proton carrier and delivers electrons to complex III or cytochrome *c* reductase, where it is oxidized back to Q (Wang and Hekimi 2016). The TCA cycle enzyme succinate dehydrogenase (SDH) or Complex II can also reduce Q to QH_2. When succinate is oxidized to fumarate, two electrons are transferred to FAD located within complex II, producing $FADH_2$ (Cecchini 2003; Nelson et al. 2008). These electrons are then passed to iron-sulfur (Fe-S) clusters and finally to Q. Contrary to complex I, this complex does not transport protons across the inner mitochondrial membrane, leading to less ATP being produced by this pathway.

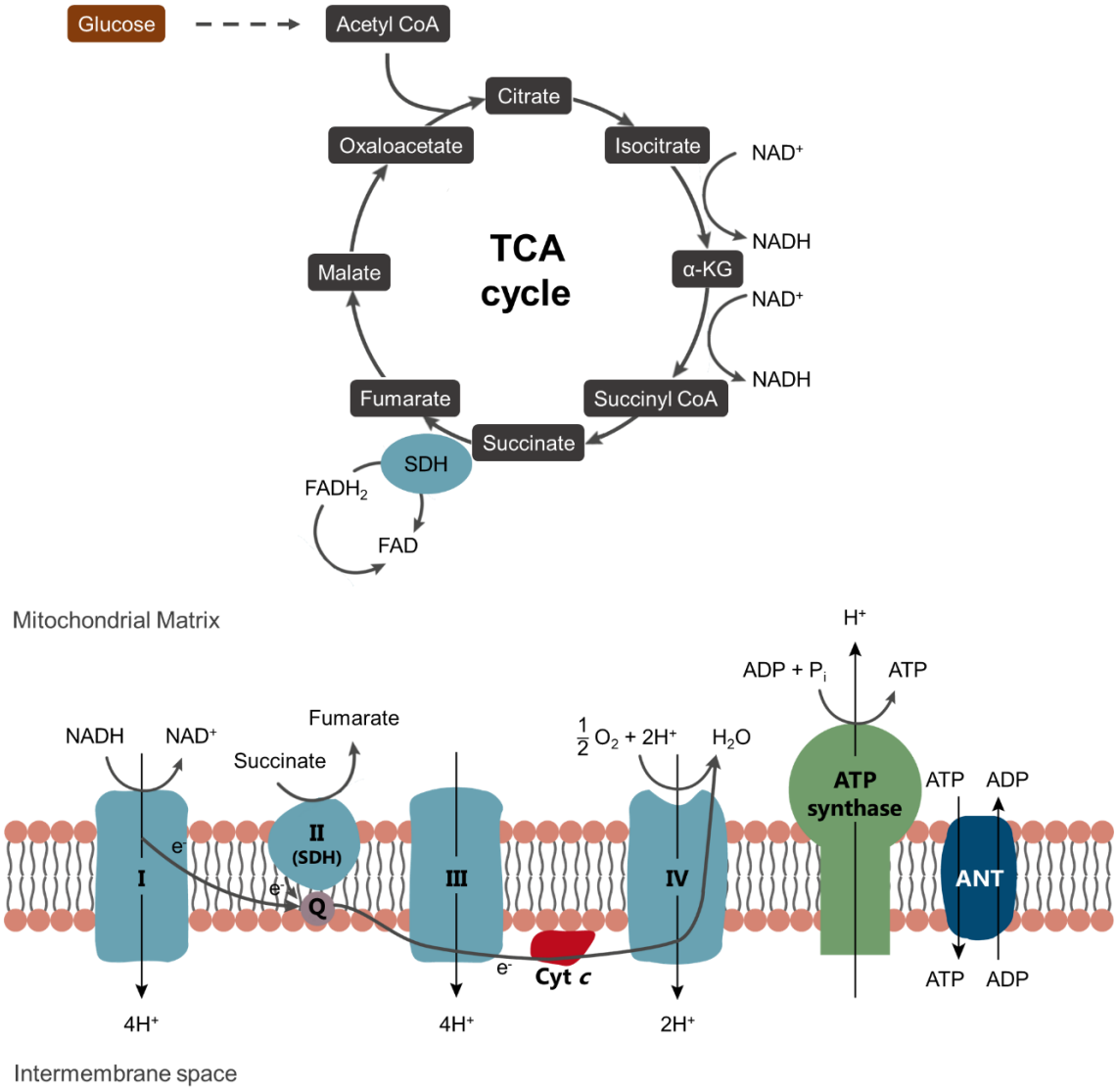

Fig. 1.1 – Simplified schematic representation of the reactions involved in the TCA cycle and electron transfer system (ETS).

The electrons from QH_2 originated from complex I and complex II are transferred to cytochrome *c* by complex III coupled with the transport of protons from the matrix to the intermembrane space (Nelson et al. 2008; Banerjee et al. 2021). Cytochrome *c* is a soluble protein of the intermembrane space that transfers electrons and contains a heme group, which switches between Fe^{2+} and Fe^{3+} (Nelson et al. 2008). Reduced cytochrome *c* donates its electron to complex IV, also known as cytochrome *c* oxidase (CcO), which ultimately reduces molecular O_2 to H_2O while concurrently pumping a total of four protons to the intermembrane space.

Although the electron transport through complexes and carriers is usually named the electron transport chain, more recently the term electron transfer system (ETS) has been used to emphasize this convergent and non-linear electron flow from complexes I and II to the Q pool (Gnaiger et al. 2020; Banerjee et al. 2021). As such, henceforth this process will be referred as ETS.

The electrochemical energy created by the proton gradient at the mitochondrial inner membrane is termed the proton-motive force. This stored energy is composed of a chemical potential energy, due to the concentration gradient (ΔpH), and an electrical potential energy, due to the charge distribution ($\Delta\psi$) across the membrane (Nelson et al. 2008). The proton motive-force is used for ATP production by ATP synthase, an F-type ATPase that uses the flow of protons from the intermembrane space to the matrix to fuel ATP production from ADP and inorganic phosphate (P_i), producing one molecule of ATP for every four protons (Junge and Nelson 2015). The proton motive force is also used by the adenine nucleotide translocase (ANT), which is an antiporter at the inner mitochondrial membrane, trading ADP for ATP. (Nelson et al. 2008).

It is important to keep in mind that under certain conditions pyruvate produced in glycolysis, rather than being used in the TCA, can be reduced to lactate in the cytoplasm by lactate dehydrogenase (LDH), as shown in eq. (2). This reaction can become relevant since it allows the replenishment of NAD^+ levels which are necessary to maintain the glycolytic flux. Lactate has even been proposed to be the actual glycolysis end-point (Schurr 2014, 2018), which seems to be even more plausible in the context of the brain (Barros et al. 2020).

$$\text{Pyruvate} + \text{NADH} \rightleftharpoons \text{Lactate} + \text{NAD}^+ \qquad (2)$$

Mitochondria also play several other key roles in the cell, including production of the so called reactive oxygen species (ROS) such as superoxide radical ($O_2^{\bullet -}$) and hydrogen peroxide (H_2O_2), that act as signaling molecules involved in cell functions, the maintenance of calcium (Ca^{2+}) homeostasis, besides actively participating in apoptosis (Goldenthal and Marín-García 2004; Davis and Williams 2012). Furthermore, changes in mitochondrial function have been reported in several neurological and neurodegenerative disorders (Lin and Beal 2006; McBride et al. 2006), hence the importance of studying brain mitochondrial function. Among all the mitochondria

functions, metabolism and oxidative phosphorylation are particularly affected (Cabral-Costa and Kowaltowski 2020).

1.2. Brain energy metabolism

As already mentioned, at the organ level, brain metabolism is almost fully oxidative. At rest, the ratio between the rate of O_2 (CMR_{O2}) and glucose (CMR_{glc}) utilization by the brain is close to the theoretical maximum value of 6.0 (6 O_2 + 1 glucose $\rightarrow$ 6 CO_2 + 6 H_2O), meaning that almost all the glucose is fully oxidized (Dienel 2019). However, during activity the CMR_{O2}/CMR_{glc} decreases (Fox et al. 1988), which has in part been attributed to lactate production (Dienel 2019). Concomitant measurements of lactate, O_2 and glucose point to oxidation of this lactate in the brain (Hu and Wilson 1997; Schurr 2018). A study in healthy humans suggested that, under physiological conditions, lactate contributes 10% to brain metabolism, but in situations in which supraphysiological plasma lactate concentrations are observed, it may contribute as much as 60% (Boumezbeur et al. 2010). Importantly, lactate can cross the blood brain barrier (BBB) and enter the brain through monocarboxylate transporters (MCT) and has been shown to support neuronal activity in brain tissue *per se* (Schurr et al. 1988; Halestrap and Wilson 2012).

Lactate can also be produced *in loco* (Hu and Wilson 1997; Bingul et al. 2020; Forderhase et al. 2020; Zuend et al. 2020). Several studies have shown that, at least in part, the end product of aerobic glycolysis is lactate rather than pyruvate. As shown in Eq. (2), the reduction of pyruvate to lactate by LDH allows the rapid regeneration of NAD^+, a requirement for maintaining the fast upregulation of glycolytic rate in neural cells upon activation. Supporting this is the fact that, under physiological conditions, blood and tissue lactate levels are higher than those of pyruvate, reflected in a lactate/pyruvate ratio higher than 10 (Havel et al. 1950). Furthermore, mitochondria contain both MCT and LDH (Hashimoto et al. 2008; Passarella et al. 2014), which allow lactate uptake and oxidation to pyruvate that then fuels the TCA cycle in the mitochondrial matrix.

Although the importance of glucose as a substrate for the brain is undisputable, the concept of lactate as an energy substrate has gained traction, while still remaining controversial (Hertz and Chen 2017; Magistretti and Allaman 2018; Schurr 2018; Bak and Walls 2018a, b; Barros and Weber 2018; Yellen 2018; Dienel 2019). The importance of lactate in brain metabolism was purposed by the demonstration that glutamate uptake in astrocytes stimulated aerobic glycolysis and lactate release to the extracellular medium (Pellerin and Magistretti 1994). This pioneering work led to the proposal of the “Astrocyte-Neuron Lactate Shuttle” (ANLS) model, according to which glutamatergic activity induces glucose uptake and lactate release by astrocytes. The extruded lactate can subsequently be taken up by neurons to support metabolic activity (Pellerin

and Magistretti 1994; Magistretti and Allaman 2018) – **Fig. 1.2**. This hypothesis is supported by several pieces of evidence, including the observed metabolic differences between neurons and astrocytes.

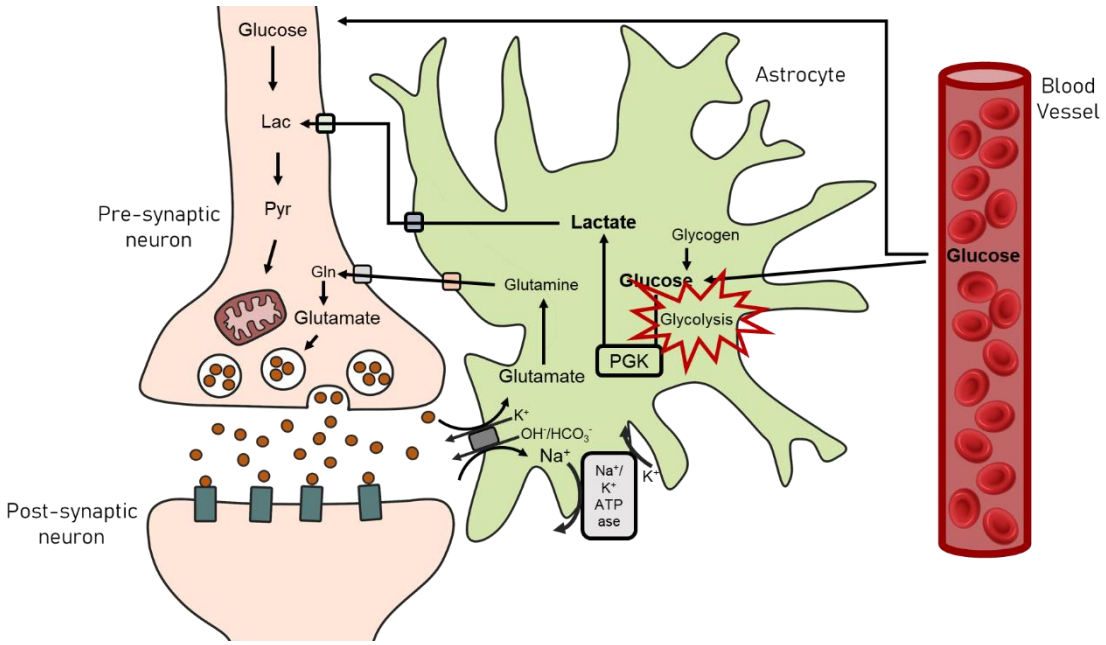

Fig. 1.2 – Schematic representation of the astrocyte-neuron lactate shuttle (ANLS) model. Uptake of glutamate by astrocytes during glutamatergic neurotransmission activates glycolysis in astrocytes. The lactate produced is released into the extracellular space and can be taken up by neurons.

1.2.1. Metabolic differences in neurons and astrocytes

There are cell-specific metabolic profiles in various organs and tissues. In the brain, it is estimated that both neurons and astrocytes uptake glucose at the same rate under basal conditions, despite neurons accounting for 70-80% of energy consumption in the brain (Nehlig et al. 2004; Chuquet et al. 2010; Howarth et al. 2012). This suggests that neurons display a higher rate of oxidative metabolism, while astrocytes are predominantly glycolytic (Bouzier-Sore et al., 2006; Itoh et al., 2003; Lovatt et al., 2007; Zhang et al., 2014). Neurons display low activity of 6-phosphofructo-2-kinase/fructose-2,6-biphosphatase-3 due to constant proteasomal degradation. As a result, production of the potent 6-phosphofructo-1-kinase (PFK1) activator, fructose-2,6-bisphosphate ($F2,6P_2$), is deficient, hindering neuronal ability to upregulate glycolytic rate (Almeida et al. 2001; Herrero-Mendez et al. 2009). In astrocytes, this enzyme is fully active, allowing the upregulation of glycolysis. On the other hand, astrocytes possess glycogen stores and glycogen-derived lactate can be an energy reserve and sustain neuronal function (Brown and Ransom 2007). Furthermore, neurons and astrocytes have been shown to have differential expression of pyruvate kinase (PK)

isoforms. Contrary to astrocytes that express the isoform PK2, neurons express PK1 which is not allosterically regulated, ultimately leading to a steady glycolytic rate in these cells (Zhang et al., 2014).

One other key enzyme which has been shown differential expression between neurons and astrocytes is LDH. Neurons express the LDH1 isoform which favors the conversion of lactate to pyruvate in lactate-consuming tissues. The conversion of lactate to pyruvate is further favored in neurons due to a lower NADH/NAD^+ ratio (Mongeon et al. 2016). Astrocytes, on the other hand, express LDH5, an isoform found in lactate-producing tissues, such as skeletal muscle (Bittar et al. 1996).

In line with this, when lactate concentration in circulation is increased, accumulation of lactate was found to be higher in neurons as compared to astrocytes, indicating that the latter have higher basal lactate levels (Mächler et al. 2016).

Finally, the expression pattern of MCT isoforms is also cell specific. Neurons express the high affinity MCT2 isoform (K_M of 0.5-0.75 mM for lactate) while astrocytes express the low affinity MCT4 and MCT1 isoforms (K_M of 22-28 mM and 3.5-10 mM for lactate, respectively) (Dimmer et al. 2000; Bergersen 2015; Pérez-Escuredo et al. 2016). Given this scenario, one may conclude that neurons are better equipped to uptake lactate even when its concentration in the extracellular medium is low.

Together, these differential expression patterns support the notion that the end-product of glycolysis in astrocytes might in fact be lactate, which can be extruded to the extracellular space and used by neurons to fuel oxidative metabolism under situations of increased energetic demand. Lactate can also be released from astrocytes through ion channels in response to K^+ (Sotelo-Hitschfeld et al. 2015; Ruminot et al. 2019).

It is thus not surprising that neuronal function and viability have been shown to be affected by pharmacological or genetic dysfunction of both neuronal and glial MCT isoforms (Newman et al. 2011; Mazuel et al. 2017). Interestingly, lactate could rescue neuronal function when glial MCT were dysfunctional but not for neuronal MCT dysfunction, highlighting the neuronal needs for extracellular lactate.

1.2.2. Brain lactate concentration dynamics

The lactate concentration dynamics in the brain has been studied with different methodologies in cells, brain tissue and *in vivo*. As already mentioned, the work of Pellerin and Magistretti showed that, in cultured astrocytes, glutamate uptake triggered lactate release to the medium (Pellerin and Magistretti 1994). The single-point measurement performed with an enzymatic

spectrophotometric method provided no information on the temporal lactate concentration dynamics. Using a similar method in acute hippocampal slices, Schurr *et al*. also showed that stimulation with glutamate for 15 min led to an increase in lactate production by the tissue. Total tissue lactate content was measured at discrete time points, revealing an increase during stimulation followed by a decrease 15 min after glutamate washout. Additionally, the increase in lactate was augmented when neuronal lactate uptake had been inhibited, pointing towards lactate uptake and use by these cells in response to glutamatergic stimulation (Schurr et al. 1999).

Other methods, based on electrochemical sensors or genetically encoded Förster Resonance Energy Transfer (FRET) lactate nanosensors, have allowed measurements of lactate concentration dynamics with high temporal resolution. These methods will be further discussed in section 1.7.2.

These have shown that neural activation induces a brief decrease in extracellular lactate which is followed by a sustained increase (Hu and Wilson 1997; Mangia et al. 2003; Lourenço et al. 2017b; Bingul et al. 2020; Forderhase et al. 2020). Most of these studies showed this biphasic profile of lactate concentration dynamics *in vivo*, independent of technique, stimulation paradigm, or brain region. This increase in extracellular lactate is presumed to be due to an increase in astrocytic lactate production and release, but the source of lactate has to date not been directly confirmed.

The use of a genetically encoded fluorescence nanosensor (Laconic) coupled to either confocal or two-photon microscopy has made it possible to follow intracellular and extracellular lactate dynamics at the cell level with high temporal resolution. Using this nanosensor, it was shown that astrocytes (in culture, cortical slices, and *in vivo*) maintain a steady-state reservoir of lactate (Sotelo-Hitschfeld et al. 2015). Neuronal depolarization or a physiological increase in extracellular K^+ induced an immediate release of this reservoir through an ion channel. A subsequent study in awake animals showed arousal-stimulated cortical activity induced release of lactate into the extracellular space with a concomitant dip in lactate concentration in astrocytes, leading the authors to infer that astrocytes release lactate into the extracellular space (Zuend et al. 2020) . The observed transient dip in astrocytic lactate was followed by an increase above baseline level, most likely the result of a fast increase in lactate production by astrocytes in excess to lactate release. Shortly after, neuronal lactate increased, coinciding with a slowing of the rise in extracellular lactate, which the authors interpreted as an increase in neuronal lactate uptake. After stimulation, the overshoot in lactate gradually returned to baseline in all compartments (extracellular, astrocytic, and neuronal). Importantly, astrocytes appeared to maintain a higher *in vivo* intracellular lactate level than neurons, which had already been demonstrated previously (Mächler et al. 2016) and corroborated by this study.

1.3. Brain ischemia and ischemia/reperfusion

The World Health Organization (WHO) defined stroke in 1970 as "rapidly developing clinical signs of focal (or global) disturbance of cerebral function, with symptoms lasting 24 hours or longer, or leading to death, with no apparent cause other than of vascular origin" (Aho et al. 1980). More recently, an updated definition has been proposed by the American Stroke Association to include clinical and tissue criteria based on significant advances made on the knowledge of the "nature, timing, clinical recognition of stroke and its mimics, and imaging findings" (Sacco et al. 2013). Regardless of its definition, stroke is one of the leading causes of mortality and morbidity worldwide (Feigin et al. 2021). Due to the high prevalence of stroke and its outcomes, it is of outmost importance to study how it occurs, its consequences, how to prevent it and how to improve patient outcome. Part of this work is focused on a strategy to improve the consequences of ischemic stroke.

Stroke is classified as either ischemic, when caused by a blockade of blood supply, or hemorrhagic, when caused by rupture of a blood vessel, with ischemic stroke being the most prevalent. As mentioned, the brain is particularly susceptible to loss in blood supply, since it relies heavily on O_2 and glucose for energy production, while mostly lacking energy reserves (Kalogeris et al. 2012). Thus, the impaired blood supply to brain tissue accompanied by ischemia leads to a series of molecular and cellular events that can end in cell death. Limited glucose and O_2 supply caused by hypoperfusion leads to energy failure in neurons within minutes due to rapid depletion of ATP (Wagner and Lanier 1994). Certain brain regions, such as the hippocampus, are more vulnerable to ischemia than others (Kirino and Sano 1984). Without enough ATP, the activity of Na^+/K^+-ATPase ceases, causing ionic imbalance with influx of Na^+, Cl^-, and Ca^{2+} and an efflux of K^+ (Hansen 1985; Daniele et al. 2021). Accumulation of Na^+ and Cl^- leads to cell swelling, damage to the cell membrane and necrosis (Iadecola and Anrather 2011) and widespread anoxic depolarization results in a massive release of neurotransmitters, including glutamate, leading to excitotoxicity (Mayor and Tymianski 2018). Excessive activation of *N*-methyl-D-aspartate (NMDA) type glutamate receptors leads to an increase in intracellular Ca^{2+}, activating proteases as well as other enzymes involved in the production of nitric oxide ($^{\bullet}NO$), free radicals and arachidonic acid metabolites (Iadecola and Anrather 2011). The overall consequence of these processes is cell death, either by necrosis or programmed cell death.

Reperfusion, i.e., reactivation of blood supply to the affected area, is urgent in order to re-establish O_2 and glucose delivery and avoid neuronal death. Reperfusion after stroke can occur spontaneously or require surgical procedures or medication (Lin et al. 2016). However, reperfusion can have deleterious effects and aggravate brain damage. This is demonstrated in a

rodent model, for example, by the fact that the infarct volume was increased with reperfusion compared to permanent occlusion with middle cerebral artery occlusion (MCAO) (Zhang et al., 1994). Reperfusion injury is associated with complex and multifactorial mechanisms including oxidative distress, pronounced inflammatory responses, platelet activation and aggregation, and disruption of the BBB, that ultimately cause neuronal death (Kalogeris et al. 2012; Lin et al. 2016). The level of damage provoked by reperfusion depends on the duration of the ischemic event (Hossmann 2012). Therefore, the ideal therapeutic strategy consists in reverting or preventing the damage resulting from both ischemia and reperfusion (I/R).

1.3.1. Production of ROS in ischemia/reperfusion

Throughout this document, the term ROS is used to refer solely to H_2O_2 and $O_2^{\bullet-}$ since these species are involved in redox signaling, contrary to other reactive species that most likely do not participate in redox signaling (Egea et al. 2017).

In physiological conditions, ROS are important second messengers participating in several cellular pathways (Finkel 2011). However, during I/R there is both an overproduction of these species and depletion of antioxidant defenses. This results in ROS triggering toxic cascades leading to oxidative damage of macromolecules, such as lipids, proteins, and DNA, as well as leading to injury through activation of certain signaling pathways, such as caspase-mediated apoptosis (Namba et al. 2001; Chan 2001; Chouchani et al. 2013).

The acute damage upon reperfusion is initially due to a burst in ROS production by mitochondria, which also initiates other damaging mechanisms that occur within a much longer time frame (from minutes to weeks) (Loor et al. 2011; Chouchani et al. 2016). Other sources of ROS in the cell that may have a role in I/R injury include xanthine oxidase and NADPH oxidases (Linas et al. 1990; Braunersreuther et al. 2013). However, these other sources produce ROS after the initial burst originating from mitochondria and their role in developing further damage is unclear (Abramov et al. 2007).

Mitochondrial production of ROS upon I/R originates mainly from the ETS complexes (Sanderson et al. 2013; Carinci et al. 2021). Limited O_2 supply during ischemia leads to accumulation of electrons upstream of complex IV, resulting in a reduced ETS. Upon reperfusion, there is a rapid increase in transfer of electrons as O_2 is again available, resulting in increased ROS production (Kunimatsu et al. 2011). As such, inhibiting the sources of ROS in the ETS can be protective in I/R.

The burst in ROS production upon reperfusion from the ETS is mainly due to $O_2^{\bullet-}$ production, which has been observed in various tissues and types of I/R injury (Chouchani et al. 2016). For

example, *in vivo* $O_2^{\bullet-}$ production measured with a biosensor increased during cerebral I/R (1h of MCAO followed by reperfusion) (Fabian et al. 1995). Superoxide radical is not only damaging *per se*, but also leads to production of more potent oxidants including H_2O_2, hydroperoxyl radical ($HOO^{\bullet}$), hydroxyl ($^{\bullet}OH$), or peroxynitrite ($ONOO^-$, by reaction with $^{\bullet}NO$) (Murphy 2009; Kalogeris et al. 2012).

In physiological conditions, mitochondrial $O_2^{\bullet-}$ can have various sources but is mainly produced by complexes I and III. However, in I/R complex I is generally recognized as the main source of $O_2^{\bullet-}$ upon reperfusion (Chouchani et al. 2016; Galkin and Moncada 2017). The mechanism of $O_2^{\bullet-}$ production at complex I during I/R is still not completely understood, but it seems to be due to reverse electron transport (RET) from complex II, as electrons are forced backward through complex I under conditions of hyperpolarization (Stepanova et al. 2017; Hernansanz-Agustín and Enríquez 2021). Accumulation of succinate during ischemia can act as a potential electron store for complex II and cause RET (Chouchani et al. 2016).

Since complex I is a major site of ROS production upon I/R, inhibiting this complex should be protective under these conditions. In fact, rotenone, an irreversible complex I inhibitor, is protective during ischemia (Lesnefsky et al. 2004). However, as this inhibition is irreversible, oxidative phosphorylation through complex I cannot resume after reperfusion. Therefore, for protection upon I/R, it would be more adequate to use reversible inhibitors. Reversible complex I inhibitors have been shown to protect against I/R injury, namely amobarbitol (Chen et al. 2006), MitoSNO – a mitochondria-selective *S*-nitrosating agent (Chouchani et al. 2013), and metformin (Cahova et al. 2015; Vial et al. 2019). Nitric oxide can also inhibit complex I through nitrosation of critical thiols (Shiva et al. 2007b; Galkin and Moncada 2017). Importantly, this is a reversible process (Galkin and Moncada 2007). Nitrite (NO_2^-) can be a metabolic precursor of $^{\bullet}NO$ via one-electron reduction and has been shown to be protective during brain I/R (Jung et al. 2006). Nitrite has also been shown to reduce brain mitochondria ROS production after cardiac arrest (Dezfulian et al. 2016). This reduction in ROS production has been associated with nitrosation of complex I (Shiva et al. 2007b; Chouchani et al. 2013). The redox conversion of $^{\bullet}NO$ /nitrite will be further developed in this work.

1.3.2. Experimental models of stroke

Although stroke is a complex disorder, some characteristics can be modeled for experimentation. Nonetheless, one must consider the intrinsic differences between humans and animals that occur at the level of genome and epigenome, brain and vascular anatomy, brain functional organization, immune system, and others (reviewed in (Sommer 2017)).

A variety of animal models for stroke are available, divided into two major types: global and local or focal ischemia. Global ischemic models mimic cardiac arrest or coronary occlusion in humans, while focal models aim at better reproducing stroke symptoms (Tajiri et al. 2013). In *in vivo* global ischemic models, vertebral and/or carotid arteries are ligated. Models of focal ischemia rely on the ligation or occlusion of the middle cerebral artery (MCA), since most thromboembolic infarcts in humans occur in regions affected by this artery (Olsen et al. 1985). As in ischemic stroke, irreversible damage occurs within minutes in a specific area – the infarct core. In the surrounding tissue, the penumbra, the reduction in blood supply is not as severe, resulting in maintenance of structural integrity while neuronal function is lost. This region becomes incorporated into the infarct core if blood supply is not re-established (Sommer 2017).

The complex nature of ischemic stroke is hard to model with *in vitro* systems, due to the absence of blood flow. However, *in vitro* models allow the study of biochemical and molecular mechanisms in conditions of lack of energy that occur in ischemia. The main approach used to model ischemia *in vitro* includes removal of energy substrates and O_2 from the medium. Alternatively, metabolism can be either chemically or enzymatically inhibited, although these are less relevant methods (Kurian and Pemaih 2014; Holloway and Gavins 2016). Oxygen and glucose deprivation (OGD) is widely used in both cells and tissues. In hippocampal slices, the lack of glucose and O_2 supply leads to a silencing of synaptic function in the first few minutes and cannot be recovered 12 min after reperfusion (Dong et al. 1988; Taylor et al. 1999). In tissue models, OGD can be applied to the whole tissue or to just a part of it, to better mimic the focal ischemic stroke. Using this approach, initial rapid neuronal depolarization has been observed within the ischemic core, followed by progressive depolarization in the penumbra region, with synaptic transmission abolished within 50 min of OGD (Richard et al. 2010).

1.4. Nitric oxide

Nitric oxide is a free radical that functions as a ubiquitous messenger, being involved in several physiological processes in the brain, such as neurovascular coupling, neurotransmitter release, synaptic plasticity, and neurometabolism (Ledo et al. 2005, 2010, 2021; Lourenço et al. 2014b, a, 2017a; Picón-Pagès et al. 2019). Its small size, free radical nature, hydrophobicity, and high diffusivity give this molecule a high range of biological targets and pathways in which it is involved (Guix et al. 2005; Toledo and Augusto 2012).

Conversely to other messenger molecules, $^{\bullet}NO$ does not interact specifically with targets on basis of structural complementarity. Being highly diffusional, its reactions are dictated by rate constants and abundance of potential targets. Among these, molecules with unpaired electrons, such as other

free radicals and transition metals, undergo the fastest reactions with •NO (Hill et al. 2010). As such, given its abundance, hemeproteins are obvious targets for •NO in biological systems. In fact, the majority of its relevant biological reactions involve the binding of •NO to ferrous iron in hemeproteins, a process termed nitrosylation (Wink and Mitchell 1998; Toledo and Augusto 2012). Examples of these proteins are the soluble guanylate cyclase (sGC), cytochrome *c* oxidase, and hemoglobin. Another, although indirect, effect of •NO is the nitrosation of proteins, which consists in the covalent addition of a nitroso group (−NO) to thiol, amines, and hydroxyl residues. This posttranslational modification of proteins has been associated to the regulation of several proteins, with physiologic and pathologic effects (Foster et al. 2009). An additional indirect modification caused by •NO is nitration which consists in the addition of a nitro group ($–NO_2$) to aromatic and aliphatic residues in proteins or to the aliphatic chain of fatty acids, mainly through formation of $ONOO^-$ and nitrogen dioxide ($^{\bullet}NO_2$). In proteins, this posttranslational modification occurs mainly at tyrosine residues, with implications in physiological and pathological processes (Ischiropoulos 2009).

Although at lower rates as compared with its reaction with free radicals and hemeproteins, •NO can also react with O_2 to produce nitrite. In aqueous phase, this reaction involves the following steps (Toledo and Augusto 2012):

$$^{\bullet}NO + O_2 \rightarrow 2\,^{\bullet}NO_2 \quad (3)$$

$$^{\bullet}NO + {}^{\bullet}NO_2 \rightleftharpoons N_2O_3 \quad (4)$$

$$N_2O_3 + H_2O \rightarrow 2NO_2^- + 2H^+ \quad (5)$$

This •NO auto-oxidation is only significant for higher •NO concentrations (and O_2 concentrations), meaning that its half-life depends on its concentration (Kharitonov et al. 1994). Due to both substances being hydrophobic, •NO and O_2 preferentially partition in hydrophobic milieus resulting in this auto-oxidation reaction taking place in cell membranes (Liu et al. 1998; Moller et al. 2005; Möller and Denicola 2018).

However, one must note that the reaction of •NO with O_2 *in vivo* under physiological conditions (low O_2) is negligible because it is competed out by other faster reactions of •NO, as mentioned earlier (hemeproteins, radicals).

Nitric oxide can be produced enzymatically by nitric oxide synthase (NOS) in a reaction in which L-arginine is the substrate and O_2 and NADPH are co-substrates. This enzyme also requires several co-factors, including FAD, FMN, heme and biopterin (Alderton et al. 2001). There are three main isoforms of NOS: neuronal NOS (nNOS or NOS I), inducible NOS (iNOS or NOS II), and endothelial NOS (eNOS or NOS III) – **Fig. 1.3**. While both nNOS and eNOS are Ca^{2+}-

dependent and constitutively expressed, iNOS is Ca^{2+} independent and inducible (Moncada et al. 1991). In neurons, •NO is mainly produced by nNOS, an enzyme that is coupled to the glutamate NMDA receptor (Christopherson et al. 1999) via protein-protein interaction mediated by the scaffold protein PSD-95 (post-synaptic density protein 95). This results in ready •NO production via an increase in intracellular Ca^{2+}, upon activation of this receptor.

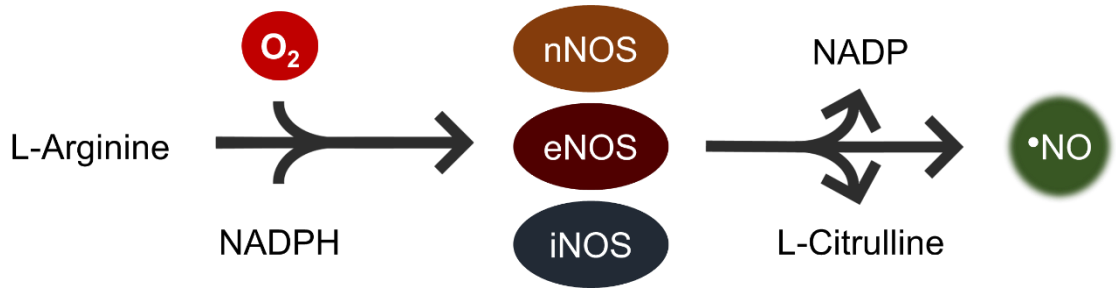

Fig. 1.3 – Nitric oxide (•NO) enzymatic production pathway. The three isoforms of the Nitric Oxide Synthase (NOS) – neuronal, endothelial, and inducible – convert L-Arginine to L-Citrulline, in an O_2-dependent reaction.

1.4.1. Modulation of energy metabolism by nitric oxide

One relevant target for •NO is cytochrome *c* oxidase, complex IV of the ETS. The effect of •NO on cytochrome *c* oxidase activity depends on O_2 concentration (**Fig. 1.4**). When O_2 concentration is high, the enzyme is predominantly in its oxidized state, consuming O_2 and metabolizing •NO to nitrite. In this case, •NO binds to the oxidized Cu_B center and inhibits enzyme activity in an uncompetitive mechanism (Antunes et al. 2007; Taylor and Moncada 2010). However, when O_2 concentration is low, cytochrome *c* oxidase is predominantly in a reduced state, and •NO binds to the heme a_3 (ferrous) competing with O_2 which results in reversible competitive inhibition of cytochrome *c* oxidase activity (Antunes et al., 2004; Taylor & Moncada, 2010). This competition allows for a fine tuning of mitochondrial respiration and a redistribution of O_2 toward locations with higher demand (Giulivi 2003; Victor et al. 2009). It also prevents hypoxia, by decreasing O_2 consumption. On the other hand, excessive inhibition of respiration is prevented by cytochrome *c* oxidase acting as a sink for •NO by metabolizing it for higher O_2 concentrations, thereby decreasing •NO concentration. In addition to dependence on O_2 concentration, the prevalence of one of these types of interaction between •NO and cytochrome *c* oxidase also depends on turnover conditions and concentrations of •NO, physiological substrates, and cytochrome *c* (Sarti et al. 2012).

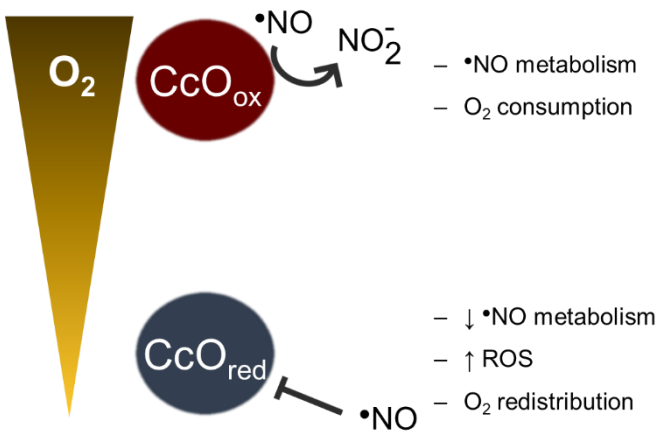

Fig. 1.4 – Nitric oxide inhibition of cytochrome *c* oxidase (CcO) depends on O_2 availability. At high O_2 concentration, •NO is metabolized, while at low oxygen concentration it inhibits the enzyme.

In the brain, •NO seems to affect energy metabolism differently in astrocytes and neurons. Although respiration is inhibited in the same proportion in both cell types, only in astrocytes is glycolytic rate increased in response to •NO through a mechanism which depends on activation of a master regulator of PFK1 via an increase in the concentration of its positive allosteric activator, $F2,6P_2$ (Almeida et al. 2001, 2004). As mentioned above, this pathway is not available in neurons. Nitric oxide can also upregulate the expression of GLUT in both neurons and astrocytes and increases glucose uptake in astrocytes (Bolaños et al. 2008).

Another target of •NO in the ETS is complex I, which is inhibited through nitrosation of critical thiol groups (Shiva et al. 2007b; Galkin and Moncada 2017). This is a reversible process and complex I activity can be restored by thiol-reducing agents (Galkin and Moncada 2007). Irreversible inhibition of complex I by •NO can also occur through nitration by $ONOO^-$ but this process is prevented if nitrosation occurs first, which protects the critical thiols from nitration (Galkin and Moncada 2017). Inhibition of complex I can, under certain conditions, lead to increased mitochondrial production of ROS and is associated with some of the possible deleterious effects of •NO (Brown and Borutaite 2004). However, when O_2 supply is insufficient, such as in ischemia, inhibition of complex I results in an oxidative phosphorylation sustained by complex II, limiting ROS generation, Ca^{2+} overload, and the release of cytochrome *c* (Shiva et al. 2007b). Interestingly, in situations in which O_2 supply is limited, NOS activity is hindered. In these conditions, •NO can be produced from nitrite as discussed in the next section.

1.5. Nitrite as a source of nitric oxide

In addition to NOS activity, •NO can be produced from nitrite, which takes place under hypoxic and acidic conditions (Lundberg et al. 2008). The NOS pathway is O_2-dependent (**Fig. 1.3**) and during hypoxia this form of •NO production is compromised. However, studies have shown that the lack of NOS activity during hypoxia does not block vasodilation as would be expected due to •NO being a critical mediator of vasodilation via its interaction with soluble guanylate cyclase in vascular smooth muscle cells (Millar 1995). Thus, nitrite reduction poses as a mechanism that ensures •NO production when the O_2 present is not sufficient (Shiva 2013). The conversion of nitrite into •NO involves a one-electron reduction and can take place through several mechanisms which may involve hemoglobin (Cosby et al. 2003) and myoglobin (Rassaf et al. 2007), xanthine oxidoreductase (Zhang et al. 1997), ascorbate (Carlsson et al. 2001), polyphenols (Gago et al. 2007), and protons (Benjamin et al. 1994).

1.5.1. The nitrate-nitrite-nitric oxide pathway

The concentration of nitrite in circulation is in the nanomolar range and can vary significantly with diet (Lundberg and Govoni 2004). A certain amount of nitrite originates from dietary sources. Although it is present in cured meat, the main source of nitrite is green leafy vegetables, which contain nitrate (NO_3^-) that, in turn, can be enzymatically reduced by commensal bacteria in human saliva to nitrite – **Fig. 1.5**. Thus, it is clear that whereas in the past both nitrate and nitrite were considered toxic substances, they can actually represent biological precursors of •NO, although nitrite can also be a product of •NO metabolism. Mediterranean and Japanese diets, generally considered healthy, contain foods with high-nitrate content. Both diets are associated with decreased incidence of cardiovascular disease as well as increased longevity (Lidder and Webb 2013). Plasma levels of nitrate, and hence nitrite, can also be increased with regular exercise (Jungersten et al. 1997), which however also stimulates eNOS expression and activity (Green et al. 2004).

Nitrate levels in plasma are normally in the micromolar range and, following a nitrate-rich meal its levels increase and remain high for hours (Lundberg and Govoni 2004). Nitrite levels in plasma also increase after nitrate ingestion. Most is excreted in urine (**Fig. 1.5**), but some is taken up by the salivary glands, leading to a 20-fold increase in concentration in saliva. Once in the oral cavity, commensal facultative anaerobic bacteria use nitrate as an alternative electron acceptor, thus producing nitrite (Duncan et al. 1995). These bacteria possess specific and effective nitrate reductases that are absent in mammals, allowing them to readily reduce nitrate to nitrite. Nitrite

is then swallowed into the stomach and, due to the acidic environment, part of it is immediately protonated to nitrous acid (HNO_2), which is then decomposed to several nitrogen oxides, such as $^{\bullet}NO$, nitrogen dioxide ($^{\bullet}NO_2$), and dinitrogen trioxide (N_2O_3) (McKnight et al. 1997). A part of the nitrite is not protonated and, in the intestine, it enters systemic circulation, reaching the peripheral organs (Lundberg et al. 2008), including the brain, where increased nitrite levels are observed in the cerebrospinal fluid (Pluta et al. 2005). Additionally, as already mentioned, nitrite may originate *in vivo* from $^{\bullet}NO$ oxidation. However, this can hardly be considered a major acute source of nitrite as compared with diet due to the slow kinetics of the reaction and the limited concentration of O_2.

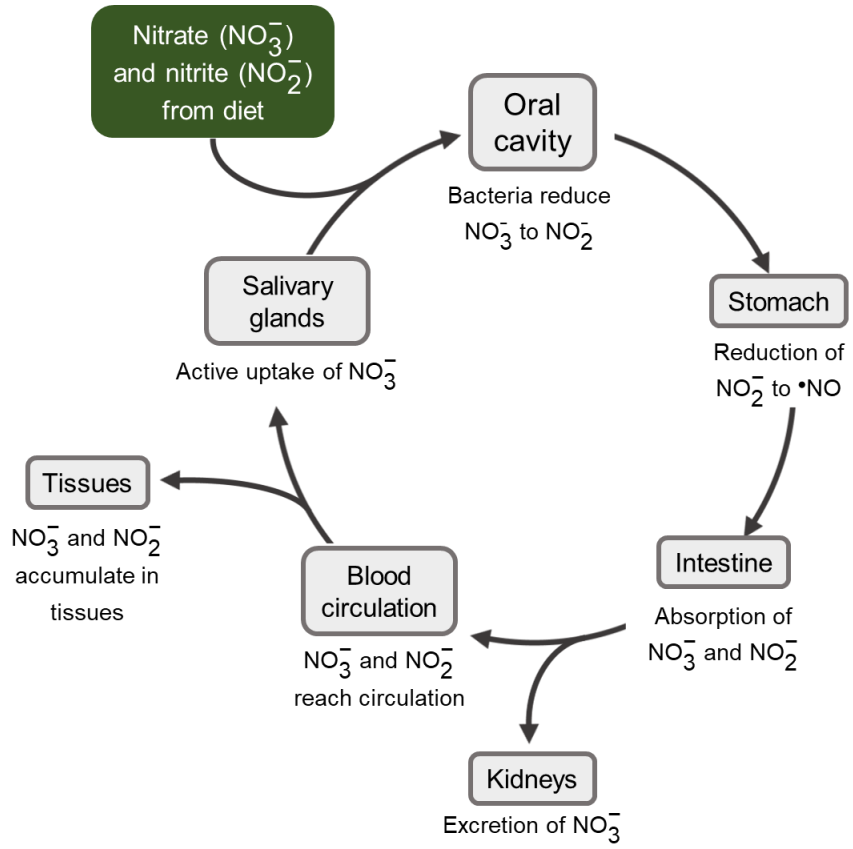

Fig. 1.5 – The entero-salivary nitrate-nitrite-nitric oxide pathway. In the oral cavity, nitrate is partially converted to nitrite by commensal bacteria that possess nitrate reductases. The nitrite produced and nitrate are swallowed into the stomach where in the acidic environment most of nitrite is reduced to $^{\bullet}NO$. The remaining nitrite and nitrate are absorbed in the small intestine, entering circulation. Through circulation they can accumulate in tissues and nitrate that reaches the salivary glands is actively taken up.

1.5.2. Nitrite and nitrate in brain ischemia

Nitrite has been shown to be protective during ischemia and I/R in a variety of organs (Murillo et al. 2011; Kapil et al. 2020). In the brain, administration of nitrite in a rodent model of I/R at the

time of reperfusion reduced infarction volume, increased local cerebral blood flow, and improved cognitive function after middle cerebral artery occlusion in a •NO dependent fashion (Jung et al. 2006). Other animal studies have also demonstrated that nitrite, applied at different time points in I/R, improved neurological function and reduced mortality (Fukuda et al. 2015; Dezfulian et al. 2016). Likewise, in a model of global cerebral ischemia, nitrate administered prior and immediately after the start of ischemia was also protective regarding neurological disorders and mortality (Kuzenkov and Krushinskii 2014).

However, despite the promising results supporting a beneficial role for nitrite in animal models of cerebral ischemia, human studies are limited. A recent study in patients of aneurysmal subarachnoid hemorrhage (a type of stroke) showed that intravenous infusion of nitrite during the early phase of brain injury (first 72h) led to an improvement of electroencephalography ischemic markers (indicative of neuronal function) in the patients that did not develop delayed brain injury (Luettich et al. 2021). For the smaller percentage of patients that did develop delayed brain injury, the effect was inconsistent. Importantly, these markers are not affected by nitrite in healthy individuals (Franko et al. 2019). In this context of stroke, to the best of my knowledge no other studies are available to date. As such, other studies are needed to evaluate the potential beneficial effects in brain ischemia.

The cytoprotective effect of nitrite in I/R injury is usually attributed to both direct and indirect pathways, the latter implicating production of •NO. These mechanisms include improvement of mitochondrial function through reversible inhibition of complex I, decrease in ROS production, Ca^{2+} influx and cytochrome *c* release, reversible inhibition of complex IV, inhibition of O_2 consumption with consequent preservation of high energy reserves during I/R, and activation of cGMP production, which is associated with decreased mitochondrial Ca^{2+} accumulation and prevention of mitochondrial permeability transition pore opening (Murillo et al. 2011). Other cytoprotective mechanisms include the suppression of platelet activation and adhesion and anti-inflammatory effects (Kapil et al. 2020). However, most of these studies have been carried out in I/R in organs other than the brain and a more in depth understanding of the mechanisms is still needed. In a model of global brain I/R, Dezfulian and colleagues showed that nitrite administered shortly after asphyxia-induced cardiac arrest and resuscitation accumulated in cerebrospinal fluid (CSF) and led to a reduction in neuronal ROS production (Dezfulian et al. 2016). It also reverted ATP reduction observed in placebo treated animals. These results were associated with increased *S*-nitrosation of brain mitochondrial proteins. In the same study, using an *in vitro* model of ischemia (OGD in cultured primary cortical neurons), nitrite decreased cell death, which was dependent on •NO formation. Furthermore, nitrite added at the moment of reperfusion abolished ROS production resulting from OGD. This study highlights the notion that nitrite can have a protection in brain I/R although the mechanistic intricacies still require further clarification.

1.6. The hippocampus

The hippocampus is a structure of the medial temporal lobe that is involved in the processes of memory and learning (Bird and Burgess 2008). Its basic layout is consistent in all mammals, comprising three different sub-regions consisting of pyramidal principal cells (CA – *Cornu Ammonis*): CA3, CA2, and CA1 (Andersen et al., 2007) – **Fig. 1.6**. In the human hippocampus, CA2 has a fairly compact and narrow pyramidal cell layer, with its borders being hard to establish and it is even less well defined in the rat hippocampus (Freund and Buzsáki 1996; Schultz and Engelhardt 2014). These hippocampal sub-regions have essentially one principal cell layer, comprised of pyramidal neurons. The hippocampus is part of the hippocampal formation, that also includes the dentate gyrus (DG, comprising granular principal cells), subiculum complex and entorhinal cortex (Andersen et al. 2007). The hippocampal formation, with highly plastic synapses, receives and integrates information from a variety of other brain regions, including the amygdala, thalamus, and hypothalamus (Andersen et al., 2007; Schultz & Engelhardt, 2014).

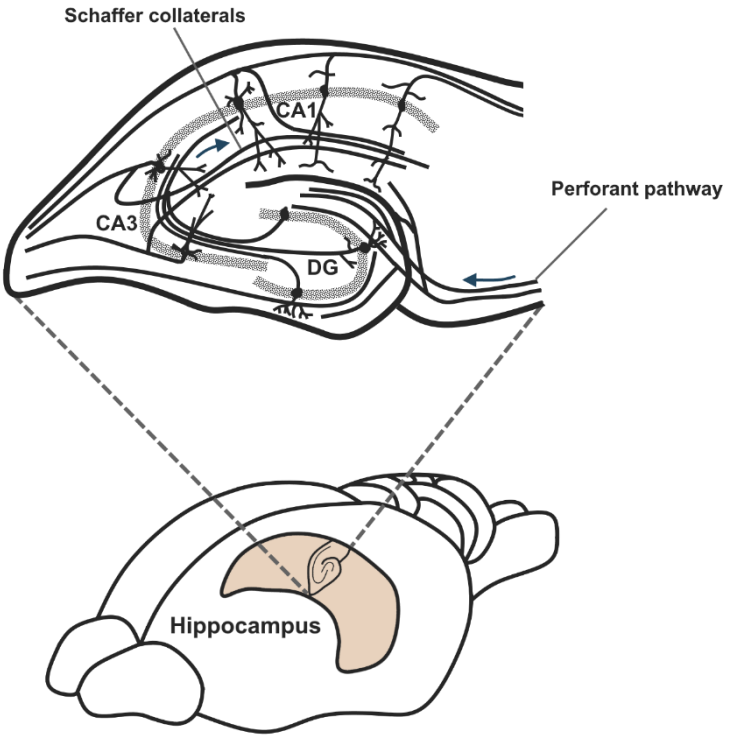

Fig. 1.6 – Location of the hippocampus within the rat brain and transversal slice, with representation of its subregions (CA1 and CA3), the dentate gyrus (DG) and neuronal circuitry.

The hippocampus represents an attractive brain structure for neurobiology studies due to its simple distribution of principal cell layers and laminar organization with a set of largely unidirectional excitatory (glutamatergic) pathways. This unidirectional flow of information is unique since the other brain regions have a reciprocal flow (Andersen et al. 2007). This occurs within a closed circuit, as represented in **Fig. 1.6**. First, the dentate gyrus receives information from the entorhinal cortex via the perforant path, which is then passed to the CA3 sub-region through the mossy fibers, the distinctive axons of the dentate granule cells (Witter and Amaral 1991). The pyramidal cells in CA3 project to other CA3 levels, subcortical regions and to CA1, which is the major input system to this sub-region (Schaffer collaterals pathway). Finally, the CA1 cells project mostly to the subiculum (Andersen et al. 2007; Schultz and Engelhardt 2014).

At the cell level, the pyramidal layers in the hippocampus consist of glutamatergic neurons that have a low firing threshold, leading to a high level of plasticity in this structure. Glutamate is the main excitatory neurotransmitter in the mammal central nervous system, and around 90% of the hippocampal neurons are glutamatergic, a much higher proportion than other parts of the cortex (Olbrich and Braak 1985). The remaining 10% are inhibitory GABAergic interneurons, which regulate the excitatory glutamatergic circuit of the principal neurons (Freund and Buzsáki 1996). Glutamate is stored in pre-synaptic vesicles and released upon stimulation. Once in the synaptic cleft, the neurotransmitter binds to specific receptors, triggering a response in the post-synaptic terminal. Glutamate receptors can be divided into two major types, ionotropic or ligand-gated ion channels and metabotropic G-protein coupled receptors (Niciu et al. 2012). Ionotropic glutamate receptors can be classified according to their different biophysical and pharmacological properties, named from exogenous agonists: NMDA, AMPA (α-amino-3-hydroxy-5-methyl-4-isoxazolepropionic acid), and KA (kainic acid). While AMPA and KA receptors have very fast kinetics, NMDA receptors have slow kinetics and can continue to mediate ion flux after clearance of glutamate from the synaptic cleft (Andersen et al., 2007). As already mentioned, $^{\bullet}NO$ is produced in response to activation of NMDA receptors, to which nNOS is coupled via protein-protein interactions mediated by PSD-95 (Christopherson et al. 1999).

In addition to the already mentioned features of the hippocampus that make it one of the most studied brain regions is the possibility of obtaining transverse slices that maintain its cytoarchitecture and functional circuitry (Lein et al. 2011) – **Fig. 1.6**. Acute slices are obtained from rodents at almost any age and can be maintained for several hours without compromising their viability and functionality.

Finally, the hippocampus is particularly affected in certain pathologies, including Alzheimer's disease and ischemia and reperfusion (Kirino and Sano 1984; West et al. 2004). Within the hippocampal formation, CA1 is the most affected region in ischemia and other insults, compared to CA3 and DG (Back et al. 2004; Ouyang et al. 2007; Alkadhi 2019). It has been suggested that

this higher susceptibility of CA1 to insults relies on the unique properties of the hippocampal formation, as CA1 neuronal death is dependent on functional CA3 input, and the higher density of NMDA receptors in this region (Onodera et al. 1986; Benveniste et al. 1989; Martens et al. 1998; Lahtinen et al. 2001). However, the exact mechanisms that lead to this specific vulnerability are still not fully understood, although mitochondrial dysfunction and changes in brain energy metabolism in the hippocampus appear to be a common denominator.

1.7. Evaluation of brain bioenergetic metabolism

As evidenced above, mitochondria play a central role in cell bioenergetics. Besides the obvious importance of oxidative phosphorylation in mitochondrial bioenergetics, there are other factors impacting energy production by mitochondria, including mitochondrial dynamics, mitochondrial transport, inter-organelle communication, biogenesis and degradation. As such, all of these parameters must be evaluated to better understand mitochondrial bioenergetics and how it is affected under pathophysiological conditions.

There are several possible ways of evaluating mitochondrial bioenergetics, including measurements of O_2 consumption at various mitochondrial respiratory states, mitochondrial membrane potential, ROS production, Ca^{2+} fluxes, redox equivalents (NADH, Ubiquinone, Cytochromes, etc.) and others (Palmeira and Moreno 2018). Evaluation of oxidative phosphorylation is typically determined indirectly through measurement of O_2 consumption or respiration. The focus in this work will be mainly the determination of respiration at different respiratory states in brain samples. As such, an emphasis will be given on how these measurements are processed and their implications.

1.7.1. Measurement of oxygen consumption rate

One widely used method for the evaluation of oxidative metabolism is through determination of O_2 consumption at different respiratory states in biological samples. This is done by observing changes in respiratory rates resulting from substrate-uncoupler-inhibitor-titration (SUIT) protocols, i.e., the successive addition of different substrates and drugs to either increase or inhibit the activity of the different complexes of the ETS. The information gathered by these studies varies depending on the type of sample, which can range from isolated mitochondria, to permeabilized cells or tissues, or intact cells or tissues. The definition of mitochondrial respiratory states based on substrate additions was first established by Chance and Williams using isolated mitochondria (Chance and Williams 1955). These definitions have since evolved and recently a

consensus between innumerous authors led by Gnaiger has been made on the nomenclature and definitions of such states (Gnaiger et al. 2020). This will be the definition used throughout this document.

1.7.1.1. Methodology

There is an array of methods that allow the monitoring of O_2 concentration in biological samples or *in vivo*, some more direct than the others. These include optical recording of intrinsic signals (ORIS), near-infrared spectroscopy (NIRS), electron paramagnetic resonance (EPR) oximetry, fluorescence oximetry and electrochemical oximetry (Ahmad & Kuppusamy, 2010; Diepart et al., 2010; Horan et al., 2012; Perry et al., 2013; Zhao et al., 2009). Among these the ones most commonly used for *in vitro* measurements are EPR, the Clark-type O_2 electrodes, and fluorescence oximetry.

Oximetry with EPR is a technique that explores the paramagnetic properties of O_2 (Ahmad and Kuppusamy 2010). Molecular oxygen has two unpaired rapidly relaxing electrons. Since the relaxation time is too fast to measure directly, a paramagnetic probe must be used (Gertsenshteyn et al. 2021). The external spin probe consist of paramagnetic material and there is a linear relationship between the relaxation rate of the spin probe and O_2 concentration (Ahmad and Kuppusamy 2010). This technique presents many advantages over other oximetry methods, including high sensitivity and specificity. The spin probes are generally nontoxic, stable and do not consume O_2 (Diepart et al. 2010; Ahmad and Kuppusamy 2010). However, its main limitation relies on the fact that it is not possible to add compounds during experiments, in addition to the cost and technical difficulties (Diepart et al. 2010).

The Clark electrode, developed by Leland Clark (Clark et al. 1953), employs amperometry to measure O_2 concentration within a closed chamber and has since been largely used in bioenergetics studies, mainly using isolated mitochondria. The electrochemical cell is comprised of a silver anode reference electrode and a platinum or gold cathode electrode bathed by an electrolyte (typically KCl) and covered by semipermeable membrane to reduce interferences and biofouling (Silva and Oliveira 2018). A working potential of -0.7 to -0.8 V vs. Ag/AgCl is applied and the following reactions take place:

$$4H^+ + 4e^- + O_2 \rightarrow 2H_2O \quad (5)$$

$$4Ag + 4Cl^- \rightarrow 4AgCl + 4e^- \quad (6)$$

The resulting current is proportional to the O_2 concentration in solution. The Oxygraph-2k system (O2k system; Oroboros Instruments, Innsbruck, Austria) is based on the Clark electrode. It comprises two separate amperometric sensors and allows the measurement of O_2 concentration with high resolution and accuracy (Gnaiger et al., 1995; Gnaiger, 2001; Hütter et al., 2006). The chamber design and construction materials combined with the O_2 sensor and electronics (highly stable temperature regulation) guarantee higher stability and lower noise of the amperometric signal resulting from the O_2 reduction reaction (Hütter et al. 2006; Gnaiger 2008). The requirement for smaller amounts of sample increases time resolution, as the rate of O_2 depletion from the medium is decreased (Gnaiger 2008).

Another widely used method for measurement of O_2 consumption is the fluorescence based XF Extracellular Flux Analyzer (Seahorse Bioscience), which is a high-throughput system since it allows measurements in 24- or 96-well plates (Horan et al. 2012; Perry et al. 2013). However, since it only allows for 4 additions during the experiments, the number of states studied per run are limited and there is low versatility in what can be added.

The studies herein conducted were aimed at developing and applying a methodology to study alterations in brain mitochondrial function and brain metabolism, requiring high resolution and versatility for which the O2k system is best suited.

1.7.1.2. Sample treatment

As already mentioned, SUIT protocols allow for the determination of O_2 consumption rates or O_2 fluxes (rates presented per mass or volume, for example) at several respiratory states (Gnaiger et al. 2020). These consist in adding specific substrates or compounds targeting an electron transfer pathway. However, many of these substrates or compounds do not cross the plasma membrane, including ADP and succinate, for example. In order to study all the parameters, isolated mitochondria or permeabilized cells/tissue must be used.

Although isolated mitochondria allow more direct evaluation without possible confounding factors from the cellular environment, it also removes the contribution of important factors such as mitochondrial dynamics and inter-communication, as well as morphology. Mitochondria are extremely dynamic organelles and multiple mechanisms allow the maintenance of their homeostasis and function, including fission, fusion and movement through the cytoskeleton, among others (Ni et al. 2015). Furthermore, the isolation process results in the alteration of mitochondrial morphology and function (Picard et al. 2011). Another issue with isolation is that pathological processes may lead to different levels of sensitivity of mitochondria to centrifugation

(Piper et al. 1985), resulting in loss of mitochondrial subpopulations during isolation (Figueiredo et al. 2008).

Some of the issues associated with isolation of mitochondria can be overcome with permeabilization of the plasma membrane in intact cells. Since the cholesterol content of the plasma membrane is higher than that of intracellular membranes, permeabilization of the plasma membrane can be achieved with mild detergents that extract cholesterol, such as saponin or digitonin (Korn 1969; Kuznetsov et al. 2008). By carefully titrating the detergent, the plasma membrane is selectively permeabilized while maintaining the integrity of organelles or the cytoskeleton, including the mitochondrial membranes (Fiskum et al. 1980; Kuznetsov et al. 2008). Comparative studies using isolated mitochondria and permeabilized tissue have produced disparate results. For example, studying muscle aging effects produced different results when measurements were carried out in isolated mitochondria or in permeabilized tissue, with more pronounced effects observed for isolated mitochondria (Picard et al. 2010). Another advantage of using permeabilized cells or tissue over isolated mitochondria is that much smaller amounts of sample are required.

Although permeabilized cells or tissue may be a better option as compared to isolated mitochondria, there is still loss of the physiological environment with permeabilization, since the cytoplasmic environment is lost. The issues that arise from isolation or permeabilization can be overcome by using intact cells (Dubinsky 2009; Brand and Nicholls 2011). While maintaining mitochondria in a physiological environment, the use of intact cells presents other limitations, such as limited access of substrates and drugs to mitochondria, and the lack of intercellular interaction remains an issue of concern. The use of intact tissue, while challenging, is advantageous in the sense that cell-to-cell interactions are preserved, which is particularly relevant in the context of brain.

1.7.1.3. Respiratory states

Mitochondrial bioenergetic parameters, such as O_2 consumption rate, are measured over different respiratory states. Respiratory states in isolated mitochondria or permeabilized cells/tissue are obtained with substrates for a determined pathway, which is achieved through the use of different substrates and inhibitors. Some of the substrates and inhibitors of each pathway/complex are presented in **Table 1.1**. Respiratory states have two complementary components: the coupling control state and the pathway control state (Gnaiger et al. 2020). The definitions of coupling

control states and pathway control states are summarized in **Table 1.2**. These states are usually obtained with saturating concentrations of substrates (including O_2).

Table 1.1 – Selected substates and inhibitors for components of the ETS.

Site of action	Substrates	Inhibitors
Complex I or NADH pathway	Pyruvate, malate, glutamate	Rotenone
Complex II or succinate pathway	Succinate	Malonic acid
Complex III		Antimycin A, Myxothiazol
Complex IV	Ascorbate, TMPD, cytochrome *c*	Sodium azide, cyanide
Complex V	ADP, ATP	Oligomycin
ANT	ADP, ATP	Atractyloside Carboxyatractyloside

The coupling control state, as the name indicates, refers to the coupling of the ETS, i.e., if the electron transfer is coupled to ATP production. There are three coupling states: Leak, OxPhos, and Electron Transfer (ET) – **Table 1.2**.

The Leak state depends on intrinsic uncoupling due to proton leak, proton slip, electron leak, and cation cycling (Doerrier et al. 2018). Proton leak refers to the leak of protons through the inner mitochondrial membrane and can be partly due to uncoupling proteins. Proton slip occurs when the number of protons translocated across the membrane by the proton pumps is decreased while all the other factors remain unchanged (Brown 1992). Protons can also slip through ATP synthase without contributing to ATP production (Brown 1992; Gnaiger et al. 2020). Electron leak refers to the leakage of electron from the ETS without reaching the point of reduction of O_2 to H_2O, reacting instead with O_2 to produce $O_2^{\bullet -}$ (Jastroch et al. 2010). Cation cycling results from the contribution of other cations to leak current, including Ca^{2+} and Mg^{2+} (Gnaiger et al. 2020). The Leak state can be achieved experimentally in the absence of adenylates (AMP, ADP, and ATP), after complete depletion of ATP, or with phosphorylation inhibitors.

Table 1.2 – Respiratory states in isolated mitochondria or permeabilized cells/tissues. Respiratory states are a combination of coupling control states and pathway control states. ROX is neither a coupling control state nor a pathway control state, as oxygen consumption from the ETS is inhibited.

	Respiratory states					
	Coupling control states			*Pathway control states*		*ROX*
	Leak	OxPhos	ET (Electron transfer)	NADH (complex I)	Succinate (complex II)	
Definition	Non-phosphorylating O_2 consumption (compensation for proton leak, etc.)	Maximal capacity for oxidative phosphorylation	Maximal electron transfer or respiratory capacity (collapsed protonmotive force)	Electron flux through complex I obtained with substrates linked to NADH production	Electron flux through complex II	Residual O_2 consumption not related to electron transfer (due to oxidative reactions)
Substrates / drugs	- Substrates* without ADP or after depletion of ATP - Inhibitor of ATP synthase (e.g. oligomycin) or ANT (e.g. carboxyatractyloside)	- Substrates* with saturating ADP	- Substrates* with uncoupler (e.g. FCCP, CCCP)	- Pyruvate - Malate - Glutamate	- Succinate	- Complex III inhibitor (e.g. antimycin A)

*Substrates include pyruvate, malate, glutamate, and succinate at saturating concentrations.

The OxPhos state is that in which oxidative phosphorylation occurs with saturating concentrations of respiratory substrates, such as pyruvate, malate, glutamate, and succinate, as well as ADP and inorganic phosphate (P_i). This results in an estimate of the maximal capacity for oxidative phosphorylation (Gnaiger et al. 2020).

The ET state is the state at which maximal electron transfer occurs, yielding an estimate of the maximal respiratory capacity associated with the ETS. This is a noncoupled state obtained by carefully titrating an uncoupler to obtain maximum O_2 consumption. Uncouplers (e.g. FCCP, CCCP) are weak lipid-soluble acids that act as protonophores, allowing protons to cross the inner mitochondrial membrane down their electrochemical gradient back to the mitochondrial matrix, collapsing the protonmotive force (Mitchell 2011). In this case O_2 consumption is not limited by oxidative phosphorylation since there is no dependence on ATP synthase activity to transport protons back to the matrix.

The pathway control state indicates which electron transfer pathway is active through the addition of saturating exogenous substrates after depletion of endogenous substrates (Gnaiger et al. 2020). The main pathways are the NADH pathway and the succinate pathway, with active flux of electrons through complex I and complex II, respectively – **Table 1.2**. These are obtained by adding saturating concentrations of either substrates that lead to NADH production (pyruvate, malate, glutamate, etc.) or succinate. Importantly, it may also be required to add inhibitors. For example, if the aim is to activate the succinate pathway only, complex I must firstly be inhibited. So respiratory states consist of a combination of both the coupling control state and the pathway control state. For example, for isolated mitochondria respiring on pyruvate and malate (NADH producing substrates) but without ADP in the medium, the respiratory state would be Leak in the NADH pathway. Another state is ROX (**Table 1.2**), which is the state with residual O_2 consumption, provoked by oxidative reactions not due to the ETS. This is obtained by inhibiting complex III. Inhibition of complex IV would be the more obvious way to obtain this state, but the known inhibitors of this complex (cyanide and azide) also inhibit catalase and other peroxidases, leading to an underestimation of the O_2 consumption at this state (Kengen et al. 2001). The O_2 consumption rate at this state should be subtracted from the rates at other states in order to remove this component from calculations.

In the case of intact, i.e., non-permeabilized cells or tissue, respiratory states are defined differently due to the inability of using substrates targeting specific pathways. There are three main states that can be evaluated: Routine, Leak, and ETS (Doerrier et al. 2018). Routine respiration is supported by exogenous substrates, either in culture media or another appropriate medium. The O_2 consumption rate at this state depends on energy demand, energy turnover, and the degree of coupling. The degree of coupling depends on the intrinsic uncoupling and pathological decoupling (Gnaiger et al. 2020). Leak respiration in intact cells is the same as for

isolated mitochondria or permeabilized cells/tissue but can only be obtained by inhibiting ATP synthesis with oligomycin, atractyloside, or carboxyatractyloside – **Table 1.1** and **Table 1.2**. Equally, ET capacity is also the same and obtained with titration of uncouplers. Residual O_2 consumption is obtained in the ROX state after inhibition of the ET pathway and is used for correction the O_2 consumption rates at the Leak, OxPhos and ET states (Doerrier et al. 2018).

1.7.2. Other approaches for studying brain energy metabolism

A plethora of technical approaches can be used to study brain metabolism, all of which with limitations and strengths. The choice of which one to use depends largely on the question at hand and obviously the availability of resources. These techniques have different time and spatial resolutions, allowing the study of different parts of the hierarchical structure of the brain. For example, some techniques only allow for measurements at the organ level, while others allow for a study at the organelle level or even at the molecular level (Barros et al. 2018). A greater focus on the techniques used for measurements related to lactate dynamics and oxidative metabolism will be given, as these relate more directly with the work shown here.

1.7.2.1. Lactate measurements

The lactate measurements in the studies mentioned in section 1.2.2. were mostly obtained either with electrochemical sensors (Hu and Wilson 1997; Lourenço et al. 2017b; Bingul et al. 2020; Forderhase et al. 2020) or with genetically encoded FRET lactate nanosensors (Sotelo-Hitschfeld et al. 2015; Mächler et al. 2016; Ruminot et al. 2019; Forderhase et al. 2020), but also with time-resolved proton magnetic resonance spectroscopy (^{1}H-MRS) (Mangia et al. 2003).

Real-time measurements of electroactive species can be obtained with microelectrodes coupled to electrochemical techniques, such as amperometry, high-speed chronoamperometry, square wave voltammetry (SWV) and fast cyclic voltammetry (FCV) (Robinson et al. 2008). They provide high sensitivity and temporal resolution, with minimal interference and damage to the brain (Dale et al. 2005; Barros et al. 2018). Compared to microdialysis, considered the golden standard for monitoring brain neurochemistry, they provide higher temporal and spatial resolution and cause less disruption to the tissue. This is a highly versatile technique, allowing for *ex vivo* and *in vivo* measurements with the possibility of simultaneously measuring several compounds and being used in parallel with other techniques, such as electrophysiology (Robinson et al. 2008). As microsensors can be calibrated before experiments, they can provide concentration estimates in real-time. The most common materials used for microelectrode fabrication are carbon and

noble metals (e.g., platinum). Carbon fiber microelectrodes (CFM) are particularly attractive, due to their small size (fibers can go down to 5 µm in diameter), low cost, ease of fabrication and potential for customization. The detection of non-electroactive species, such as lactate, can be achieved using microbiosensors based on microelectrodes with an appropriate enzyme immobilized at their surface (Dale et al. 2005; Bingul et al. 2020; Forderhase et al. 2020). This methodology usually involves the use of oxidases that produce H_2O_2, an electroactive substance (Weltin et al. 2016). Hydrogen peroxide acts as a reporter molecule and its electrochemical detection is optimal at electrodes comprised of platinum or platinum alloys. However, CFM can also be used in these microbiosensors by modifying their surface with deposition of platinum, representing a more inexpensive solution (Lourenço et al. 2019). Additionally, these microbiosensors can provide the opportunity of reducing size compared to conventional platinum electrodes (Meyerhoff et al. 1999; Lourenço et al. 2019).

The use of genetically encoded fluorescent nanosensors is a more recent development for the detection of metabolites. These are chimeric proteins that change their optical properties upon binding to a ligand (Barros et al. 2018). The expression of these nanosensors in cellular compartments can be detected by microscopy, with the spatial resolution and depth of measurements varying according to the microscopy technique chosen (wide field, confocal or two-photon). As such, they allow for the detection of metabolite dynamics at the cell level or lower levels. Specifically, the one used for lactate measurements (Laconic) is based on intramolecular FRET. The nanosensor uses a bacterial transcription regulator (LlDR), containing a lactate binding domain, sandwiched between two fluorescent proteins (mTFP and Venus) (San Martín et al. 2013). The major disadvantage of this technique is that these nanosensors are difficult to calibrate and their different expression level in different cells hinders the direct comparison between cells. However, it is possible to partly circumvent this issue, which is more feasible in cell cultures or tissue slices. Nonetheless, the technique can only provide estimations of concentration.

Magnetic resonance microscopy (MRS) is a noninvasive method that allows the visualization and quantification of a high number of brain metabolites, including lactate. It relies on the magnetic resonance from the nuclei in atoms of individual molecules to create a spectrum that graphically shows the detected signals as a function of their temporal frequencies (Buonocore and Maddock 2015). Measurements are done in a volume of interest or voxel, that is maintained throughout the experiments. Most lactate measurements are done with proton MRS (^{1}H-MRS), since the hydrogen nucleus produces a stronger signal than for example with ^{13}C, by using smaller voxels and having faster scan times (Buonocore and Maddock 2015; Barros et al. 2018). However, this technique has rather low temporal and spatial resolutions.

1.7.2.2. Brain oxidative metabolism

Neural activity is tightly coupled to oxidative metabolism, due to its high energy demand. Oxidative phosphorylation is usually studied by respirometry, as already described in section 1.7.1. As mentioned, it can be done with isolated mitochondria, cells or even tissue. Oxygen measurements in brain tissue or *in vivo* can also be performed with microelectrodes coupled to electrochemical techniques (Ledo et al. 2010, 2017a, b; Lourenço et al. 2017b; Fernández-Moncada et al. 2018). As already discussed, these allow for high spatial and temporal resolution, while being minimally invasive. However, measurements are carried out in open chamber, meaning that oxygen is continuously replenished, which can affect the measured concentration dynamics.

Brain oxidative metabolism can also be studied by determining changes in metabolites by *in vivo* MRS or *ex vivo* nuclear magnetic resonance (NMR). For example, ^{13}C NMR allows the quantification of TCA cycle intermediates by determining the exact positions of the labeled carbons of each detected metabolite (Rodrigues et al. 2013). Furthermore, ^{31}P NMR can be used to detect ATP. However, these techniques are less sensitive and have low temporal resolution.

1.8. Aims and outline

The brain is a complex and highly oxidative organ and, since it mostly lacks energy reserves, it depends greatly on delivery of energy substrates, mainly glucose and O_2, for energy production to maintain its viability and functionality.

Under physiological conditions, neurometabolism seems to involve an intricate mechanism that allows for a rapid supply of energy substrates during activity, with lactate playing an important role. This involves tight neurometabolic coupling between neurons and astrocytes, where net transfer of lactate from astrocytes to neurons allows for adequate fulfillment of energetic demands arising from activity. Evidence shows complimentary energy profiles in both cell types, supporting the notion of a neurometabolic coupling while neurons are markedly oxidative, astrocytes appear to rely more on the glycolytic pathway, being able to release lactate produced even when O_2 is readily available. Still, the role of lactate and the mechanisms involved in this neurometabolic coupling need further clarification.

Due to such high energy demand, the brain is particularly susceptible to failure of blood perfusion, with the consequent limitation of both glucose and O_2 supply. Indeed, various neurological pathologies are related to such failure and strategies to red uce its impact are greatly relevant. This

is particularly patent in stroke, where blood perfusion to certain brain areas can be completely blocked. As stroke is one of the leading causes of mortality and morbidity worldwide, improving its outcome can improve survivability and quality of life for patients. One of such strategies is through the modulation of mitochondrial metabolism to reduce the production of deleterious molecules that worsen the prognosis of stroke. In this regard, the redox conversion between nitrite and •NO has been linked to the modulation of mitochondrial respiration, thus affecting brain metabolism.

Therefore, the main purpose of this work is to study the modulation of neurometabolism under both physiological and pathological conditions with focus on the modulatory effects of lactate and nitrite. Under physiological conditions, the modulation of oxidative metabolism by lactate will be demonstrated in the context of neurometabolic coupling in the central nervous system, namely the hippocampus. Using an *in vitro* model of stroke, the potential of nitrite as a modulator of oxidative metabolism in the same brain region will be assessed.

The hippocampus appears as a brain region adequate for these studies as it is involved in memory and learning and is particularly susceptible to ischemia resulting from loss in blood perfusion. Additionally, it is possible to obtain tissue slices from this region that are biochemically and electrophysiologically functional. By using hippocampal slices, neurometabolism studies can be conducted in a preparation that better represents the *in vivo* conditions as compared to isolated cells, for example, while also providing a better control of the extracellular environment when compared to *in vivo* studies.

With this main purpose in mind, this work is divided in three chapters to address the following specific aims:

- Design, characterization, and evaluation of novel methodologies to investigate bioenergetic metabolism using hippocampal slices, namely optimization of a respirometry protocol capable of evaluating whole tissue O_2 consumption while maintaining tissue integrity, as a mean of evaluating oxidative metabolism, and an oxidase-based lactate microbiosensor using platinized carbon fiber microelectrodes to monitor extracellular lactate dynamics in real time in hippocampal slices (Chapter 3);
- Study the role of endogenous and exogenous lactate as an energy substrate in the hippocampus, both under resting conditions and in response to stimulation, using the new methodologies previously characterized along with pharmacological tools to quantify the contributions of both neurons and glia (Chapter 4);
- Evaluation of the protective role of nitrite during ischemia/reperfusion by modulation of oxidative neurometabolism in whole hippocampal tissue and elucidation of the underlying molecular mechanisms (Chapter 5).

2. Materials and Methods

2.1. Chemicals and reagents

Fatty acid free bovine serum albumin (FAF-BSA) and carboxyatractyloside were obtained from Calbiochem. Magnesium chloride hexahydrate was purchased from Fluka, sodium chloride from OmniPur, and carbonylcyanide-4-(trifluoromethoxy)-phenylhydrazone (FCCP) from Enzo Life Sciences. Carbogen gas mixture (O_2/CO_2 95:5) and nitrogen (N_2) were obtained from Linde. All other chemicals were analytical-grade and purchased from Sigma-Aldrich.

2.2. Media and solutions

All aqueous solutions and media were prepared using ultra-pure deionized water (R ≥ 18.2 MΩ cm), obtained from a Milli-Q system (Millipore Integral 10, MA, USA).

Mitochondrial Respiration Medium

The medium used in the evaluation of interferences to measurements provoked by the holder and with permeabilized slices was Mitochondrial Respiration medium 05 (MiR05, *p*H 7.1), which was prepared as described by Oroboros Instruments with the following composition (in mM): 0.5 EGTA, 3 $MgCl_2$, 60 Lactobionic acid, 20 Taurine, 10 KH_2PO_4, 20 HEPES, 110 D-Sucrose. The medium was supplemented with fatty acid free BSA (1 g L^{-1}).

Biopsy Preservation Solution

Biopsy preservation solution (BIOPS; prepared according to Oroboros Instruments) consisted of (in mM) 2.77 CaK_2EGTA, 7.23 K_2EGTA, 5.77 Na_2ATP, 6.56 $MgCl_2$, 20 Taurine, 15 Na_2Phosphocreatine, 20 Imidazole, 0.5 Dithiothreitol, and 50 MES.

Artificial Cerebrospinal Fluid

The medium used for hippocampal slice dissection and recovery period was a modified artificial cerebrospinal fluid (aCSF) with the following composition (in mM): 124 NaCl, 2 KCl, 25 $NaHCO_3$, 1.25 NaH_2PO_4, 1 $MgCl_2$, 1.5 $CaCl_2$, 0.2 ascorbate, 1 L-glutathione reduced, and 10 D-glucose. For experiments with hippocampal slices, aCSF with the following composition was used (in mM): 124 NaCl, 2 KCl, 25 $NaHCO_3$, 1.25 NaH_2PO_4, 1 $MgCl_2$, 1.5 $CaCl_2$ and substrate depending on the experiment (0.1, 0.5, 10 or 15 mM D-glucose, 10 or 15 mM sodium L-lactate, 10 mM pyruvate). Both were continuously bubbled with carbogen for appropriate O_2 supply and to maintain *p*H 7.4. In respirometry experiments, aCSF was additionally supplemented with 20

mM HEPES for *p*H buffering and 5 mg mL^{-1} FAF-BSA to facilitate drug diffusion. For O_2 and glucose deprivation, respirometry aCSF lacked glucose.

Phosphate Buffer Saline

The *in vitro* evaluation of microbiosensors was carried out in 0.05 M phosphate buffer saline (PBS) at *p*H 7.4 with the following composition (in mM): 100 NaCl, 10 NaH_2PO_4 and 40 Na_2HPO_4.

Stock solutions

Sodium dithionite stock solution (10 mM) was prepared in phosphate buffer, 50 mM, *p*H 8. Malate (L-malic acid; 0.4 M) and glutamate (L-Glutamic acid, monosodium salt hydrate; 2 M) stock solutions were prepared in ultra-pure water with *p*H adjusted to 7 with 5 M KOH. The stock solutions of ADP were prepared in ultra-pure water with *p*H adjusted to 7 with 5 M KOH and 0.3 M of $MgCl_2$ was added in the end. Sodium pyruvate (2 M), carboxyatractyloside (5 mM), succinate (1 M), azide (NaN_3, 4 M), propidium iodide (1.5 mM), nitrite ($NaNO_2$, 4 mM), carboxy-PTIO (100 mM), and cytochrome *c* (4 mM) stock solutions were prepared in ultra-pure deionized water. Myoglobin stock solution (saturated, ~3 mM) was prepared by adding myoglobin to a defined volume of ultra-pure water until saturation.

Oligomycin (4 mg mL^{-1}), CCCP (1 mM), FCCP (10 mM), rotenone (1 mM), antimycin A (5 mM), and α-cyano-4-hydroxycinnamic acid (4-CIN) stock solutions were prepared with absolute ethanol. The AR-C155858 (0.5 M) stock solution was prepared in DMSO.

The fluorocitrate (FC) solution was prepared as follows: 8 mg of DL-fluorocitric acid barium salt (Sigma) were dissolved in 105 µL of 0.57 M HCl, Ba^{2+} was precipitated with 0.7 M Na_2SO_4 (43 µL) and then 32 µL of 0.94 M $NaCO_3$ were added. The suspension was centrifuged at 1000xg for 5 min and the supernatant recovered.

Lactate (1 M), glutamate for stimulation (L-Glutamic acid, monosodium salt hydrate; 0.5 M), and potassium chloride (3 M) stock solutions were prepared in aCSF without glucose. Saponin stock solution (5 mg mL^{-1}) was prepared in MiR05. Nitrate ($NaNO_3$, 1 mM) was prepared in the animals drinking water.

The 0.4% H_2PtCl_6 solution was prepared in 0.1 M H_2SO_4.

2.3. Sample holder

A sample holder was manufactured to hold hippocampal slices in the recording chamber of the O2k system (Oroboros Instruments, Innsbruck, Austria). The purpose of this holder was to avoid

the damage provoked by direct contact of hippocampal slices with the stirring bar, thus preserving tissue integrity throughout the experiment. This holder consisted of a nylon mesh (1 mm^2 area square holes) glued with cyanoacrylate onto a polypropylene plastic ring with a diameter of 1.6 cm and a height of 3 mm (**Fig. 2.1**). These properties allowed for a perfect fit of the holder in the O2k system chambers without movement.

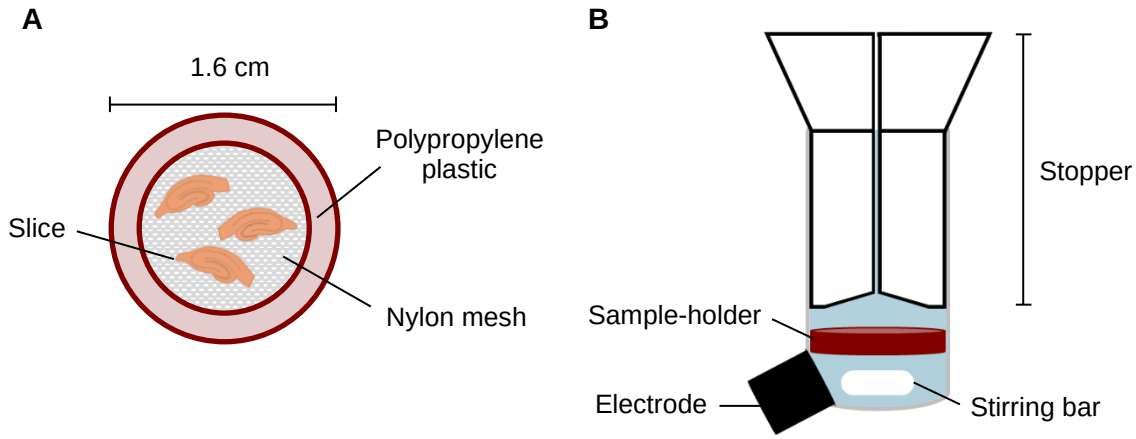

Fig. 2.1 – Schematic representation of (A) hippocampal slices resting on the homemade holder, top view and (B) chamber cross-section showing the holder positioning (in red; between the stirring bar and the stopper). Slices are placed on this holder to prevent damage from the stirring bar in the chamber.

2.4. Effect of the sample holder on chamber vertical mixing

Oxygen concentration was measured in MIR05 with the O2k system (Oroboros Instruments, Innsbruck, Austria), at 32ºC with a sampling rate of 0.5 Hz. Calibration was performed according to manufacturer's instructions. The system has two chambers, giving the possibility of performing two experiments at the same time. The sample holder was placed in one of the chambers while the other had only medium. The holder positioning in the chamber is shown in **Fig. 2.1B** (fitted between the stirring bar and the stopper). Dithionite (70 µM) was added to both chambers to decrease O_2 concentration to a defined level, but not completely deplete it. In a different vertical mixing interference test, stirrer tests were carried out, consisting in stopping stirring for a defined period of time (30 s in this case) and restarting it, as allowed by the equipment software. In this case, the O_2 concentration was measured at a frequency of 5 Hz to allow for higher time resolution.

2.5. Lactate microbiosensors

Carbon fiber microelectrodes were fabricated as previously described (Santos et al. 2008) – **Fig. 2.2A**. Briefly, a single carbon fiber (30 µm Textron Lowell, MA) was inserted into a borosilicate glass capillary (1.16 mm i.d., 2 mm o.d., Harvard Apparatus Ltd. UK) which was then pulled on a vertical puller (Harvard Apparatus Ltd. UK). The protruding carbon fiber was cut to a tip length of 100-180 µm with tweezers under an inverted optical microscope. The electrical contact between the carbon fiber and the copper wire was provided by conductive silver paint (RS, UK). The microelectrodes were pretreated and tested for their general recording properties in PBS by fast cyclic voltammetry at a scan rate of 400 V s^{-1}, between −0.4 and + 1.6 V vs. Ag/AgCl, for 1 s (MultiPalmSens4, PalmSens BV, The Netherlands).

The electrodeposition of platinum nanoparticles on the carbon surface – **Fig. 2.2A** – was carried out using a deoxygenated 0.4% chloroplatinic acid solution in 0.1 M H_2SO_4, in a two-electrode electrochemical cell comprising the CFM as a working electrode, and Ag/AgCl in 3M NaCl as a reference electrode (RE-5B, BAS Inc, West Lafayette, IN, USA). Potentiostatic electrodeposition was performed by applying a holding potential of -0.2 V vs. Ag/AgCl for 10 s (Lourenço et al. 2019).

Lactate oxidase (EC 1.1.3.2, from *Aerococcus viridans* lyophilized powder) was immobilized at the platinized CFM (CFM/Pt) surface by crosslinking with glutaraldehyde. The CFM/Pt tip was dipped for 5 min in a drop of a mixture of 1 mg mL^{-1} of enzyme, 10% BSA, and 0.125% glutaraldehyde. The procedure was repeated 3 times, with a 1 min drying interval. The same procedure was applied to obtain sentinel sensors (with glutaraldehyde and BSA only, lacking enzyme).

After enzyme immobilization, the sensors were stored dry and protected from light, and at room temperature conditions for at least 72h to allow for stabilization of the matrix. To limit lactate diffusion and thus increase the apparent K_M for lactate, the sensors were coated with a polyurethane membrane by dipping three times for 5 s with 10 min interval between each dipping in a solution containing 2% polyurethane in 98% tetrahydrofuran and 2% dimethylformamide.

Finally, before experiments, the sensor surface was modified with an exclusion layer of polymerized 1,3-phenylenediamine (*m*-PD) to decrease the putative interference from oxidation of certain electroactive molecules present in brain tissue. Electrodeposition of *m*-PD (10 mM) was achieved by cyclic voltammetry at a scan rate of 50 mV s^{-1}, between +0.25 and +0.75 V vs. Ag/AgCl for 20 min (FAST MKII, Quanteon LLC, USA) in deoxygenated PBS. A schematic representation of lactate and sentinel/null microbiosensor design is shown in **Fig. 2.2B**.

2.6. Scanning electron microscopy

A microphotograph of the tip of CFM (**Fig. 2.2A**) was obtained with high-resolution scanning electron microscopy (SEM) with a field emission scanning electron microscope coupled with energy dispersed X-ray spectroscopy (EDS; Zeiss Merlin coupled to a GEMINI II column). The microelectrodes were held on the specimen holder with conductive carbon adhesive tabs. Images were recorded with an acceleration voltage of 25 kV.

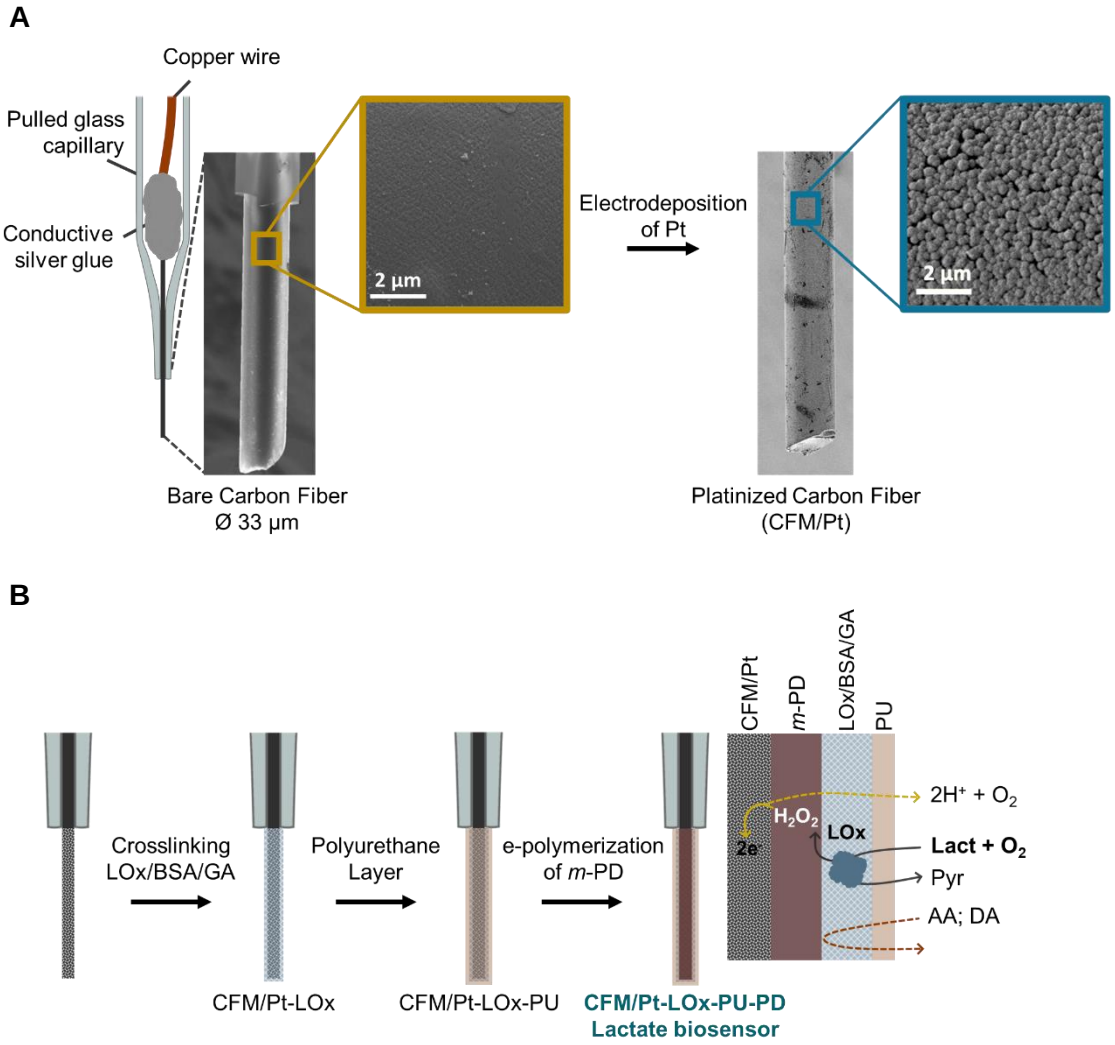

Fig. 2.2 – (A) Schematic representation of a carbon fiber microelectrode, showing a scanning electron microscopy (SEM) micrograph of the carbon tip before and after platinization. The blow-up image in the far right shows the surface morphology of the Pt particles on the carbon fiber. (B) CFM/Pt-LOx-PU-PD microbiosensor construction. In the far right, scheme of microelectrode operation. LOx – lactate oxidase, GA – glutaraldehyde, *m*-PD – *m*-phenyenediamine, PU – polyurethane, Lact – lactate, Pyr – pyruvate, AA – ascorbic acid, DA – dopamine.

2.7. Animals

All animal procedures were performed in accordance with the European Union Council Directive for the Care and Use of Laboratory animals, 2010/63/EU, and were approved by the local ethics committee (ORBEA 146_2016/31102016) and the Portuguese Directorate-General for Food and Veterinary. The animals were purchased from Charles River Laboratory (Barcelona, Spain) and maintained at the local animal facility (Faculty of Medicine, University of Coimbra). In the animal facility, rooms for housing were kept under a controlled environment: a temperature of 22–24 °C, a relative humidity of 45–65%, 15 air exchanges per hour and a 12:12 light/dark cycle. Animals were fed with a standard rodent chow and were provided chlorinated water, both *ad libitum*. Cage bedding of standard corn cob was changed three times a week and environmental enrichment was provided with tissue paper and a cardboard tube. For homogenate experiments, 1 male C57 BL/6N mouse (aged 4 months) was used. For evaluation of respirometric states in rat and mice, 7 female Wistar rats (aged 8–10 weeks) and 5 male CD-1 mice (aged 8 weeks) were used. For the experiments conducted in chapter 4, male Wistar rats (8-12 w.o.) were used. In chapter 5, male C57BL/6 mice (5-6 m.o.) were used for hypoxia studies. Male Wistar rats (9-13 w.o.) were used in OGD and anoxia/reoxygenation (A/R) experiments. Three-month-old Wistar male rats received nitrate (1 mM) in their drinking water for 5-7 weeks and were used in A/R experiments. Their water and food intake were measured every 2 days, at which time their water was replaced. The experiments with the Alzheimer's disease model were performed using the male triple transgenic mouse model of Alzheimer's disease (3xTgAD) as described by Oddo and colleagues (Oddo et al. 2003). Both 3xTgAD mice and background strain, wild-type nontransgenic mice (NTg) (C57BL6/129sv) were supplied from a colony implemented in the animal facility of the Center for Neuroscience and Cell Biology (Coimbra) obtained from Dr Frank LaFerla's Laboratory at the Department of Neurobiology and Behavior and Institute for Brain Aging and Dementia, University of California at Irvine. Animals from each genotype were divided into 2 age groups: young (3-6 months old; N = 14 for NTg and N = 12 for 3xTgAD) and middle-aged (12 months old; N = 8 for both NTg and 3xTgAD).

2.8. Brain homogenate preparation

For preparation of brain homogenate, a mouse was killed by cervical displacement and the brain was rapidly removed and placed in ice-cold BIOPS. The forebrain was washed, and all membranes and blood vessels were removed. All procedures were carried out on ice. The wet weight was determined, and the tissue was cut into small pieces. After washing the pieces with

BIOPS, the tissue was homogenized in MiR05 (100 mg_{wt} mL^{-1}) using a micro tissue grinder with a Teflon pestle (4 strokes). The homogenate was added to the O2k chamber containing MiR05 at the final concentration of 1 mg_{wt} mL^{-1}.

2.9. Hippocampal slices preparation

Rats (under anesthesia, isoflurane) and mice were killed by cervical displacement. Following decapitation, the brain was rapidly removed and placed in ice-cold modified aCSF Having the brain in ice-cold modified aCSF continuously bubbled with humified carbogen (95% O_2/5% CO_2) for *p*H buffering (*p*H 7.4) and oxygenation, the hippocampi were dissected and 250-µm or 400-µm transverse slices were prepared using a vibratome (Vibroslice, World Precision Instruments, Inc., UK). The thickness of tissue for each species was optimized as to allow a compromise between tissue viability (ratio between surface damage and healthy core tissue) and access of substrates/drugs to the tissue core. Slices were then transferred into a pre-incubation chamber (BSC-PC, Harvard Apparatus) containing modified aCSF at room temperature, also continuously bubbled with carbogen and allowed to recover for at least 1 h under these conditions.

2.10. High-resolution respirometry

Oxygen flux is the O_2 consumption rate when expressed as a size-specific quantity (for example, per mass or per volume) (Gnaiger et al. 2020). Oxygen flux (pmol s^{-1} mg^{-1}) was measured by high-resolution respirometry with the Oxygraph-2k system (Oroboros Instruments, Innsbruck, Austria) controlled by DatLab software v. 5.1.1.9 or v. 7.4.0.4. Air calibration was performed according to the manufacturer instructions. Measurements were carried out with continuous stirring (750 rpm) in 2 mL of medium.

2.10.1.1. Evaluation of interference from the sample holder

The medium used for the brain homogenate experiments evaluating interference from the holder was MiR05. Experiments were carried out at 37ºC and at air O_2 concentration (~180 µM). The manufactured sample-holder was placed in one of the chambers while the other only had medium – **Fig. 2.3**. The same brain homogenate and in the same amount (1 mg_{wt} mL^{-1}) was added to both chambers. A standard SUIT protocol was carried out: pyruvate (5 mM), malate (2 mM) and glutamate (10 mM) – PMG – were added as NADH linked substrates, followed by ADP (2.5 mM)

to start oxidative phosphorylation. Then, complex II linked substrate succinate (10 mM; succ) was added. To test for integrity of the mitochondrial outer membrane, cytochrome *c* (10 µM; cyt *c*) was added. The maximal capacity of the ETS – ET capacity – was determined by adding CCCP stepwise (0.5 µM steps). Finally, rotenone (0.5 µM; rot) was added for complex I inhibition, followed by antimycin A (2.5 µM; ama) for complex III inhibition. Reoxygenation was carried out whenever needed by opening the chamber.

2.10.1.2. Intact hippocampal slices

The experiments with hippocampal slices were carried out in aCSF supplemented with HEPES and FAF-BSA at 32ºC. Measurements were carried out with continuous stirring (750 rpm) in 2 mL of aCSF and at high O_2 concentration (between 700 and 900 µM) to ensure proper oxygenation of the slices core (Ledo et al. 2005, 2017b), except for measurements in hypoxia, that were carried out at lower O_2 concentration (~150-200 µM). To increase O_2 concentration, the medium was saturated with carbogen using a syringe with the stoppers in place without completely closing the chamber and without immersing the needle. The manufactured sample-holder was used to sustain the tissue in the chamber during the recording to avoid slice damage by the stirring bar present in the recording chamber – **Fig. 2.3**.

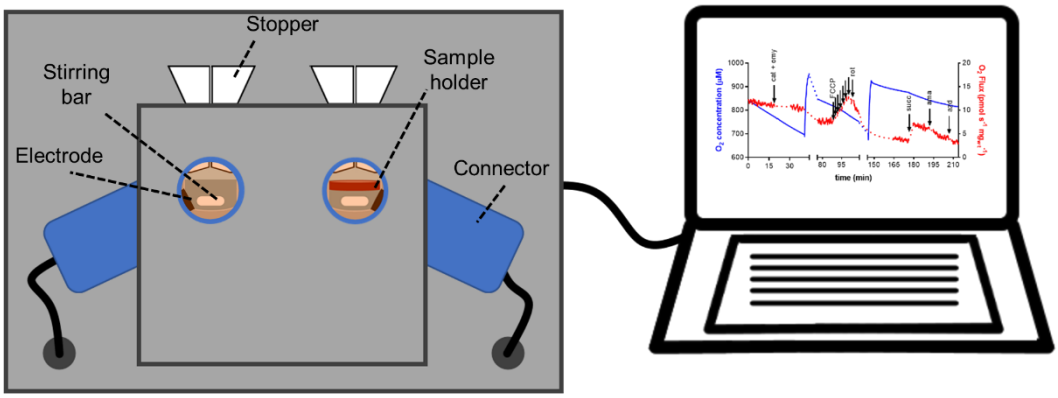

Fig. 2.3 – Representation of the O2k system with a sample holder fitted into one of its two chambers, connected to a computer that controls both the equipment and processes the recording.

The DatLab software allows for a correction for instrumental background. This was performed prior to experiments with the same aCSF medium used during experiments and with each manufactured holder in place in the respective chamber. Initially, the O_2 concentration of the medium was increased to values near saturation with carbogen. After stabilization, the O_2 concentration was decreased by briefly opening the chamber. This background correction

experiment was performed within the O_2 levels used in the experiments (~700–900 µM), and stable fluxes were obtained for approximately 900, 700 µM and two concentrations in between these two values. This background correction was also performed for lower levels O_2 concentration (~150-200 µM) for the hypoxia experiments.

With O_2 concentration already within the 700-900 µM (or at air concentration for hypoxia experiments), slices were placed in the chamber on the slice-holder using a brush, followed by reoxygenation and closing of the chambers. Reoxygenation was carried out whenever the O_2 concentration in the medium reached values of approximately 700 µM (or 150 µM in hypoxia experiments). For each experiment 3 (rat; 250 µm thick) or 4 (mouse; 400 µm thick) slices were used, with an average wet weight of tissue of 5–10 mg. This amount of tissue allowed for an ideal basal O_2 flux (Pesta and Gnaiger 2012), as a higher or lower amount of tissue results in rapid depletion of O_2 in the medium or loss of resolution, respectively. The O_2 flux was normalized between experiments by determination of the wet weight of the slices used in each individual recording. Slices were gently transferred into a pre-weighed slice holder and excess media was dried by gently tapping the holder on tissue paper.

Evaluation of respiratory states: a SUIT protocol was used, in which substrates, inhibitors and uncouplers were added to the recording chamber in the following order: carboxyatractyloside (12.5 µM) and oligomycin (20 µg mL^{-1}) for Leak, FCCP (20 µM, titration) for ET capacity (maximum respiration), rotenone (2.2 µM), succinate (11 mM), antimycin A (12.5 µM) and azide (20 mM) for ROX. Each addition was only performed after the signal had been stable for at least 5 min. When appropriate, nitrite ($NaNO_2$) was added to the chamber at a 10 or 100 µM concentration before placing the slices.

Evaluation of the effect of different substrates: substrate composition of the medium varied according to the experiments: 0.1, 0.5, 10 or 15 mM glucose, or 10 mM lactate. Lactate (15 mM) was added to the chamber when slices were in 0.5 or 15 mM glucose. Inhibition of glial oxidative metabolism was achieved by adding 100 µM of FC to the recording chamber for a minimum period of 1.5 h. Inhibition of monocarboxylate transport into neurons was achieved by adding 4-CIN (200 µM) into the recording chamber for a minimum of 20 min. The time-dependent inhibition of O_2 flux in the presence of FC and 4-CIN and stabilization after 1.5 h and 20 min, respectively, is shown in **Fig. 4.2**. Then, slices were stimulated with either glutamate (5 mM) or KCl (60 mM).

Oxygen and glucose deprivation (OGD): this was performed in the O2k chamber, having respirometry aCSF without glucose and at low O_2 concentration (< 10 µM), which was achieved with nitrogen (N_2), and by placing the slices afterwards – **Fig. 5.2A**. Slices were in OGD for varying times (5, 10, 15, and 30 min) following which glucose (10 mM) was added to the chamber and O_2 was increased to ~800 µM with carbogen (reperfusion), at which time the chamber was

closed. Measurements were carried out at a higher frequency (5 Hz) as opposed to the normally used (0.5 Hz) to allow for higher time resolution. The signal was smoothed (150 points average) for analysis, since the O_2 flux noise was dramatically increased due to the higher acquisition frequency. The control (0'OGD) consisted of placing the slices in the chamber at low O_2 but immediately increasing the O_2 concentration. The controls with complex I, complex III, and complex IV inhibition were achieved by ensuring that inhibition was complete (decrease in O_2 flux until stable) and only then OGD was performed. Inhibition of complex I or complex IV was carried out with 2.2 µM rotenone (Rot) and 0.2 M azide (Azd), respectively. Analysis of O_2 flux after OGD and reperfusion was performed at 6 and 15 min after the start of reoxygenation (median of a 15 s portion). When ~40 min had passed after OGD and reperfusion, signal acquisition frequency was changed to 0.5 Hz, BSA was added to the chamber (5 mg/mL) and measurements of Routine (R), ET capacity (E) and ROX were carried out. For nitrite effect on O_2 consumption after OGD and reperfusion, nitrite ($NaNO_2$) at either 10 or 50 µM was added before placing the slices, which were then in OGD for 15 min. Myoglobin (150 µM) was added to the chamber before slices. Due to its labile nature, C-PTIO (1 mM) was added immediately before adding glucose and reoxygenation.

2.10.1.3. Permeabilized hippocampal slices

In experiments with permeabilized hippocampal slice pieces, three slices were weighted and placed in ice-cold modified aCSF and cut into small pieces (~ 1 mm^2). The pieces were then transferred to ice-cold MiR05 and after 1 min, washed twice in MiR05. The pieces were then transferred to the O2k chamber that contained MiR05 at 32ºC and air O_2 concentration (~180 µM). Saponin permeabilization was first tested as previously described (Herbst and Holloway 2015). Pyruvate (5 mM), malate (2mM), glutamate (10 mM) and ADP (2.5 mM) were added to the chamber. Then, saponin was added in increments of 10 mg mL^{-1} first and then of 5 mg mL^{-1}. After O_2 flux stopped increasing, cytochrome *c* (10 µM) was added to evaluate permeabilization of mitochondrial membranes. For experiments, 20 mg mL^{-1} of saponin was added after placing the slices in the chamber containing MiR05, followed by pyruvate, malate, and glutamate (PMG) and ADP, to obtain complex I linked respiration. After a stable O_2 flux was obtained, O_2 concentration was decreased with N_2 and anoxia (considered as O_2 concentration below 10 µM) was maintained for 15 min. Then, reoxygenation was carried out by opening the chamber until the same level of concentration before anoxia was reached. For control, O_2 concentration was maintained at ~180-220 µM. Nitrite (10 or 100 µM) was added right before decreasing O_2 concentration for anoxia. The effect of dietary nitrate was evaluated in rats that received nitrate

in their drinking water and experiments were carried out the same way, except no nitrite was added in this case.

2.11. Propidium iodide staining

Hippocampal slices were incubated in 3 μM propidium iodide for 30 min (in a pre-incubation chamber with oxygenated aCSF). The slices were transferred to fresh aCSF to a 48-well plate, and PI fluorescence was observed using the 5x objective of a Zeiss P.A.L.M. Laser Dissecting Microscope (Germany) using a red filter (558 nm excitation and 583 nm emission). Images were acquired with an AxioCam HR camera coupled with Axiovision software (version 3.1). Densitometric analysis of fluorescence of regions of interest (ROI) was performed using ImageJ. Each ROI had 445.62 × 531.47 microns and areas with low cell bodies density were selected. Before quantification, the background was normalized using subtract background filter (rolling ball radius 50px, 8-bit images). The percentage of PI-stained areas was determined from the binary image.

2.12. Lactate measurements in hippocampal slices

Electrochemical recordings of lactate in hippocampal slices were carried out by amperometry at +0.7 V vs. Ag/AgCl with CFM/Pt-LOx-PU-PD microbiosensors. The slices were immobilized in an immersion recording chamber (BSC-BU with BSC-ZT top, Harvard Apparatus Ltd., UK), perfused with aCSF continuously bubbled with humidified carbogen at 32ºC and at a flow rate of 2 mL min^{-1} – **Fig. 2.4**. All experiments were performed with both the lactate sensor (CFM/Pt-LOx-PU-PD) and a sentinel sensor (CFM/Pt-Null-PU-PD) to ensure that the changes in current were due exclusively to changes in lactate concentration and not due to other electroactive species. The lactate microbiosensor was placed in the pyramidal cell layer of the CA1 subregion at a depth of 150-200 μm with the sentinel sensor in close proximity (ca. 100 μm tip-to-tip distance). All experiments were carried out in either 0.5 or 15 mM glucose aCSF, except for those where the glucose concentration was varied within the interval of 0 to 15 mM glucose. After stabilization of the background current, the composition of the perfusion medium was changed. The lactate concentration in perfusion was increased by changing the perfusion to aCSF containing successively higher concentrations of lactate (final concentrations in the 0.2-15 mM range). For stimulation, the perfusion was changed to aCSF supplemented with 5 mM glutamate or 60 mM KCl for 5 min, and then changed back to only aCSF. For inhibition of monocarboxylate transport into neurons, the perfusion was changed to aCSF supplemented with 20 nM AR-C155858 for 30

min, followed by stimulation with KCl in the presence of this inhibitor. In these experiments AR-C155858 was used instead of 4-CIN due to 4-CIN being electroactive and greatly detected by the sensors at the concentration used (200 µM).

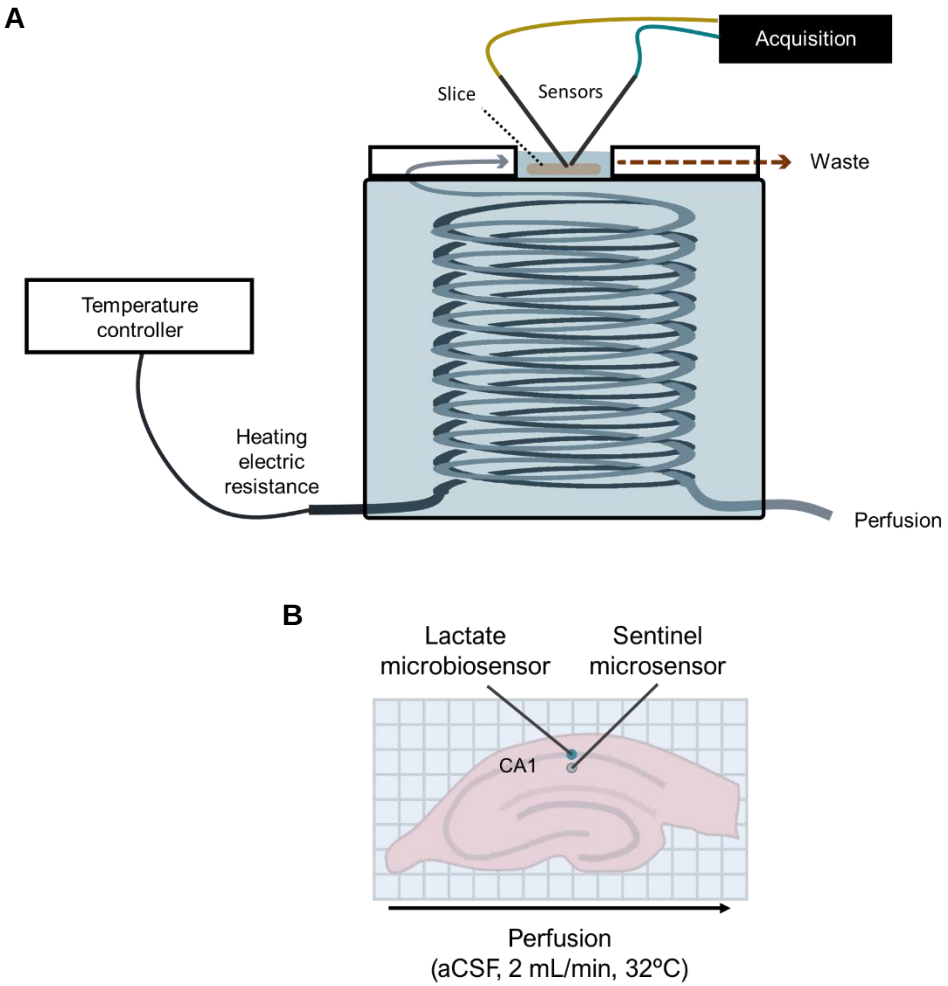

Fig. 2.4 – (A) Representation of perfusion system used in lactate measurements in hippocampal slices. (B) Hippocampal slice in perfusion (aCSF) with local of insertion for both the lactate and sentinel microsensors in the CA1 sub-region.

2.13. Evaluation of H_2O_2 sensitivity with biofouling

Brain homogenates were prepared by homogenizing brain tissue with an ice-cold glass/Teflon potter with 3 strokes. The sensors (CFM/Pt-Null-PU) were placed in homogenates for 2h at room temperature. The H_2O_2 sensitivity was determined in PBS at 32ºC both before and after placing the sensor in the homogenate. The sensors were then washed in 1% Triton X-100 in PBS under vigorous stirring for 20 min, at room temperature. The H_2O_2 sensitivity was again determined.

2.14. Calculation of flux control ratios

The mass-specific O_2 fluxes (expressed in pmol s^{-1} mg^{-1} tissue wet weight, as defined in (Gnaiger 1993)) can be normalized for a reference state, such as the maximum rate or electron transfer (ET) capacity obtained with FCCP, to determine what have been designated as flux control ratios (FCR). Values for FCR with ET capacity as the reference state (FCR per ET capacity) are independent of mitochondrial content and cell size and are theoretically limited between 0.0 and 1.0. The FCRs were calculated as described by Gnaiger (Gnaiger 2008), using ET capacity as the reference for normalization, as follows:

ET capacity (E) = maximum flux – residual flux (ROX)

Routine control ratio = (basal flux – residual flux) / E

Leak control ratio = (leak flux – residual flux) / E

*net*Routine = (Routine c r. – Leak c. r.) / E

Residual = ROX / maximum flux

2.15. Data analysis

For the respirometry experiments, data acquisition and analysis were performed using DatLab software v. 5.1.1.9 or v. 7.4.0.4 (Oroboros Instruments, Innsbruck, Austria). Data is presented as O_2 flux (pmol s^{-1} mg_{wt}^{-1}), which corresponds to the O_2 consumption rate normalized for the wet tissue (wt) weight determined for each individual experiment. A portion of the recording at timepoints of interest was selected when respiration was stable for at least 5 min and their median was used, except for the analyses of the response to stimulation. In these cases, a portion of the signal with the maximal O_2 flux was selected and the median was used. This means that respiration was evaluated around 1-3 min after stimulation started. Flux control ratios (FCR; 0-1) are normalized O_2 fluxes for the maximal level (FCR per ET capacity) or for the basal level with only glucose in the medium (FCR per glucose; O_2 flux / glucose O_2 flux).
OriginLab 2016 (OriginLab Corporation, Northampton, MA, USA) was used for determination of $\Delta t_{50\%-90\%}$. It was also used for smoothing (150 ppts average) of the O_2 flux signal after OGD and reperfusion and for analysis of the signal at discreet time points (median of a 15s segment at

6, 7, 8, 9, 10, 12.5, 15, 17.5, and 20 min after starting reoxygenation). The response curve of lactate microbiosensors as a function of temperature was calculated as the ratio between the recorded current and the maximum recorded current for the same electrode (I / I_{max}) and then fitted by interpolation using the cubic b-spline function and the maximum of the resulting curve was determined.

GraphPad Prism 5.0 (GraphPad Software, Inc.) was used for kinetic analysis of the microbiosensors. The data from each individual curve was fitted to a Michaelis-Menten type equation, allowing the determination of the apparent Michaelis constant ($K_{M,app}$) for lactate and the maximum steady-state current response (I_{max}). The individual fit of the curve $[glucose]_{aCSF}$ vs $[lactate]_{ECS}$ for each replicate was done using the specific binding with Hill slope equation and the results were included when the R^2 of the fit was >0.990.

The lactate sensitivity was determined by linear regression in the range between 0.15 and 0.6 mM. The limit of detection (LOD) for lactate was calculated according to the following expression:

$$3 \times SD_{baseline}/m$$

where $SD_{baseline}$ represents the standard deviation of the baseline and m the slope of the calibration curve. The ascorbate and H_2O_2 sensitivities were determined by measuring the current in response to 100 and 40 µM, respectively. The selectivity against ascorbate was determined as the ratio of sensitivities towards lactate and ascorbate. The analytical parameters of the microbiosensors after use in slices were defined as a percentage of the values for the same sensor before insertion in slices, except for ascorbate sensitivity (some of the pre-calibration values were 0). The H_2O_2 sensitivity after biofouling in brain homogenate was also defined as a percentage of the value for the same sensor before placing it in the homogenate.

2.16. Statistical analysis

Statistical analysis was performed using GraphPad Prism 5.0 (GraphPad Software, Inc.). All data is expressed as mean ± S.E.M., unless stated otherwise. In all cases, normality of data was determined. Statistical significance of differences between two parameters was evaluated by one or two-tailed paired t-test (or Wilcoxon test in the case of a non-normal distribution). Evaluation of comparison between multiple parameters was performed with one-way ANOVA with Holm-Sidak's multiple comparisons test or Kruskall-Wallis test with Dunn's multiple comparisons test. two-way ANOVA and Sidak post-test with correction for multiple comparisons or three-way

ANOVA and Bonferroni post-test with correction for multiple comparisons. Results for two-way ANOVA analysis are presented as $F_{(DFn, DFd)}$ and *P* value.

3. Novel Bioanalytical Tools to Study Bioenergetic Metabolism in Hippocampal Slices

Part of the work presented in this chapter was published in:

Dias C, Lourenço CF, Barbosa RM, Laranjinha J, Ledo A. Analysis of respiratory capacity in brain tissue preparations: high-resolution respirometry for intact hippocampal slices. Anal Biochem. 2018;551:43-50. doi:10.1016/j.ab.2018.05.010

Dias C, Lourenco CF, Ferreiro E, Barbosa RM, Laranjinha J, Ledo A. Age-dependent changes in the glutamate-nitric oxide pathway in the hippocampus of the triple transgenic model of Alzheimer's disease: implications for neurometabolic regulation. Neurobiol Aging. 2016;46:84-95. doi:10.1016/j.neurobiolaging.2016.06.012

Dias C, Fernandes E, Barbosa RM, Ledo A. Monitoring Extracellular Lactate in Hippocampal Brain Slices with Oxidase-Based Microbiosensors. Bioelectrochem. Submitted

3.1. Introduction

The brain is an organ with high index of metabolic activity and although it comprises only 2% of the human body mass, its O_2 and glucose requirements amount to 20% and 25% of the total body consumption, respectively (Magistretti et al. 1999). This high energy demand results mainly from the maintenance and restoration of ion gradients, generation of action potentials and neurotransmitter uptake (Attwell and Laughlin 2001). As such, the brain is particularly susceptible to alterations in energy metabolism and multiple cerebral disorders have been related to deficits in energy metabolism (Camandola and Mattson 2017; Watts et al. 2018; Cabral-Costa and Kowaltowski 2020). Thus, the development of novel methodologies to study brain energy metabolism is needed to better understand its intricate mechanisms and how they are affected in pathological conditions.

Mitochondrial oxidative phosphorylation, being a major source of ATP, is an important part of brain energy metabolism and mitochondrial bioenergetics and is particularly affected in several pathologies (Cabral-Costa and Kowaltowski 2020). One widely used method for the evaluation of oxidative metabolism is through determination of respiratory states in biological samples. This is done by observing changes in respiratory rates resulting from different respiratory states, which are achieved by increasing or inhibiting the activity of the different complexes of the ETS. Using a closed chamber, the measurement of O_2 consumption rates can be accomplished with the use of O_2 electrodes. The Oxygraph-2k system comprises two separate amperometric O_2 sensors and allows the measurement of O_2 concentration with high resolution and accuracy, overcoming putative limitations associated with classical Clark-type electrodes (Gnaiger et al., 1995; Gnaiger, 2001; Hütter et al., 2006). This higher resolution derives from the design and materials used, allowing for smaller amounts of sample to be used, which increases time resolution (Gnaiger 2008).

Establishing respiratory states requires the access of substrates and drugs to the complexes of the mitochondrial ETS, leading most researchers to use isolated mitochondria in their studies (Cardoso et al. 2010; Aidt et al. 2013; Jørgensen et al. 2015; Mottahedin et al. 2017). However, the study of mitochondrial respiration in discrete structures of the rodent brain, such as the hippocampus, has been hindered by the impossibility of isolating adequate amounts of mitochondria to perform classical bioenergetics studies. The use of whole tissue preparations coupled to high-resolution respirometry affords a powerful tool to study mitochondrial respiration and metabolic fluxes in the brain tissue, because only a small amount of tissue (5–10 mg) is required (Pesta and Gnaiger 2012). Furthermore, this approach allows the maintenance of cytoarchitecture, inter-cellular communication and connectivity (Lein et al. 2011). An additional

advantage of using whole tissue preparations is that it avoids the loss of the physiological environment that occurs during isolation of mitochondria, under which both mitochondrial morphology and function are altered (Picard et al. 2011). Mitochondria are extremely dynamic organelles and multiple mechanisms allow the maintenance of their homeostasis and function, including fission, fusion and movement through the cytoskeleton, among others (Ni et al. 2015). Comparative studies using isolated mitochondria and permeabilized tissue have produced disperse results. When studying the effects of muscle aging, measurements carried out in isolated mitochondria revealed a higher degree of compromise then measurements in permeabilized tissue (Picard et al. 2010). Although permeabilized cells or tissue may be a better option as compared to isolated mitochondria, mitochondria are still exposed to a non-physiological environment, due to the loss of cytoplasmic milieu. The issues that arise from isolation or permeabilization can be overcome by using intact cells (Dubinsky 2009; Brand and Nicholls 2011). While maintaining mitochondria in a physiological environment, the use of intact cells presents other limitations, such as access of substrates and drugs to mitochondria, and the lack of intercellular interaction remains an issue of concern.

The use of intact tissue, while challenging, is advantageous in the sense that cell-to-cell interactions are preserved. Hippocampal slices have been used in measurements of O_2 consumption before using either microelectrodes inserted in the tissue or a system based on fluorescence detection (Kudin et al. 1999; Kunz et al. 1999; Ledo et al. 2005, 2010; Schuh et al. 2011; Ivanov et al. 2014). Here, we present a method that allows the study of intact tissue brain bioenergetics using this system for high-resolution respirometry.

The role of lactate in brain metabolism has received much attention in the last years. While glucose is the primary brain substrate in physiological conditions, lactate can also act as an energy substrate, particularly in conditions of increased energy demand (Magistretti and Allaman 2018; Barros and Weber 2018). Although mounting evidence seems to support the existence of an astrocyte-to-neuron lactate shuttle, further clarifying the role of lactate in brain metabolism is required. As such the development of tools for direct and real time measurement of lactate concentration dynamics in the brain extracellular space is of great interest. Importantly, as the brain is highly dynamic, these tools should have high spatial and temporal resolution.

In the rodent brain, the extracellular concentration of lactate *in vivo* is reported to range between 1-3 mM (Harada et al. 1993; Abi-Saab et al. 2002; Yager et al. 2002; Dong et al. 2003; Zilberter et al. 2010). The use of microelectrodes coupled to electrochemical techniques represents an interesting option for measurements of lactate concentration dynamics, as they provide high sensitivity and spatial resolution, with minimal interference and damage to the brain (Barros et al. 2018). Carbon fiber microelectrodes are particularly attractive, due to their small size (fibers can go down to 5 μm in diameter), low cost, ease of fabrication and potential for customization.

The detection of non-electroactive species, such as lactate, can be achieved using microbiosensors based on microelectrodes with an appropriate enzyme immobilized at their surface. This methodology usually involves the use of oxidase enzymes that produce H_2O_2, an electroactive substance (Weltin et al. 2016). Hydrogen peroxide acts as a reporter molecule and its electrochemical detection is optimal at electrodes comprised of platinum or platinum alloys. Carbon fiber microelectrodes can also be used in these microbiosensors by modifying their surface with deposition of platinum, representing an inexpensive solution. Additionally, these microbiosensors can provide the opportunity of reducing the size compared to conventional platinum electrodes (Meyerhoff et al. 1999; Lourenço et al. 2019).

Rodent brain slices are widely used to study neurophysiology since they allow for a better control of the extracellular milieu compared to *in vivo*, facilitating changes in medium composition for drug delivery and substrate composition alteration, for example, and by removing the interferences from blood perfusion and anesthesia. As such, brain slices have been widely used in brain metabolism studies (Hertz 2012).

The goal of this chapter was to design novel bioanalytical tools to study brain energy metabolism in whole brain tissue, namely the hippocampal slice. These tools provide a mean of determining whole tissue O_2 consumption to evaluate oxidative metabolism, and also to determine lactate dynamics in the tissue. To this purpose, the Oroboros O2k system was adapted to be used with whole tissue, by designing and manufacturing a sample holder fitting this system. This holder was tested for possible interferences with measurements and then used to measure O_2 consumption at different respiratory states in hippocampal slices from two rodent species. Finally, the use of this method was further validated by evaluating the same respiratory states in hippocampal slices from an Alzheimer's disease model and its evolution with age.

Additionally, lactate microbiosensors were designed and optimized for monitoring extracellular lactate concentration dynamics in brain slices. Their analytical performance was evaluated *in vitro*¸ including sensitivity, selectivity, and operational stability for monitoring changes in lactate concentration in the extracellular space in hippocampal slices. The microbiosensors were further tested by evaluating changes in lactate dynamics evoked by stimulation with glutamate and investigating the dependency of these lactate dynamics in response to glucose supply.

3.2. Results

3.2.1. Adaptation of high-resolution respirometry for intact tissue

The purpose of this work was to establish a protocol for the evaluation of different respiratory states in whole brain tissue preparation, specifically intact hippocampal slices, using high-resolution respirometry. At the time, only one protocol was available in the literature, in which authors placed slices into the recording chamber (Kudin et al. 1999). We found that under such conditions, the brain tissue became fragmented due to stirring and by the end of the experiment, a homogenate rather than brain tissue was present in the recording chamber. In order to maintain tissue integrity throughout the time span of the recording, we designed a sample holder that was placed in a fixed position in the recording chamber (**Fig. 2.1**). To validate its suitability, we evaluated the putative interference introduced by the sample holder on measurements.

3.2.1.1. Evaluation of sample holder interferences on measurements

One possible source of interference introduced by the sample holder is decreased/delayed vertical mixing, thereby impacting medium homogenization in the chamber. The O_2 sensor is located at the bottom part of the chamber next to the stirring bar and placing the sample holder in the middle of the chamber (**Fig. 2.1B**) could create 2 sub-chambers, above and below the holder mesh, with different O_2 concentrations, which would influence the accuracy of real-time measurements. As such, the effect of the holder on vertical mixing was evaluated in two tests. First, a known amount of dithionite, which reduces O_2, was added to the chamber in the presence or absence of the holder whilst recording O_2 concentration. As can be appreciated in **Fig. 3.1A**, the rate and amplitude of the decrease in O_2 concentration measured was unaffected by the presence of the holder. When the holder was present, after the O_2 concentration decreased to a minimum, it started increasing gradually until it reached a plateau that was close to the plateau level obtained without the holder. This is probably due to the materials used in the holder, which can adsorb O_2 and then release it slowly to the medium.

We next evaluated the effect of the sample holder on vertical mixing by performing an open chamber stirrer test which consists in stopping stirring for a defined period of time (as allowed by the equipment software) and restarting stirring automatically, while maintaining a constant O_2 supply (open chamber). This is a highly reproducible process, as it is automatically controlled by the software. The representative traces in **Fig. 3.1B** show that the profile of change of O_2 concentration produced by transiently stopping stirring is similar in the absence and presence of the holder. When stirring is turned off, convective mixing of O_2 ceases, and only diffusive mixing

is present, thus resulting in a decrease in the O_2 concentration measured at the sensor location. When stirring is turned back on, the O_2 reaching the vicinity of the sensor is no longer dependent on diffusion only and concentration increases. The time taken for the measured O_2 concentration to increase after restarting stirring can be affected by how long it takes for the medium in the chamber to become completely homogeneous. When we analyzed how long it took the O_2 concentration to increase from 50% to 90% ($\Delta t_{50\%-90\%}$) of the maximum concentration obtained after the stirring was back on (**Fig. 3.1C**), no difference was observed between the two conditions tested (N = 6, *P* = 0.6901). These results confirm that vertical mixing and O_2 diffusion in the chamber are not affected by the presence of the holder.

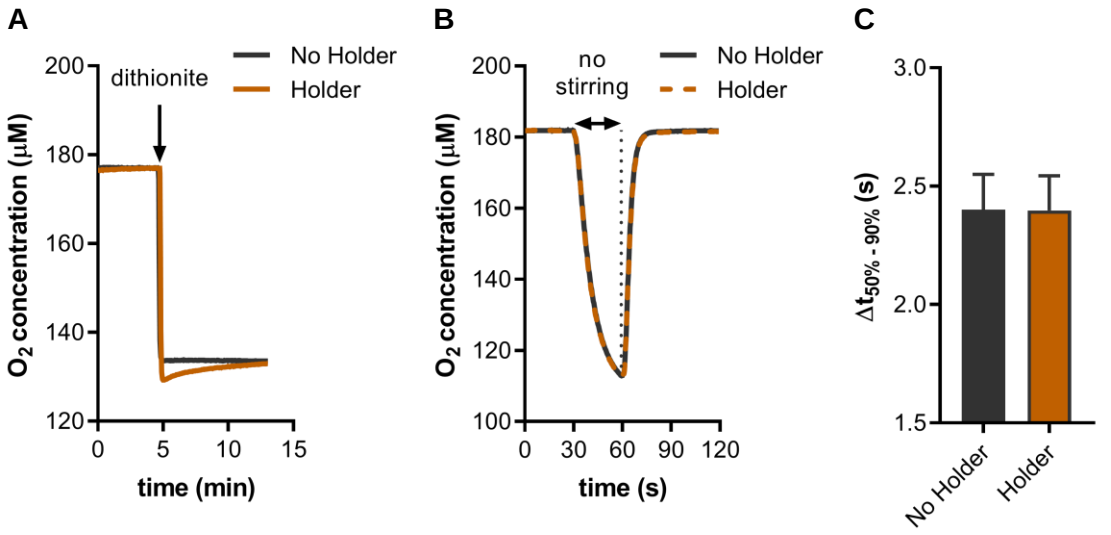

Fig. 3.1 – Evaluation of vertical mixing in the chamber in the presence of the sample holder. (A) Response to dithionite injection in the presence (orange) and absence of the holder (grey). (B) Stirrer test (stirring stopped for 30s and restarted) in the presence and absence of the holder. (C) Variation of oxygen kinetics during the stirrer test (time for the signal to go from 50% to 90% when stirring was turned back on – $\Delta t_{50\%-90\%}$**, s**). Values represent mean ± S.E.M.

Having determined that the sample holder did not affect vertical mixing in the recording chamber, we tested whether it interfered with measurements of O_2 flux in biological samples (**Fig. 3.2**). For that we performed a standard SUIT experiment using brain homogenate with or without the holder present in the recording chamber. The homogenate allowed us to have the exact same conditions in both chambers and to simultaneously run the experiment with or without the holder. Several respiratory states were evaluated, and as shown in **Fig. 3.2A** the O_2 flux traces obtained under the two conditions are superimposed. The only difference observed occurred during reoxygenation of the chamber. As can be appreciated in **Fig. 3.2B**, reoxygenation was slower in the presence of

the holder. Reoxygenation is achieved by pushing back the stopper that seals the solution in the recording chamber and allowing an air bubble to form at the surface of the medium. The exchange of O_2 between air bubble and medium depends on the contact area between the two, with a larger area resulting in faster exchange. With the holder in the chamber, the contact area was visibly smaller as compared to when the holder was not present, as depicted in **Fig. 3.3**, resulting in a longer oxygenation time. Thus, we can conclude that the holder does not affect closed chamber measurements but does lead to longer oxygenation time, which has no major impact in experiments.

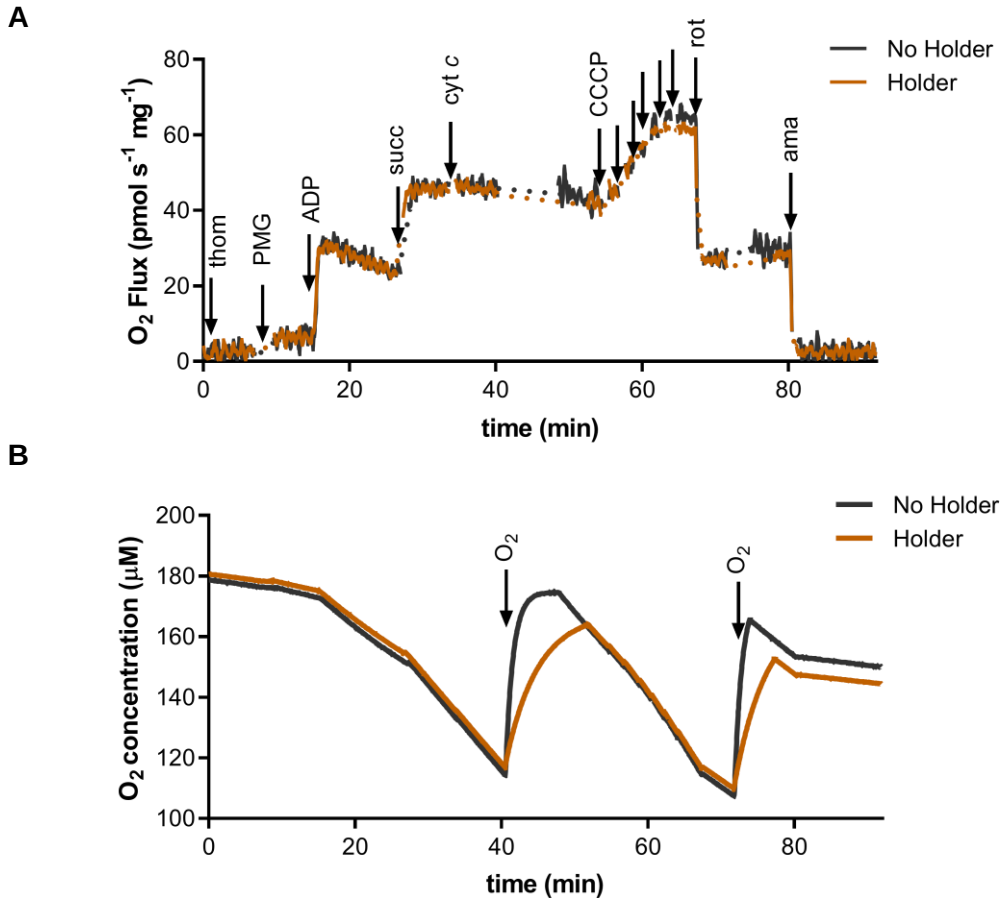

Fig. 3.2 – Evaluation of sample holder effects on O_2/ O_2 flux measurements with biological sample (tissue homogenate) during a typical experiment. One chamber contained only the sample (dark grey), while the other contained both the sample and the holder (orange). (A) O_2 flux (pmol s^{-1} mg^{-1}) measurements. (B) O_2 concentration (µM) recording. The arrows indicate the moment of addition of sample/drug/substrate: tissue homogenate (thom); pyruvate + malate + glutamate (PMG); ADP; succinate (succ); cytochrome *c* (cyt *c*); CCCP (added stepwise); rotenone (rot); antimycin A (ama).

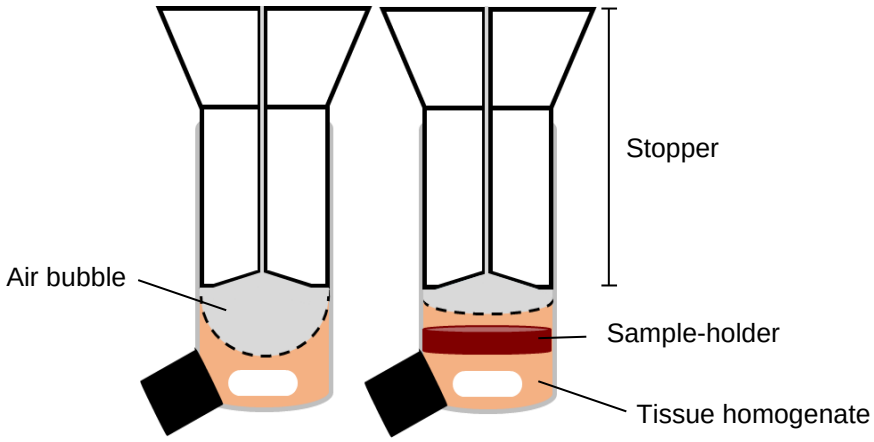

Fig. 3.3 – Schematic representation of oxygenation of the O2k chamber in the presence and absence of the sample holder (in red). Oxygenation is carried out by opening the chamber by setting the stopper higher and allowing an air bubble to enter. The contact area between the air bubble and the medium (dashed lines) is affected by the holder.

3.2.1.2. Evaluation of mitochondrial respiration in intact hippocampal slices using high-resolution respirometry

We proceeded to optimize a SUIT protocol for the evaluation of different respiratory states in intact hippocampal slices using high-resolution respirometry. Both mouse and rat hippocampal slices were tested under conditions of high O_2 concentration to maximize tissue viability at 32 °C (Erecińska and Silver 2001; Ledo et al. 2005). As shown in **Fig. 3.4**, we successfully implemented a SUIT protocol, from which key respirometric parameters were determined in order to compare metabolic parameters between hippocampal slices obtained from rats and mice. Using this protocol, we determined Routine respiration, Leak respiration, ET capacity and non-ETS O_2 consumption. We compared parameters from hippocampal slices from rat and mouse and normalized the O_2 fluxes obtained for maximum respiration (FCR per ET capacity).

Routine respiration

Routine respiration rate is the basal tissue O_2 flux supported by an exogenously supplied endogenous substrate – in this case, glucose and pyruvate. High concentrations of glucose (10 mM) were used to keep a constant source of substrates and allow adequate supply to the whole slice. In order to guarantee that the rate of glycolysis did not limit the O_2 flux, pyruvate, a substrate of the TCA cycle, was added to the medium. As observed in the initial 20 min segment of **Fig. 3.4A**, a stable O_2 flux was obtained under these conditions. As shown in **Fig. 3.4B**, the average Routine O_2 flux was determined to be 12.4 ± 1.2 and 8.3 ± 1.1 pmol s^{-1} mg_{wt}^{-1} for rat and mouse

hippocampal slices, respectively. Although not statistically different, mouse slices appeared to have lower basal respiration.

Leak respiration

During oxidative phosphorylation, proton leak across the inner mitochondrial membrane occurs, resulting in partial uncoupling between substrate oxidation and ATP synthesis. The extent of this leak can be determined by measuring O_2 flux under conditions of inhibited ATP synthesis

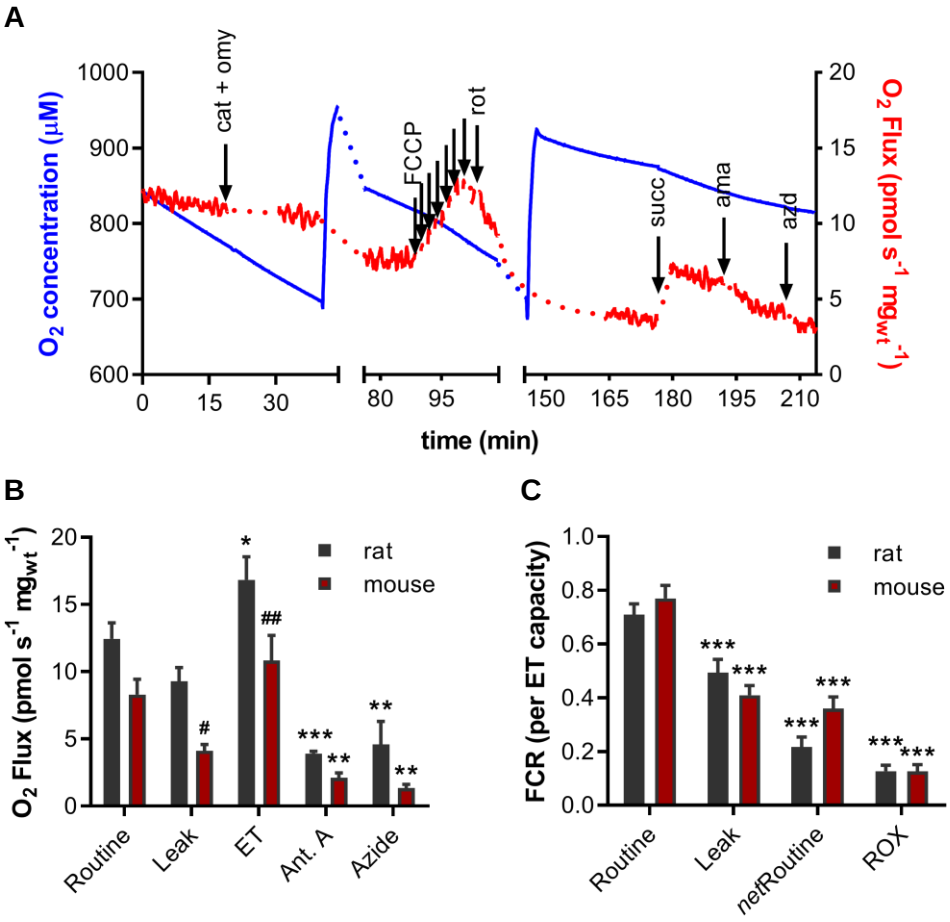

Fig. 3.4 – Evaluation of mitochondrial respiration in hippocampal slices from two rodent species (*Rattus norvegicus* and *Mus musculus*). (A) Representative oxygraphic trace: O_2 concentration (blue line; µM) and O_2 flux (red line; pmol s^{-1} mg_{wt}^{-1}); the arrows indicate the moment of addition of each drug/substrate: carboxyatractyloside (cat) and oligomycin (omy), FCCP (added stepwise), rotenone (rot), succinate (succ), antimycin A (ama), and azide (azd). (B) Average O_2 flux values at different respiratory states (Routine, Leak, ET capacity, and ROX – Ant. A + Azide) determined for mouse and rat hippocampal slices. (C) Flux control ratios (normalization to ET capacity) for hippocampal slices from mouse and rat. *P < 0.05, **P < 0.01, ***P < 0.001 for comparison to basal in (B) and to Routine in (C); $^{\#}$P < 0.05, $^{\#\#}$P < 0.01 for comparison between rodent species.

(Divakaruni and Brand 2011). We determined the level of Leak respiration by adding oligomycin, an ATP synthase inhibitor, and carboxyatractyloside (cat), an ANT inhibitor. As shown in **Fig. 3.4A**, this produced a slow decrease in O_2 flux to 9.3 ± 1.0 and 4.1 ± 0.5 pmol s^{-1} mg_{wt}^{-1} for rat and mouse hippocampal slices, respectively (**Fig. 3.4B**). Although this decrease from Routine respiration was not statistically significant for neither rat nor mouse, we found that Leak was significantly lower in slices obtained from mouse when compared to rat ($F_{(1,87)}$ = 22.01, P < 0.0001).

ET capacity

The maximal respiratory or ET capacity can be determined by completely uncoupling O_2 consumption from ATP synthesis. Exogenous uncouplers such as FCCP dissipate the proton gradient across the inner mitochondrial membrane (Terada 1990), dissociating electron transfer from the proton gradient, which is normally used by ATP synthase. To determine ET capacity, FCCP was added in a stepwise fashion (titration) until no further effect was observed (**Fig. 3.4A**). The maximal O_2 flux was 16.8 ± 1.7 and 10.8 ± 1.9 pmol s^{-1} mg_{wt}^{-1} for hippocampal slices obtained from rat and mouse, respectively (**Fig. 3.4B**). This increase from basal respiration was significant for rat ($F_{(4, 87)}$ = 24.51, P < 0.0001) but not mouse. Furthermore, the ET capacity was significantly lower in mouse when compared to rat ($F_{(1,87)}$ = 22.01, P < 0.0001).

Residual oxygen consumption - ROX

When evaluating O_2 consumption in cells or tissues, it is important to consider the occurrence of cellular reactions that consume O_2 independently of the mitochondrial ETS. Thus, to evaluate the level of ROX, i.e., non-ETS O_2 consumption, we determined O_2 flux under conditions of total inhibition of the ETS by adding antimycin A (ama) and azide (azd), inhibitors of complexes III and IV, respectively. As can be observed in **Fig. 3.4A** and **B**, this caused O_2 flux to decrease to levels close to zero. When compared to Routine respiration, ROX O_2 flux was significantly lower for both rat and mouse ($F_{(4, 87)}$ = 24.51, P < 0.0001). No difference was observed between the 2 species.

Flux control ratios

When O_2 fluxes are normalized for maximum flux (ET capacity), flux control ratios (FCR) are determined, which are independent of mitochondrial content and cell size and are theoretically limited between 0.0 and 1.0 (Gnaiger 2008). The Routine control ratio corresponds to normalized Routine respiration and is an indication of how close basal respiration is to ET capacity (Pesta and Gnaiger 2012). As shown in **Fig. 3.4C**, the Routine control ratio was found to be relatively

high for hippocampal slices obtained from both rat and mouse. The Leak control ratio, which reflects the level of uncoupled respiration, was found to be significantly decreased relative to Routine for hippocampal slices from both rat and mouse. The *net*Routine control ratio, which is a measure of the fraction of O_2 consumption that is coupled to ATP synthesis, was significantly lower than Routine control ratio. Finally, residual respiration was found to be lower when compared to the other FCR (**Fig. 3.4C**), indicating that only a small fraction of measured O_2 consumption is subverted towards production of ROS or other O_2 consuming reactions in the tissue. Interestingly, contrary to what was observed for the O_2 flux values (**Fig. 3.4B**), no inter-species difference was observed for the FCR values ($F_{(1, 90)} = 0.9855$, $P = 0.3235$). However, within each species, the distinct FCR values were found to be significantly different ($F_{(3,90)} = 73.27$, $P < 0.0001$). No significant interaction between the two parameters (species and FCR) was observed ($F_{(3, 90)} = 2.538$, $P = 0.0616$).

For the sake of comparison and validation, in **Table 3.1** we compared the FCR values obtained here to those published by other authors using different cell preparations, all obtained using the Oxygraph-2k system. As observed, Routine, Leak and Residual FCR values in intact slices were higher than those reported for cell preparations, while *net*ROUTINE control ratio values were

Table 3.1 – Comparative table showing values for Electron Transfer (ET) capacity, Flux Control Ratios with ET capacity as reference (FCR per ET capacity) and Residual Oxygen Consumption (ROX) obtained here, using hippocampal slices obtained from rat and mouse (first 2 rows) and values reported by other authors and obtained with different cellular preparations. Values represent mean ± S.D.

	ET capacity	Routine	Leak	*net*Routine	ROX	Ref
Rat hippocampal slices	**17 ± 6**	**0.71 ± 0.16**	**0.49 ± 0.20**	**0.22 ± 0.15**	**0.15 ± 0.11**	-
Mouse hippocampal slices	**11 ± 6**	**0.77 ± 0.15**	**0.41 ± 0.11**	**0.36 ± 0.13**	**0.13 ± 0.07**	-
Rat insulinoma cell line (INS-1 832/13)		0.493 ± 0.014[a]	0.250 ± 0.022[a]	0.239 ± 0.020[a]		(Hals et al. 2015)
Human non-small cell lung carcinoma (H1299)		0.229 ± 0.01	0.034 ± 0.004	0.194 ± 0.004		(Hall et al. 2013)
Transformed human embryonic kidney cells (HEK 293)	14 ± 2	0.31 ± 0.03	0.09 ± 0.00	0.23 ± 0.02	0.01 ± 0.00	(Aguirre et al. 2010)
Mouse parental hematopoietic cells (32D)	81 ± 11	0.39 ± 0.02	0.10 ± 0.02	0.29 ± 0.02	0.03 ± 0.01	(Gnaiger 2008)
Human umbilical vein endothelial cells (HUVEC)	114 ± 18	0.26 ± 0.02	0.13 ± 0.02	0.13 ± 0.00	0.05 ± 0.04	(Hütter et al. 2006)
Human peritoneal mesothelial cells (HPMC)	181 ± 58	0.40 ± 0.09	0.09 ± 0.01	0.31 ± 0.08	0.02 ± 0.01	(Stadlmann et al. 2006)
Human foreskin fibroblasts	111 ± 24	0.34 ± 0.03	0.14 ± 0.02	0.20 ± 0.02	0.07 ± 0.03	(Hütter et al. 2004)

[a] ± S.E.M

similar to those reported for isolated cells. Curiously, the ET capacity determined for hippocampal slices were relatively low when compared to most cell preparations, although similar to those reported for HEK293 cells.

Evaluation of tissue viability

When evaluating mitochondrial respiration in intact tissue samples, it is important to control tissue viability – the presence of cells within the tissue with compromised membrane integrity can distort readings as a result of higher accessibility of substrates and inhibitors to mitochondria. To assess tissue viability, we performed an intra-experimental control by determining the response to succinate added after inhibition of mitochondrial complex I with rotenone (**Fig. 3.4A**). Succinate, a substrate of complex II, does not permeate cellular membranes and therefore, exogenous succinate will stimulate respiration only in cells with compromised membrane integrity (Pesta and Gnaiger 2012). As shown in **Fig. 3.4A**, while rotenone decreased O_2 flux in slices from both rat and mouse, subsequent addition of succinate increased O_2 flux (**Fig. 3.4A**), indicating the existence of a population of cells within the tissue slices with compromised plasmatic membrane integrity. We determined the respirometric viability index (RVI; the ratio between O_2 consumption following addition of succinate subtracted of the level after antimycin A inhibition and maximum flux) and found the average value of 0.21 ± 0.07 and 0.46 ± 0.09 for rat and mouse, respectively. Slices from mouse showed significantly lower tissue viability (expressed as a higher RVI value) when compared to rat ($P < 0.05$). As can be appreciated from the example recording presented in **Fig. 3.4A**, these experiments are timely. We determined cell permeability using propidium iodide (PI) staining to assess whether the maintenance of the tissue for such a long period under such conditions alters cellular viability. Because PI does not cross cell membranes, this DNA stain enters only cells with compromised membrane integrity. As shown in **Fig. 3.5A**, control slices maintained in aCSF in the slice pre-chamber (not used for respirometry experiment) showed a low level of PI staining. Slices collected from the recording chamber after a full experiment revealed a small increase in PI staining. However, this increase is minor when compared to the positive control (permeabilized cells), where the staining is significantly increased throughout the slice. The fluorescence intensity was quantified in two regions of interest (ROI, inset boxed shown in **Fig. 3.5A**) and as shown in **Fig. 3.5B**, there was no significant difference between the level of PI staining in control slices and slices collected from the Oxygraph-2k chamber after a full SUIT experiment. Furthermore, the level of PI staining is significantly lower for slices from experiments when compared to a positive control of permeabilized slices.

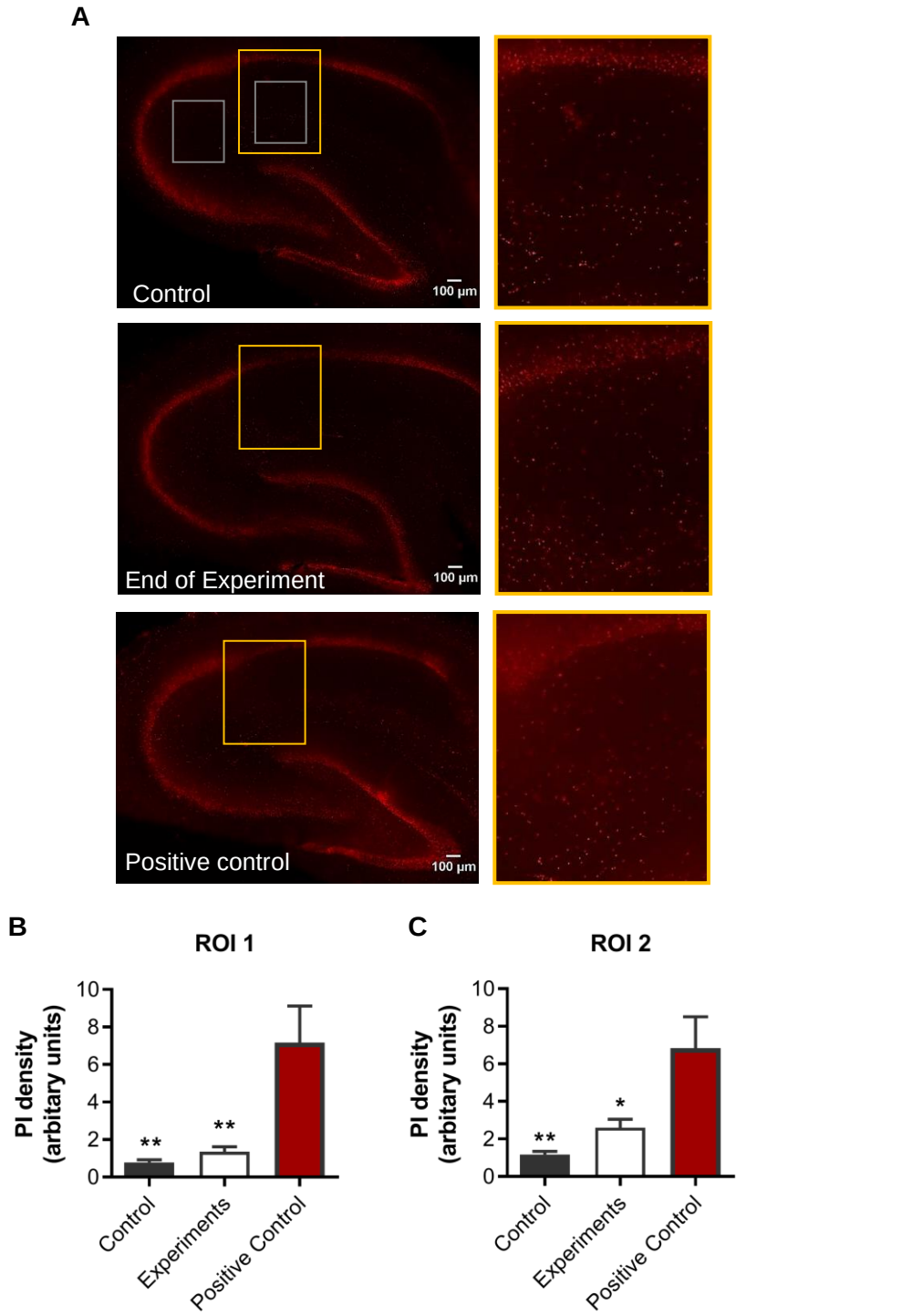

Fig. 3.5 – Propidium iodide (PI) staining of rat hippocampal slices. (A) Microphotographs obtained from hippocampal slices stained with PI under different conditions. Left panel shows full slice image while right panel is a blowup of the region in yellow. (B) Average PI staining intensity quantified from two different regions of interest (ROI1 and ROI2, as indicated in A). Values represent mean ± S.E.M. **P* < 0.05, ***P* < 0.01 for comparison to positive control.

3.2.1.3. *Evaluation of respiratory parameters in a rodent model of Alzheimer's disease*

To further validate this protocol, we evaluated if we could observe differences in respiratory states in the hippocampus of a rodent model of Alzheimer's disease (AD). Alzheimer's disease has been shown to affect mitochondrial respiration (Young-Collier et al. 2012; Swerdlow 2018), but the studies reported this in either isolated mitochondria or homogenates, which can distort results, as already mentioned.

We used the protocol described in 3.2.1.2. to compare respiratory states between slices from the triple transgenic mouse model for Alzheimer's disease (3xTgAD) and nontransgenic mice (NTg). Considering the progressive nature of AD, which is recapitulated in 3xTgAD mice (Oddo et al. 2003), we evaluated O_2 consumption at two ages: young (3-6 mo) and middle-aged (12mo). These age groups were chosen based on a study done by others on our colony of 3xTgAD mice confirming the expected spatiotemporal progression of AD histopathology as initially described (Oddo et al. 2003). At 3 months of age, intraneuronal Aβ immunoreactivity was observed, which progressed to extracellular Aβ plaques at 15 months in both cortex and hippocampal regions of 3xTgAD mice. At 15 months old, there was also hyperphosphorylated tau in the hippocampus (Mota et al. 2014). We determined Routine respiration, ET capacity (maximal respiration), Leak, and ROX (**Fig. 3.6A**) in hippocampal slices obtained from these animals at both age points. Our evaluations showed that Routine O_2 flux (supported by exogenously supplied glucose and pyruvate) and ET O_2 flux (resulting from uncoupled ETS working at maximal speed) were the respiratory states most affected as a function of age in both genotypes, although the tendency was more pronounced for 3xTgAD mice. Determination of the fractional change in O_2 flux from Routine in response to the addition of inhibitors and/or uncouplers (**Fig. 3.6B**) revealed an age-dependent decrease in ET capacity for both genotypes, supporting the observation of lower maximal respiratory capacity. Statistical analysis revealed that age, but not genotype, significantly contributed to the variation observed ($F = 14.29$, $P = 0.0006$). We were not able to perform this analysis in slices obtained from old-aged animals (18 months) due to the fact that basal O_2 flux was too low, and no response was elicited by additions during the SUIT protocol, which highlights the significant compromise of oxidative metabolism in the aged hippocampus. These results emphasize the use and application of the method here described.

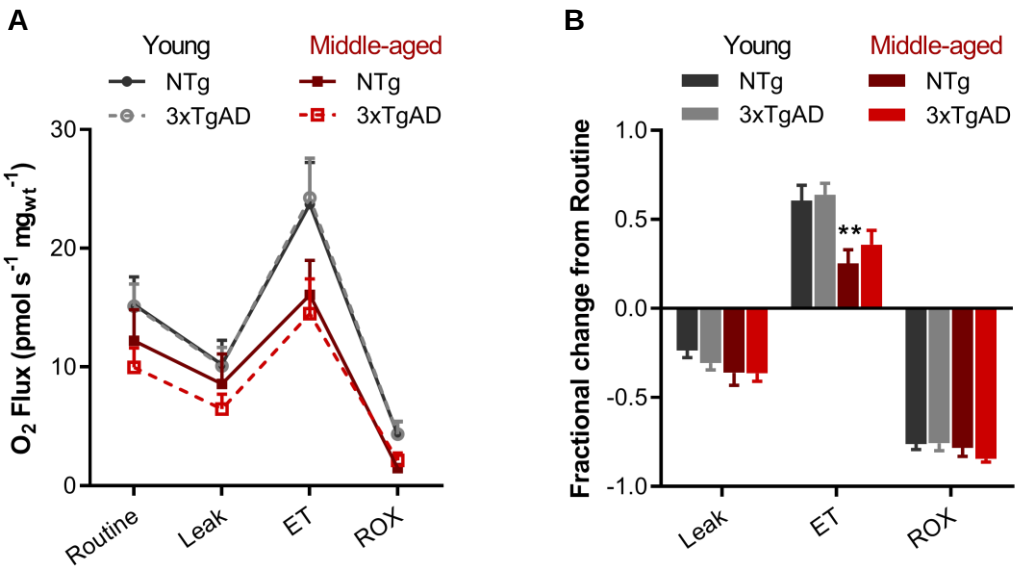

Fig. 3.6 – Evaluation of respiratory states in intact hippocampal slices from young and middle-aged mice using high-resolution respirometry. (A) Average O_2 flux determined at four states, namely Routine, Leak, ET capacity, and ROX. (B) Fractional change from Routine O_2 flux to Leak, ET capacity, and ROX. **P < 0.01 compared to young-aged same genotype.

3.2.2. Oxidase-based microbiosensors for monitoring extracellular lactate in brain tissue

In order to understand the role of lactate in hippocampal energy metabolism, we aimed to measure lactate concentration dynamics in brain tissue. To this purpose, an electrochemical lactate microbiosensor was designed based on immobilization of lactate oxidase on the surface of platinized CFM (CFM/Pt). This strategy encompassed the oxidation of lactate by lactate oxidase, producing the electroactive reporter molecule H_2O_2 that is readily detected at the CFM/Pt, as depicted in **Fig. 2.2**. In the following sections we describe the evaluation of the lactate microbiosensor analytical properties and validate their applicability in monitoring extracellular lactate concentration dynamics in hippocampal slices.

3.2.2.1. Analytical properties of CFM/Pt-based lactate microbiosensors

The active surface of CFM was first modified by electrodeposition of platinum. The deposition of these particles could be observed with scanning electron microscopy (SEM), showing the coverage of the carbon surface with spherical particles (**Fig. 2.2A**). The platinum provides a

platform for the design of oxidase based microbiosensors due to its ability to detect H_2O_2 (Lourenço et al. 2019). As schematized in **Fig. 2.2B**, lactate oxidase (LOx) was then immobilized on the active surface via cross-linking with glutaraldehyde and BSA to obtain a lactate microbiosensor. A polyurethane (PU) membrane was applied over the enzyme layer (CFM/Pt-LOx-PU) to limit lactate diffusion to the enzyme and increase the linear range by increasing the apparent K_M of the sensor (Burmeister et al. 2005; Spehar-Délèze et al. 2021). At the same time, a sentinel sensor (CFM/Pt-Null-PU) that consisted of a microsensor identical to the lactate microbiosensor except it lacked enzyme was used as a selectivity control, assuring changes recorded at the CFM/Pt-LOx-PU resulted exclusively from changes in lactate concentration.

The CFM/Pt-LOx-PU were tested for their analytical properties in PBS *p*H 7.4, at 32ºC, which is the temperature used for recording in hippocampal slices. A typical amperometric recording of the response of the sensor and sentinel to successive additions of lactate concentrations is presented in **Fig. 3.7**. The CFM/Pt-LOx-PU displayed a typical Michaelis-Menten behavior with saturation above 15 mM, while de CFM/Pt-Null-PU showed no response to added lactate. The data was then fitted using a Michaelis-Menten model, from which the average $K_{M.app}$ was determined to be 1.4 ± 0.2 mM, with an average I_{max} of 6.8 ± 2.6 nA (**Table 3.2**). Microbiosensor sensitivity was determined in the linear concentration range of 0.15 – 0.6 mM and other analytical parameters are presented in **Table 3.2**.

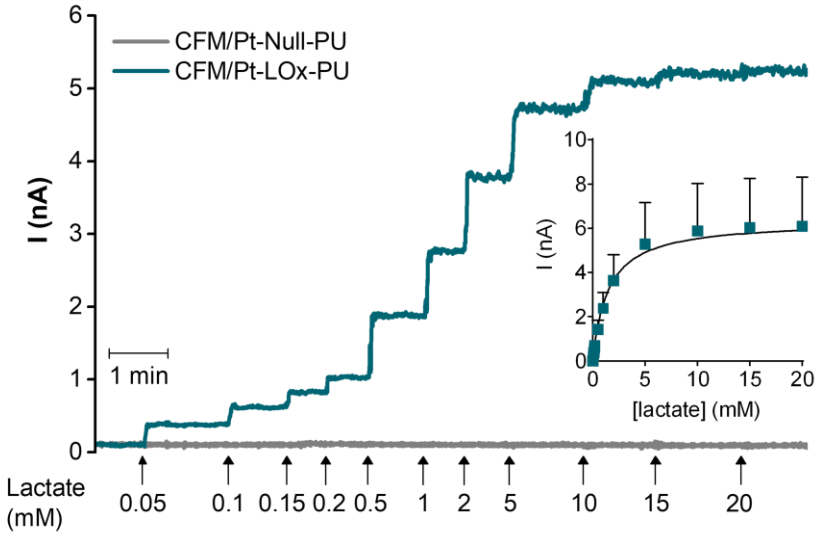

Fig. 3.7 – Representative recording of the CFM/Pt-LOx-PU (blue) and CFM/Pt-Null-PU (grey) response to increasing lactate concentrations. The successive additions and their final concentrations are indicated by arrows. The measurements were performed by amperometry at +0.7 V vs. Ag/AgCl at 32ºC. Inset: Data fitted to the Michaelis-Menten equation.

Table 3.2 – Enzyme kinetic and analytical parameters for the CFM/Pt-LOx-PU microbiosensors. Lactate sensitivity was determined for the 0.15 – 0.6 mM range.

Microbiosensor	$K_{M,app}$ (mM)	I_{max} (nA)	Sensitivity (nA mM^{-1})	R^2	LOD (µM)
CFM/Pt-LOx-PU (N=8)	1.4 ± 0.2	6.8 ± 2.6	2.2 ± 0.7	0.993 ± 0.002	41 ± 12

I_{max} – Maximal current; LOD – Limit of Detection

Biosensor performance is influenced by temperature which can affect enzymatic activity, membrane permeability, and O_2 solubility (Vaddiraju et al. 2011). As such, temperature dependency of the microbiosensors response to lactate was evaluated. The response of the CFM/Pt-LOx-PU to a bolus addition of lactate 0.5 mM was measured for temperatures between 30-40 ºC (N=3; **Fig. 3.8**), revealing that maximal activity was observed between the 32-34ºC range, which is ideal for recording in hippocampal brain slices which are maintained at 32 ºC.

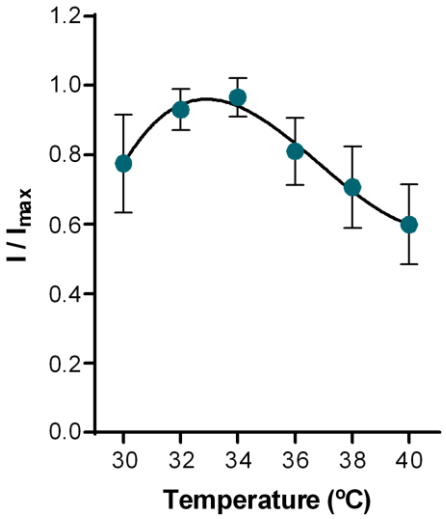

Fig. 3.8 – Effect of temperature variation on recorded current by CFM/Pt-LOx-PU in response to 0.5 mM lactate (N=3). Maximal response was observed for a temperature in the 32-34ºC interval.

The brain extracellular milieu contains several electroactive species, including ascorbate, which is oxidized at a lower potential than H_2O_2. Ascorbate is not only present in the brain extracellular space at high concentration (250-500 µM), but its concentration can vary in response to glutamatergic neurotransmission (Rice 2000; Ferreira et al. 2013, 2018). To mimic conditions in brain slices, the microbiosensors were calibrated in the presence of this potential interferent. As

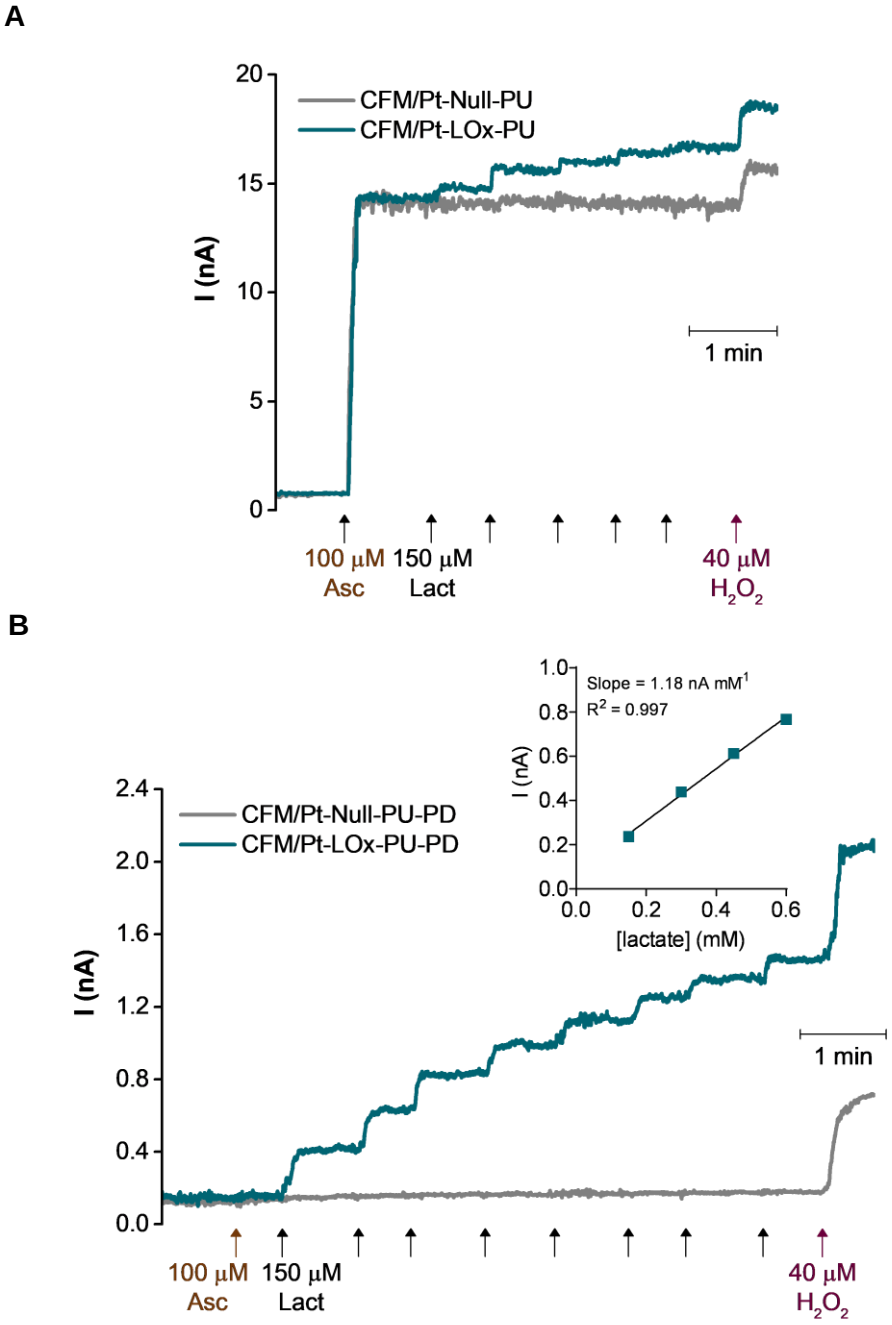

Fig. 3.9 – Representative recording of the calibration curves of CFM/Pt-based lactate microbiosensors (CFM/Pt-LOx-PU; blue) and sentinel microsensors (CFM/Pt-Null-PU; grey) in the presence of ascorbate (A) and with PD coating (B). In the end, the response to H_2O_2 was also tested. The additions and their final concentrations are indicated by arrows. The measurements were performed by amperometry at +0.7 V vs. Ag/AgCl at 32ºC. Inset: Linear regression of the calibration curve in the 0.15 – 0.6 mM range.

can be observed in **Fig. 3.9A**, there was a considerable response to 100 µM ascorbate, with the mean selectivity (lactate sensitivity/ascorbate sensitivity) of 0.15 ± 0.06 (N=8). To increase selectivity, we added a permselective coating by electropolymerization of 1,3-phenylenediamine (*m*-PD). This film forms a size exclusion layer that prevents larger molecules such as ascorbate and dopamine from reaching the electrode surface, while still allowing for smaller molecules such as H_2O_2 and lactate to permeate (Burmeister et al. 2008; Bucur et al. 2021). As seen in **Fig. 3.9B,** this significantly reduced the microbiosensor response to ascorbate and the selectivity increased to 5.31 ± 1.37 (N=6), with two additional sensors presenting no measurable response to ascorbate. Importantly, the fact that experiments are performed with a sentinel sensor ensures that interferences from this and other molecules are minimized. Addition of this permselective film decreased the sensor response both to lactate (0.6 ± 0.2 nA mM^{-1}; N=8) and H_2O_2 (33 ± 11 nA mM^{-1}; N=8). Nonetheless, the lactate sensitivity is still within the desired values for this application.

3.2.2.2. Evaluation of the operational stability of the lactate microbiosensor

Many authors have shown a decay of the analytical performance of sensors and biosensors following recording in brain tissue as a result of biofouling and/or damage to the coatings (Wisniewski et al. 2000; Singh et al. 2011). Therefore, we assessed the analytical parameters of the lactate microbiosensors after being used in successive recording sessions in slices (**Table 3.3**).

Table 3.3 – Analytical parameters of CFM/Pt-LOx-PU-PD before (pre-calibration) and after each successive recording session in slices (1-4, N) as a percentage of the pre-calibration values or in nA mM^{-1} (ascorbate sensitivity). *P < 0.05, for comparison to pre-calibration value.

Number of recordings (N)	Analytical parameters			
	Lactate sensitivity (%)	Lactate LOD (%)	H_2O_2 sensitivity (%)	Ascorbate sensitivity (nA mM^{-1})
Pre-calibration (14)	100	100	100	0.20 ± 0.07
1 (6)	90.0 ± 9.4	171.5 ± 32.4*	92.8 ± 4.0	0.08 ± 0.08
2 (4)	91.0 ± 16.1	133.3 ± 11.6*	74.8 ± 7.4*	0.12 ± 0.12
3 (8)	90.8 ± 5.6	127.0 ± 22.6	71.4 ± 10.8*	0.58 ± 0.15*
4 (4)	74.0 ± 17.2	249.0 ± 82.1	61.8 ± 7.5*	0.69 ± 0.49

The sensitivity towards lactate decreased by ~10% after the sensors were used in the first slice, remained stable with the use in a second and third slice, and decreased again after being used in a fourth slice (26%). However, these changes in sensitivity were not statistically significant when compared to pre-calibration values. The limit of detection (LOD), increased after use in the first slice and remained unchanged after recording in slices 2 and 3. The H_2O_2 sensitivity decreased significantly after the second, third and fourth slices. As for ascorbate sensitivity, it increased after the third slice.

The decrease in H_2O_2 sensitivity was greater than for lactate, which was unexpected as lactate detection depends on sensor sensitivity to H_2O_2. We hypothesized that this discrepancy might result from the fact that, in the *in vitro* evaluation, H_2O_2 added to the bulk solution must diffuse to CFM/Pt surface across not only the enzyme matrix but also cellular debris which remains attached to the tip upon removal from tissue. It is possible that bulk H_2O_2 might react with biomolecules such as proteins and lipids in this cellular debris. On the other hand, lactate sensitivity would not be as affected by this as H_2O_2 is generated by LOx within the immobilized matrix. To test this hypothesis, sensitivity was evaluated before and after immersion of sensors in brain homogenate for 2h (Singh et al. 2011). The H_2O_2 sensitivity was significantly decreased by 36.6 ± 2.8 % (N=6; P<0.05) and was partially recovered by washing in mild detergent to remove attached debris – **Fig. 3.10**. After washing, the H_2O_2 sensitivity was decreased by only 24.8 ± 3.3 % compared to the initial value, which was significantly different than before washing

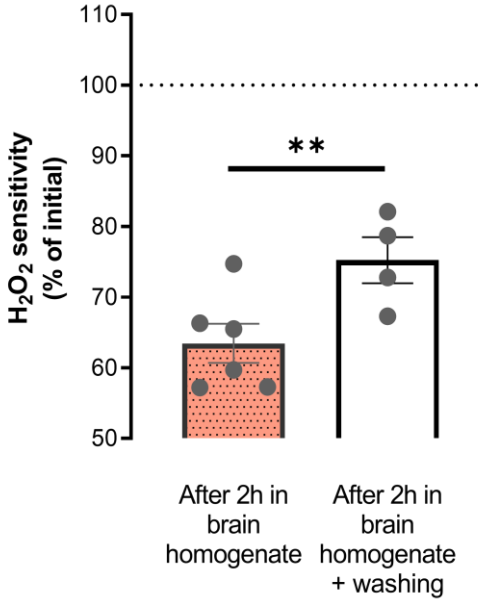

Fig. 3.10 – Hydrogen peroxide sensitivity (in percentage of H_2O_2 sensitivity before placing in the homogenate – 100 %) of CFM/Pt-Null-PU microsensors after the sensor was placed in brain homogenate for 2h to induce biofouling (A) followed by washing with diluted detergent for 20 min (B). $^{**}P < 0.01$

($P<0.01$). The loss of H_2O_2 sensitivity but not lactate sensitivity results from the fact that, in the latter, H_2O_2 is produced within the enzyme layer, not having to cross the debris to reach the active platinum surface.

3.2.2.3. Lactate measurements in hippocampal slices

The lactate microbiosensors with *m*-PD coating (CFM/Pt-LOx-PU-PD) were used to evaluate lactate dynamics in hippocampal slices. The lactate microbiosensor was inserted in the CA1 subregion with the sentinel sensor immediately below, as represented in **Fig. 3.11A.** The concentration of lactate in the perfusion medium (aCSF) was gradually increased from 0 to 15 mM. This experiment was performed in the absence of glucose as to not confound the signal resulting from exogenously added lactate with that of endogenous lactate, resulting from aerobic glycolysis (Magistretti and Allaman 2018; Barros et al. 2020, 2021). As can be observed in **Fig.**

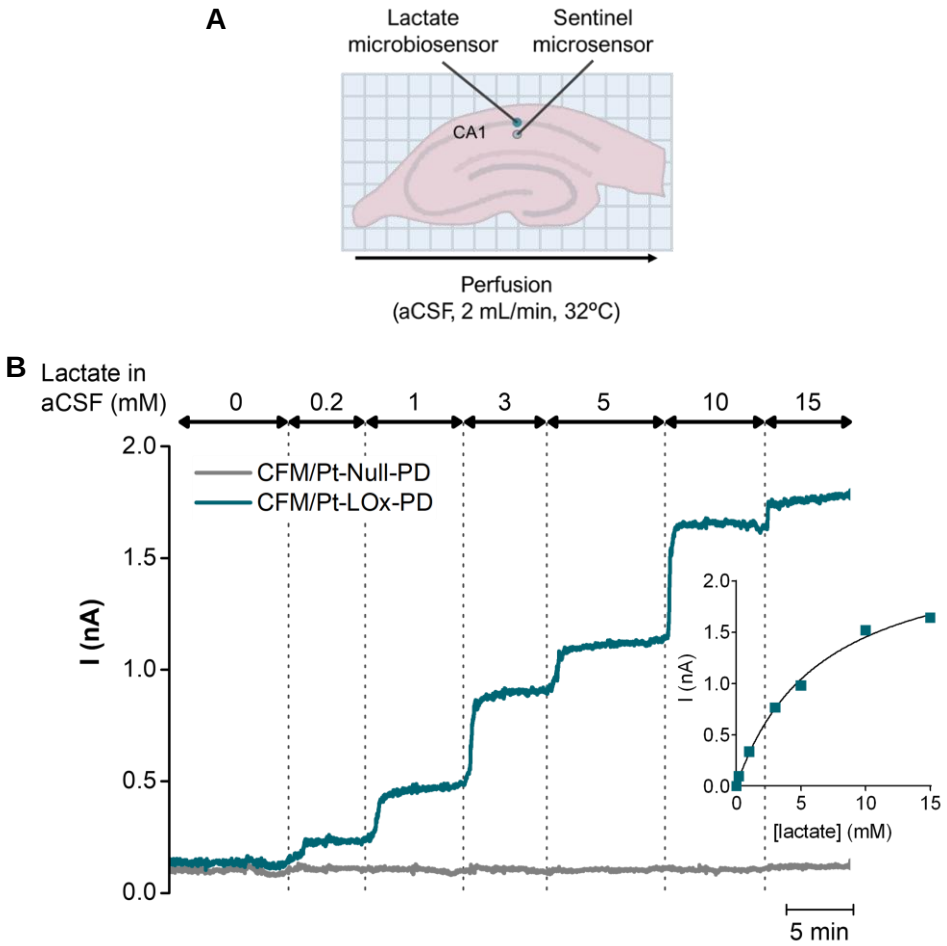

Fig. 3.11 – Lactate measurements with CFM/Pt-based lactate microbiosensors (CFM/Pt-LOx-PU-PD; blue) in hippocampal slices in the presence of a sentinel microsensor (CFM/Pt-Null-PU-PD; grey). (A) Schematic representation of insertion sites for both the lactate and sentinel microsensors in the hippocampal slice, CA1 subregion. (B) Response to increasing lactate concentrations in the perfusion medium (aCSF).

3.11B, incremental changes in lactate resulted in an increase in the current (I, nA) measured by the lactate sensor, while the current from the sentinel sensor remained unchanged. This validates the suitability of the lactate microbiosensor to monitor changes in extracellular lactate in brain slices.

3.2.2.4. Changes in extracellular lactate in the CA1 subregion evoked by glutamate stimulation

Stimulation of glutamatergic neurotransmission has been shown to stimulate lactate release from astrocytes and uptake by neurons to satisfy metabolic needs (Magistretti and Allaman 2018). The concentration dynamics of lactate in hippocampal slices was evaluated in response to a transient

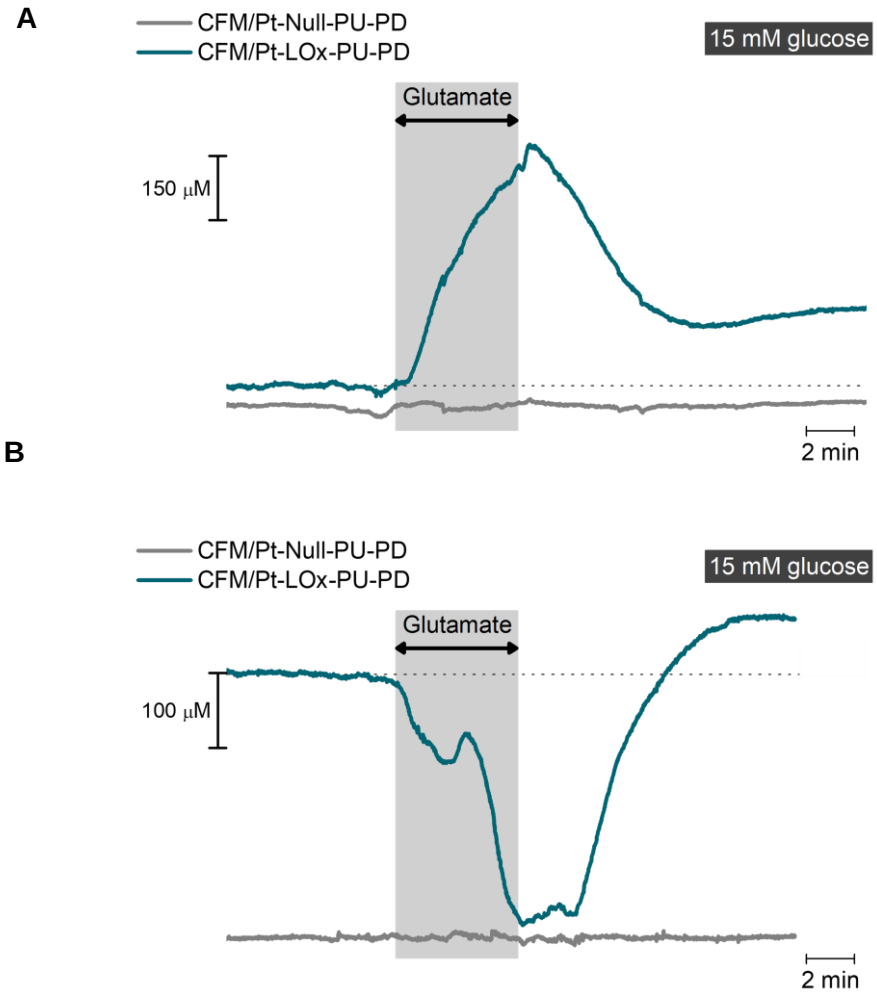

Fig. 3.12 – Lactate measurements with CFM/Pt-based lactate microbiosensors (CFM/Pt-LOx-PU-PD; blue) in the CA1 subregion of hippocampal slices in the presence of a sentinel microsensor (CFM/Pt-Null-PU-PD; grey) with bath glutamate stimulation (5 mM; 5 min) in the presence of 15 mM glucose. Two different types of response were observed: increasing (A) and decreasing (B) extracellular lactate with stimulation.

stimulation with glutamate (5 mM, 5 min) in the presence of 15 mM glucose. From the total of 10 individual recordings, we observed 2 types of responses represented in a 50/50 proportion. As observed in **Fig. 3.12,** for profile A, stimulation of glutamatergic neurotransmission resulted in a transient increase in extracellular lactate concentration ($\Delta_{Lactate}$ = 420.0 ± 214.1 µM, N=5) which was followed by a smaller overshoot after recovery of baseline ($\Delta_{Lactate}$ = 108.6 ± 45.0 µM, N=5). For profile B, glutamate induced a transient decrease in the extracellular concentration of lactate ($\Delta_{Lactate}$ = -284.6 ± 64.12 µM, N=5), followed by an overshoot ($\Delta_{Lactate}$ = 118.2 ± 28.3 µM, N=5). Extracellular lactate is mainly derived from aerobic glycolysis, and thus is dependent on glucose supply. When slices perfused with a low concentration of glucose (0.5 mM) were stimulated with glutamate (5 mM, 5 min) either a small increase ($\Delta_{Lactate}$ = 57.2 ± 15.7 µM, N=4, **Fig. 3.13A**) or no change in extracellular lactate (**Fig. 3.13B**) were observed (N=2). Furthermore, no overshoot was observed under these conditions and in fact, following profile A, a decrease in baseline level was observed (-14.6 ± 6.0 µM, N=4).

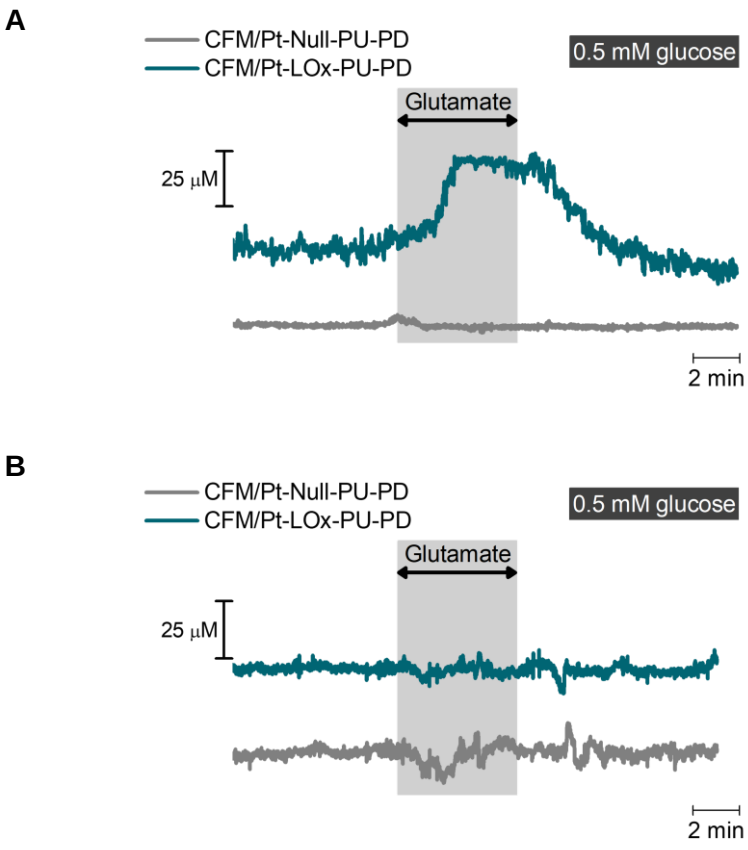

Fig. 3.13 – Lactate measurements with CFM/Pt-based lactate microbiosensors (CFM/Pt-LOx-PU-PD; blue) in the CA1 subregion of hippocampal slices in the presence of a sentinel microsensor (CFM/Pt-Null-PU-PD; grey) with bath glutamate stimulation (5 mM; 5 min) in the presence of 0.5 mM glucose. Two different types of response were observed: increasing (A) and unchanged (B) extracellular lactate with stimulation.

3.3. Discussion

The brain is highly dependent on energy metabolism to function properly, meaning that any alteration in brain bioenergetics will have profound consequences. Thus, unraveling the complex mechanisms of brain energy metabolism is of great importance and the development of new methodologies and bioanalytical tools can help advance our current knowledge. In this chapter, two new methodologies are presented to study brain energy metabolism in brain slices, namely hippocampal slices. Hippocampal slices preserve cytoarchitectural integrity, intercellular communication, and connectivity, retaining biochemical and electrophysiological functionality (Lein et al. 2011). Furthermore, this structure of the temporal medial lobe is involved in memory and learning (Jarrard 1995) and is particularly affected in several brain pathologies, such as Alzheimer's disease (Halliday 2017), making it an attractive region to study.

3.3.1. Adaptation of respirometry measurements to intact hippocampal slices

Oxidative phosphorylation allows cells to obtain the highest amount of energy (ATP) from the complete oxidation of glucose to CO_2. Many diseases, including neurodegenerative disorders such as Alzheimer's disease, have been associated with mitochondrial dysfunction (Lin and Beal 2006; McBride et al. 2006; Monzio Compagnoni et al. 2020). Therefore, it is important to develop methodologies for evaluating mitochondrial respiration and metabolic fluxes in complex preparations, such as the hippocampal slice. The use of complex biological preparations to study mitochondrial function, in particular mitochondrial respiration, can be advantageous, albeit challenging. As opposed to isolated mitochondria or cells, intact tissue preparations are a better representation of the physiological setting, maintaining a more physiological environment for mitochondria and preserving intercellular interactions. In the present study, we adapted a high-resolution respirometry protocol – a methodology that allows the instantaneous on-line recording of O_2 fluxes (Hütter et al., 2006) – for intact tissue preparations, namely hippocampal slices.

To this purpose we designed a sample holder to preserve tissue integrity throughout the experiment and optimized and validated this methodology, establishing adequate SUIT protocols for acute hippocampal slices from both rat and mouse.

The custom sample holder was manufactured from a nylon mesh fitted to a polypropylene ring. This holder fitted into the instrument recording chamber and slices were placed in the nylon mesh, thus protected from the stirring bar. We found that the sample holder had no measurable effect on vertical mixing in the chamber, although the polypropylene plastic used in the ring is porous and permeable to O_2 (Myers et al. 1959; Bastarrachea et al. 2011; Kim et al. 2013), leading to

adsorption of O_2 which could be slowly released back into the medium when O_2 concentration decreased. This issue could be solved by using different materials. The holder increased the time required for reoxygenation of media due to the decrease in the contact area between medium and air during oxygenation, which did not impact on measurable respiratory states.

We then optimized a SUIT protocol for evaluation of respiratory states in hippocampal slices and compared O_2 fluxes between rat and mouse measured under defined coupling and pathway-controlled states and normalized the O_2 fluxes obtained for maximum respiration to determine relevant FCR values. In general, all parameters were lower for slices from mouse compared to those from rat. In particular, the mean values for Leak and ET capacity respiration were significantly lower in mouse slice preparations.

The significantly lower level of Leak respiration for slices from mouse suggests that the tissue is in a more coupled state when compared to hippocampal slices obtained from rat. This difference may be due to intrinsic differences of the tissue or to differences in tissue viability. One report has shown that the distribution of uncoupling proteins isoforms differ between rat and mouse brain tissue (Alán et al. 2009). On the other hand, the intra-experimental evaluation of tissue viability, measured as RVI, showed that slices obtained from mouse had a lower viability index when compared to rat, suggesting a higher ratio of damaged-to-intact cells, possibly as a result of higher difficulty in slice preparation due to the smaller size of the mouse hippocampus. Finally, the Leak control ratio was not different between the two species, strongly suggesting that the difference observed between mouse and rat slices is most likely a result of different functional mitochondrial count. Notwithstanding, the Leak control ratios obtained here are higher than those reported in other studies using isolated cells. A high level of leak respiration may be an indication that respiration is uncoupled to ATP synthesis, possibly as a result of trauma caused by the preparation of the slices. In a study comparing organotypic and acute hippocampal slices, Schuh et al. reported a decrease in O_2 consumption upon addition of oligomycin of ∼50% for acute slices and ∼75% for organotypic slices (Schuh et al. 2011). We observed more modest decreases of ∼40% and ∼25% for mouse and rat slices, respectively. In organotypic slice cultures, the layers of damaged cells are removed, and tissue slices are significantly thinner when compared to acute slice preparations.

Increased maximal respiratory or ET capacity in slices from rat may also explain the differences observed in the absolute values of proton leak. The results for maximal respiration obtained are similar to those reported for transformed human embryonic kidney cells (HEK 293). Our results are also in agreement with the study by Schuh et al., where an increase of 150% from basal respiration was obtained when FCCP was added (Schuh et al. 2011) (our results show an increase of ∼130%).

Although not significantly different, there was a tendency for a lower basal or Routine respiration for hippocampal slices obtained from mouse, which may suggest less active oxidative metabolism. When Routine respiration was normalized for maximal respiration (Routine control ratio), a similar level was obtained for both rat and mouse hippocampal slices and both were higher than those determined for cells. Interestingly, we found that the *net*Routine control ratio, i.e., the fraction of O_2 consumption directly linked to ATP synthesis, was similar to the one reported for isolated cells. Thus, although basal respiration is increased in slices, this is not translated into higher ATP output, but rather is mainly the result of elevated proton leak.

Oxygen consumption not associated to the ETS was similar between the two species. When comparing to cells (**Table 3.1**), synaptosomes (Joyce et al. 2003), and organotypic hippocampal slices (Schuh et al. 2011), the level of ROX was higher. This may be due to an increased level of cells with dysfunctional mitochondria.

To further demonstrate the potential of this method and the ability to detect differences in respiratory states from intact tissues, we carried out similar experiments in hippocampal slices from the triple transgenic mouse model for Alzheimer's disease (3xTgAD). This rodent model of AD expresses 3 transgenes, namely $PS1_{M146V}$, APP_{SWE}, and tau_{P301L}. Phenotypically, these mice progressively develop plaque and tangle histopathology, which are preceded by age-related deficits in LTP plasticity. As such, this model recapitulates the hallmark events of AD (Oddo et al. 2003). Changes in cellular energy metabolism are proposed to occur at the onset and progression of AD. Decrease in cerebral glucose consumption rate is an early predictor of AD (Hoyer et al. 1988; Cunnane et al. 2011), and brain metabolism is declined at least one decade before diagnosis (Wang et al., 2007).

Using the same SUIT protocol in hippocampal slices from this mouse model, we found an age-dependent decrease in oxidative phosphorylation function in both the 3xTgAD and NTg genotypes. Besides the tendency for decrease in basal or Routine respiration, the decrease in maximal respiratory or ET capacity is suggestive of a decreased ability to adequately respond to situations of increased energy demand, such as those imposed by synaptic transmission. Total brain mitochondria isolated from 3xTgAD mice have shown decay in respiratory parameters such as respiratory control rate, membrane potential, and ATP/ADP ratio, as well as an imbalance between mitochondrial biogenesis and autophagy in both mitochondria from the hippocampus and the cortex (Carvalho et al. 2015). Decline in the activity of both pyruvate dehydrogenase and cytochrome *c* oxidase has also been observed in brain tissue of AD patients (Blass et al. 2000). Furthermore, oxidative damage of proteins has been reported in the hippocampus of the 3xTgAD mouse model as early as 3 months of age, namely in proteins involved in energy metabolism such as enolase 1, glyceraldehyde-3-phosphate dehydrogenase, and phosphoglycerate kinase 1 (Shen et al. 2015).

Interestingly, we found no differences between the two genotypes for both ages evaluated. It is possible that these metabolic changes only become more exacerbated in the older aged 3xTgAD. However, due to extremely low basal respiratory rate is the slice preparations at this age, we were unable to perform this evaluation in slices from old-aged NTg and 3xTgAD samples.

3.3.2. Monitoring lactate in hippocampal slices with lactate oxidase-based microbiosensors

Although lactate was classically viewed as a metabolic endpoint of glycolysis, it has been demonstrated more recently that lactate can play an important role in brain metabolism. While glucose is the primary brain substrate under physiological conditions, lactate can also act as an energy substrate, particularly in conditions of increased energy demand (Magistretti and Allaman 2018; Barros and Weber 2018). Lactate is apparently shuttled between astrocytes and neurons, supporting the notion of a tight neurometabolic coupling between these cells. This has been supported by several studies, but there is still a need to further clarify the role of lactate in brain metabolism. Direct and real time monitoring of lactate concentration dynamics in the brain extracellular space can help elucidate the underlying mechanisms that support this neurometabolic coupling. For that, we designed a microbiosensor based on platinized CFM and using lactate oxidase to measure lactate dynamics in brain slices.

To create a platform for H_2O_2 detection, the active surface of the CFM was first modified by electrodeposition of platinum particles, resulting in the coverage of the carbon surface with spherical platinum particles. These platinized CFM have been previously shown to have good analytical performance towards detection of H_2O_2, and are thus a suitable platform for the design of oxidase based microbiosensors (Lourenço et al. 2019). After immobilization of lactate oxidase (LOx), a polyurethane membrane was applied over the enzyme layer to limit lactate diffusion to the enzyme and increase the linear range by increasing the apparent K_M of the sensor (Burmeister et al. 2005; Lourenço et al. 2017b; Spehar-Délèze et al. 2021). In addition to the lactate microbiosensor, sentinel microsensors were built in the same way, but lacked lactate oxidase. The use of these sentinel microsensors allows real-time monitoring of putative interferents, detected by both the active and null sensors, increasing the specificity of measurements (Bucur et al., 2021; Burmeister et al., 2005; Patel, 2020).

Recording in hippocampal slices is typically performed at temperatures below 37 ºC (Teyler 1980; Reid et al. 1988; Panuccio et al. 2018; Manz et al. 2021) and in our case in particular, recordings in slices are usually performed at 32ºC. As such, the analytical properties of the lactate microbiosensors here described were carried out at this temperature. The sensors showed a typical

Michaelis-Menten behavior with saturation above 15 mM, while the sentinel showed no response to added lactate. The K_M of the enzyme used in this study (lactate oxidase from *Aerococcus viridans*) has been estimated to be in the range from 0.12 to 0.94 mM (Yorita et al. 2000; Taurino et al. 2013). The mean $K_{M.app}$ here reported for the biosensors (1.4 mM) is higher, indicating that addition of polyurethane successfully increased the biosensor $K_{M.app}$. The sensitivity displayed by the sensors (2.2 nA mM^{-1}) was within acceptable values for this purpose, since lactate concentrations *in vivo* in rodents are reported to range between 1-3 mM (Harada et al. 1993; Abi-Saab et al. 2002; Yager et al. 2002; Dong et al. 2003; Zilberter et al. 2010).

The performance of biosensors can be affected by temperature, due to changes in enzymatic activity, membrane permeability, and O_2 solubility (Vaddiraju et al. 2011). The biosensors here described revealed optimal temperature performance for hippocampal slice recordings, since the maximal activity was observed between the 32-34ºC range.

In the brain, there are several electroactive species that can vary in concentration, particularly in response to stimulation, and some are oxidized at a lower potential than H_2O_2. One of such molecules is ascorbate, which is present at a high concentration (Rice 2000; Ferreira et al. 2013, 2018). We found that addition of a permselective coating of polymerized *m*-PD increased microbiosensor selectivity against ascorbate to a level suitable for recording in hippocampal slices. This film forms a size exclusion layer that prevents larger molecules such as ascorbate and dopamine from reaching the electrode surface, while still allowing for smaller molecules such as H_2O_2 and lactate to permeate (Burmeister et al. 2008; Bucur et al. 2021). In addition to this coating, the fact that experiments are performed with a sentinel sensor ensures that interferences from this molecule and others are minimized. The drawback of using an *m*-PD coating was that the sensitivity of the biosensors decreased for both lactate and H_2O_2. This has been described before for glucose microbiosensors prepared in a fashion similar to that described here (Lourenço et al. 2019) and it may be due to modifications of the platinum surface properties (Katsounaros et al. 2012). Nonetheless, the lactate sensitivity was still within the desired values for this application.

The use of sensors and biosensors in brain tissue can lead to a decay in analytical performance as a result of biofouling and/or damage to the coatings (Wisniewski et al. 2000; Singh et al. 2011). The lactate microbiosensors showed minor changes in analytical properties when used successively in three slices. The maintenance of most analytical parameters is likely due to the *m*-PD and the polyurethane coatings, as both have been shown to reduce biofouling (Wahono et al. 2012; Fang et al. 2017; Bucur et al. 2021).

The ability of the lactate microbiosensors with *m*-PD coating to monitor lactate dynamics in hippocampal slices was validated by showing that they responded adequately to increase in lactate in the perfusion medium. The current measured by the sentinel sensor remained unchanged,

confirming that the current measured by the microbiosensor was only due to lactate. This experiment validated the suitability of the lactate microbiosensor to monitor changes in extracellular lactate in brain slices.

To further confirm the suitability of these lactate biosensors for recording lactate concentration dynamics in brain slices, the response of slices to glutamatergic activation was evaluated. Stimulation of glutamatergic neurotransmission has been shown to induce lactate release from astrocytes and uptake by neurons to satisfy metabolic needs (Magistretti and Allaman 2018). The profile of response during stimulation with glutamate varied, with half the cases showing a net increase in extracellular lactate while the other half displayed a net decrease. In the aftermath of glutamate stimulation, all recordings showed an overshoot in extracellular lactate. Most relevant is that in all recordings no change in the sentinel sensor was detected, confirming that changes in the microbiosensor resulted exclusively from changes in lactate. The concentration of lactate in the extracellular space results from the balance between extrusion and uptake and changes result from a net flux in which either extrusion rate exceeds uptake/consumption, leading to an increase in extracellular lactate, or vice-versa, leading to a decrease. This balance is emphasized in our recordings when lactate decreases during stimulation, where after lactate decreases there is briefly an increase, only for lactate to start decreasing again. Importantly, neuronal activity has been shown to remain normal for the concentration of glutamate used (Schurr et al. 1999), which excludes any possible excitotoxic effect.

In a study using acute hippocampal slices and a comparable stimulation paradigm, a similar result to our profile with an increase in lactate during stimulation was obtained, albeit using a lower glucose concentration (4 mM) in the slice perfusion media (Schurr et al. 1999). However, these measurements were indirect (using an enzymatic kit to measure lactate in slice perfusate) and lacked the temporal resolution presented here. Some *in vivo* studies have shown the occurrence of an initial dip in lactate concentration immediately after stimulation, followed by an increase (Hu and Wilson 1997; Mangia et al. 2003; Bingul et al. 2020). This dip could have the same origin as seen in the decreasing lactate profile. This emphasizes the existence of a balance between lactate extrusion (putatively by astrocytes) and uptake, which is reflected on the extracellular lactate dynamics. Studies performed *in vivo* measuring lactate have shown an increase in extracellular lactate after brief stimulation, consistent with our results that show an overshoot in extracellular lactate after stimulation (Hu and Wilson 1997; Bingul et al. 2020; Forderhase et al. 2020; Zuend et al. 2020). However, the neurovascular response observed *in vivo* can alter the delivery of energy substrates to the brain tissue from circulation, including lactate (Dalsgaard 2005; Mächler et al. 2016) and result in a more robust overshoot then that observed in slices devoid of functional blood flow.

This observation of two distinct profiles highlights the relevance of monitoring other neurophysiological parameters, such as intracellular Ca^{2+} dynamics and/or extracellular field potential, in order to access neuronal response to glutamate stimulation and how it correlates with the observed lactate dynamics. Importantly, it is possible to use electrochemical biosensors and simultaneously monitor these parameters (Shew et al. 2010; Hinzman et al. 2015; Ledo et al. 2018).

Extracellular lactate is mainly derived from aerobic glycolysis, and thus is dependent on glucose supply. The same stimulation paradigm used with a lower glucose concentration (0.5 mM) produced either a smaller increase or no change in extracellular lactate. Furthermore, no post-stimulation overshoot was observed under these conditions. The lower availability of glucose means that less lactate can be produced and extruded to the extracellular space, explaining the lack of decrease in lactate during stimulation, as observed in the experiments with higher glucose. Previous studies have shown that decreasing the glucose concentration from 10 mM to 4 mM decreases extracellular lactate concentration (Schurr et al. 1999) and synaptic function in hippocampal slices has been shown to be silenced for glucose concentrations below 2 mM (Schurr et al. 1989; An et al. 2008). This silencing could be at least partly related to the effect of low glucose on ATP-sensitive potassium channels (K_{ATP} channels). These channels are blocked by ATP, but when glucose in the medium is low (< 1 mM) leading to low intracellular ATP they open, leading to neuron hyperpolarization in hypothalamic slices (Parsons and Hirasawa 2010). Indeed, these channels are activated in extreme metabolic deprivation, such as in anoxia and ischemia (Pierrefiche et al. 1996; Allen and Brown 2004). The high expression of K_{ATP} channels in the hippocampus suggests that a similar effect may be observed in this brain region (Dunn-Meynell et al. 1998; Salamone et al. 1999). In fact, overstimulation causes neuronal post-hyperpolarization mediated by K_{ATP} channels in the hippocampus (Tanner et al. 2011).

3.4. Conclusions

In this chapter, two novel bioanalytical methodologies to study bioenergetics metabolism in hippocampal slices were described and were shown to be suitable for their purpose, i.e., to measure O_2 consumption as a measure of oxidative metabolism and to monitor extracellular lactate concentration dynamics in whole hippocampal slices.

We have demonstrated that it is possible to obtain stable O_2 fluxes with intact acute hippocampal slices from both rat and mouse through high-resolution respirometry by using a manufactured sample holder and adapted SUIT protocol. Importantly, the presence of the holder does not affect measurements. There was an effective response to addition of inhibitors of the complexes of the ETS and other drugs targeting mitochondria, and all had the expected effects on respiration. We further established the use of this methodology in intact tissue, by evaluating differences in respiratory states in hippocampal slices from a mouse model for Alzheimer's disease and its evolution with age. We found a tendency for decrease in some of the parameters tested that was more dependent on age. We have demonstrated that this methodology can be used for assessment of mitochondrial function in a preparation closer to the physiological state. This methodology can be valuable for other applications, such as the study of energy substrates in the brain. Furthermore, the sample holder here described could have further uses other than with intact tissue. It could for example be used to prevent damage to permeabilized tissue or even be used with whole smaller living organisms.

The designed lactate microbiosensor based on lactate oxidase immobilized on the surface of platinized carbon fiber microelectrodes was used in monitoring rapid changes in extracellular lactate linked to glutamate stimulation in hippocampal slices. The *in vitro* characterization revealed suitable analytical performance, namely high sensitivity and selectivity, low LOD, and also extended operational stability. Two distinct profiles of change in lactate flux in hippocampal slices upon glutamate stimulation were obtained while after stimulation an overshoot in lactate concentration was always observed. Decreasing glucose concentration to 0.5 mM completely abolished the consumption of extracellular lactate upon glutamate stimulation as well as the post-stimulation overshoot, highlighting that the monocarboxylic acid is continuously produced from glucose in healthy brain tissue. In conclusion, the lactate microbiosensors here described can allow us to elucidate the role of lactate in neurometabolic coupling using brain slices, as demonstrated by showing the complex profile in change elicited by glutamatergic stimulation.

3.5. Future Directions

The sample holder should be further improved, using materials impermeable to O_2 and decreasing its size to a minimum while still maintaining stability inside the chamber (ongoing collaboration with Oroboros Instruments). The methodology could be tested for its application to permeabilized tissue, to decrease the damage provoked by stirring. Furthermore, a comparison between the different brain regions and even other tissues could be carried out. The lactate microbiosensors should be tested for their ability of measuring lactate dynamics *in vivo*.

4. Aerobic Glycolysis in the Hippocampus Sustains Extracellular Lactate to Support Neuronal Oxidative Metabolism

4.1. Introduction

Glucose is the primary energy substrate for the human brain (Sokoloff 1977) which consumes a paramount 20% of total glucose-derived energy, despite accounting for only 2% of total body weight (Mergenthaler et al. 2013; Yellen 2018). It enters cells through GLUT and can be metabolized through glycolysis. Pyruvate can then either undergo oxidative decarboxylation to acetyl CoA, which in turn is completely oxidized to CO_2 through the TCA cycle, or alternatively be reduced to lactate by LDH. In fact, lactate has been proposed to be the actual end-point of glycolysis (Schurr 2014, 2018), a concept which seems to be even more plausible in the context of the brain (Barros et al. 2020). The amount of lactate in the brain is at least 10 times higher than pyruvate, due to the high affinity of LDH for pyruvate and mitochondrial pyruvate consumption (Olesen 1970; Gjedde and Magistretti 2011; Barros et al. 2020). The conversion of pyruvate to lactate by LDH is also important for the cytosolic replenishment of NAD^+ for glycolysis.

Although the importance of glucose as a substrate for the brain is unquestionable, the concept of lactate also acting as an energetic substrate has gained traction, while still remaining controversial (Hertz and Chen 2017; Magistretti and Allaman 2018; Schurr 2018; Bak and Walls 2018a, b; Barros and Weber 2018; Yellen 2018; Dienel 2019). The decisive work of Pellerin and Magistretti showing that glutamate uptake stimulates aerobic glycolysis in primary astrocyte cultures associated with lactate release led to the proposal of the "Astrocyte Neuron Lactate Shuttle" (ANLS) model. According to this model, glutamatergic activity induces glucose uptake and lactate release by astrocytes, which is subsequently taken up by neurons to support metabolic activity (Pellerin and Magistretti 1994; Magistretti and Allaman 2018). Since then, mounting evidence has supported the ANLS model (Magistretti and Allaman 2018; Barros and Weber 2018).

It is estimated that both neurons and astrocytes uptake glucose at the same rate in basal conditions, despite neurons accounting for 70-80% of energy consumption in the brain (Nehlig et al. 2004; Chuquet et al. 2010; Howarth et al. 2012). However, neurons not only display a lower glycolytic rate than astrocytes, but lack the ability to upregulate glycolytic rate, explained by low activity of 6-phosphofructo-2-kinase/fructose-2,6-biphosphatase-3 in these cells which results in deficient production of $F2,6P_2$, a potent activator of PFK1 (Almeida et al. 2001; Herrero-Mendez et al. 2009). On the other hand, astrocytes possess glycogen stores and glycogen-derived lactate can be an energy reserve and sustain neuronal function (Brown and Ransom 2007). Neurons keep lower lactate levels at rest compared to astrocytes (Mächler et al. 2016) and have lower $NADH/NAD^+$, favoring lactate to pyruvate conversion (Mongeon et al. 2016). Furthermore, the expression of

LDH isoforms was found to be cell specific: LDH1, which favors the oxidation of lactate to pyruvate, is found in neurons while LDH5 is expressed in astrocytes and is associated to the production of lactate from pyruvate (Bittar et al. 1996). Also, MCT are differentially expressed among brain cells: neurons express a high affinity isoform (MCT2), while astrocytes low affinity isoforms (mostly MCT4 and also MCT1) (Bergersen 2015). Finally, increased neural activity has been shown to increase extracellular lactate (Lourenço et al. 2017b; Bingul et al. 2020), accompanied by a decrease in lactate in astrocytes (Zuend et al. 2020) while neurons seem to preferably use lactate over glucose (van Hall et al. 2009; Wyss et al. 2011).

In sum, lactate appears to play an important role in meeting the acute energy demands of neurons that results from increased activity and many studies support the notion that lactate is transferred from astrocytes to neurons. With the work described in this chapter, we aimed at better understanding the role of lactate in the context of neurometabolism by performing a quantitative evaluation of oxidative metabolism linked to substrate utilization and correlating it to dynamic changes in extracellular lactate in the hippocampus. We used high resolution respirometry in whole hippocampal slices and microbiosensor technology, according to what was described in the previous chapter, along with pharmacological modulation to study the role of lactate as an oxidative substrate in the hippocampus. By using rat hippocampal slices, the cytoarchitecture and cells interactions are preserved, while allowing easy manipulation of the extracellular medium composition.

4.2. Results

4.2.1. Oxygen consumption rate in hippocampal slices is dependent on glucose concentration and is stimulated by addition of lactate

Evaluation of oxidative phosphorylation is typically performed under saturating concentration of substrates, which, in the case of intact hippocampal slices, is glucose. To ascertain how the concentration of glucose added to hippocampal slice media impacted tissue O_2 consumption, we determined basal O_2 flux as a function of added glucose, using the methodology described in chapter 3 (**Fig. 4.1A**). Raising the glucose concentration from 0.1 to 0.5 mM resulted in a significant increase in O_2 flux from 8.47 ± 0.55 (N = 7) to 10.87 ± 0.23 pmol s^{-1} mg_{wt}^{-1} (N = 31). Further raise in glucose concentrations produced a tendency for increase in O_2 flux to 11.56 ± 0.58 pmol s^{-1} mg_{wt}^{-1} (N = 6) for 10 mM and 11.75 ± 0.36 pmol s^{-1} mg_{wt}^{-1} (N = 27) at 15 mM. When glucose was replaced with lactate at 10 mM, the O_2 flux in hippocampal slices was similar to that observed for glucose (11.97 ± 0.77 pmol s^{-1} mg_{wt}^{-1}; N = 6). These results indicate that O_2 consumption in hippocampal slices is only limited for very low glucose concentrations and that lactate can fully replace glucose as a fuel for oxidative phosphorylation.

In a physiological setting, both lactate and glucose are expected to be found in the brain extracellular space and so we assessed whether adding lactate on top of glucose could "boost" O_2 flux. We evaluated the effect of adding exogenous lactate both under conditions of low (0.5 mM) and high (15 mM) glucose. The lower concentration was chosen to be in the low end of the expected extracellular concentration of glucose found in the brain, which ranges from 0.5 to 4.4 mM (Silver and Erecińska 1994; McNay and Gold 1999; Kirchner et al. 2006; Slais et al. 2008) without limiting O_2 flux in hippocampal slices, as observed. The higher concentration of glucose aimed to guarantee saturating substrate conditions, considering these experiments are performed in a closed chamber. In slice neurophysiological studies, glucose concentration is typically 10 mM glucose, which has been shown to maximize responses to 'physiological' stimuli. Furthermore, lowering glucose concentration to values bellow 2 mM impairs brain slice functional indicators (An et al. 2008). Additionally, in slice preparations, the distance for metabolite diffusion is higher than the distance between capillaries, which is on average ca. 50 μm (LaManna et al. 2004), meaning that glucose diffusion can limit availability in the tissue core.

As can be seen in **Fig. 4.1B** and **C**, addition of lactate (15 mM) increased O_2 flux in hippocampal slices both when glucose concentration was low (0.5 mM, red) and high (15 mM, black) by 9.8 ± 1.8 % (N = 16) and 8.7 ± 1.5 % (N = 13), respectively. So, even when extracellular glucose concentration is not limiting, increase in lactate can "boost" the rate of oxidative phosphorylation

in the hippocampus. Although the concentration of lactate chosen here may appear excessive, blood lactate concentration can reach 20 mM with exercise and can enter the brain parenchyma (Rasmussen et al. 2010; Dienel 2019).

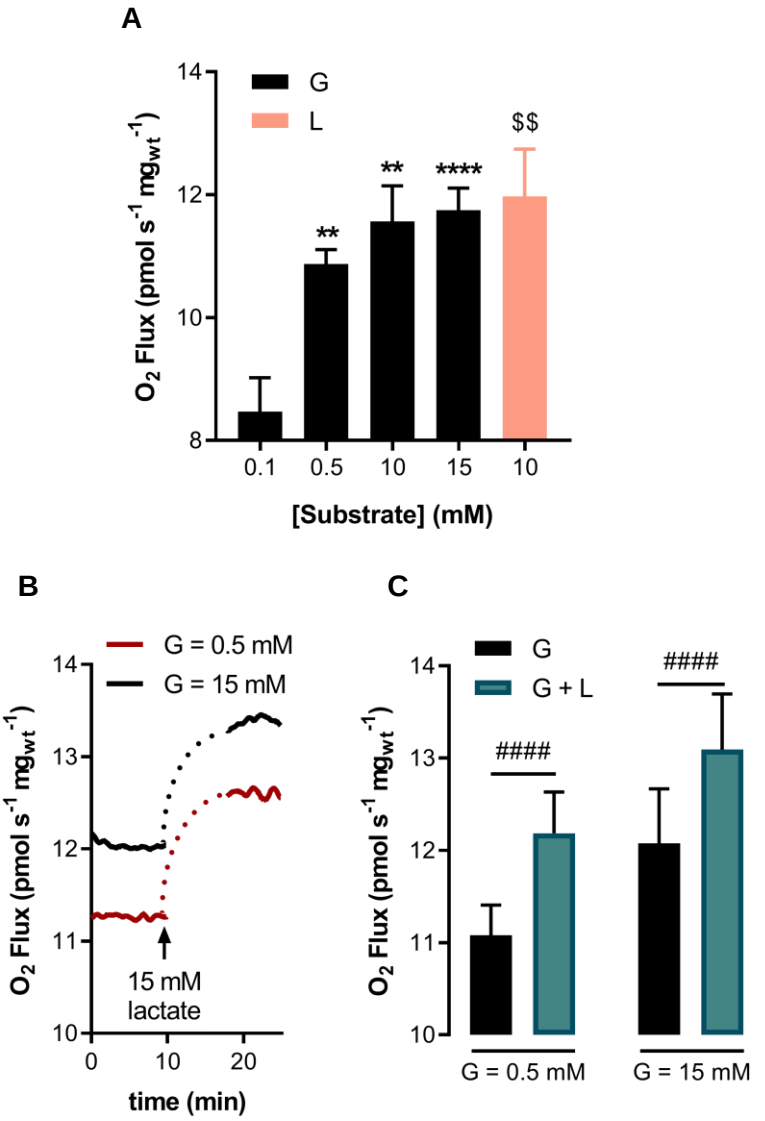

Fig. 4.1 – Basal O_2 flux measures in intact hippocampal slices using high resolution respirometry. (A) Average basal respiration (O_2 flux; pmol s^{-1} mg_{wt}^{-1}) measured in hippocampal slices with different concentrations of glucose (G; 0.1-15 mM) or lactate (L; 10 mM) in aCSF media. (B) Representative recording of O_2 flux measured in hippocampal slices, showing the increase in basal O_2 flux observed upon addition of lactate (15mM, arrow) to media containing either 0.5 (red) or 15 (black) mM glucose (G). (C) Mean basal O_2 flux measured under different conditions of glucose and lactate concentration. **P < 0.01, ****P < 0.0001 for comparison to 0.1 mM glucose; $^{\$\$}$P < 0.01 for comparison between 0.1 mM glucose and lactate; $^{\#\#\#\#}$P < 0.0001 for comparison between same glucose concentration with or without lactate.

Since lactate as the sole substrate can induce neural bursts in slices, which were suppressed by adding a low concentration of glucose (Hollnagel et al. 2020), we decided to evaluate the role of lactate (15 mM) in the presence of a low amount of glucose (0.5 mM) to better replicate physiological conditions, instead of using lactate alone.

4.2.2. Inhibition of astrocytic TCA cycle and neuronal MCT2 decreases oxygen consumption in hippocampal slices

In order to better understand glucose vs. lactate utilization by the different cellular elements in hippocampal slices, we explored pharmacological tools to inhibit oxidative phosphorylation in glial cells (fluorocitrate, FC), and lactate uptake in neurons (4-CIN). Fluorocitrate is an inhibitor of aconitase (Fonnum et al. 1997) which is preferentially taken up by glia but not neurons (Hassel et al. 1995), while 4-CIN is an inhibitor of the monocarboxylate transporter 2 (MCT2) expressed in neurons. At the concentration used here (200 µM), 4-CIN inhibits MCT2 (IC_{50} = 24 µM), but not MCT1 (IC_{50} = 425 µM; endothelial cells) nor MCT4 (IC_{50} = 990 µM; astrocytes) (Bröer et al. 1999; Bergersen 2015). We first optimized incubation time for each inhibitor. As shown in **Fig. 4.2**, both FC (100 µM) and 4-CIN (200 µM) inhibited hippocampal slice O_2 flux with maximal effect observed at 1.5h and 1h, respectively.

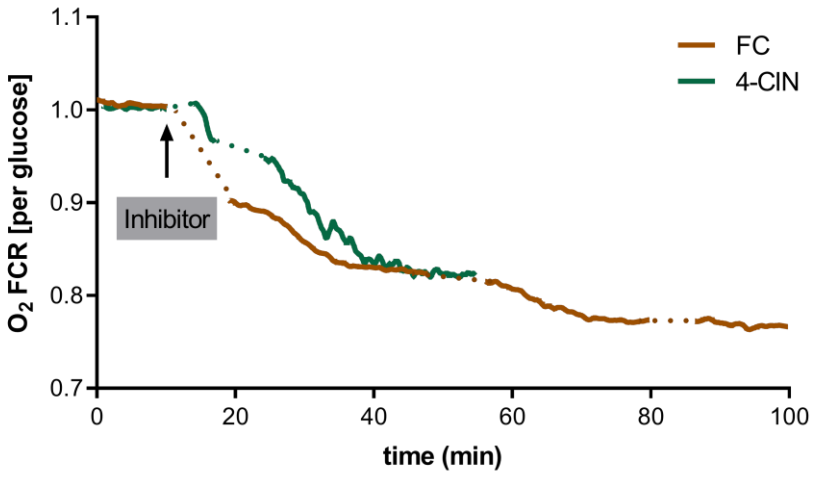

Fig. 4.2 - Pharmacological inhibition of glial TCA cycle by fluorocitrate (FC) and neuronal lactate uptake by 4-CIN decrease hippocampal slice respiration in 15 mM glucose. Representative traces of O_2 flux normalized to level with only glucose in the medium (O_2 Flux Control Ratio – FCR – per glucose). The dotted segments in each recording represent moments of chamber re-oxygenation.

We then explored the effect of these inhibitors on slice respiration in conditions of low or high glucose, and with added lactate.

Inhibition with FC resulted in a decrease in hippocampal slice respiration for all the conditions tested: low and high glucose, with or without lactate (**Fig. 4.3A**), supporting the existence of oxidative phosphorylation in glial cells. By normalizing measured O_2 fluxes to the basal value (only glucose) we can observe that the relative effect of FC was most pronounced under low glucose plus lactate (~35%), while for all other conditions it was about 25% (**Fig. 4.3B**). This difference, although non-significant, may suggest that when glucose supply is low, astrocytes also use lactate as a fuel for oxidative phosphorylation.

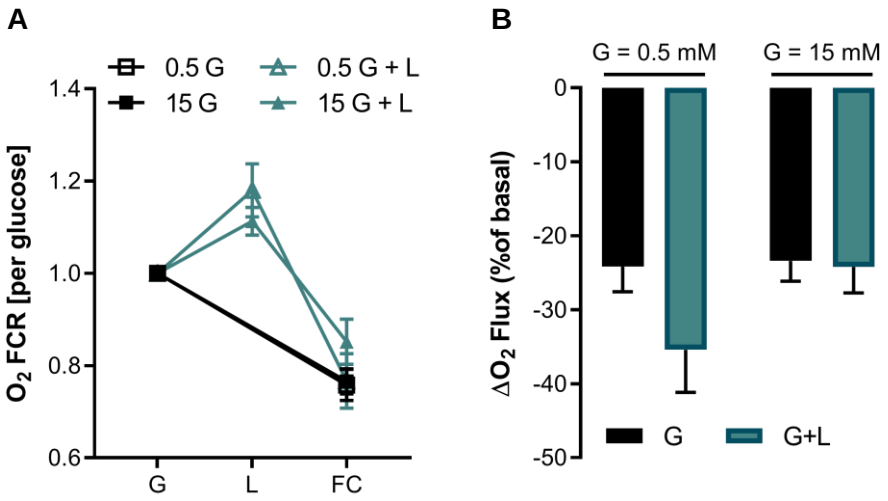

Fig. 4.3 – Pharmacological inhibition of glial TCA cycle by FC decreased O_2 consumption in hippocampal slices. (A) O_2 FCR is decreased with inhibition of glial TCA cycle both when slices are supplied with only glucose (G; black) and when lactate is added as well (L; blue). Values are shown normalized for the value of O_2 flux observed with glucose (O_2 Flux Control Ratio – FCR – per glucose). (B) Percentage change in O_2 flux (ΔO_2 Flux) from basal (O_2 flux observed with glucose) observed following inhibition of glial TCA cycle with FC.

Inhibition of lactate transport into neurons reversed the increased O_2 FCR evoked by adding lactate in blue, supporting the notion that the increase in O_2 flux observed upon addition of a surplus of lactate is the result of increased oxidative phosphorylation in neurons (in blue in **Fig. 4.4A**). Interestingly, 4-CIN also inhibited O_2 flux when only glucose was added to media (in black in **Fig. 4.4A**). This suggests that even when only glucose is supplied to hippocampal slices, not only is lactate present in the extracellular media, but also that it is used by neurons to support oxidative phosphorylation. As shown in **Fig. 4.4B**, the relative inhibition of O_2 flux induced by

4-CIN was most pronounced for low glucose (**Fig. 4.4**; P = 0.0758, comparing to 0.5 mM glucose + lactate; P = 0.0591, comparing to 15 mM glucose), suggesting that under these conditions (low glucose supply) neurons are more dependent on lactate uptake to support oxidative phosphorylation.

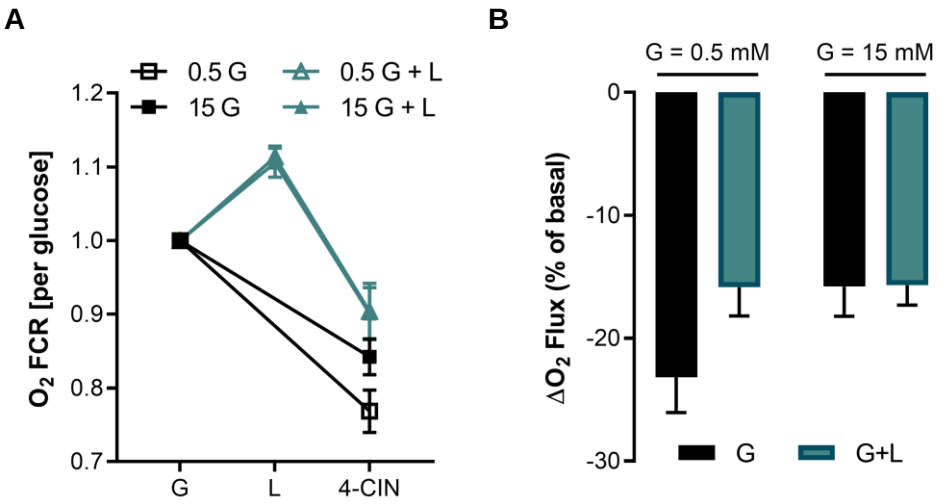

Fig. 4.4 – Pharmacological inhibition of MCT2 in neurons by 4-CIN decreased O_2 consumption in hippocampal slices. (A) O_2 FCR is decreased with inhibition of MCT2 by 4-CIN both when slices are supplied with only glucose (G; black) and when lactate is added as well (L; blue). Values are shown normalized for the value of O_2 flux observed with glucose (O_2 Flux Control Ratio – FCR – per glucose). (B) Percentage change in O_2 flux (ΔO_2 Flux) from basal (O_2 flux observed with glucose) following inhibition of MCT2 with 4-CIN.

4.2.3. Lactate production by hippocampal slices as a function of glucose concentration

These results prompted us to investigate how changes in extracellular glucose concentration affected lactate concentration in the extracellular space ($[lactate]_{ECS}$) in hippocampal slices. To this purpose we measured extracellular lactate concentration using the lactate microbiosensors described in chapter 3. As can be observed in the representative recording of extracellular lactate concentration shown in **Fig. 4.5A**, we found that, as the concentration of glucose was increased in the perfusion media, extracellular lactate concentration increased in a stepwise fashion until saturation was achieved, revealing a dose-dependent behavior. To exclude the possibility of saturation of the lactate microbiosensor response, we added 2 mM lactate on top of the 15 mM

glucose, which elicited an increase in the signal confirming that it was still responsive to changes in lactate. At the end of the recording, both lactate and glucose were removed from the perfusion media and the current value was found to be lower than that observed in the presence of 0.5 mM

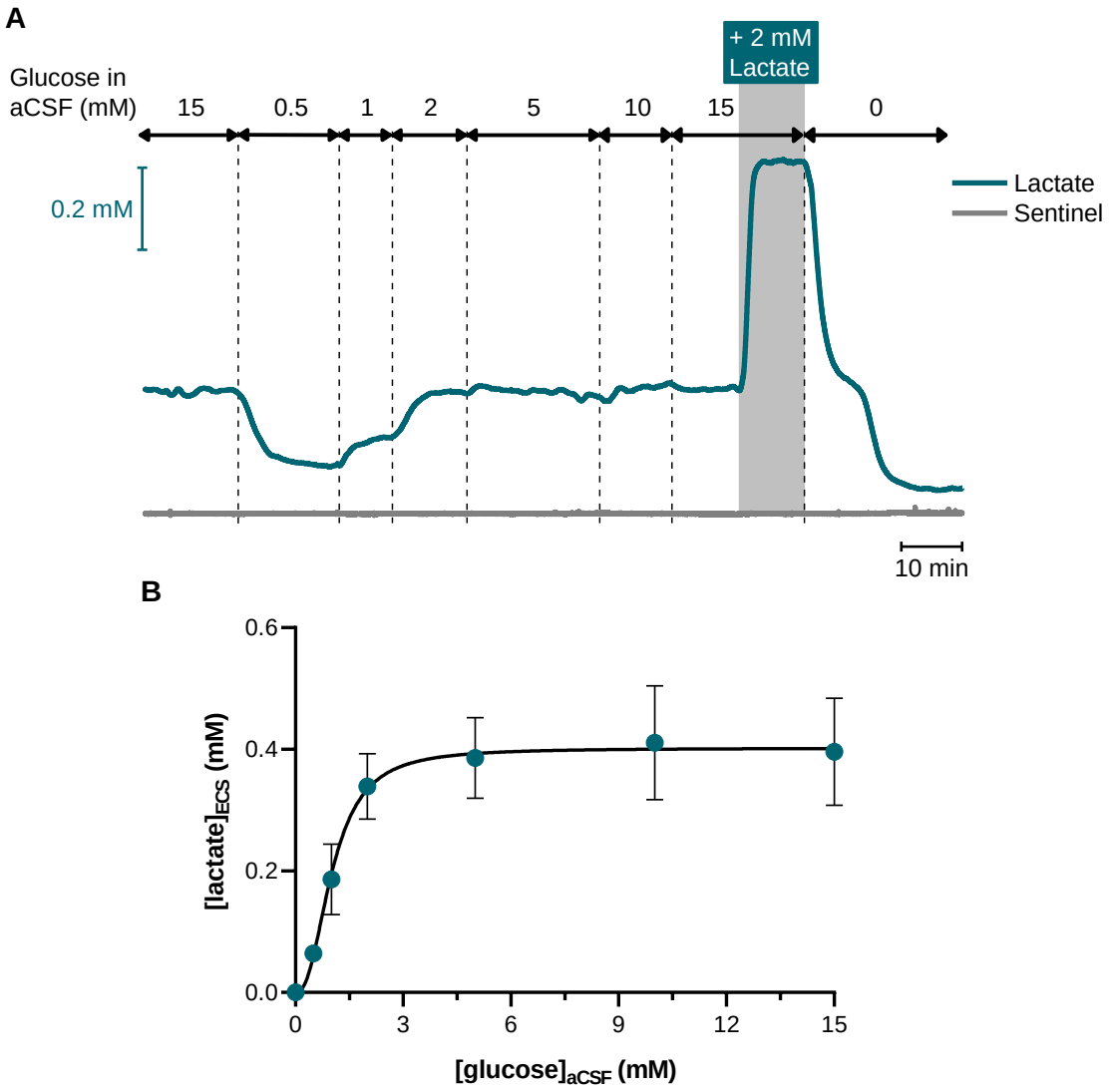

Fig. 4.5 – Measurement of lactate in the extracellular space of hippocampal slices. (A) Representative recording in hippocampal slice showing current recorded at the lactate microbiosensor (blue) and sentinel/null sensor (grey). Changes in extracellular lactate concentration were monitored as the concentration of glucose in perfusion aCSF was changed from 15 to 0.5 mM and then incrementally to 15 mM. To confirm that lack of further increase in signal at the lactate sensor was not derived from sensor saturation, 2 mM lactate were added, showing that the lactate sensor was still responsive to increasing lactate concentrations. At the end of the recording, both lactate and glucose were removed in order to estimate absolute zero concentration of lactate in the extracellular space. (B) Mean concentration of extracellular lactate concentration ($[lactate]_{ECS}$) determined for different aCSF glucose concentrations with curve fitting in black.

glucose, indicating that even under conditions of low glucose availability, the hippocampal cells actively produce and release lactate to the extracellular media. Fitting the curve $[glucose]_{aCSF}$ vs. $[lactate]_{ECS}$ showed that the maximum lactate concentration obtained is 0.37 ± 0.06 mM, with the half-maximum obtained with 0.81 ± 0.05 mM glucose (N = 8; **Fig. 4.5B**). **Table 4.1** shows the mean extracellular lactate concentration obtained for each glucose concentration. Thus, when glucose is readily available, in particular for the range expected to be found in the healthy brain, lactate concentration is maintained within a stringent range.

Table 4.1 - Effect of supplied glucose concentration ($[glucose]_{aCSF}$; mM) on hippocampal slice extracellular lactate concentration ($[lactate]_{ECS}$; mM).

$[glucose]_{aCSF}$ (mM)	$[lactate]_{ECS}$ (mM)
0.5	0.064 ± 0.001 (N = 8)
1	0.186 ± 0.058 (N = 4)
2	0.339 ± 0.054 (N = 8)
5	0.470 ± 0.053 (N = 5)
10	0.411 ± 0.093 (N = 5)
15	0.396 ± 0.088 (N = 5)

4.2.4. Lactate supports oxidative phosphorylation in hippocampal slices upon stimulation

Having shown that lactate is continuously extruded to the extracellular space in hippocampal slices and that neurons use lactate to support oxidative phosphorylation under resting conditions, we next investigated the role of lactate in supporting oxidative phosphorylation under conditions in which neural activity is increased. We stimulated hippocampal slices with glutamate (5 mM) and KCl (60 mM) and as can be observed in **Fig. 4.6A** both stimuli produced an immediate increase in tissue respiration. The maximal change in O_2 flux evoked by each stimulus was determined to be 83.6 ± 4.8 % for glutamate (N = 7) and 198.4 ± 12.73 % for KCl (N = 16; **Fig. 4.6B**). The increase incited by KCl was significantly higher ($P < 0.0001$) when compared to glutamate.

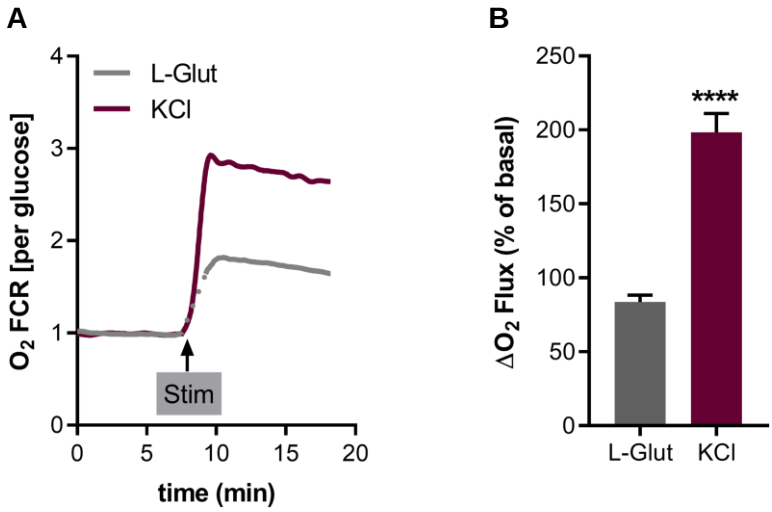

Fig. 4.6 – Stimulation of hippocampal slices increases basal O_2 flux. (A) Representative trace of O_2 flux normalized to glucose respiration level (O_2 Flux Control Ratio – FCR – per glucose) from slices in 15 mM glucose showing the effect of different stimuli (glutamate, 5 mM; KCl, 60 mM). (B) Percentage change in O_2 flux (ΔO_2 Flux) from basal elicited by each stimulus. ****P < 0.0001 for comparison between stimulation level with glutamate and KCl.

For each one of these conditions, we investigated the effect of lowering glucose concentration as well as that of adding lactate on the observed increase in O_2 flux. Stimulation of glutamate neurotransmission imposes an increase in energy demand in hippocampal slices, translated into an increase in O_2 flux. As can be observed in **Fig. 4.7A** in the grey columns, the percentage increase in O_2 flux induced by glutamate stimulation was similar for hippocampal slices respiring under conditions of low (0.5 mM) and high (15 mM) glucose (116.3 ± 11.9 %, N = 10 and 128.3 ± 13.8 %, N = 16, respectively). The addition of lactate allowed for a more robust increase in O_2 flux upon glutamatergic stimulation, most notability when glucose concentration was low ($F_{(1, 42)}$ = 6.559, P = 0.0141). Post-hoc analysis revealed that this increase was significant when adding lactate to low glucose (P < 0.05).

In order to access whether both neurons and astrocytes contribute to the increased O_2 flux observed upon glutamatergic stimulation, we inhibited oxidative phosphorylation in astrocytes with FC. Observing the orange columns in **Fig. 4.7A** we found that in the presence of FC the response to glutamate stimulation was lowered for all conditions ($F_{(1, 62)}$ = 22.24, P < 0.0001), indicating that under these conditions, both glia and neurons contribute to increased O_2 flux.

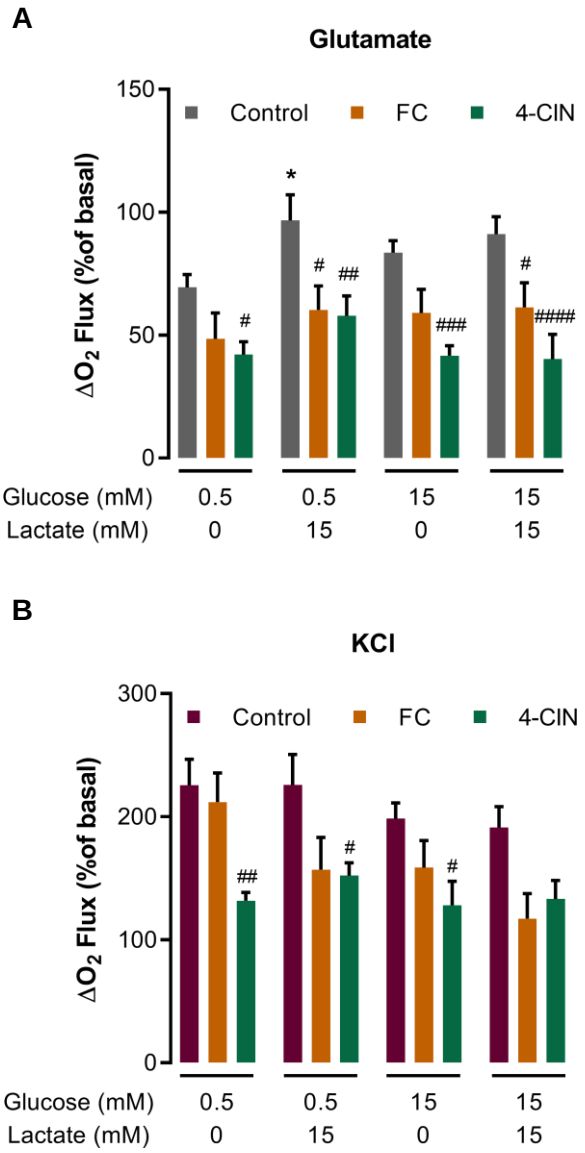

Fig. 4.7 – Stimulation of hippocampal slice respiration in response to glutamate or KCl. (A) Stimulation of O_2 flux by glutamate with 0.5 or 15 mM glucose, with or without lactate, in control conditions (grey) or with fluorocitrate (FC; orange) or 4-CIN (green). (B) Stimulation of O_2 flux by KCl with 0.5 or 15 mM glucose, with or without lactate, in control conditions (burgundy) or with fluorocitrate (FC; orange) or 4-CIN (green). Values are shown in percentage of basal flux (with glucose or glucose + lactate). *P < 0.05 for comparison to only glucose in the medium at the same concentration; #P < 0.05, ##P < 0.01, ###P < 0.001, ####P < 0.0001 for comparison to control with same substrate composition.

Post-hoc analysis revealed that this decrease was significant for conditions in which both glucose and lactate were present in the bathing media. Most interestingly, FC reversed the effect of adding lactate on top of glucose, suggesting that lactate is used by astrocytes to support energy metabolism upon glutamate stimulation. Similarly, inhibition of MCT2 (shown in green in **Fig.**

4.7A) limited the glutamate-evoked increase in O_2 flux in hippocampal slices ($F_{(1, 67)} = 59.44$, $P < 0.0001$), with substrate composition affecting the variance observed ($F_{(3, 67)} = 2.918$, $P = 0.0404$). This supports the notion that extracellular lactate enters neurons and is used to support oxidative phosphorylation under situations of increased energy demand such as those imposed by glutamatergic neurotransmission.

Stimulation of brain tissue with high K^+ concentration induces depolarization in neurons, which in turn leads to an increase in energy metabolism to support the activity of pumps and channels that re-establish ionic gradients. As shown by the burgundy columns in **Fig. 4.7B**, KCl stimulation produced an increase in O_2 flux under all conditions evaluated, and addition of lactate did not further increase O_2 flux. Inhibition of TCA in astrocytes using FC produced a tendency for limited increase in O_2 flux upon KCl-induced depolarization ($F_{(1, 43)} = 10.27$, $P = 0.0025$), with substrate composition also accounting for the variance observed ($F_{(3, 43)} = 3.13$, $P = 0.0353$), but no significant interaction between the two factors. These results suggest limited involvement of increased astrocyte oxidative phosphorylation in handling the increased energy demand imposed by K^+-evoked depolarization. On the other hand, blocking neuronal uptake of lactate by inhibition of MCT2 significantly restricted the increase in O_2 flux induced by KCl for all conditions ($F_{(1, 41)} = 37.5$, $P < 0.0001$), without being affected by substrate composition, which can be interpreted as a demonstration that neurons indeed use lactate as a substrate to increase respiration in response to KCl.

Considering that (1) stimulation with KCl produced a more robust increase in hippocampal oxidative metabolism, (2) glutamate may act as a metabolic substrate for astrocytes, confounding observed results, and (3) stimulation with glutamate produced inconsistent results in terms of observed changes in extracellular lactate concentration dynamics, as seen in chapter 3, we opted to focus on how stimulation with KCl affected exogenous extracellular lactate concentration dynamics in hippocampal slices, in the presence of 15 mM glucose in the perfusion media.

In the representative amperometric recording shown in **Fig. 4.8A**, perfusion of hippocampal slices with KCl induced an average net decrease in lactate (arrow "a" in **Fig. 4.8A**) of 0.36 ± 0.06 mM (N = 8). After stimulation (5 min) a transient lactate overshoot above baseline (arrow "b" in **Fig. 4.8A**) was observed, reaching a maximum increase from baseline of 0.23 ± 0.15 mM (N = 8) (**Fig. 4.8C**). Throughout the duration of the recording, no change in the recorded current at the sentinel sensor was observed, guaranteeing that changes recorded at the lactate sensor are solely the result of changes in extracellular lactate concentration.

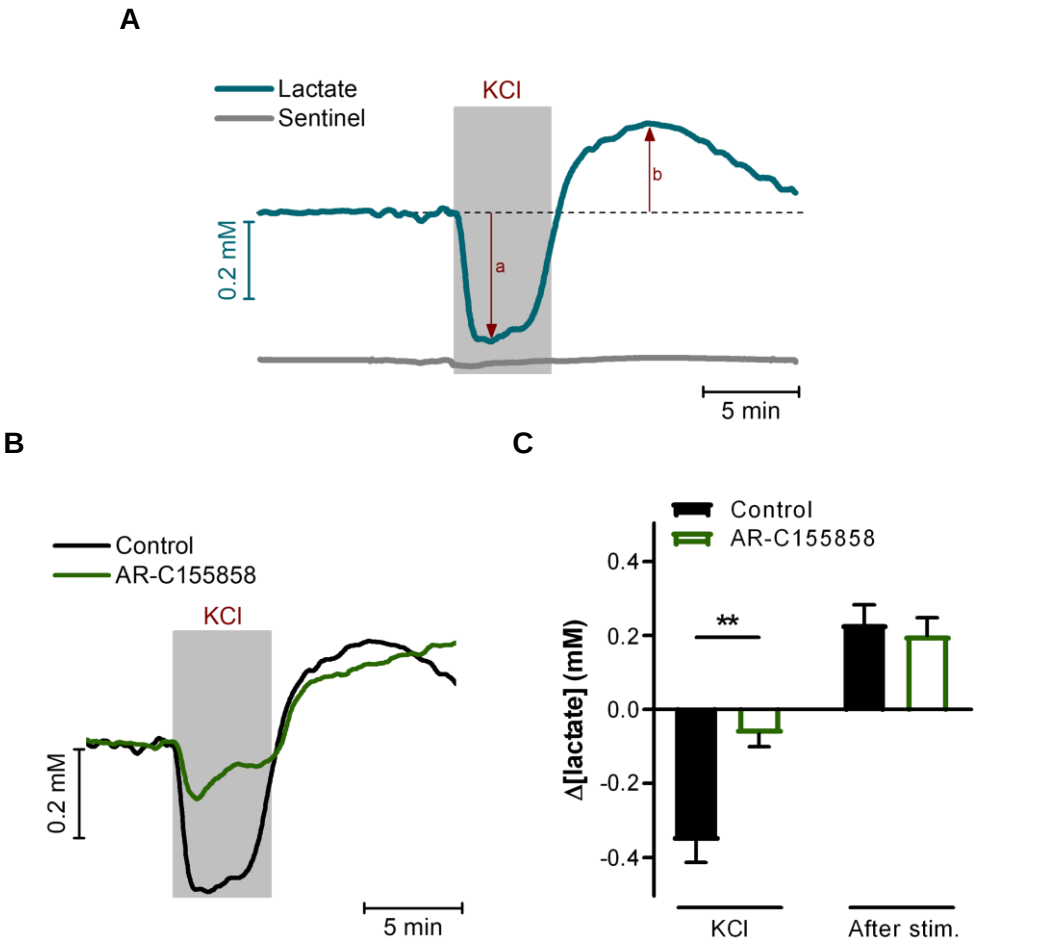

Fig. 4.8 – Changes in extracellular lactate concentration in hippocampal slices in response to K^+ stimulation, with 15 mM glucose in the perfusion media. (A) Representative recording of extracellular lactate concentration (in blue) with sentinel (in grey) and response to KCl stimulation. Grey block indicates period of KCl perfusion (5 min) and dashed black line shows extension of baseline from the lactate sensor. (B) Representative recording of extracellular lactate concentration observed upon KCl stimulation for control conditions (in black) and in the presence of AR-C155858 (in green) for neuronal lactate uptake inhibition. Grey block indicates period of KCl perfusion. (C) Mean maximal change in extracellular lactate (Δ[lactate], mM) observed during KCl stimulation (arrow "a" in A) and after stimulation (arrow "b" in A) for control conditions and in the presence of AR-C155858. **P < 0.01 for comparison between control and AR-C155858.

In order to confirm that the decrease in extracellular lactate concentration observed upon stimulation resulted from neuron uptake, we inhibited neuronal lactate uptake using the MCT2 inhibitor AR-C155858. This is a potent inhibitor for MCT2 (K_i < 10 nM) and MCT1 (K_i = 2.3 nM), but does not inhibit MCT4 (Ovens et al. 2010). In this case, 4-CIN (used above in respirometry studies) could not be used due to its interference in the electrochemical measurements, since it is electroactive. As can be observed in **Fig. 4.8B** and **C**, inhibition of

neuronal lactate uptake hindered the net consumption of extracellular lactate by hippocampal slices upon KCl stimulation ($N = 6$; $P < 0.01$). Furthermore, no significant difference was seen for the overshoot phase. Taken together, this shows that the initial decrease in lactate is the result of uptake by neurons, however, the subsequent increase in extracellular lactate is not derived from neurons, leaving astrocytes to be the source.

.

4.3. Discussion

Understanding neurometabolism in physiology and pathophysiology is a challenging endeavor, namely when considering the intricate metabolite fluxes that are proposed to occur between the main cellular elements of the brain tissue: neurons and astrocytes. This implies that valuable information can be uncovered from studies in preparations such as brain slices. In the present work we investigated the putative role of lactate as a metabolic fuel in the hippocampus, a structure of the temporal lobe implicated in memory and learning and sensitive to damage in brain pathologies such as neurodegeneration in Alzheimer´s disease or sclerosis in temporal lobe epilepsy (Scheff and Price 2006; Dawe et al. 2020; Ren and Curia 2021).

To this purpose we used high-resolution respirometry to evaluate oxidative metabolism at the whole tissue level to determine how different substrate combinations (glucose and lactate) modulate respiration in hippocampal slices. To our knowledge, such studies have never been done in a closed chamber environment and measuring whole tissue O_2 consumption. As compared to *in vivo* studies, the merit of using slice preparations resides mainly on the fact that the composition of the extracellular milieu can be easily modulated, as explored in the present study. Additionally, the lack of cerebral blood flow removes the confounding effects that can arise from glucose and lactate supply from the blood stream, allowing the focus to be on the neuron-astrocyte interplay. Additionally, we evaluated extracellular lactate dynamics using carbon fiber microelectrode-based lactate biosensors to better understand how changes in oxidative phosphorylation relate to lactate production and consumption by different cell types.

We observed that O_2 consumption in hippocampal slices could be modulated by decreasing glucose concentrations. A previous report had failed to see such a dependency in brain tissue (Levasseur et al. 2006). However, the authors used thicker tissue slices, air O_2 concentration, no buffering system in the medium, and a higher range of glucose concentrations (1.1-100 mM as compared to 0.1-15 mM used here). Additionally, the high-resolution respirometer used in the present study has improved time and signal resolutions as compared to the "Cartesian diver" microrespirometer used by the authors, which may have allowed us to discriminate small differences not observable with other equipment. Interestingly, we observed that the extracellular concentration of lactate also varies as a function of glucose concentration between 0.5 and 5 mM and saturated for higher concentrations of glucose. In fact, the maximal extracellular concentration of lactate measured in hippocampal slices was 0.37 mM and half-maximal concentration was achieved for a glucose concentration of 0.81 mM. In the brain of normoglycemic rodents, the extracellular concentration of glucose *in vivo* is reported to range

between 0.5 to 4.4 mM (Silver and Erecińska 1994; McNay and Gold 1999; Kirchner et al. 2006; Slais et al. 2008), while values for extracellular lactate range from 1 mM to 3 mM (Abi-Saab et al. 2002; Dong et al. 2003; Zilberter et al. 2010). Of course, *in vivo* extracellular levels also reflect glucose and lactate levels in plasma. However, our data shows that from the standpoint of neural cells, extracellular lactate concentration is maintained in a relative narrow range of concentrations. This limitation may be due to a limited glycolytic capacity. For example, the K_M of brain hexokinase is only 0.03 mM (Wilson 2003). Interestingly, the glucose concentration range for which oxidative phosphorylation is limited (<0.5 mM) is also that for which extracellular lactate levels are quite sensitive to glucose concentration. Thus, we can conclude that, at least in the hippocampus, aerobic glycolysis is continuous, even at rest, maintaining a steady state concentration of extracellular lactate available to fuel oxidative metabolism.

While glucose is classically viewed as the main energy substrate in the brain, lactate can also be an energy source for brain metabolism (McIlwain, 1953; van Hall et al., 2009) and, in hippocampal slices, it can sustain synaptic activity as a sole energy substrate (Schurr et al. 1988). We observed not only that basal O_2 consumption can be maintained with lactate, but also that lactate (15 mM) can further stimulate O_2 consumption in the presence of glucose. This is in accordance to what has been observed in excised sympathetic ganglia, where the total CO_2 output from the tissue was higher when both glucose and lactate were present (Larrabee 1996). Elevated blood lactate concentrations can be achieved *in vivo* with exercise and enter the brain parenchyma, reaching concentrations as high as 20 mM (Rasmussen et al. 2010; Dienel 2019).

As has been largely discussed, different brain cells appear to display different metabolic profiles: while neurons are more oxidative, astrocytes rely mostly on glycolysis (reviewed in (Magistretti and Allaman 2015)). As expected, we found that inhibition of MCT2, the monocarboxylate transporter isoform expressed in neurons, led to a decrease in O_2 flux for all conditions tested, with most robust inhibition observed for low glucose concentration, suggesting that under these conditions not only is lactate being produced to the extracellular media, but is actively supporting neuronal oxidative phosphorylation. Interestingly, blocking oxidative phosphorylation in astrocytes with FC produced the most robust inhibition of tissue O_2 consumption when low glucose was supplemented with lactate, while for all other conditions, the expected 25% inhibition was observed (Serres et al. 2007; Ivanov et al. 2014). Fluorocitrate inhibits aconitase activity and is only taken up by glia, without affecting neuronal activity (Stone et al. 1990; Hassel et al. 1995; Fonnum et al. 1997). This observation suggests that when available glucose is low, astrocytes will also use available lactate to fuel oxidative metabolism. The K_M for lactate transport of MCT4 (the MCT isoform more prevalent in astrocytes) is higher than the lactate concentration used here (~22-28 mM) (Dimmer et al. 2000; Pérez-Escuredo et al. 2016), although recent studies indicate

that this K_M value may be in the lower mM range (Contreras-Baeza et al. 2019). Accordingly, an increase in cytosolic lactate has been observed when astrocytes were exposed to 10 mM lactate (Sotelo-Hitschfeld et al. 2015). This phenomenon has also been observed *in vivo* with an increase in blood lactate resulting in an increase of intracellular lactate in astrocytes (Mächler et al. 2016). Both stimulation of glutamatergic neurotransmission and depolarization with high [K^+] significantly increased hippocampal slice respiration for all substrate conditions, including low glucose (0.5 mM), despite the fact that synaptic function has been shown to be silenced in hippocampal slices when glucose concentration is lowered below 2 mM (Schurr et al. 1989; An et al. 2008). Astrocytes uptake glutamate through active transporters (GLAST and GLT1) that are Na^+-dependent (Danbolt 2001; McKenna 2013), with Na^+ gradients then being re-established by the Na^+/K^+-ATPase (McKenna 2013). This energetic expenditure is compensated by a portion of glutamate being metabolized by astrocytes, after being converted to α-ketoglutarate and entering the TCA cycle (as reviewed in (Dienel 2013; McKenna 2013)). Therefore, the increased O_2 consumption observed with glutamate might be due not only to neuronal activation but also to glutamate metabolism by astrocytes. Adding lactate led to a more robust increase in O_2 flux in response to glutamate for both low and high glucose, suggesting that lactate is used to satisfy the increased energetic demand provoked by glutamatergic activity in slices, in good agreement with previous studies showing that lactate in the presence of glucose significantly increased the O_2 consumption, NAD(P)H oxidation phase, and efficacy of synaptic transmission during prolonged stimulation (Ivanov et al., 2011).

Inhibition of astrocytic oxidative phosphorylation hindered the increase in O_2 consumption, suggesting that at least part of the response results from increased astrocytic oxidative metabolism. Since this was more evident when lactate was added, we hypothesize that astrocytes also use lactate to fuel oxidative metabolism upon glutamatergic stimulation, particularly when extracellular lactate is high (in line with the low affinity MTC found in these cells). Increased O_2 consumption with glutamate has also been observed in astrocytes in culture (Eriksson et al. 1995). Contradictorily, another study showed that cortical astrocytes in culture display a decrease in O_2 consumption in response to glutamate (Azarias et al. 2011). However, these results were obtained in a different medium (DMEM) and with pyruvate present.

On the other hand, the blunted glutamate-evoked O_2 consumption response observed under MCT2 inhibition with 4-CIN clearly demonstrated neuronal use of extracellular lactate as an energetic fuel. The fact that the effect of 4-CIN was evident even when lactate was not added to the media suggests that hippocampal cells actively consume glucose and extrude lactate, as already suggested by Pellerin and Magistretti and many others (Pellerin and Magistretti 2012; Magistretti and Allaman 2018; Barros and Weber 2018).

Stimulation with high K^+ concentration caused a more robust increase in tissue O_2 consumption, consistent with previous reports in brain slices (Ashford and Dixon 1935; Dickens and Greville 1935; Hertz and Schou 1962). High K^+ (60 mM) depolarizes neurons and stimulates both neuronal and astrocytic metabolism, as demonstrated using neuronal and neuron-glial mixed cultures (Honegger and Pardo 1999).

Contrary to what was observed with glutamate-stimulation, adding lactate did not further increase O_2 consumption response to high KCl concentration, most likely due to the fact that K^+ stimulates lactate release from astrocytes (Sotelo-Hitschfeld et al. 2015), which appears to not involve MCT. Inhibition of oxidative metabolism in astrocytes revealed that these cells are responsible for a fraction of the increased O_2 consumption in response to stimulation with KCl for all conditions, except for when glucose concentration is low. In fact, it has been previously observed that a higher concentration of K^+ induced an increase in O_2 consumption by cultured astrocytes, in the presence of only glucose (7 mM) (Hertz et al. 1973). Considering that for low glucose FC could inhibit basal O_2 consumption but had no effect on the response to KCl stimulation, one might speculate that under the latter condition, all glucose consumed by astrocytes may be diverted to lactate to be extruded to the extracellular space, thus decreasing astrocytic oxidative metabolism. Indeed, we observed that 0.5 mM glucose limits the availability of extracellular lactate to a great extent. It has also been previously observed that K^+ leads to a stimulation of astrocytic ATP accumulation, while O_2 consumption by these cells is inhibited, due to glycolytic stimulation via the Na^+-bicarbonate cotransporter NBCe1 (Fernández-Moncada et al. 2018). However, the concentration of K^+ used in this case was much lower, which can make a difference as discussed before (Hertz et al. 2013). Another interesting observation is that the effect of FC seems to be higher whenever lactate is present, supporting the assertion that astrocytes can consume lactate when its concentration is greatly increased above the K_M of the MCT4 and MCT1 expressed in these cells (Dimmer et al. 2000; Bergersen 2015; Pérez-Escuredo et al. 2016), as is expected to be observed following exercise.

Using microbiosensors we were also able to investigate the effect of KCl stimulation on extracellular lactate dynamics, which reflects the net balance between lactate release and uptake by the different cell types in the hippocampal slice. We found that KCl led to an initial decrease in extracellular lactate, indicating a net consumption of lactate by the tissue, followed by an overshoot. A similar pattern was previously observed in freely moving animals with long-term potentiation in the dentate gyrus of the hippocampus (Bingul et al. 2020).

Inhibition of neuron lactate uptake diminished not only the KCl-evoked increase in O_2 flux as well as the decrease in extracellular lactate, corroborating that lactate is indeed transported into

neurons to fuel oxidative metabolism in response to depolarization. The lack of effect of neuronal MCT inhibition on the lactate overshoot suggests that this is the result of astrocytic release.

4.4. Conclusions

The role of lactate in brain oxidative metabolism is still not entirely understood. In this chapter we investigated how lactate is used to support the metabolic demands both at rest and upon stimulation by measuring tissue O_2 consumption and extracellular lactate concentration dynamics in hippocampal slices, a preparation that better represents a physiological setting compared to cell culture and that allows a precise modulation of the extracellular fluid.

Our results show that glucose concentration modulates the rate of tissue O_2 consumption within a limited and physiological range as well as the extracellular lactate concentration, supporting the notion that lactate is continuously released to the extracellular space in brain tissue, independent of system supply. Furthermore, increasing extracellular lactate concentration increases the rate of respiration at rest independently of glucose concentration. In response to stimulation, astrocytes can consume lactate, at least when present in a higher concentration. Additionally, it was clearly demonstrated that neurons can use lactate to better respond to the metabolic demands created by stimulation.

In conclusion, the work in this chapter shows that glucose is continuously converted to lactate through aerobic glycolysis in neural cells (most likely astrocytes) and released to the extracellular space in the hippocampus to be used as an oxidative substrate by neurons under both resting and stimulation.

4.5. Future Directions

The impact of glutamate in astrocytic oxidative metabolism could be further studied by inhibiting its uptake. The lactate dynamics in response to stimulation could be evaluated using other types of stimulation paradigms, as we have seen differences between stimulation with glutamate and KCl. Furthermore, these studies would greatly benefit from combining information on the dynamics of both extracellular and intracellular lactate concentrations.

5. Modulation of Oxidative Neurometabolism in Ischemia/Reperfusion by Nitrite

5.1. Introduction

Stroke is one of the leading causes of mortality and morbidity worldwide (Feigin et al. 2021). Ischemic stroke, the most common type of stroke, is caused by a temporary or permanent interruption of blood supply to a part of the brain, resulting in tissue damage. The brain is particularly susceptible to loss in blood supply, since it relies heavily on O_2 and glucose for energy production, while lacking energy reserves (Kalogeris et al. 2012). Rapid restoration of blood supply (reperfusion) is then needed to re-establish O_2 and glucose delivery to avoid neuronal death. Reperfusion commonly occurs spontaneously after stroke or can be achieved through surgical procedures or with medication (Lin et al. 2016). While reperfusion is necessary to restore cell metabolism and avoid cell death, it can also have deleterious effects and aggravate brain damage. This is demonstrated, for example, by the fact that the infarct volume was increased with reperfusion compared to permanent occlusion with middle cerebral artery occlusion (MCAO) in the rat (Zhang et al., 1994). As such, the ideal therapeutic strategy consists in restoring blood supply while minimizing the damage from reperfusion.

One major source of damage after ischemia/reperfusion (I/R) is the production of oxidants and ROS[1] in mitochondria, particularly along the ETS (Cadenas and Davies 2000; Sanderson et al. 2013). When the supply of O_2 is reduced during ischemia, the limited transfer of electrons through complex IV leads to an upstream accumulation of electrons, resulting in a reduced ETS. With reperfusion, there is a rapid increase in transfer of electrons as O_2 is again available as the final electron acceptor, resulting in increased ROS production (Kunimatsu et al. 2011). As such, inhibiting the sources of ROS in the ETS can be protective in I/R.

The burst of ROS production upon reperfusion from the ETS is mainly due to $O_2^{\bullet -}$ production, which has been observed in various tissues and types of I/R injury (Chouchani et al. 2016). Superoxide radical can suffer spontaneous or catalyzed dismutation to H_2O_2 and O_2 but can also generate $ONOO^-$, a strong oxidant and nitrating species which is produced in the diffusion-limited reaction with $^{\bullet}NO$ (Murphy 2009; Kalogeris et al. 2012). There are a few possible sites for ROS production within mitochondrial ETS, but complex I is generally recognized one of the main source of ROS upon reperfusion (Chouchani et al. 2016; Galkin and Moncada 2017).

Nitric oxide is proposed to exert multiple direct and indirect effects on the complexes of the ETS, thus regulating mitochondrial function. Besides binding to complex IV in competition with O_2, $^{\bullet}NO$ can also inhibit complex I through nitrosation of critical thiols in this complex (Shiva et al.

[1] Please note that the term reactive oxygen species (ROS) includes, among other species, signaling physiological species, such as hydrogen peroxide and superoxide radical. These species are involved in redox signaling, contrary to other more reactive species that most likely do not participate in redox signaling (Egea et al. 2017).

2007b; Galkin and Moncada 2017). Importantly, this might be a reversible process and complex I activity can be restored by thiol-reducing agents (Galkin and Moncada 2007). Irreversible inhibition of complex I can also occur through nitration by $ONOO^-$, but this process is prevented if nitrosation occurs first that results in protection of critical thiols to nitration (Galkin and Moncada 2017; Galkin 2019). As mentioned, •NO can also reversibly inhibit O_2 consumption in conditions of low O_2 concentration through competitive inhibition of cytochrome *c* oxidase, the complex IV of the respiratory chain in mitochondria (Antunes et al. 2004; Brunori et al. 2006; Taylor and Moncada 2010). The latter happens due to the binding of •NO to the binding site of O_2 when cytochrome *c* oxidase is in its reduced form. This competition allows for a fine tuning of mitochondrial respiration and a redistribution of O_2 toward locations with higher demand (Giulivi 2003; Victor et al. 2009).

Classically, •NO is synthesized by a family of nitric oxide synthases (NOS) in an O_2 dependent reaction. However, nitrite can be a bioprecursor of •NO, particularly under acidic conditions caused by hypoxia (Lundberg et al., 2008), a situation in which the enzymatic pathway for its synthesis by NOS is attenuated due to low availability of O_2. Thus, the one-electron reduction of nitrite to •NO poses as a physiological mechanism that ensures •NO production when O_2 bioavailability is not sufficient (Shiva, 2013). Nitrite concentration *in vivo* can be increased through diet, and although it is present in cured meats, the main source of nitrite is green leafy vegetables. These contain nitrate that can be reduced to nitrite by commensal bacteria in saliva. Nitrate in circulation is secreted and concentrated in salivary glands, where these nitrate reductase-containing bacteria reduce it to nitrite which is then absorbed back into circulation (Lundberg et al. 2008). Increasing nitrite in circulation leads to its accumulation in various organs, including the brain (Bryan et al. 2005). On the other hand, plasma levels of nitrate and nitrite can originate from endogenous sources via oxidation of •NO. For instance, under inflammatory conditions where there is induction of iNOS or during regular exercise (Jungersten et al., 1997), which stimulates eNOS expression and activity (Green et al., 2004).

Nitrite has been shown to have a protective effect in situations of brain I/R. Nitrite administered at the time of reperfusion was shown to reduce infarction volume, increase local cerebral blood flow, and improve cognitive function after middle cerebral artery occlusion in rats (Jung et al. 2006). These effects were dependent on •NO and were not achieved with an equal amount of nitrate. However, the mechanism through with nitrite exerts this protection in brain I/R remains unclear. One putative target for its protective bioactivity is through modulation of mitochondrial respiration and hence ROS production. Nitrite has been shown to reduce *in vivo* brain ROS production after cardiac arrest (Dezfulian et al. 2016). This reduction in ROS production is

associated with inhibition of complex I through nitrosation (Shiva et al. 2007b; Chouchani et al. 2013).

Considering the modulation of mitochondrial respiration by •NO and •NO-derived species as well as the univalent redox conversion between nitrite and •NO, we have hypothesized that the protective action of nitrite in brain I/R might include the regulation of mitochondrial function, particularly at the level of respiration. For the experimental verification of the hypothesis, we used high-resolution respirometry to evaluate the effects of nitrite on brain tissue respiration in conditions of I/R in hippocampal slices. The experimental design involved firstly the evaluation of the effect of nitrite during hypoxia and then in the I/R model. In an attempt to elucidate the mechanism/sites of nitrite action, we used permeabilized hippocampal slices and evaluated the effect of nitrite on complex I-linked respiration during and after I/R. As nitrate is a source of nitrite, the effect of dietary nitrate was also evaluated.

5.2. Results

5.2.1. Effect of nitrite on respiratory states under chronic hypoxia

In a first set of experiments, we asked whether nitrite could modulate respiratory rates in hippocampal slices both under situations of high and low (hypoxic) O_2 concentrations. Typically, because O_2 has to diffuse from the perfusion media towards the inner slice cell layers, experiments with brain slices are conducted at high O_2 concentrations in the perfusion/bathing media (in this case, 700-800 µM) to ensure proper oxygenation of the tissue core (Ledo et al. 2005). As a model of hypoxia, we used a lower O_2 concentration in the bathing medium (150 µM; low [O_2]) and determined the effect on basal respiration (Routine), maximal respiration (ET capacity) and non-ETS O_2 consumption (ROX). As can been seen in **Fig. 5.1**, significant decreases in Routine respiration ($P < 0.0001$) and ET capacity ($P < 0.001$) were observed when O_2 concentration was decreased. Both these parameters were corrected by subtracting ROX to eliminate the contribution of non-ETS O_2 consumption. Although there was a tendency for a decrease in ROX with low O_2 concentration, this was not statistically significant. Uncoupling respiration to determine ET capacity led to a significant increase from Routine respiration for both high and low O_2 concentration ($P < 0.0001$; **Fig. 5.1A** and **B**).

Considering its proposed protective role in ischemia, we evaluated the effect of nitrite (10 and 100 µM) on slice O_2 consumption under both conditions of O_2 concentration. While 10 µM of nitrite might be considered a supraphysiological concentration *in vivo*, 100 µM is definitely an exceedingly high concentration. However, we are using a model system and have chosen this high concentration so that nitrite would not be limiting and would also allow to evaluate whether the effect of nitrite was concentration dependent.

With regards to Routine respiration (**Fig. 5.1A**), the higher nitrite concentration (100 µM) produced a non-significant decrease in O_2 consumption at high O_2 concentration while at low O_2 concentration no significant effect was observed for either nitrite concentration. Similarly, addition of nitrite had no effect on ET capacity (**Fig. 5.1B**) nor the residual O_2 consumption (ROX; **Fig. 5.1C**) under both high and low O_2 concentration.

Altogether, these results show that limiting O_2 delivery to hippocampal tissue results in decreased O_2 consumption. As for nitrite, it seems to have no significant effect on O_2 consumption under the conditions tested.

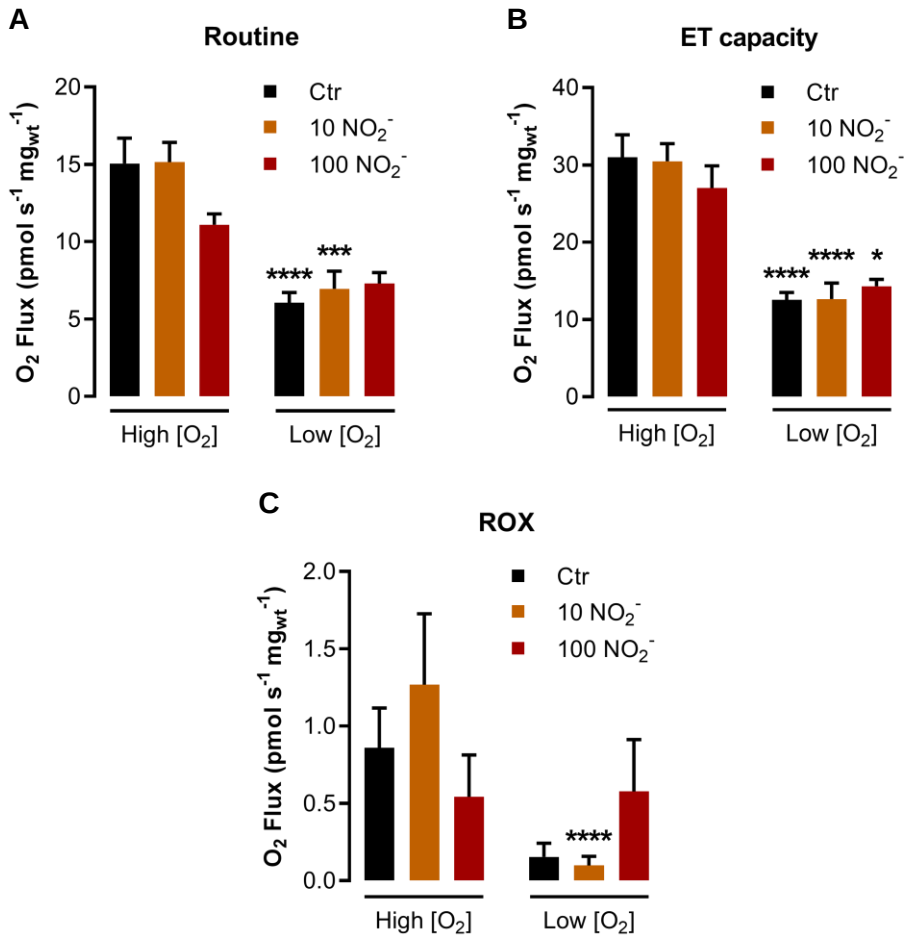

Fig. 5.1 – Changes in tissue O_2 flux as a function of O_2 concentration and nitrite (10 or 100 µM) at different states. (A) Routine respiration (basal respiration) after a stable O_2 flux was obtained corrected for ROX (non-ETS O_2 consumption). (B) ET capacity (maximal respiration) after uncoupler titration corrected for ROX. (C) ROX (residual O_2 consumption) after inhibition of complex I with rotenone and complex III with antimycin A. *P < 0.05, ***P < 0.001, ****P < 0.0001 compared to high [O_2].

5.2.2. Modulation of hippocampal slice respiration by nitrite in a model of ischemia/reperfusion

As discussed before, the damage occurring during ischemia is aggravated by subsequent reperfusion. As such, we evaluated the putative protective effect of nitrite in a model of I/R in hippocampal slices. Nitrite can be reduced to •NO in the presence of reductants such as ascorbate (AA) under the hypoxic conditions observed during ischemia, in particular due to the lowering of local *p*H and according to the following equations (Lundberg et al. 2008):

$$NO_2^- + H^+ \rightarrow HNO_2 \quad (7)$$

$$2HNO_2 + \text{Ascorbate} \rightarrow 2\,\dot{N}O + \text{dehydroAscorbate} + 2H_2O \quad (8)$$

We hypothesize that •NO resulting from this reaction can then inhibit ETS complexes, modulating the production of reactive species that has been described to occur upon reperfusion.

Hippocampal slices were subject to a period of O_2 and glucose deprivation (OGD) to simulate ischemia, followed by addition of both glucose and O_2 to simulate reperfusion. We first optimized the duration of OGD. Slices were transferred from the pre-incubation chamber (in which they are maintained at normal glucose and O_2 concentrations) into the recording chamber containing media with zero glucose and zero O_2 (OGD conditions). The slices were maintained under OGD conditions for different time periods (5, 10, 15, and 30 min), following which glucose and O_2 were added to the recording chamber to mimic reperfusion. Additionally, a control experiment was performed in which reoxygenation was performed immediately after adding slices to the recording chamber (0' OGD), in order to determine the effect of changing the O_2 concentration in the chamber for re-oxygenation on O_2 flux.

As can be observed in (**Fig. 5.2A**), O_2 flux is null during the period of OGD and upon reperfusion a significant increase is observed, that then slowly decreases and stabilizes. Only 15 min of OGD (15'OGD) produced a significant difference in the reperfusion phase when compared to 0'OGD (**Fig. 5.2B)**. In these conditions, OGD led to an increase in O_2 flux - oxidative burst - that was visible at 6 min after the start of reoxygenation (the first time point in which it was possible to measure O_2 consumption; $P < 0.001$). For each condition, we determined the O_2 flux at 6 and 15 min after reoxygenation and values are plotted in **Fig. 5.2C**, highlighting that only for the 15 min OGD protocol was there a significant ($P < 0.01$) increase in flux at both time points. As such, from this point forward we used 15'OGD followed by replenishment of O_2 and glucose as a I/R model in hippocampal slices.

To ensure that this burst of O_2 consumption was associated with the ETS and not to other O_2 consuming reactions, we performed OGD in the presence of rotenone (Rot) or azide (Azd), inhibitors of complexes I and IV, respectively. Under both conditions, a significant decrease in the O_2 consumption was observed (**Fig. 5.2B and C)** compared to all other conditions.

Following stabilization of O_2 consumption after OGD, we evaluated basal respiration (Routine, R), maximal respiration (ET capacity, E) and residual O_2 consumption (ROX) for 0' and 15'OGD – **Fig. 5.2D**. At this time point (~40 min after reoxygenation) all parameters were similar between control and OGD, indicating that the observed changes in O_2 flux were transient and limited to the moment immediately following reoxygenation.

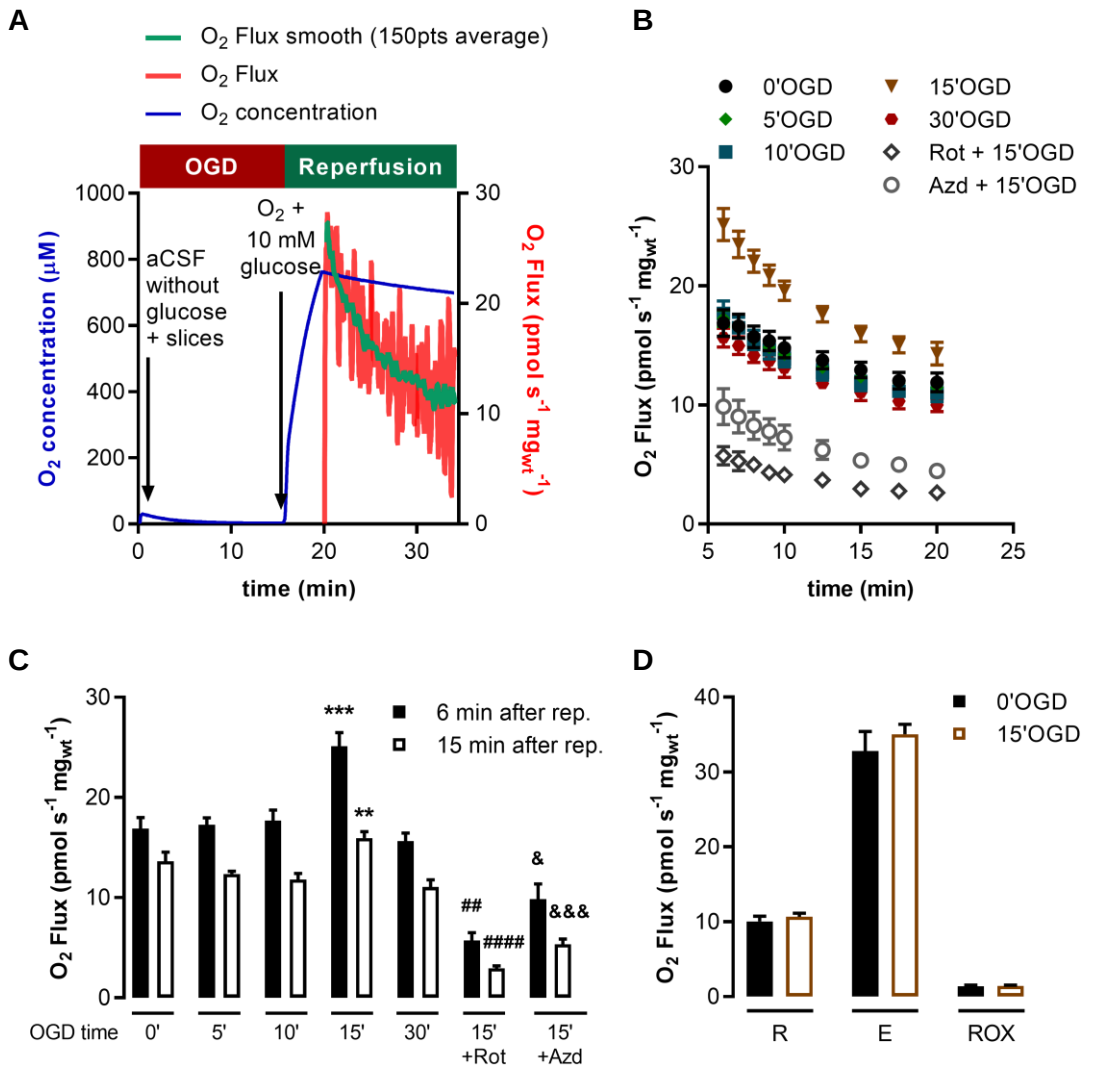

Fig. 5.2 – Oxygen and glucose deprivation (OGD) for 15 min and reperfusion in hippocampal slices leads to a burst in respiration after reoxygenation with glucose. (A) Representative trace with O_2 concentration (in blue) and O_2 flux (in red) smoothed (150 pts average) to reduce noise (in green). (B) Oxygen flux measured following different OGD times (0, 5, 10, 15, and 30 min) and with inhibition of respiratory complexes I by rotenone (Rot) and IV by azide (Azd). The time points shown correspond to O_2 flux after the start of reoxygenation. (C) Analysis of O_2 flux at 6 and 15 min after the start of reoxygenation. (D) Analysis of respiratory states after O_2 flux was stable (R – Routine, E – ET capacity, ROX – residual oxygen consumption). $^{**}P < 0.01$, $^{***}P < 0.001$ in comparison to all other conditions at the same time point; $^{\#\#}P < 0.01$, $^{\#\#\#\#}P < 0.0001$ in comparison to all other conditions at the same time point, except for 15'OGD + Azd; $^{\&}P < 0.05$, $^{\&\&}P < 0.001$ in comparison to all other conditions at the same time point, except for 15'OGD + Rot.

We then evaluated whether nitrite had any modulatory effect on the "burst phase" of O_2 consumption and have used two concentrations (10 and 50 µM). Firstly, we found that nitrite had no effect on the O_2 flux measured under control conditions (0'OGD; **Fig. 5.3A**, **B** and **C**). However, in the brain slice I/R model the presence of nitrite significantly decreased the oxidative burst (15'OGD; **Fig. 5.3A, D** and **E**). At 6 min after reoxygenation (**Fig. 5.3D**), the decrease in the oxidative burst was only significant with 50 µM nitrite ($P < 0.05$; N = 10), while for 15 min after reoxygenation (**Fig. 5.3E**) this decrease was significant for both 10 ($P < 0.05$; N = 11) and 50 µM nitrite ($P < 0.01$; N = 10). As before, the changes in Routine respiration, ET capacity and ROX were also evaluated after a stable O_2 flux had been obtained (**Fig. 5.3F**-**H**). We observed no significant changes in any of these parameters in the presence of nitrite, supporting that the observed changes are not the result of nitrite-induced toxicity.

Considering that nitrite can be reduced to •NO under conditions such as those observed in I/R, we used two •NO scavengers, namely myoglobin (Myo, 150 µM) and carboxy-PTIO (C-PTIO, 1mM) to investigate this possibility. We found that both Myo (**Fig. 5.4A**) and C-PTIO (**Fig. 5.4B**) decreased the oxidative burst observed for 15'OGD, both at 6- and 15-min following reperfusion (**Fig. 5.4C and D**). This decrease in oxidative burst was statistically significant for C-PTIO. Overall, neither Myo nor C-PTIO had any significant effect in the presence of nitrite, but it is apparent that myoglobin in the presence of nitrite allows an increased O_2 flux. Quite interestingly, the effect of nitrite, Myo and C-PTIO on the oxidative burst are similar. These results are somehow controversial and may be due to other reactions involving the scavengers used, in addition to the mere inactivation of •NO. For example, in certain conditions both C-PTIO and myoglobin can embark in redox reactions promoting the transitions between •NO and nitrite, and these reactions might be further influenced by O_2 changes.

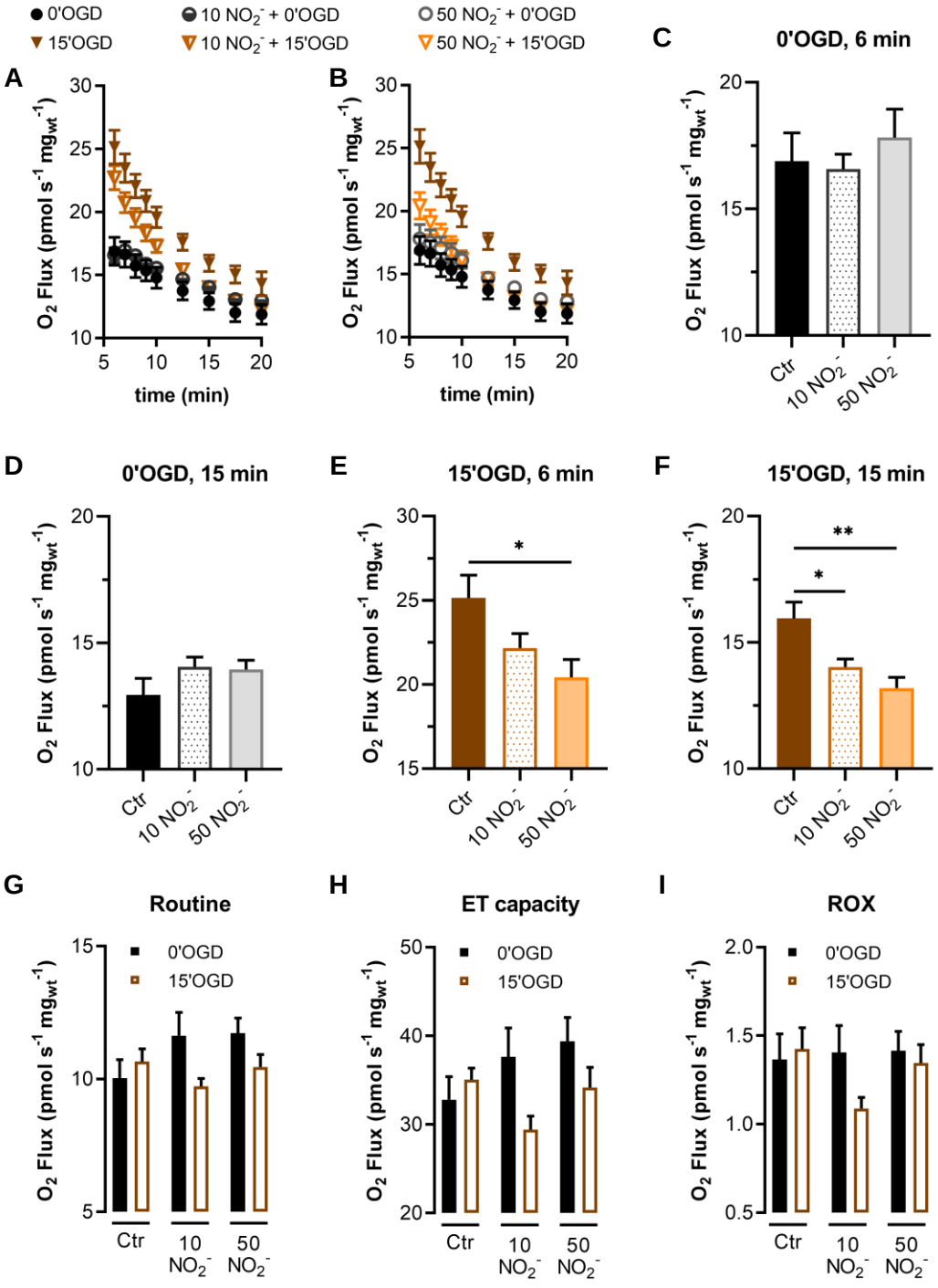

Fig. 5.3 – Nitrite decreases the burst in respiration following OGD/reperfusion in hippocampal slices. Effect of nitrite on respiration in control (0'OGD) or after 15 min of OGD (15'OGD) and reoxygenation with glucose (the time points shown correspond to O_2 flux after the start of reoxygenation) in the presence or absence of 10 µM (A) or 50 µM nitrite (B). Analysis of O_2 flux for 0'OGD at 6 min (C) or 15 min (D) after start of reoxygenation. Analysis of O_2 flux for 15'OGD at 6 min (E) or 15 min (F) after start of reoxygenation. Analysis of Routine (G), ET capacity (H), and ROX (I) after O_2 flux was stable. *$P < 0.05$, **$P < 0.01$ for comparison to control.

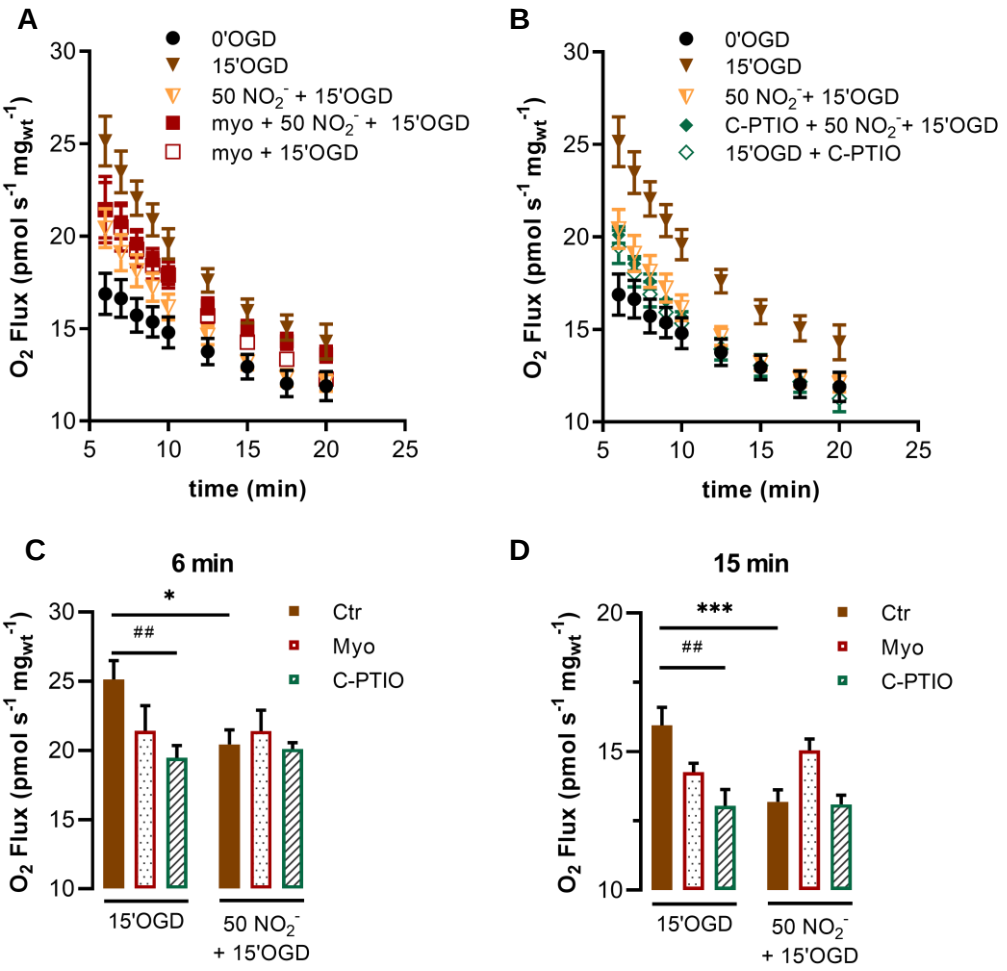

Fig. 5.4 – Effect of nitrite on the respiration burst after OGD and reperfusion dependence on •NO. (A) Effect of myoglobin (150 µM; added before OGD) on respiration after 15 min. of OGD and reoxygenation with glucose (the time points shown correspond to O_2 flux after the start of reoxygenation) in the presence or absence of 50 µM nitrite. (B) Effect of C-PTIO (1 mM; added before reoxygenation) on respiration after 15 min. of OGD and reoxygenation with glucose in the presence or absence of 50 µM nitrite. Comparison of O_2 flux at 6 min (C) or 15 min (D) after start of reoxygenation. *P < 0.05, ***P < 0.001 for comparison between 15'OGD with or without nitrite. $^{\#\#}$P < 0.01 for comparison to control.

5.2.3. Nitrite effect on hippocampal tissue oxygen consumption linked to complex I after anoxia/reoxygenation

We then asked whether the oxidative burst described above was due to an increased NADH or complex I linked respiration. In fact, other studies reported this to be the case in mitochondria from other tissues. To evaluate specific complex linked O_2 consumption, intact tissue/cells cannot be used, as most of the substrates for complexes do not cross the cell membrane. As such, we used permeabilized hippocampal slices for which we had to implement the experimental design and conditions.

Firstly, we tested the optimal concentration of saponin needed for permeabilization of cell membranes without compromising mitochondrial membranes (**Fig. 5.5**). Slices were cut into small pieces to facilitate permeabilization and a lower O_2 concentration was used (150-200 µM). After a stable O_2 flux was obtained, substrates linked to NADH production were added into the chamber – pyruvate (P), malate (M) and glutamate (G) – and then ADP, the substrate for ATP synthase. Then, 10 mg mL^{-1} of saponin was added twice (final concentration = 20 mg mL^{-1}) and then 5 mg mL^{-1} more. As expected, the O_2 flux of hippocampal slices increased following each addition of saponin as a result of increased substrate accessibility due to permeabilization of the plasma membrane. The final addition of saponin (final concentration = 25 mg mL^{-1}) had no effect on O_2 flux, indicating maximal permeability of the plasma membrane. In order to evaluate the integrity of the mitochondrial outer membrane we added cytochrome *c*, having observed no significant change in O_2 flux. This indicated that, while the plasma membrane had lost integrity

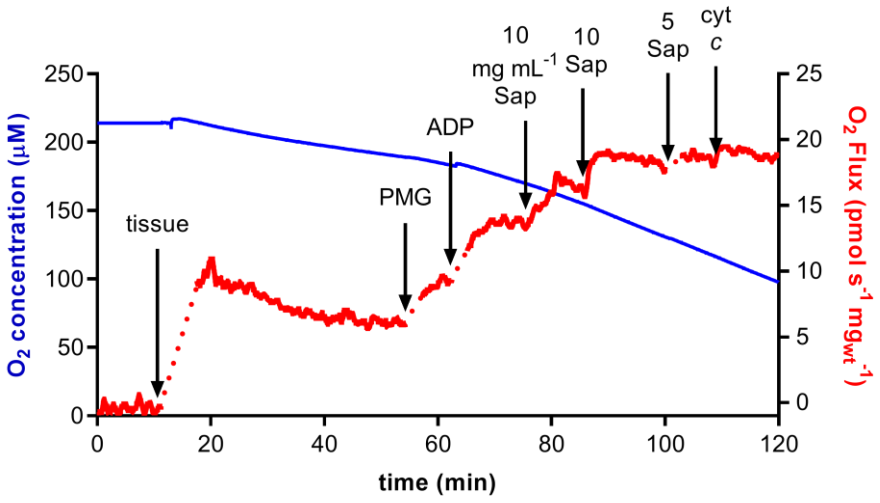

Fig. 5.5 – Determination of saponin concentration for cell membrane permeabilization in hippocampal slice pieces. Arrows point to each addition. PMG – pyruvate + malate + glutamate; Sap – saponin; cyt *c* – cytochrome *c*.

due to saponin, the mitochondrial outer membrane remained intact, blocking access of added cytochrome *c* to the intermembrane space. As such, 20 mg mL^{-1} of saponin was considered the optimal concentration for permeabilization of hippocampal slice pieces, since increasing to 25 mg mL^{-1} only led to a minor increase in O_2 flux.

Permeabilization was then carried out *in situ* by adding saponin to the recording chamber after the tissue (**Fig. 5.6A**). After that, pyruvate, malate, glutamate (PMG) and then ADP were added

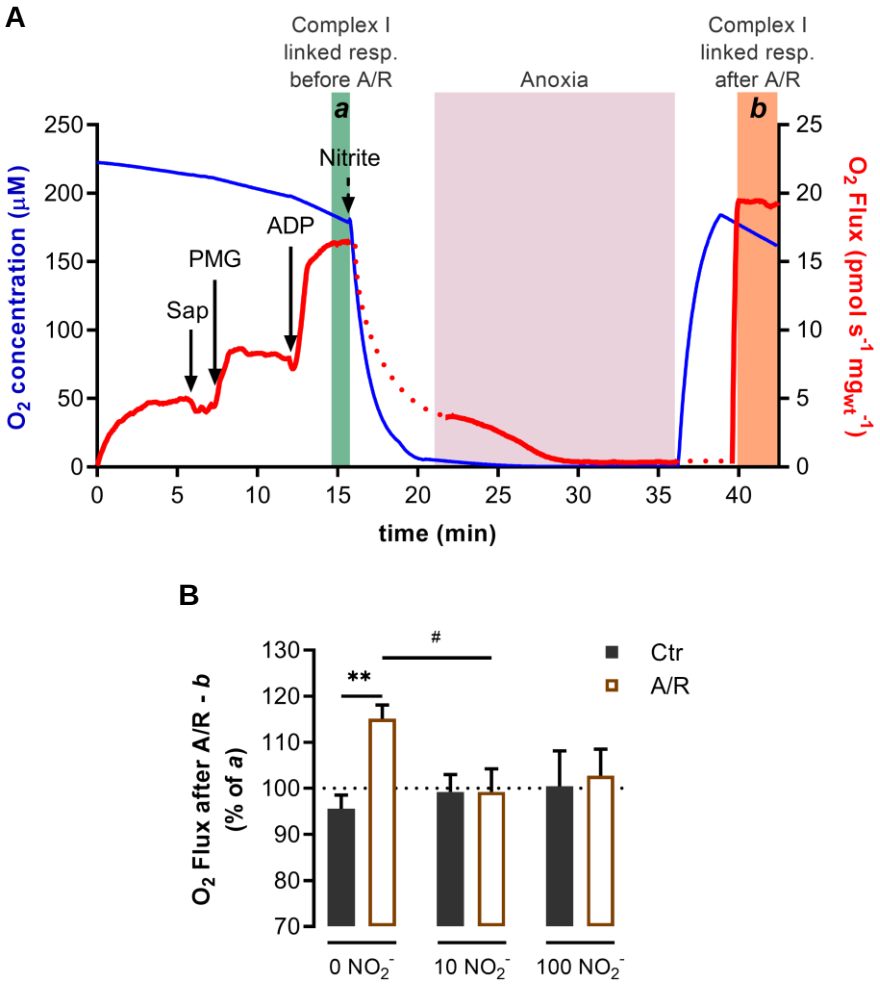

Fig. 5.6 – Nitrite decreases complex I or NADH-linked oxidative burst occurring following anoxia/reoxygenation (A/R) in permeabilized hippocampal slices. (A) Representative trace with O_2 concentration (in blue) and O_2 flux (in red) with arrows pointing each addition (saponin, pyruvate + malate + glutamate – PMG, ADP, and nitrite). Oxygen concentration was decreased, and anoxia (highlighted in pink) was carried out for 15 min. The complex I linked respiration before A/R is highlighted in green (time point *a*) while the complex I linked respiration after A/R is highlighted in orange (time point *b*). (B) Comparison in percentage between O_2 flux in complex I linked respiration before A/R (100%; highlighted in green; time point *a*) and after A/R (highlighted in orange; time point *b*) in the presence or absence of nitrite at 10 or 100 µM. $^{**}P < 0.01$ for comparison to control. $^{\#}P < 0.05$ for comparison to no nitrite.

to start complex I linked respiration (NADH linked oxidative phosphorylation). Once O_2 flux was stable in this respiratory state (time point "*a"*), O_2 concentration was decreased and after 15 min of anoxia (O_2 concentration below 10 µM), O_2 was increased to the same level as before anoxia (time point "*b"*). In control conditions, O_2 concentration was maintained in the range 180-220 µM during this period of time. This anoxia/reoxygenation (A/R) led to an increase in O_2 flux of about 15%, while in control conditions, where the tissue remained in the chamber with O_2 during the same period of time, a slight decrease in O_2 flux was observed (**Fig. 5.6B** and **C**). This increase in percentage for A/R compared to control was statistically significant ($P < 0.01$). These results are in good agreement to what we observed during OGD and reperfusion experiments in intact hippocampal slices.

Then, we evaluated how nitrite could modulate this oxidative burst in complex I linked respiration. For that, nitrite at 10 or 100 µM was added right before A/R, as shown in **Fig. 5.6A**. We found no significant changes produced by nitrite under control conditions (**Fig. 5.6B** and **C**). However, nitrite 10 µM significantly decreased ($P < 0.05$) the oxidative burst observed after A/R. At 100 µM there was also a tendency for decrease. These results show that the oxidative burst observed during OGD reperfusion and its modulation by nitrite might be, at least partly, related to complex I linked respiration.

5.2.4. Dietary supplementation of rats with nitrate and the effects on complex I linked respiration in hippocampal tissue during anoxia/reoxygenation

Nitrate ingestion leads to an increase in nitrite in blood and tissues, including the brain. As such, we evaluated if increasing nitrate intake could, via an increase in circulating nitrite, also afford protection in A/R. Nitrate was added to the drinking water of animals in a dietary concentration (~1 mM / 0.1 mg L^{-1}) for 35 days and nitrate consumption was measured by monitoring food and water intake (**Table 5.1**).

Table 5.1 – Mean nitrate intake by animals with nitrate (1 mM) in their drinking water. Food ingestion was also considered, as the chow contained nitrate. Values represent mean ± SD. $^{**}P < 0.01$ in comparison to control.

	Control	**Nitrate**
Nitrate intake (mg day^{-1} kg^{-1})	3.2 ± 0.1 (N = 5)	10.5 ± 0.8** (N = 6)
Nitrate intake (µmol day^{-1} kg^{-1})	37.7 ± 1.2 (N = 5)	123.5 ± 9.4** (N = 6)

Hippocampal slices were obtained from these animals and the effect of A/R was evaluated in permeabilized tissue with added substrates linked to NADH production. Similar to what was observed above, an oxidative burst was observed following reoxygenation (**Fig. 5.7A** and **B**) both for control and nitrate-fed animals. Slices obtained from animals fed with nitrate displayed a clear tendency for a decrease in the oxidative burst, when compared to animals with normal diet (control). However, further studies are required to achieve more robust conclusions.

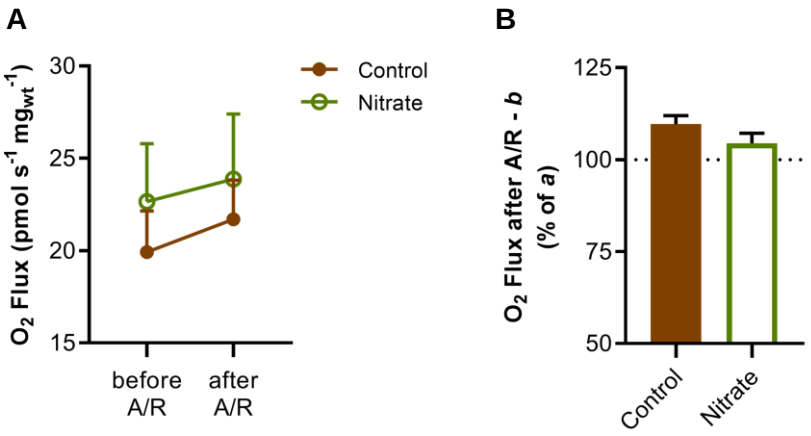

Fig. 5.7 – Dietary nitrate effect on the burst in complex I or NADH linked respiration after anoxia/reoxygenation (A/R) in permeabilized hippocampal slices. (A) Oxygen flux at each state/time point after permeabilization for control and nitrate fed animals. (B) Comparison in percentage between O_2 flux in complex I linked respiration before A/R (100%, *a*) and after A/R (*b*) for control and nitrate fed animals.

5.3. Discussion

The mammalian brain relies greatly on O_2 for energy production and is acutely vulnerable to hypoxia. Moreover, and although astrocytes do contain modest amounts of glycogen, the brain overall lacks energy reserves (Kalogeris et al. 2012). Oxygen is the final electron acceptor of the ETS, being required for complete oxidation of substrates to produce ATP during oxidative phosphorylation and, thus, the lack of sufficient O_2 compromises the efficiency of energy production, resulting in the dysfunction of multiple energy-dependent reactions.

One of the brain regions particularly affected by insufficient O_2 supply is the hippocampus (Ordy et al. 1993). As such, we aimed to study the effects of hypoxia and I/R in the rodent hippocampus at the level of oxidative phosphorylation and its putative modulation by nitrite. We used intact or permeabilized tissue to preserve the tissue cytoarchitecture and cell interactions, providing a better physiological model as opposed to isolated mitochondria.

Nitrite can be a source of $^{\bullet}NO$, particularly under conditions of hypoxia when its O_2-dependent enzymatic synthesis by the family of NOS is hindered (Lundberg et al. 2008). Nitric oxide can then inhibit complexes of the respiratory chain, including complex I, which can be protective in hypoxia due to limitation of ROS production under these circumstances (Cadenas and Davies 2000; Shiva et al. 2007b; Chouchani et al. 2013).

To study the effect of hypoxia on hippocampal tissue oxidative metabolism, we limited the O_2 supply to whole hippocampal slices by using a lower O_2 concentration (~150 µM) in the bathing medium and measured tissue O_2 consumption. In the brain, resting O_2 levels vary between 30 and 100 µM (Nair et al. 1987; Murr et al. 1994; Zauner et al. 1995; Devor et al. 2011; Kealy et al. 2013; Lourenço et al. 2017b). Typically, almost saturating O_2 concentrations are used with brain slices to ensure proper oxygenation at the core of the slice (Erecińska and Silver 2001; Ledo et al. 2005), since the tissue lacks blood circulation and O_2 must reach the core by diffusion from the medium. Our lab has previously shown that the O_2 concentration decreases steeply as a function of tissue thickness (Ledo et al. 2005). As such, decreasing the O_2 concentration in the medium bathing the tissue to 150 µM should result in most of the tissue being hypoxic. In this case, the protocol here applied is of chronic hypoxia since slices were in low O_2 for at least 50 min before starting measurements. Chronic hypoxia may elicit a wide range of potential responses to limited O_2 availability, spanning from metabolic reprogramming to changes in gene expression profiles and epigenetic modifications (Liu & Le, 2014; Mosqueira & Iturriaga, 2019; Terraneo & Samaja, 2017; Zhou et al., 2008).

We showed that the low O_2 concentration indeed limits tissue O_2 consumption without completely inhibiting it. This has been previously observed for hepatocytes (Schumacker et al. 1993) and

cardiomyocytes (Budinger et al. 1996) exposed to chronic hypoxia (minutes to hours) without showing compromised cell viability. This decrease in O_2 consumption was associated with decreased ATP concentration, an observation that can be supported by an altered cytochrome *c* oxidase activity. Indeed, isolated liver mitochondria showed decreased coupled respiration when exposed to chronic hypoxia (2h) (Chandel et al. 1995) and the effect was associated to a decrease in maximal velocity of cytochrome *c* oxidase (Chandel et al. 1996). Generally, limitation of respiration due to hypoxia leads to the activation of the transcription factor hypoxia-inducible factor-1 (HIF-1) (Wang et al., 1995), which upregulates glycolysis and downregulates oxidative phosphorylation (Papandreou et al. 2006), reducing the cell's reliance on O_2-dependent ATP production. This is due to HIF-1 upregulating glycolytic enzymes as well as pyruvate dehydrogenase kinase 1 (PDK1), which inactivates the mitochondrial enzyme pyruvate dehydrogenase, reducing the flow of pyruvate to the TCA cycle (Papandreou et al. 2006). In mice exposed to hypoxia for 30-60 min, it has been shown that HIF-1 mRNA increases in the brain (Wiener et al. 1996). Additionally, transient focal ischemia in mice triggered a strong and long-lasting HIF-1α protein increase that was mainly limited to neurons (Baranova et al. 2007).

The decrease in O_2 consumption by the tissue during hypoxia can be a protective mechanism to attenuate the effects of lower O_2 availability and prevent local anoxia (Tormos and Chandel 2010). In the face of reduced O_2 availability, cells must adapt their metabolism to maintain the reactions that rely on ATP. We found that, even under hypoxic conditions and despite the significant decrease in Routine respiration, hippocampal tissue still responded to uncoupling with a robust increase in O_2 flux, supporting the existence of spare respiratory capacity even in hypoxia. As such, inhibition of tissue O_2 consumption with hypoxia could in part be due to regulation and not only due to insufficient O_2 being present to act as a substrate for oxidative phosphorylation. As expected, we also found a tendency for decreased non-ETS O_2 consumption.

As nitrite can be a relevant source of $^{\bullet}NO$ under hypoxic conditions and considering that both inhibit complex I and complex IV of the ETS, we evaluated the effect of nitrite on hippocampal tissue O_2 consumption under these conditions. We found that nitrite had no effect on tissue O_2 flux, neither for control nor hypoxic conditions. One possible explanation could be that $^{\bullet}NO$ produced via univalent reduction of nitrite by the ETS could prevent HIF-1α stabilization (Hagen et al. 2003), removing its TCA cycle inhibitory effect. However, the relatively short time of hypoxia (~50 min) could be insufficient to observe HIF-1α effects (Zimmer et al. 2016).There is no indication to which effects can be observed in this relatively short time course as most of the studies on this subject have been done in cells with much longer hypoxia periods. Another explanation may be that, at the O_2 concentration used, there may still be enzymatic production of

$^{\bullet}$NO or the conditions are still not sufficient to provoke nitrite reduction. Indeed, the K_M for O_2 of NOS in the brain is estimated to be ~20 µM (Rengasamy and Johns 1996).

As mentioned above, during ischemia mitochondrial respiration is inhibited and ATP is depleted, resulting in a bioenergetic deficit. While reperfusion is necessary to re-establish O_2 and glucose delivery and restore cellular metabolism, reperfusion itself aggravates mitochondrial damage and tissue injury (Lin et al., 2016). In fact, the reduced state of ETS components during ischemia might partially reduce O_2 as soon as it is again available as the final electron acceptor, resulting in a burst of $O_2^{\bullet-}$ production. The resulting oxidative distress and the opening of the mitochondrial transition pore with cytochrome *c* release ultimately result in triggering of the apoptotic cascade (Stone et al. 1989; Jemmerson et al. 2005). In the end, I/R in the brain leads to oxidative distress, mitochondrial dysregulation, blood-brain barrier disruption, inflammation, and increased neuronal apoptosis (Lin et al. 2016).

Considering the abovementioned, we next investigated the putative protective role of nitrite during reperfusion. For that, we took advantage of the method described in chapter 3 and applied an I/R model in slices while measuring O_2 consumption. This allowed us to determine O_2 fluxes immediately after reperfusion. Slices were subjected to OGD for different time periods, followed by reperfusion, which consisted in adding glucose to the medium and reoxygenation. This protocol has been widely used to mimic stroke (Holloway and Gavins 2016), particularly in organotypic brain slice cultures (Sommer 2017), but to our knowledge has never been used in this context. Using this method in acute brain slices has the advantage that measurements can be carried out at the same time as OGD is applied. Oxygen deprivation was achieved at hypoxic concentrations (< 10 µM). We found that 15 min of OGD followed by reperfusion resulted in an oxidative burst that was still observable 15 min after the start of reoxygenation but not after ~40 min. Furthermore, inhibition of complexes I and IV abolished the oxidative burst, confirming that it is the result of O_2 consumption by the ETS. For shorter or longer periods of OGD, we observed no difference compared to control upon reperfusion. Shorter periods of OGD may not be sufficient to induce damage and with longer periods there may already be some neuronal death (Juzekaeva et al. 2020). It is noteworthy that our results are hardly comparable to *in vivo* studies in terms of timings, as OGD results in a higher rate of neuronal death in slices than during ischemia *in vivo*, due to a stronger cytotoxic edema and Ca^{2+} load, as discussed by others (Juzekaeva et al. 2020). The observed oxidative burst can be associated with the burst in ROS generation *in vivo* after global cerebral I/R (Peters et al. 1998; Kunimatsu et al. 2011). To our knowledge, this burst in tissue respiration has never been observed, not even in isolated mitochondria from various organs, including brain (Feng et al., 2008; Maruyama et al., 2013; Morin et al., 2003; Perry et al., 2019; Schild & Reiser, 2005; Shiva, Sack, et al., 2007). In fact, this oxidative burst immediately after

reperfusion could be expected, since ROS production is more pronounced during the initial 15 min after reperfusion in global cerebral ischemia (Kunimatsu et al. 2011). Additionally, Sanderson and colleagues have argued that isolated mitochondria cannot represent what happens *in vivo* during I/R, since isolated mitochondria have a higher mitochondrial membrane potential compared to mitochondria in intact cells (150-200 mV vs 80-140 mV) leading to an inability to hyperpolarize during reperfusion (Sanderson et al. 2013). The hyperpolarization observed after reperfusion should lead to increased oxidative phosphorylation and ROS production due to overly active complexes of the ETS.

In our model, following OGD and reperfusion, general respiratory states were evaluated. We found that Routine tissue respiration, ET capacity, and ROX were unaltered, showing that our model of OGD produced transient alterations in O_2 consumption only in the time frame immediately after reperfusion.

We hypothesized that nitrite could reduce this oxidative burst and be protective in avoiding ROS production upon reperfusion. While nitrite produced no effect in control conditions, it decreased the oxidative burst observed at both 10 and 50 µM. Nitrite has been previously shown to reduce O_2 consumption and ROS production after I/R in liver isolated mitochondria with complex I substrates (Shiva et al. 2007b). Nitrite was also shown to reduce brain ROS production *in vivo* upon cardiac arrest and resuscitation, a model of global brain I/R (Dezfulian et al. 2016).

The effect of nitrite has been largely attributed to its reduction to •NO (Shiva 2013; Dezfulian et al. 2016). Thus, we aimed at determining if the inhibition of the oxidative burst was dependent on nitrite reduction by performing the experiments in the presence of two known •NO scavengers, myoglobin and C-PTIO. However, our results were inconclusive. Although the scavengers did not abolish the effect of nitrite, we cannot attribute this to a •NO independent effect of nitrite, since the scavengers also seemed to reduce the oxidative burst after OGD and reperfusion in the absence of nitrite. In fact, •NO scavengers have been previously shown to reduce the effects of nitrite after I/R, suggesting the need of nitrite reduction to •NO for effects to be observed (Jung et al. 2006; Shiva et al. 2007b). Our observations may be attributed to competing reactions of the scavengers. For example, C-PTIO can embark in reactions with both nitrite and •NO, yielding different products depending on the ratio of nitrite and C-PTIO and •NO steady state concentration (Pfeiffer et al. 1997; Goldstein et al. 2003). Deoxymyoglobin, in turn, can also reduce nitrite to •NO (Shiva et al. 2007a). Having the whole tissue present is an advantage in terms of brain model but, in turn, may potentiate these other competing reactions for C-PTIO and myoglobin.

One putative target for nitrite is complex I of the ETS, a major source of ROS during I/R (Chouchani et al. 2016) that can be inhibited by •NO-derived metabolites through S-nitrosation (Chouchani et al. 2013). Furthermore, complex I inhibitors, such as rotenone, decrease ROS

production and are protective in I/R (Lesnefsky et al. 2004; Chen et al. 2006) and previous work suggests that nitrite inhibits complex I linked respiration in hepatic I/R (Shiva et al. 2007b). To understand whether the observed effects of nitrite in tissue O_2 consumption after I/R were related to complex I inhibition, we ran an anoxia and reoxygenation (A/R) protocol in permeabilized hippocampal slices using substrates linked to NADH production. An oxidative burst was observed that was similar to that observed for intact (non-permeabilized) tissue, increasing by ~15% immediately after reoxygenation. Such increase was significantly attenuated by 10 µM nitrite, suggesting that the decrease in oxidative burst in the presence of nitrite might be mediated via complex I. Of note, an inhibition in complex I linked respiration by nitrite was observed in isolated liver mitochondria, as mentioned before, although the authors did not observe a burst in O_2 consumption (Shiva et al. 2007b). However, one cannot rule out a possible inhibition of complex IV inhibition by nitrite-derived $^{\bullet}NO$ in competition with molecular O_2 for the binuclear center or even an effect on other complexes of the ETS that were not assessed here.

In vivo nitrite can be produced from nitrate through the entero-salivary pathway, resulting in an increase of nitrite levels in circulation (Lundberg et al. 2008) and consequently in tissues, including the brain (Bryan et al. 2005). In line with this, nitrate has been associated with beneficial cardiovascular effects during I/R (Webb et al. 2008). Thus, we hypothesized that dietary nitrate might produce an effect similar to that of nitrite added to slices, decreasing the complex I linked oxidative burst observed after A/R. We thus evaluated this in hippocampal slices obtained from animals treated with nitrate in their diet (added to drinking water) for a one-month period. Although not significant, a clear tendency for decreased complex I linked oxidative burst was observed following A/R. This non-significant decrease could be due to a relatively low nitrate concentration being used (1 mM; 10 mg day^{-1} kg^{-1}; 0.12 mmol day^{-1} kg^{-1}), as other studies showing cognitive improvements with nitrate supplementation have used much higher doses (Gilchrist et al. 2014; Thompson et al. 2015). Nonetheless, the daily amount of nitrate ingested by the rats during the supplementation experiments here described (~0.1 mmol kg^{-1}) is approximately the same dose of nitrate (~5 mg day^{-1}) that has been shown to produce effects in the blood pressure of rats following distal middle cerebral artery occlusion (Allan et al. 2018). A similar acute dose of nitrate also improved neurological assessment after occlusion of both carotids in rats (Kuzenkov and Krushinskii 2014). The same nitrate dose also led to reduced blood pressure and brain blood flow fluctuations in humans (Fan et al. 2020). However, the nitrate dose cannot be directly compared between humans and rats, as rats have been shown to produce a lower amount of nitrite from circulating nitrate (Montenegro et al. 2016). The reason for this difference is still unknown. One other possible explanation for the lack of a clear effect of nitrate diet on the oxidative burst resided on the fact that nitrite may no longer be present at a relevant concentration in the tissue due to the excision and preparation process.

5.4. Conclusions

The brain relies greatly on O_2 for energy production and is particularly susceptible to damage by hypoxia. Nitrite has been shown to be protective in brain I/R and appears to be responsible for decreased ROS production. The work described in this chapter focused on the putative modulation of brain energy metabolism in I/R by nitrite and clarification of the underlying mechanisms.

We first observed that brain hippocampal tissue in hypoxia presented lower O_2 consumption, suggesting a metabolic reprogramming since there was still spare respiratory capacity to increase O_2 consumption even under hypoxia. Nitrite exerted no effect under these conditions.

Although it is necessary to re-establish circulation, reperfusion aggravates injury. Immediately after *in vitro* I/R, we observed an increase in hippocampal slice oxidative metabolism, or oxidative burst that, to our knowledge, is described for the first time, and that could be associated with increased ROS production from the ETS. This oxidative burst was decreased by nitrite, but it could not be determined whether this effect required the reduction of this anion to $^{\bullet}NO$. Although the results indicate that the effect of nitrite might be related to modulation of complex I activity, one cannot dismiss the inhibition of cytochrome *c* oxidase as a contributor to the observed decrease of oxidative burst. In fact, $^{\bullet}NO$ might inhibit complex I via nitrosation of critical cysteine residues and at lower concentrations, although within the same order of magnitude, $^{\bullet}NO$ can compete with O_2 for cytochrome *c* oxidase (Cadenas and Davies 2000).

An *in vivo* experiment designed to explore the sequential reduction of nitrate to $^{\bullet}NO$ via the nitrate-nitrite-$^{\bullet}NO$ pathway revealed that slices obtained from rats supplemented with dietary nitrate showed a clear tendency to undergo less intense oxidative burst following an A/R protocol.

In conclusion, we provided evidence that nitrite plays a protective role in brain I/R by decreasing the reperfusion-coupled oxidative burst through a mechanism that points to complex I-linked respiration inhibition. The molecular mechanisms, however, remain to be fully discerned.

5.5. Future Directions

The work developed in this chapter leads to other questions to further understand the mechanism through which nitrite can be protective in brain I/R, particularly concerning the ETS. As such, other complexes of the ETS should be evaluated to identify possible targets for nitrite, notably the inhibition of cytochrome *c* oxidase. A correlation with the production of ROS, notably $O_2^{\bullet -}$ and H_2O_2, should concomitantly be investigated with the attenuation of the burst of O_2 consumption by the ETS. Furthermore, since reverse electron transport (RET) from complex II to complex I could be involved in ROS production during I/R, the role of this phenomenon and modulation by nitrite should also be assessed. Finally, considering the well-known effects of $^{\bullet}NO$ on the components of the ETS, the production of $^{\bullet}NO$ under these conditions should be measured in order to clearly verify the hypothesis that the effects of nitrite are mediated by its reduction to $^{\bullet}NO$.

6. Final conclusions

The brain is heavily dependent on appropriate energy metabolism to maintain its high-level functionality due to its metabolic needs. Thus, there must be mechanisms that ensure such needs are met in a timely manner and fine-tuned in time and space with activity level. The work presented in this thesis investigated brain bioenergetics mechanisms in physiology and pathology. More specifically, the role of lactate in neurometabolism and the modulation of brain tissue response to I/R by nitrite. For that, new tools were designed and characterized, allowing for novel insights into this field. The data and its analysis here presented allowed the following main conclusions to be reached:

i. The development of a sample holder allowed for monitoring of whole brain tissue O_2 consumption as a means of evaluating oxidative metabolism, while maintaining the tissue intact throughout the time course of respirometry experiments. The holder did not cause interference to measurements, allowing stable O_2 fluxes and the adaptation of protocols to study brain oxidative metabolism in a tissue preparation that better represents the *in vivo* conditions.

ii. The newly designed lactate microbiosensor based on LOx immobilized on the surface of CFM/Pt showed suitable analytical performance – high sensitivity and selectivity, low limit of detection, and extended operational stability – for measuring lactate concentration in brain tissue, allowing monitoring of rapid changes in extracellular lactate in response to stimulation. These microbiosensors are an asset to elucidate the role of lactate in neurometabolic coupling.

iii. By using these novel methodologies, it was shown that glucose modulates not only tissue O_2 consumption within a limited and physiological range but also extracellular lactate concentration. Lactate is continuously produced from glucose through aerobic glycolysis and released to the extracellular space, presumably by astrocytes.

iv. Neurons uptake extracellular lactate to fuel oxidative metabolism both under resting and neural activation conditions to better respond to the metabolic demands.

v. In an *in vitro* model of I/R in the hippocampus, there is an oxidative burst immediately after reperfusion, which is possibly associated with ROS production. Nitrite decreases this oxidative burst by mechanisms not yet clear but that are likely related to the modulation of mitochondrial respiration, in particular with the inhibition of complex I linked respiration.

7. Bibliography

Abi-Saab WM, Maggs DG, Jones T, et al (2002) Striking Differences in Glucose and Lactate Levels Between Brain Extracellular Fluid and Plasma in Conscious Human Subjects: Effects of Hyperglycemia and Hypoglycemia. J Cereb Blood Flow Metab 22:271–279. https://doi.org/10.1097/00004647-200203000-00004

Abramov AY, Scorziello A, Duchen MR (2007) Three Distinct Mechanisms Generate Oxygen Free Radicals in Neurons and Contribute to Cell Death during Anoxia and Reoxygenation. J Neurosci 27:1129 LP – 1138. https://doi.org/10.1523/JNEUROSCI.4468-06.2007

Aguirre E, Rodríguez-Juárez F, Bellelli A, et al (2010) Kinetic model of the inhibition of respiration by endogenous nitric oxide in intact cells. Biochim Biophys Acta - Bioenerg 1797:557–565. https://doi.org/https://doi.org/10.1016/j.bbabio.2010.01.033

Ahmad R, Kuppusamy P (2010) Theory, Instrumentation, and Applications of Electron Paramagnetic Resonance Oximetry. Chem Rev 110:3212–3236. https://doi.org/10.1021/cr900396q

Aho K, Harmsen P, Hatano S, et al (1980) Cerebrovascular disease in the community: results of a WHO collaborative study. Bull World Health Organ 58:113–130

Aidt FH, Nielsen SMB, Kanters J, et al (2013) Dysfunctional mitochondrial respiration in the striatum of the Huntington's disease transgenic R6/2 mouse model. PLoS Curr 5:. https://doi.org/10.1371/currents.hd.d8917b4862929772c5a2f2a34ef1c201

Alán L, Smolková K, Kronusová E, et al (2009) Absolute levels of transcripts for mitochondrial uncoupling proteins UCP2, UCP3, UCP4, and UCP5 show different patterns in rat and mice tissues. J Bioenerg Biomembr 41:71. https://doi.org/10.1007/s10863-009-9201-2

Alderton WK, Cooper CE, Knowles RG (2001) Nitric oxide synthases: structure, function and inhibition. Biochem J 357:593–615. https://doi.org/10.1042/bj3570593

Alkadhi KA (2019) Cellular and Molecular Differences Between Area CA1 and the Dentate Gyrus of the Hippocampus. Mol Neurobiol 56:6566–6580. https://doi.org/10.1007/s12035-019-1541-2

Allan PD, Tzeng Y-C, Gowing EK, et al (2018) Dietary nitrate supplementation reduces low frequency blood pressure fluctuations in rats following distal middle cerebral artery occlusion. J Appl Physiol 125:862–869. https://doi.org/10.1152/japplphysiol.01081.2017

Allen TGJ, Brown DA (2004) Modulation of the excitability of cholinergic basal forebrain neurones by KATP channels. J Physiol 554:353–370. https://doi.org/https://doi.org/10.1113/jphysiol.2003.055889

Almeida A, Almeida J, Bolaños JP, Moncada S (2001) Different responses of astrocytes and neurons to nitric oxide: The role of glycolytically generated ATP in astrocyte protection. Proc Natl Acad Sci 98:15294 LP – 15299. https://doi.org/10.1073/pnas.261560998

Almeida A, Moncada S, Bolaños JP (2004) Nitric oxide switches on glycolysis through the AMP protein kinase and 6-phosphofructo-2-kinase pathway. Nat Cell Biol 6:45–51. https://doi.org/10.1038/ncb1080

An JH, Su Y, Radman T, Bikson M (2008) Effects of glucose and glutamine concentration in the formulation of the artificial cerebrospinal fluid (ACSF). Brain Res 1218:77–86. https://doi.org/10.1016/j.brainres.2008.04.007

Andersen P, Morris R, Amaral DG, et al (2007) The hippocampus book. Oxford University Press, New York, NY, US

Antunes F, Boveris A, Cadenas E (2007) On the Biologic Role of the Reaction of NO with Oxidized Cytochrome c Oxidase. Antioxid Redox Signal 9:1569–1580. https://doi.org/10.1089/ars.2007.1677

Antunes F, Boveris A, Cadenas E (2004) On the mechanism and biology of cytochrome oxidase inhibition by nitric oxide. Proc Natl Acad Sci U S A 101:16774 LP – 16779. https://doi.org/10.1073/pnas.0405368101

Ashford CA, Dixon KC (1935) The effect of potassium on the glucolysis of brain tissue with reference to the Pasteur effect. Biochem J 29:157–168. https://doi.org/10.1042/bj0290157

Attwell D, Laughlin SB (2001) An Energy Budget for Signaling in the Grey Matter of the Brain. J Cereb Blood Flow Metab 21:1133–1145. https://doi.org/10.1097/00004647-200110000-00001

Azarias G, Perreten H, Lengacher S, et al (2011) Glutamate Transport Decreases Mitochondrial pH and Modulates Oxidative Metabolism in Astrocytes. J Neurosci 31:3550 LP – 3559. https://doi.org/10.1523/JNEUROSCI.4378-10.2011

Back T, Hemmen T, Schüler OG (2004) Lesion evolution in cerebralischemia. J Neurol 251:388–397. https://doi.org/10.1007/s00415-004-0399-y

Bak LK, Walls AB (2018a) CrossTalk opposing view: lack of evidence supporting an astrocyte-to-neuron lactate shuttle coupling neuronal activity to glucose utilisation in the brain. J Physiol 596:351–353. https://doi.org/10.1113/JP274945

Bak LK, Walls AB (2018b) Rebuttal from Lasse K. Bak and Anne B. Walls. J Physiol 596:357. https://doi.org/10.1113/JP275507

Banerjee R, Purhonen J, Kallijärvi J (2021) The mitochondrial coenzyme Q junction and complex III: biochemistry and pathophysiology. FEBS J. https://doi.org/10.1111/febs.16164

Baranova O, Miranda LF, Pichiule P, et al (2007) Neuron-Specific Inactivation of the Hypoxia Inducible Factor 1α Increases Brain Injury in a Mouse Model of Transient Focal Cerebral Ischemia. J Neurosci 27:6320 LP – 6332. https://doi.org/10.1523/JNEUROSCI.0449-07.2007

Barros LF, Bolaños JP, Bonvento G, et al (2018) Current technical approaches to brain energy metabolism. Glia 66:1138–1159. https://doi.org/https://doi.org/10.1002/glia.23248

Barros LF, Ruminot I, San Martín A, et al (2021) Aerobic Glycolysis in the Brain: Warburg and Crabtree Contra Pasteur. Neurochem Res 46:15–22. https://doi.org/10.1007/s11064-020-02964-w

Barros LF, San Martín A, Ruminot I, et al (2020) Fluid Brain Glycolysis: Limits, Speed, Location, Moonlighting, and the Fates of Glycogen and Lactate. Neurochem Res 45:1328–1334. https://doi.org/10.1007/s11064-020-03005-2

Barros LF, Weber B (2018) CrossTalk proposal: an important astrocyte-to-neuron lactate shuttle couples neuronal activity to glucose utilisation in the brain. J Physiol 596:347–350. https://doi.org/10.1113/JP274944

Bastarrachea L, Dhawan S, Sablani SS (2011) Engineering Properties of Polymeric-Based Antimicrobial Films for Food Packaging: A Review. Food Eng Rev 3:79–93. https://doi.org/10.1007/s12393-011-9034-8

Benjamin N, O'Driscoll F, Dougall H, et al (1994) Stomach NO synthesis. Nature 368:502. https://doi.org/10.1038/368502a0

Benveniste H, Jørgensen MB, Sandberg M, et al (1989) Ischemic Damage in Hippocampal CA1 is Dependent on Glutamate Release and Intact Innervation from CA3. J Cereb Blood Flow Metab 9:629–639. https://doi.org/10.1038/jcbfm.1989.90

Bergersen LH (2015) Lactate Transport and Signaling in the Brain: Potential Therapeutic Targets and Roles in Body—Brain Interaction. J Cereb Blood Flow Metab 35:176–185. https://doi.org/10.1038/jcbfm.2014.206

Bingul D, Kalra K, Murata EM, et al (2020) Persistent changes in extracellular lactate dynamics following synaptic potentiation. Neurobiol Learn Mem 175:107314. https://doi.org/10.1016/j.nlm.2020.107314

Bird CM, Burgess N (2008) The hippocampus and memory: insights from spatial processing. Nat Rev Neurosci 9:182–194. https://doi.org/10.1038/nrn2335

Bittar PG, Charnay Y, Pellerin L, et al (1996) Selective Distribution of Lactate Dehydrogenase Isoenzymes in Neurons and Astrocytes of Human Brain. J Cereb Blood Flow Metab 16:1079–1089. https://doi.org/10.1097/00004647-199611000-00001

Blass JP, Sheu REXK-F, Gibson GE (2000) Inherent Abnormalities in Energy Metabolism in Alzheimer Disease: Interaction with Cerebrovascular Compromise. Ann N Y Acad Sci 903:204–221. https://doi.org/10.1111/j.1749-6632.2000.tb06370.x

Bolaños JP, Delgado-Esteban M, Herrero-Mendez A, et al (2008) Regulation of glycolysis and pentose–

phosphate pathway by nitric oxide: Impact on neuronal survival. Biochim Biophys Acta - Bioenerg 1777:789–793. https://doi.org/10.1016/j.bbabio.2008.04.011

Boumezbeur F, Petersen KF, Cline GW, et al (2010) The Contribution of Blood Lactate to Brain Energy Metabolism in Humans Measured by Dynamic 13C Nuclear Magnetic Resonance Spectroscopy. J Neurosci 30:13983 LP – 13991. https://doi.org/10.1523/JNEUROSCI.2040-10.2010

Bouzier-Sore A-K, Voisin P, Bouchaud V, et al (2006) Competition between glucose and lactate as oxidative energy substrates in both neurons and astrocytes: a comparative NMR study. Eur J Neurosci 24:1687–1694. https://doi.org/10.1111/j.1460-9568.2006.05056.x

Brand MD, Nicholls DG (2011) Assessing mitochondrial dysfunction in cells. Biochem J 435:297–312. https://doi.org/10.1042/BJ20110162

Braunersreuther V, Montecucco F, Ashri M, et al (2013) Role of NADPH oxidase isoforms NOX1, NOX2 and NOX4 in myocardial ischemia/reperfusion injury. J Mol Cell Cardiol 64:99–107. https://doi.org/10.1016/j.yjmcc.2013.09.007

Bröer S, Bröer A, Schneider HP, et al (1999) Characterization of the high-affinity monocarboxylate transporter MCT2 in Xenopus laevis oocytes. Biochem J 341:529–535. https://doi.org/10.1042/0264-6021:3410529

Brown AM, Ransom BR (2007) Astrocyte glycogen and brain energy metabolism. Glia 55:1263–1271. https://doi.org/10.1002/glia.20557

Brown GC (1992) The leaks and slips of bioenergetic membranes. FASEB J 6:2961–2965. https://doi.org/10.1096/fasebj.6.11.1644259

Brown GC, Borutaite V (2004) Inhibition of mitochondrial respiratory complex I by nitric oxide, peroxynitrite and S-nitrosothiols. Biochim Biophys Acta - Bioenerg 1658:44–49. https://doi.org/10.1016/j.bbabio.2004.03.016

Brunori M, Forte E, Arese M, et al (2006) Nitric oxide and the respiratory enzyme. Biochim Biophys Acta 1757:1144–1154. https://doi.org/10.1016/j.bbabio.2006.05.011

Bryan NS, Fernandez BO, Bauer SM, et al (2005) Nitrite is a signaling molecule and regulator of gene expression in mammalian tissues. Nat Chem Biol 1:290–297. https://doi.org/10.1038/nchembio734

Bucur B, Purcarea C, Andreescu S, Vasilescu A (2021) Addressing the Selectivity of Enzyme Biosensors: Solutions and Perspectives. Sensors 21:3038. https://doi.org/10.3390/s21093038

Budinger GR, Chandel N, Shao ZH, et al (1996) Cellular energy utilization and supply during hypoxia in embryonic cardiac myocytes. Am J Physiol Cell Mol Physiol 270:L44–L53. https://doi.org/10.1152/ajplung.1996.270.1.L44

Buonocore MH, Maddock RJ (2015) Magnetic resonance spectroscopy of the brain: a review of physical principles and technical methods. Rev Neurosci 26:609–632. https://doi.org/doi:10.1515/revneuro-2015-0010

Burmeister JJ, Palmer M, Gerhardt GA (2005) l-lactate measures in brain tissue with ceramic-based multisite microelectrodes. Biosens Bioelectron 20:1772–1779. https://doi.org/10.1016/j.bios.2004.07.003

Burmeister JJ, Pomerleau F, Huettl P, et al (2008) Ceramic-based multisite microelectrode arrays for simultaneous measures of choline and acetylcholine in CNS. Biosens Bioelectron 23:1382–1389. https://doi.org/10.1016/j.bios.2007.12.013

Cabral-Costa J V, Kowaltowski AJ (2020) Neurological disorders and mitochondria. Mol Aspects Med 71:100826. https://doi.org/10.1016/j.mam.2019.10.003

Cadenas E, Davies KJA (2000) Mitochondrial free radical generation, oxidative stress, and aging. Free Radic Biol Med 29:222–230. https://doi.org/https://doi.org/10.1016/S0891-5849(00)00317-8

Cahova M, Palenickova E, Dankova H, et al (2015) Metformin prevents ischemia reperfusion-induced oxidative stress in the fatty liver by attenuation of reactive oxygen species formation. Am J Physiol Liver Physiol 309:G100–G111. https://doi.org/10.1152/ajpgi.00329.2014

Camandola S, Mattson MP (2017) Brain metabolism in health, aging, and neurodegeneration. EMBO J 36:1474–1492. https://doi.org/10.15252/embj.201695810

Cardoso S, Santos MS, Seiça R, Moreira PI (2010) Cortical and hippocampal mitochondria bioenergetics and oxidative status during hyperglycemia and/or insulin-induced hypoglycemia. Biochim Biophys Acta - Mol Basis Dis 1802:942–951. https://doi.org/10.1016/j.bbadis.2010.07.001

Carinci M, Vezzani B, Patergnani S, et al (2021) Different Roles of Mitochondria in Cell Death and Inflammation: Focusing on Mitochondrial Quality Control in Ischemic Stroke and Reperfusion. Biomedicines 9:169. https://doi.org/10.3390/biomedicines9020169

Carlsson S, Wiklund NP, Engstrand L, et al (2001) Effects of pH, Nitrite, and Ascorbic Acid on Nonenzymatic Nitric Oxide Generation and Bacterial Growth in Urine. Nitric Oxide 5:580–586. https://doi.org/10.1006/niox.2001.0371

Carvalho C, Santos MS, Oliveira CR, Moreira PI (2015) Alzheimer's disease and type 2 diabetes-related alterations in brain mitochondria, autophagy and synaptic markers. Biochim Biophys Acta - Mol Basis Dis 1852:1665–1675. https://doi.org/10.1016/j.bbadis.2015.05.001

Cecchini G (2003) Function and Structure of Complex II of the Respiratory Chain. Annu Rev Biochem 72:77–109. https://doi.org/10.1146/annurev.biochem.72.121801.161700

Chan PH (2001) Reactive Oxygen Radicals in Signaling and Damage in the Ischemic Brain. J Cereb Blood Flow Metab 21:2–14. https://doi.org/10.1097/00004647-200101000-00002

Chance B, Williams GR (1955) Respiratory enzymes in oxidative phosphorylation: I. Kinetics of oxygen utilization. J Biol Chem 217:383–393. https://doi.org/10.1016/S0021-9258(19)57189-7

Chandel N, Budinger GR, Kemp RA, Schumacker PT (1995) Inhibition of cytochrome-c oxidase activity during prolonged hypoxia. Am J Physiol Cell Mol Physiol 268:L918–L925. https://doi.org/10.1152/ajplung.1995.268.6.L918

Chandel NS, Budinger GRS, Schumacker PT (1996) Molecular Oxygen Modulates Cytochrome c Oxidase Function *. J Biol Chem 271:18672–18677. https://doi.org/10.1074/jbc.271.31.18672

Chen Q, Moghaddas S, Hoppel CL, Lesnefsky EJ (2006) Reversible Blockade of Electron Transport during Ischemia Protects Mitochondria and Decreases Myocardial Injury following Reperfusion. J Pharmacol Exp Ther 319:1405 LP – 1412. https://doi.org/10.1124/jpet.106.110262

Chouchani ET, Methner C, Nadtochiy SM, et al (2013) Cardioprotection by S-nitrosation of a cysteine switch on mitochondrial complex I. Nat Med 19:753–759. https://doi.org/10.1038/nm.3212

Chouchani ET, Pell VR, James AM, et al (2016) A Unifying Mechanism for Mitochondrial Superoxide Production during Ischemia-Reperfusion Injury. Cell Metab 23:254–263. https://doi.org/10.1016/j.cmet.2015.12.009

Christopherson KS, Hillier BJ, Lim WA, Bredt DS (1999) PSD-95 Assembles a Ternary Complex with the N-Methyl-d-aspartic Acid Receptor and a Bivalent Neuronal NO Synthase PDZ Domain. J Biol Chem 274:27467–27473. https://doi.org/10.1074/jbc.274.39.27467

Chuquet J, Quilichini P, Nimchinsky EA, Buzsáki G (2010) Predominant Enhancement of Glucose Uptake in Astrocytes versus Neurons during Activation of the Somatosensory Cortex. J Neurosci 30:15298 LP – 15303. https://doi.org/10.1523/JNEUROSCI.0762-10.2010

Clark LC, Wolf R, Granger D, Taylor Z (1953) Continuous Recording of Blood Oxygen Tensions by Polarography. J Appl Physiol 6:189–193. https://doi.org/10.1152/jappl.1953.6.3.189

Contreras-Baeza Y, Sandoval PY, Alarcón R, et al (2019) Monocarboxylate transporter 4 (MCT4) is a high affinity transporter capable of exporting lactate in high-lactate microenvironments. J Biol Chem 294:20135–20147. https://doi.org/10.1074/jbc.RA119.009093

Cosby K, Partovi KS, Crawford JH, et al (2003) Nitrite reduction to nitric oxide by deoxyhemoglobin vasodilates the human circulation. Nat Med 9:1498–1505. https://doi.org/10.1038/nm954

Cunnane S, Nugent S, Roy M, et al (2011) Brain fuel metabolism, aging, and Alzheimer's disease. Nutrition 27:3–20. https://doi.org/10.1016/j.nut.2010.07.021

Dale N, Hatz S, Tian F, Llaudet E (2005) Listening to the brain: microelectrode biosensors for neurochemicals. Trends Biotechnol 23:420–428. https://doi.org/10.1016/j.tibtech.2005.05.010

Dalsgaard MK (2005) Fuelling Cerebral Activity in Exercising Man. J Cereb Blood Flow Metab 26:731–750. https://doi.org/10.1038/sj.jcbfm.9600256

Danbolt NC (2001) Glutamate uptake. Prog Neurobiol 65:1–105. https://doi.org/10.1016/S0301-0082(00)00067-8

Daniele SG, Trummer G, Hossmann KA, et al (2021) Brain vulnerability and viability after ischaemia. Nat Rev Neurosci 22:553–572. https://doi.org/10.1038/s41583-021-00488-y

Davis RE, Williams M (2012) Mitochondrial Function and Dysfunction: An Update. J Pharmacol Exp Ther 342:598 LP – 607. https://doi.org/10.1124/jpet.112.192104

Dawe RJ, Yu L, Arfanakis K, et al (2020) Late-life cognitive decline is associated with hippocampal volume, above and beyond its associations with traditional neuropathologic indices. Alzheimer's Dement 16:209–218. https://doi.org/10.1002/alz.12009

Devor A, Sakadžić S, Saisan PA, et al (2011) "Overshoot" of O2 Is Required to Maintain Baseline Tissue Oxygenation at Locations Distal to Blood Vessels. J Neurosci 31:13676 LP – 13681. https://doi.org/10.1523/JNEUROSCI.1968-11.2011

Dezfulian C, Kenny E, Lamade A, et al (2016) Mechanistic characterization of nitrite-mediated neuroprotection after experimental cardiac arrest. J Neurochem 139:419–431. https://doi.org/10.1111/jnc.13764

Dickens F, Greville GD (1935) The metabolism of normal and tumour tissue: Neutral salt effects. Biochem J 29:1468–1483. https://doi.org/10.1042/bj0291468

Dienel GA (2019) Brain Glucose Metabolism: Integration of Energetics with Function. Physiol Rev 99:949–1045. https://doi.org/10.1152/physrev.00062.2017

Dienel GA (2013) Astrocytic energetics during excitatory neurotransmission: What are contributions of glutamate oxidation and glycolysis? Neurochem Int 63:244–258. https://doi.org/10.1016/j.neuint.2013.06.015

Diepart C, Verrax J, Calderon PB, et al (2010) Comparison of methods for measuring oxygen consumption in tumor cells in vitro. Anal Biochem 396:250–256. https://doi.org/10.1016/j.ab.2009.09.029

Dimmer KS, Friedrich B, Lang F, et al (2000) The low-affinity monocarboxylate transporter MCT4 is adapted to the export of lactate in highly glycolytic cells. Biochem J 350 Pt 1:219–227. https://doi.org/10.1042/0264-6021:3500219

Divakaruni AS, Brand MD (2011) The Regulation and Physiology of Mitochondrial Proton Leak.

Physiology 26:192–205. https://doi.org/10.1152/physiol.00046.2010

Doerrier C, Garcia-Souza LF, Krumschnabel G, et al (2018) High-Resolution FluoRespirometry and OXPHOS Protocols for Human Cells, Permeabilized Fibers from Small Biopsies of Muscle, and Isolated Mitochondria BT - Mitochondrial Bioenergetics: Methods and Protocols. In: Palmeira CM, Moreno AJ (eds). Springer New York, New York, NY, pp 31–70

Dong WQ, Schurr A, Reid KH, et al (1988) The rat hippocampal slice preparation as an in vitro model of ischemia. Stroke 19:498–502. https://doi.org/10.1161/01.STR.19.4.498

Dong Y, Wang L, Shangguan D, et al (2003) Analysis of glucose and lactate in hippocampal dialysates of rats during the operant conditioned reflex using microdialysis. Neurochem Int 43:67–72. https://doi.org/10.1016/S0197-0186(02)00192-4

Dubinsky JM (2009) Heterogeneity of nervous system mitochondria: Location, location, location! Exp Neurol 218:293–307. https://doi.org/10.1016/j.expneurol.2009.05.020

Duncan C, Dougall H, Johnston P, et al (1995) Chemical generation of nitric oxide in the mouth from the enterosalivary circulation of dietary nitrate. Nat Med 1:546–551. https://doi.org/10.1038/nm0695-546

Dunn-Meynell AA, Rawson NE, Levin BE (1998) Distribution and phenotype of neurons containing the ATP-sensitive K+ channel in rat brain. Brain Res 814:41–54. https://doi.org/https://doi.org/10.1016/S0006-8993(98)00956-1

Egea J, Fabregat I, Frapart YM, et al (2017) European contribution to the study of ROS: A summary of the findings and prospects for the future from the COST action BM1203 (EU-ROS). Redox Biol 13:94–162. https://doi.org/10.1016/j.redox.2017.05.007

Erecińska M, Silver IA (2001) Tissue oxygen tension and brain sensitivity to hypoxia. Respir Physiol 128:263–276. https://doi.org/10.1016/S0034-5687(01)00306-1

Eriksson G, Peterson A, Iverfeldt K, Walum E (1995) Sodium-dependent glutamate uptake as an activator of oxidative metabolism in primary astrocyte cultures from newborn rat. Glia 15:152–156. https://doi.org/10.1002/glia.440150207

Fabian RH, DeWitt DS, Kent TA (1995) In vivo Detection of Superoxide Anion Production by the Brain Using a Cytochrome c Electrode. J Cereb Blood Flow Metab 15:242–247. https://doi.org/10.1038/jcbfm.1995.30

Fan J-L, O'Donnell T, Lanford J, et al (2020) Dietary nitrate reduces blood pressure and cerebral artery velocity fluctuations and improves cerebral autoregulation in transient ischemic attack patients. J Appl Physiol 129:547–557. https://doi.org/10.1152/japplphysiol.00160.2020

Fang L, Liang B, Yang G, et al (2017) A needle-type glucose biosensor based on PANI nanofibers and PU/E-PU membrane for long-term invasive continuous monitoring. Biosens Bioelectron 97:196–202. https://doi.org/10.1016/j.bios.2017.04.043

Feigin VL, Stark BA, Johnson CO, et al (2021) Global, regional, and national burden of stroke and its risk factors, 1990-2019: a systematic analysis for the Global Burden of Disease Study 2019. Lancet Neurol 20:795–820. https://doi.org/10.1016/S1474-4422(21)00252-0

Feng Y, Lu Y, Lin X, et al (2008) Endomorphins and morphine limit anoxia–reoxygenation-induced brain mitochondrial dysfunction in the mouse. Life Sci 82:752–763. https://doi.org/10.1016/j.lfs.2008.01.004

Fernández-Moncada I, Ruminot I, Robles-Maldonado D, et al (2018) Neuronal control of astrocytic respiration through a variant of the Crabtree effect. Proc Natl Acad Sci 115:1623–1628. https://doi.org/10.1073/pnas.1716469115

Ferreira NR, Ledo A, Laranjinha J, et al (2018) Simultaneous measurements of ascorbate and glutamate in vivo in the rat brain using carbon fiber nanocomposite sensors and microbiosensor arrays. Bioelectrochemistry 121:142–150. https://doi.org/10.1016/j.bioelechem.2018.01.009

Ferreira NR, Santos RM, Laranjinha J, Barbosa RM (2013) Real Time In Vivo Measurement of Ascorbate in the Brain Using Carbon Nanotube-Modified Microelectrodes. Electroanalysis 25:1757–1763. https://doi.org/10.1002/elan.201300053

Figueiredo PA, Ferreira RM, Appell HJ, Duarte JA (2008) Age-Induced Morphological, Biochemical, and Functional Alterations in Isolated Mitochondria From Murine Skeletal Muscle. Journals Gerontol Ser A 63:350–359. https://doi.org/10.1093/gerona/63.4.350

Finkel T (2011) Signal transduction by reactive oxygen species. J Cell Biol 194:7–15. https://doi.org/10.1083/jcb.201102095

Fiskum G, Craig SW, Decker GL, Lehninger AL (1980) The cytoskeleton of digitonin-treated rat hepatocytes. Proc Natl Acad Sci 77:3430 LP – 3434. https://doi.org/10.1073/pnas.77.6.3430

Fonnum F, Johnsen A, Hassel B (1997) Use of fluorocitrate and fluoroacetate in the study of brain metabolism. Glia 21:106–113. https://doi.org/10.1002/(SICI)1098-1136(199709)21:1<106::AID-GLIA12>3.0.CO;2-W

Forderhase AG, Styers HC, Lee CA, Sombers LA (2020) Simultaneous voltammetric detection of glucose and lactate fluctuations in rat striatum evoked by electrical stimulation of the midbrain. Anal Bioanal Chem 412:6611–6624. https://doi.org/10.1007/s00216-020-02797-0

Foster MW, Hess DT, Stamler JS (2009) Protein S-nitrosylation in health and disease: a current perspective. Trends Mol Med 15:391–404. https://doi.org/10.1016/j.molmed.2009.06.007

Fox PT, Raichle ME, Mintun MA, Dence C (1988) Nonoxidative glucose consumption during focal physiologic neural activity. Science (80-) 241:462 LP – 464. https://doi.org/10.1126/science.3260686

Franko E, Ezra M, Crockett DC, et al (2019) Effect of nitrite on the electroencephalographic activity in the healthy brain. Nitric Oxide 90:47–54. https://doi.org/10.1016/j.niox.2019.06.002

Freund TF, Buzsáki G (1996) Interneurons of the hippocampus. Hippocampus 6:347–470. https://doi.org/10.1002/(SICI)1098-1063(1996)6:4<347::AID-HIPO1>3.0.CO;2-I

Fukuda T, Kakinohana M, Takayama C, et al (2015) Dietary supplementation with sodium nitrite can exert neuroprotective effects on global cerebral ischemia/reperfusion in mice. J Anesth 29:609–617. https://doi.org/10.1007/s00540-014-1968-6

Gago B, Lundberg JO, Barbosa RM, Laranjinha J (2007) Red wine-dependent reduction of nitrite to nitric oxide in the stomach. Free Radic Biol Med 43:1233–1242. https://doi.org/10.1016/j.freeradbiomed.2007.06.007

Galkin A (2019) Brain Ischemia/Reperfusion Injury and Mitochondrial Complex I Damage. Biochem 84:1411–1423. https://doi.org/10.1134/S0006297919110154

Galkin A, Moncada S (2017) Modulation of the conformational state of mitochondrial complex I as a target for therapeutic intervention. Interface Focus 7:20160104. https://doi.org/10.1098/rsfs.2016.0104

Galkin A, Moncada S (2007) S-Nitrosation of Mitochondrial Complex I Depends on Its Structural Conformation*. J Biol Chem 282:37448–37453. https://doi.org/10.1074/jbc.M707543200

Gertsenshteyn I, Giurcanu M, Vaupel P, Halpern H (2021) Biological validation of electron paramagnetic resonance (EPR) image oxygen thresholds in tissue. J Physiol 599:1759–1767. https://doi.org/10.1113/JP278816

Gilchrist M, Winyard PG, Fulford J, et al (2014) Dietary nitrate supplementation improves reaction time in type 2 diabetes: Development and application of a novel nitrate-depleted beetroot juice placebo. Nitric Oxide 40:67–74. https://doi.org/10.1016/j.niox.2014.05.003

Giulivi C (2003) Characterization and function of mitochondrial nitric-oxide synthase. Free Radic Biol Med 34:397–408. https://doi.org/10.1016/S0891-5849(02)01298-4

Gjedde A, Magistretti P (2011) Cellular Mechanisms of Brain Energy Metabolism. In: Youmans neurological surgery. Volume 1. pp 123–146

Gnaiger E (2001) Bioenergetics at low oxygen: dependence of respiration and phosphorylation on oxygen and adenosine diphosphate supply. Respir Physiol 128:277–297. https://doi.org/10.1016/S0034-5687(01)00307-3

Gnaiger E (2008) Polarographic Oxygen Sensors, the Oxygraph, and High-Resolution Respirometry to Assess Mitochondrial Function. In: Drug-Induced Mitochondrial Dysfunction. pp 325–352

Gnaiger E (1993) Nonequilibrium thermodynamics of energy transformations. Pure Appl Chem 65:1983–2002. https://doi.org/10.1351/pac199365091983

Gnaiger E, et al, ― MitoEAGLE Task Group (2020) Mitochondrial physiology. Bioenerg Commun 2020.1: https://doi.org/10.26124/bec:2020-0001.v1

Gnaiger E, Steinlechner-Maran R, Méndez G, et al (1995) Control of mitochondrial and cellular respiration by oxygen. J Bioenerg Biomembr 27:583–596. https://doi.org/10.1007/BF02111656

Goldenthal MJ, Marín-García J (2004) Mitochondrial signaling pathways: A receiver/integrator organelle. Mol Cell Biochem 262:1–16. https://doi.org/10.1023/B:MCBI.0000038228.85494.3b

Goldstein S, Russo A, Samuni A (2003) Reactions of PTIO and Carboxy-PTIO with ·NO, ·NO2, and O2.¯*. J Biol Chem 278:50949–50955. https://doi.org/10.1074/jbc.M308317200

Green DJ, Maiorana A, O'Driscoll G, Taylor R (2004) Effect of exercise training on endothelium-derived nitric oxide function in humans. J Physiol 561:1–25. https://doi.org/10.1113/jphysiol.2004.068197

Guix FX, Uribesalgo I, Coma M, Muñoz FJ (2005) The physiology and pathophysiology of nitric oxide in the brain. Prog Neurobiol 76:126–152. https://doi.org/10.1016/j.pneurobio.2005.06.001

Hagen T, Taylor CT, Lam F, Moncada S (2003) Redistribution of Intracellular Oxygen in Hypoxia by Nitric Oxide: Effect on HIF1α. Science (80-) 302:1975 LP – 1978. https://doi.org/10.1126/science.1088805

Halestrap AP, Wilson MC (2012) The monocarboxylate transporter family—Role and regulation. IUBMB Life 64:109–119. https://doi.org/10.1002/iub.572

Hall A, Larsen AK, Parhamifar L, et al (2013) High resolution respirometry analysis of polyethylenimine-mediated mitochondrial energy crisis and cellular stress: Mitochondrial proton leak and inhibition of the electron transport system. Biochim Biophys Acta - Bioenerg 1827:1213–1225. https://doi.org/10.1016/j.bbabio.2013.07.001

Halliday G (2017) Pathology and hippocampal atrophy in Alzheimer's disease. Lancet Neurol 16:862–864. https://doi.org/10.1016/S1474-4422(17)30343-5

Hals IK, Bruerberg SG, Ma Z, et al (2015) Mitochondrial Respiration in Insulin-Producing β-Cells: General Characteristics and Adaptive Effects of Hypoxia. PLoS One 10:e0138558. https://doi.org/10.1371/journal.pone.0138558

Hansen AJ (1985) Effect of anoxia on ion distribution in the brain. Physiol Rev 65:101–148. https://doi.org/10.1152/physrev.1985.65.1.101

Harada M, Sawa T, Okuda C, et al (1993) Effects of glucose load on brain extracellular lactate concentration in conscious rats using a microdialysis technique. Horm Metab Res 25:560–3. https://doi.org/10.1055/s-2007-1002177

Harris JJ, Jolivet R, Attwell D (2012) Synaptic Energy Use and Supply. Neuron 75:762–777. https://doi.org/10.1016/j.neuron.2012.08.019

Hassel B, Westergaard N, Schousboe A, Fonnum F (1995) Metabolic differences between primary cultures of astrocytes and neurons from cerebellum and cerebral cortex. Effects of fluorocitrate. Neurochem Res 20:413–420. https://doi.org/10.1007/BF00973096

Herbst EAF, Holloway GP (2015) Permeabilization of brain tissue in situ enables multiregion analysis of mitochondrial function in a single mouse brain. J Physiol 593:787–801. https://doi.org/10.1113/jphysiol.2014.285379

Hernansanz-Agustín P, Enríquez JA (2021) Generation of Reactive Oxygen Species by Mitochondria. Antioxidants 10:. https://doi.org/10.3390/antiox10030415

Herrero-Mendez A, Almeida A, Fernández E, et al (2009) The bioenergetic and antioxidant status of neurons is controlled by continuous degradation of a key glycolytic enzyme by APC/C-Cdh1. Nat Cell Biol 11:747–752. https://doi.org/10.1038/ncb1881

Hertz L (2012) Metabolic Studies in Brain Slices – Past, Present, and Future. Front Pharmacol 3:26. https://doi.org/10.3389/fphar.2012.00026

Hertz L, Chen Y (2017) Integration between Glycolysis and Glutamate-Glutamine Cycle Flux May Explain Preferential Glycolytic Increase during Brain Activation, Requiring Glutamate. Front Integr Neurosci 11:18. https://doi.org/10.3389/fnint.2017.00018

Hertz L, Dittmann L, Mandel P (1973) K+ induced stimulation of oxygen uptake in cultured cerebral glial cells. Brain Res 60:517–520. https://doi.org/10.1016/0006-8993(73)90814-7

Hertz L, Schou M (1962) Univalent cations and the respiration of brain-cortex slices. Biochem J 85:93–104. https://doi.org/10.1042/bj0850093

Hertz L, Xu J, Song D, et al (2013) Astrocytic and neuronal accumulation of elevated extracellular K+ with a 2/3 K+/Na+ flux ratio - consequences for energy metabolism, osmolarity and higher brain function. Front Comput Neurosci 7:114. https://doi.org/10.3389/fncom.2013.00114

Hill BG, Dranka BP, Bailey SM, et al (2010) What Part of NO Don't You Understand? Some Answers to the Cardinal Questions in Nitric Oxide Biology *. J Biol Chem 285:19699–19704. https://doi.org/10.1074/jbc.R110.101618

Hinzman JM, DiNapoli VA, Mahoney EJ, et al (2015) Spreading depolarizations mediate excitotoxicity in

the development of acute cortical lesions. Exp Neurol 267:243–253. https://doi.org/10.1016/j.expneurol.2015.03.014

Hirst J (2013) Mitochondrial Complex I. Annu Rev Biochem 82:551–575. https://doi.org/10.1146/annurev-biochem-070511-103700

Hollnagel J-O, Cesetti T, Schneider J, et al (2020) Lactate Attenuates Synaptic Transmission and Affects Brain Rhythms Featuring High Energy Expenditure. iScience 23:. https://doi.org/10.1016/j.isci.2020.101316

Holloway PM, Gavins FNE (2016) Modeling Ischemic Stroke In Vitro: Status Quo and Future Perspectives. Stroke 47:561–569. https://doi.org/10.1161/STROKEAHA.115.011932

Honegger P, Pardo B (1999) Separate Neuronal and Glial Na+,K+-ATPase Isoforms Regulate Glucose Utilization in Response to Membrane Depolarization and Elevated Extracellular Potassium. J Cereb Blood Flow Metab 19:1051–1059. https://doi.org/10.1097/00004647-199909000-00013

Horan MP, Pichaud N, Ballard JWO (2012) Review: Quantifying Mitochondrial Dysfunction in Complex Diseases of Aging. Journals Gerontol Ser A 67:1022–1035. https://doi.org/10.1093/gerona/glr263

Hossmann K-A (2012) The Two Pathophysiologies of Focal Brain Ischemia: Implications for Translational Stroke Research. J Cereb Blood Flow Metab 32:1310–1316. https://doi.org/10.1038/jcbfm.2011.186

Howarth C, Gleeson P, Attwell D (2012) Updated energy budgets for neural computation in the neocortex and cerebellum. J Cereb blood flow Metab 32:1222–1232. https://doi.org/10.1038/jcbfm.2012.35

Hoyer S, Oesterreich K, Wagner O (1988) Glucose metabolism as the site of the primary abnormality in early-onset dementia of Alzheimer type? J Neurol 235:143–148. https://doi.org/10.1007/BF00314304

Hu Y, Wilson GS (1997) A Temporary Local Energy Pool Coupled to Neuronal Activity: Fluctuations of Extracellular Lactate Levels in Rat Brain Monitored with Rapid-Response Enzyme-Based Sensor. J Neurochem 69:1484–1490. https://doi.org/10.1046/j.1471-4159.1997.69041484.x

Hütter E, Renner K, Pfister G, et al (2004) Senescence-associated changes in respiration and oxidative phosphorylation in primary human fibroblasts. Biochem J 380:919–928. https://doi.org/10.1042/bj20040095

Hütter E, Unterluggauer H, Garedew A, et al (2006) High-resolution respirometry–a modern tool in aging research. Exp Gerontol 41:103–109. https://doi.org/10.1016/j.exger.2005.09.011

Iadecola C, Anrather J (2011) The immunology of stroke: from mechanisms to translation. Nat Med 17:796–808. https://doi.org/10.1038/nm.2399

Ischiropoulos H (2009) Protein tyrosine nitration - An update. Arch Biochem Biophys 484:117–121.

https://doi.org/10.1016/j.abb.2008.10.034

Itoh Y, Esaki T, Shimoji K, et al (2003) Dichloroacetate effects on glucose and lactate oxidation by neurons and astroglia in vitro and on glucose utilization by brain in vivo. Proc Natl Acad Sci 100:4879 LP – 4884. https://doi.org/10.1073/pnas.0831078100

Ivanov AI, Malkov AE, Waseem T, et al (2014) Glycolysis and Oxidative Phosphorylation in Neurons and Astrocytes during Network Activity in Hippocampal Slices. J Cereb Blood Flow Metab 34:397–407. https://doi.org/10.1038/jcbfm.2013.222

Jarrard LE (1995) What does the hippocampus really do? Behav Brain Res 71:1–10. https://doi.org/10.1016/0166-4328(95)00034-8

Jastroch M, Divakaruni AS, Mookerjee S, et al (2010) Mitochondrial proton and electron leaks. Essays Biochem 47:53–67. https://doi.org/10.1042/bse0470053

Jemmerson R, Dubinsky JM, Brustovetsky N (2005) Cytochrome c Release from CNS Mitochondria and Potential for Clinical Intervention in Apoptosis-Mediated CNS Diseases. Antioxid Redox Signal 7:1158–1172. https://doi.org/10.1089/ars.2005.7.1158

Jørgensen T, Grunnet N, Quistorff B (2015) One-Year High Fat Diet Affects Muscle-But Not Brain Mitochondria. J Cereb Blood Flow Metab 35:943–950. https://doi.org/10.1038/jcbfm.2015.27

Joyce OJP, Farmer MK, Tipton KF, Porter RK (2003) Oxidative phosphorylation by in situ synaptosomal mitochondria from whole brain of young and old rats. J Neurochem 86:1032–1041. https://doi.org/10.1046/j.1471-4159.2003.01915.x

Jung KH, Chu K, Ko SY, et al (2006) Early intravenous infusion of sodium nitrite protects brain against in vivo ischemia-reperfusion injury. Stroke 37:2744–2750. https://doi.org/10.1161/01.STR.0000245116.40163.1c

Junge W, Nelson N (2015) ATP Synthase. Annu Rev Biochem 84:631–657. https://doi.org/10.1146/annurev-biochem-060614-034124

Jungersten L, Ambring A, Wall B, Wennmalm Å (1997) Both physical fitness and acute exercise regulate nitric oxide formation in healthy humans. J Appl Physiol 82:760–764. https://doi.org/10.1152/jappl.1997.82.3.760

Juzekaeva E, Gainutdinov A, Mukhtarov M, Khazipov R (2020) Reappraisal of anoxic spreading depolarization as a terminal event during oxygen–glucose deprivation in brain slices in vitro. Sci Rep 10:18970. https://doi.org/10.1038/s41598-020-75975-w

Kalogeris T, Baines CP, Krenz M, Korthuis RJ (2012) Chapter Six - Cell Biology of Ischemia/Reperfusion Injury. In: Jeon KWBT-IR of C and MB (ed). Academic Press, pp 229–317

Kapil V, Khambata RS, Jones DA, et al (2020) The Noncanonical Pathway for In Vivo Nitric Oxide Generation: The Nitrate-Nitrite-Nitric Oxide Pathway. Pharmacol Rev 72:692 LP – 766. https://doi.org/10.1124/pr.120.019240

Katsounaros I, Schneider WB, Meier JC, et al (2012) Hydrogen peroxide electrochemistry on platinum: towards understanding the oxygen reduction reaction mechanism. Phys Chem Chem Phys 14:7384–7391. https://doi.org/10.1039/C2CP40616K

Kealy J, Bennett R, Lowry JP (2013) Simultaneous recording of hippocampal oxygen and glucose in real time using constant potential amperometry in the freely-moving rat. J Neurosci Methods 215:110–120. https://doi.org/10.1016/j.jneumeth.2013.02.016

Kengen SW, Bikker FJ, Hagen WR, et al (2001) Characterization of a catalase-peroxidase from the hyperthermophilic archaeon Archaeoglobus fulgidus. Extremophiles 5:323–332. https://doi.org/10.1007/s007920100208

Kharitonov VG, Sundquist AR, Sharma VS (1994) Kinetics of nitric oxide autoxidation in aqueous solution. J Biol Chem 269:5881–5883. https://doi.org/10.1016/S0021-9258(17)37543-9

Kim SJ, Song E, Jo K, et al (2013) Composite oxygen-barrier coating on a polypropylene food container. Thin Solid Films 540:112–117. https://doi.org/10.1016/j.tsf.2013.06.009

Kirchner A, Velíšková J, Velíšek L (2006) Differential effects of low glucose concentrations on seizures and epileptiform activity in vivo and in vitro. Eur J Neurosci 23:1512–1522. https://doi.org/10.1111/j.1460-9568.2006.04665.x

Kirino T, Sano K (1984) Selective vulnerability in the gerbil hippocampus following transient ischemia. Acta Neuropathol 62:201–208. https://doi.org/10.1007/BF00691853

Korn ED (1969) Cell Membranes: Structure and Synthesis. Annu Rev Biochem 38:263–288. https://doi.org/10.1146/annurev.bi.38.070169.001403

Kudin A, Vielhaber S, Beck H, et al (1999) Quantitative investigation of mitochondrial function in single rat hippocampal slices: a novel application of high-resolution respirometry and laser-excited fluorescence spectroscopy. Brain Res Protoc 4:329–334. https://doi.org/10.1016/S1385-299X(99)00037-9

Kunimatsu T, Kobayashi K, Yamashita A, et al (2011) Cerebral reactive oxygen species assessed by electron spin resonance spectroscopy in the initial stage of ischemia–reperfusion are not associated with hypothermic neuroprotection. J Clin Neurosci 18:545–548. https://doi.org/10.1016/j.jocn.2010.07.140

Kunz WS, Goussakov I V, Beck H, Elger CE (1999) Altered mitochondrial oxidative phosphorylation in hippocampal slices of kainate-treated rats. Brain Res 826:236–242. https://doi.org/10.1016/S0006-

8993(99)01279-2

Kurian GA, Pemaih B (2014) Standardization of in vitro Cell-based Model for Renal Ischemia and Reperfusion Injury. Indian J Pharm Sci 76:348–353. https://doi.org/10.4103/0250-474X.139930

Kuzenkov VS, Krushinskii AL (2014) Protective Effect of Magnesium Nitrate against Neurological Disorders Provoked by Cerebral Ischemia in Rats. Bull Exp Biol Med 157:721–723. https://doi.org/10.1007/s10517-014-2651-5

Kuznetsov A V, Veksler V, Gellerich FN, et al (2008) Analysis of mitochondrial function in situ in permeabilized muscle fibers, tissues and cells. Nat Protoc 3:965–976. https://doi.org/10.1038/nprot.2008.61

Lahtinen H, Autere A-M, Paalasmaa P, et al (2001) Post-insult activity is a major cause of delayed neuronal death in organotypic hippocampal slices exposed to glutamate. Neuroscience 105:131–137. https://doi.org/10.1016/S0306-4522(01)00168-3

LaManna JC, Chavez JC, Pichiule P (2004) Structural and functional adaptation to hypoxia in the rat brain. J Exp Biol 207:3163–3169. https://doi.org/10.1242/jeb.00976

Larrabee MG (1996) Partitioning of CO2 Production Between Glucose and Lactate in Excised Sympathetic Ganglia, with Implications for Brain. J Neurochem 67:1726–1734. https://doi.org/10.1046/j.1471-4159.1996.67041726.x

Ledo A, Barbosa R, Cadenas E, Laranjinha J (2010) Dynamic and interacting profiles of *NO and O2 in rat hippocampal slices. Free Radic Biol Med 48:1044–50. https://doi.org/10.1016/j.freeradbiomed.2010.01.024

Ledo A, Barbosa RM, Gerhardt GA, et al (2005) Concentration dynamics of nitric oxide in rat hippocampal subregions evoked by stimulation of the NMDA glutamate receptor. Proc Natl Acad Sci U S A 102:17483–17488. https://doi.org/10.1073/pnas.0503624102

Ledo A, Lourenço CF, Cadenas E, et al (2021) The bioactivity of neuronal-derived nitric oxide in aging and neurodegeneration: Switching signaling to degeneration. Free Radic Biol Med 162:500–513. https://doi.org/https://doi.org/10.1016/j.freeradbiomed.2020.11.005

Ledo A, Lourenço CF, Laranjinha J, et al (2017a) Ceramic-Based Multisite Platinum Microelectrode Arrays: Morphological Characteristics and Electrochemical Performance for Extracellular Oxygen Measurements in Brain Tissue. Anal Chem 89:1674–1683. https://doi.org/10.1021/acs.analchem.6b03772

Ledo A, Lourenço CF, Laranjinha J, et al (2018) Concurrent measurements of neurochemical and electrophysiological activity with microelectrode arrays: New perspectives for constant potential amperometry. Curr Opin Electrochem 12:129–140. https://doi.org/10.1016/j.coelec.2018.05.018

Ledo A, Lourenço CF, Laranjinha J, et al (2017b) Combined in Vivo Amperometric Oximetry and Electrophysiology in a Single Sensor: A Tool for Epilepsy Research. Anal Chem 89:12383–12390. https://doi.org/10.1021/acs.analchem.7b03452

Lein PJ, Barnhart CD, Pessah IN (2011) Acute hippocampal slice preparation and hippocampal slice cultures. Methods Mol Biol 758:115–134. https://doi.org/10.1007/978-1-61779-170-3_8

Lesnefsky EJ, Chen Q, Moghaddas S, et al (2004) Blockade of Electron Transport during Ischemia Protects Cardiac Mitochondria *. J Biol Chem 279:47961–47967. https://doi.org/10.1074/jbc.M409720200

Levasseur JE, Alessandri B, Reinert M, et al (2006) Lactate, not glucose, up-regulates mitochondrial oxygen consumption both in sham and lateral fluid percussed rat brains. Neurosurgery 59:1122–1131. https://doi.org/10.1227/01.NEU.0000245581.00908.AF

Lidder S, Webb AJ (2013) Vascular effects of dietary nitrate (as found in green leafy vegetables and beetroot) via the nitrate-nitrite-nitric oxide pathway. Br J Clin Pharmacol 75:677–696. https://doi.org/10.1111/j.1365-2125.2012.04420.x

Lin L, Wang X, Yu Z (2016) Ischemia-reperfusion Injury in the Brain: Mechanisms and Potential Therapeutic Strategies. Biochem Pharmacol 5:213. https://doi.org/10.4172/2167-0501.1000213

Lin MT, Beal MF (2006) Mitochondrial dysfunction and oxidative stress in neurodegenerative diseases. Nature 443:787–795. https://doi.org/10.1038/nature05292

Linas SL, Whittenburg D, Repine JE (1990) Role of xanthine oxidase in ischemia/reperfusion injury. Am J Physiol Physiol 258:F711–F716. https://doi.org/10.1152/ajprenal.1990.258.3.F711

Liu H, Le W (2014) Epigenetic modifications of chronic hypoxia-mediated neurodegeneration in Alzheimer's disease. Transl Neurodegener 3:7. https://doi.org/10.1186/2047-9158-3-7

Liu X, Miller MJS, Joshi MS, et al (1998) Accelerated reaction of nitric oxide with O_2 within the hydrophobic interior of biological membranes. Proc Natl Acad Sci 95:2175 LP – 2179. https://doi.org/10.1073/pnas.95.5.2175

Loor G, Kondapalli J, Iwase H, et al (2011) Mitochondrial oxidant stress triggers cell death in simulated ischemia–reperfusion. Biochim Biophys Acta - Mol Cell Res 1813:1382–1394. https://doi.org/10.1016/j.bbamcr.2010.12.008

Lourenço CF, Caetano M, Ledo A, Barbosa RM (2019) Platinized carbon fiber-based glucose microbiosensor designed for metabolic studies in brain slices. Bioelectrochemistry 130:107325. https://doi.org/10.1016/j.bioelechem.2019.06.010

Lourenço CF, Ferreira NR, Santos RM, et al (2014a) The pattern of glutamate-induced nitric oxide dynamics in vivo and its correlation with nNOS expression in rat hippocampus, cerebral cortex and

striatum. Brain Res 1554:1–11. https://doi.org/10.1016/j.brainres.2014.01.030

Lourenço CF, Ledo A, Barbosa RM, Laranjinha J (2017a) Neurovascular-neuroenergetic coupling axis in the brain: master regulation by nitric oxide and consequences in aging and neurodegeneration. Free Radic Biol Med 108:668–682. https://doi.org/10.1016/j.freeradbiomed.2017.04.026

Lourenço CF, Ledo A, Gerhardt GA, et al (2017b) Neurometabolic and electrophysiological changes during cortical spreading depolarization: multimodal approach based on a lactate-glucose dual microbiosensor arrays. Sci Rep 7:6764. https://doi.org/10.1038/s41598-017-07119-6

Lourenço CF, Santos RM, Barbosa RM, et al (2014b) Neurovascular coupling in hippocampus is mediated via diffusion by neuronal-derived nitric oxide. Free Radic Biol Med 73:421–429. https://doi.org/https://doi.org/10.1016/j.freeradbiomed.2014.05.021

Lovatt D, Sonnewald U, Waagepetersen HS, et al (2007) The Transcriptome and Metabolic Gene Signature of Protoplasmic Astrocytes in the Adult Murine Cortex. J Neurosci 27:12255 LP – 12266. https://doi.org/10.1523/JNEUROSCI.3404-07.2007

Luettich A, Franko E, Spronk DB, et al (2021) Beneficial Effect of Sodium Nitrite on EEG Ischaemic Markers in Patients with Subarachnoid Haemorrhage. Transl Stroke Res. https://doi.org/10.1007/s12975-021-00939-9

Lundberg JO, Govoni M (2004) Inorganic nitrate is a possible source for systemic generation of nitric oxide. Free Radic Biol Med 37:395–400. https://doi.org/10.1016/j.freeradbiomed.2004.04.027

Lundberg JO, Weitzberg E, Gladwin MT (2008) The nitrate–nitrite–nitric oxide pathway in physiology and therapeutics. Nat Rev Drug Discov 7:156–167. https://doi.org/10.1038/nrd2466

Mächler P, Wyss MT, Elsayed M, et al (2016) In Vivo Evidence for a Lactate Gradient from Astrocytes to Neurons. Cell Metab 23:94–102. https://doi.org/10.1016/j.cmet.2015.10.010

Magistretti PJ, Allaman I (2015) A Cellular Perspective on Brain Energy Metabolism and Functional Imaging. Neuron 86:883–901

Magistretti PJ, Allaman I (2018) Lactate in the brain: from metabolic end-product to signalling molecule. Nat Rev Neurosci 19:235–249. https://doi.org/10.1038/nrn.2018.19

Magistretti PJ, Pellerin L, Rothman DL, Shulman RG (1999) Energy on Demand. Science (80-) 283:496 LP – 497. https://doi.org/10.1126/science.283.5401.496

Mangia S, Garreffa G, Bianciardi M, et al (2003) The aerobic brain: lactate decrease at the onset of neural activity. Neuroscience 118:7–10. https://doi.org/10.1016/S0306-4522(02)00792-3

Manz KM, Siemann JK, McMahon DG, Grueter BA (2021) Patch-clamp and multi-electrode array electrophysiological analysis in acute mouse brain slices. STAR Protoc 2:100442.

https://doi.org/10.1016/j.xpro.2021.100442

Martens U, Capito B, Wree A (1998) Septotemporal distribution of [3H]MK-801, [3H]AMPA and [3H]Kainate binding sites in the rat hippocampus. Anat Embryol (Berl) 198:195–204. https://doi.org/10.1007/s004290050177

Maruyama D, Hirata N, Miyashita R, et al (2013) Substrate-dependent modulation of oxidative phosphorylation in isolated mitochondria following in vitro hypoxia and reoxygenation injury. Exp Clin Cardiol 18:158–160

Mayor D, Tymianski M (2018) Neurotransmitters in the mediation of cerebral ischemic injury. Neuropharmacology 134:178–188. https://doi.org/10.1016/j.neuropharm.2017.11.050

Mazuel L, Blanc J, Repond C, et al (2017) A neuronal MCT2 knockdown in the rat somatosensory cortex reduces both the NMR lactate signal and the BOLD response during whisker stimulation. PLoS One 12:e0174990

McBride HM, Neuspiel M, Wasiak S (2006) Mitochondria: More Than Just a Powerhouse. Curr Biol 16:R551–R560. https://doi.org/10.1016/j.cub.2006.06.054

McIlwain H (1953) Substances which support respiration and metabolic response to electrical impulses in human cerebral tissues. J Neurol Neurosurg Psychiatry 16:257–266. https://doi.org/10.1136/jnnp.16.4.257

McKenna MC (2013) Glutamate Pays Its Own Way in Astrocytes. Front Endocrinol (Lausanne) 4:191. https://doi.org/10.3389/fendo.2013.00191

McKnight GM, Smith LM, Drummond RS, et al (1997) Chemical synthesis of nitric oxide in the stomach from dietary nitrate in humans. Gut 40:211 LP – 214. https://doi.org/10.1136/gut.40.2.211

McNay EC, Gold PE (1999) Extracellular Glucose Concentrations in the Rat Hippocampus Measured by Zero-Net-Flux. J Neurochem 72:785–790. https://doi.org/10.1046/j.1471-4159.1999.720785.x

Mergenthaler P, Lindauer U, Dienel GA, Meisel A (2013) Sugar for the brain: The role of glucose in physiological and pathological brain function. Trends Neurosci. 36:587–597

Meyerhoff JB, Ewing MA, Ewing AG (1999) Ultrasmall Enzyme Electrodes with Response Time Less than 100 Milliseconds. Electroanalysis 11:308–312. https://doi.org/https://doi.org/10.1002/(SICI)1521-4109(199905)11:5<308::AID-ELAN308>3.0.CO;2-K

Millar J (1995) The nitric oxide/ascorbate cycle: How neurones may control their own oxygen supply. Med Hypotheses 45:21–26. https://doi.org/10.1016/0306-9877(95)90194-9

Mitchell P (2011) Chemiosmotic coupling in oxidative and photosynthetic phosphorylation. Biochim

Biophys Acta - Bioenerg 1807:1507–1538. https://doi.org/10.1016/j.bbabio.2011.09.018

Moller M, Botti H, Batthyany C, et al (2005) Direct measurement of nitric oxide and oxygen partitioning into liposomes and low density lipoprotein. J Biol Chem 280:8850–8854. https://doi.org/10.1074/jbc.M413699200

Möller MN, Denicola A (2018) Diffusion of nitric oxide and oxygen in lipoproteins and membranes studied by pyrene fluorescence quenching. Free Radic Biol Med 128:137–143. https://doi.org/10.1016/j.freeradbiomed.2018.04.553

Moncada S, Palmer RM, Higgs EA (1991) Nitric oxide: physiology, pathophysiology, and pharmacology. Pharmacol Rev 43:109 LP – 142

Mongeon R, Venkatachalam V, Yellen G (2016) Cytosolic NADH-NAD(+) Redox Visualized in Brain Slices by Two-Photon Fluorescence Lifetime Biosensor Imaging. Antioxid Redox Signal 25:553–563. https://doi.org/10.1089/ars.2015.6593

Montenegro MF, Sundqvist ML, Nihlén C, et al (2016) Profound differences between humans and rodents in the ability to concentrate salivary nitrate: Implications for translational research. Redox Biol 10:206–210. https://doi.org/10.1016/j.redox.2016.10.011

Monzio Compagnoni G, Di Fonzo A, Corti S, et al (2020) The Role of Mitochondria in Neurodegenerative Diseases: the Lesson from Alzheimer's Disease and Parkinson's Disease. Mol Neurobiol 57:2959–2980. https://doi.org/10.1007/s12035-020-01926-1

Mor I, Cheung EC, Vousden KH (2011) Control of Glycolysis through Regulation of PFK1: Old Friends and Recent Additions. Cold Spring Harb Symp Quant Biol 76:211–216. https://doi.org/10.1101/sqb.2011.76.010868

Morin C, Zini R, Tillement J-P (2003) Anoxia–reoxygenation-induced cytochrome c and cardiolipin release from rat brain mitochondria. Biochem Biophys Res Commun 307:477–482. https://doi.org/10.1016/S0006-291X(03)01203-8

Mosqueira M, Iturriaga R (2019) Chronic hypoxia changes gene expression profile of primary rat carotid body cells: consequences on the expression of NOS isoforms and ET-1 receptors. Physiol Genomics 51:109–124. https://doi.org/10.1152/physiolgenomics.00114.2018

Mota SI, Ferreira IL, Valero J, et al (2014) Impaired Src signaling and post-synaptic actin polymerization in Alzheimer's disease mice hippocampus — Linking NMDA receptors and the reelin pathway. Exp Neurol 261:698–709. https://doi.org/10.1016/j.expneurol.2014.07.023

Mottahedin A, Svedin P, Nair S, et al (2017) Systemic activation of Toll-like receptor 2 suppresses mitochondrial respiration and exacerbates hypoxic–ischemic injury in the developing brain. J Cereb Blood Flow Metab 37:1192–1198. https://doi.org/10.1177/0271678X17691292

Murillo D, Kamga C, Mo L, Shiva S (2011) Nitrite as a mediator of ischemic preconditioning and cytoprotection. Nitric Oxide 25:70–80. https://doi.org/10.1016/j.niox.2011.01.003

Murphy MP (2009) How mitochondria produce reactive oxygen species. Biochem J 417:1–13. https://doi.org/10.1042/BJ20081386

Murr R, Berger S, Schürer L, et al (1994) A novel, remote-controlled suspension device for brain tissue PO2 measurements with multiwire surface electrodes. Pflügers Arch 426:348–350. https://doi.org/10.1007/BF00374792

Myers AW, Stannett V, Szwarc M (1959) The permeability of polypropylene to gases and vapors. J Polym Sci 35:285–288. https://doi.org/10.1002/pol.1959.1203512830

Nair PK, Buerk DG, Halsey JH (1987) Comparisons of oxygen metabolism and tissue PO2 in cortex and hippocampus of gerbil brain. Stroke 18:616–622. https://doi.org/10.1161/01.STR.18.3.616

Namba K, Takeda Y, Sunami K, Hirakawa M (2001) Temporal Profiles of the Levels of Endogenous Antioxidants After Four-Vessel Occlusion in Rats. J Neurosurg Anesthesiol 13:. https://doi.org/10.1097/00008506-200104000-00010

Nehlig A, Wittendorp-Rechenmann E, Dao Lam C (2004) Selective Uptake of [14C]2-Deoxyglucose by Neurons and Astrocytes: High-Resolution Microautoradiographic Imaging by Cellular 14C-Trajectography Combined with Immunohistochemistry. J Cereb Blood Flow Metab 24:1004–1014. https://doi.org/10.1097/01.WCB.0000128533.84196.D8

Nelson DL (David L, Cox MM, Lehninger AL (2008) Lehninger principles of biochemistry, 5th ed. W.H. Freeman, New York

Newman LA, Korol DL, Gold PE (2011) Lactate Produced by Glycogenolysis in Astrocytes Regulates Memory Processing. PLoS One 6:e28427

Ni H-M, Williams JA, Ding W-X (2015) Mitochondrial dynamics and mitochondrial quality control. Redox Biol 4:6–13. https://doi.org/10.1016/j.redox.2014.11.006

Niciu MJ, Kelmendi B, Sanacora G (2012) Overview of glutamatergic neurotransmission in the nervous system. Pharmacol Biochem Behav 100:656–664. https://doi.org/10.1016/j.pbb.2011.08.008

Oddo S, Caccamo A, Shepherd JD, et al (2003) Triple-Transgenic Model of Alzheimer's Disease with Plaques and Tangles: Intracellular Aβ and Synaptic Dysfunction. Neuron 39:409–421. https://doi.org/10.1016/S0896-6273(03)00434-3

Olbrich H-G, Braak H (1985) Ratio of pyramidal cells versus non-pyramidal cells in sector CA1 of the human Ammon's horn. Anat Embryol (Berl) 173:105–110. https://doi.org/10.1007/BF00707308

Olesen J (1970) Total CO2, lactate, and pyruvate in brain biopsies taken after freezing the tissue in situ.

Acta Neurol Scand 46:141–148. https://doi.org/10.1111/j.1600-0404.1970.tb05613.x

Olsen TS, Skriver EB, Herning M (1985) Cause of cerebral infarction in the carotid territory. Its relation to the size and the location of the infarct and to the underlying vascular lesion. Stroke 16:459–466. https://doi.org/10.1161/01.STR.16.3.459

Onodera H, Sato G, Kogure K (1986) Lesions to Schaffer collaterals prevent ischemic death of CA1 pyramidal cells. Neurosci Lett 68:169–174. https://doi.org/10.1016/0304-3940(86)90136-9

Ordy JM, Wengenack TM, Bialobok P, et al (1993) Selective Vulnerability and Early Progression of Hippocampal CA1 Pyramidal Cell Degeneration and GFAP-Positive Astrocyte Reactivity in the Rat Four-Vessel Occlusion Model of Transient Global Ischemia. Exp Neurol 119:128–139. https://doi.org/10.1006/exnr.1993.1014

Ouyang Y-B, Voloboueva LA, Xu L-J, Giffard RG (2007) Selective Dysfunction of Hippocampal CA1 Astrocytes Contributes to Delayed Neuronal Damage after Transient Forebrain Ischemia. J Neurosci 27:4253 LP – 4260. https://doi.org/10.1523/JNEUROSCI.0211-07.2007

Ovens MJ, Davies AJ, Wilson MC, et al (2010) AR-C155858 is a potent inhibitor of monocarboxylate transporters MCT1 and MCT2 that binds to an intracellular site involving transmembrane helices 7–10. Biochem J 425:523–530. https://doi.org/10.1042/BJ20091515

Palmeira CMM, Moreno AJ (2018) Mitochondrial Bioenergetics. Methods in Molecular Biology., 2nd edn. Humana Press, Nwe York

Panuccio G, Colombi I, Chiappalone M (2018) Recording and Modulation of Epileptiform Activity in Rodent Brain Slices Coupled to Microelectrode Arrays. JoVE e57548. https://doi.org/10.3791/57548

Papandreou I, Cairns RA, Fontana L, et al (2006) HIF-1 mediates adaptation to hypoxia by actively downregulating mitochondrial oxygen consumption. Cell Metab 3:187–197. https://doi.org/10.1016/j.cmet.2006.01.012

Parsons MP, Hirasawa M (2010) ATP-Sensitive Potassium Channel-Mediated Lactate Effect on Orexin Neurons: Implications for Brain Energetics during Arousal. J Neurosci 30:8061 LP – 8070. https://doi.org/10.1523/JNEUROSCI.5741-09.2010

Patel BA (2020) Chapter 12 - Electrochemical biosensors. In: Patel BBT-E for B (ed). Elsevier, pp 267–284

Pellerin L, Magistretti PJ (1994) Glutamate uptake into astrocytes stimulates aerobic glycolysis: a mechanism coupling neuronal activity to glucose utilization. Proc Natl Acad Sci 91:10625–10629. https://doi.org/10.1073/pnas.91.22.10625

Pellerin L, Magistretti PJ (2012) Sweet sixteen for ANLS. J Cereb Blood Flow Metab 32:1152–1166.

https://doi.org/10.1038/jcbfm.2011.149

Pérez-Escuredo J, Van Hée VF, Sboarina M, et al (2016) Monocarboxylate transporters in the brain and in cancer. Biochim Biophys Acta 1863:2481–2497. https://doi.org/10.1016/j.bbamcr.2016.03.013

Perry CGR, Kane DA, Lanza IR, Neufer PD (2013) Methods for Assessing Mitochondrial Function in Diabetes. Diabetes 62:1041 LP – 1053. https://doi.org/10.2337/db12-1219

Perry JB, Davis GN, Allen ME, et al (2019) Cardioprotective effects of idebenone do not involve ROS scavenging: Evidence for mitochondrial complex I bypass in ischemia/reperfusion injury. J Mol Cell Cardiol 135:160–171. https://doi.org/10.1016/j.yjmcc.2019.08.010

Pesta D, Gnaiger E (2012) High-Resolution Respirometry: OXPHOS Protocols for Human Cells and Permeabilized Fibers from Small Biopsies of Human Muscle BT - Mitochondrial Bioenergetics: Methods and Protocols. In: Palmeira CM, Moreno AJ (eds). Humana Press, Totowa, NJ, pp 25–58

Peters O, Back T, Lindauer U, et al (1998) Increased Formation of Reactive Oxygen Species after Permanent and Reversible Middle Cerebral Artery Occlusion in the Rat. J Cereb Blood Flow Metab 18:196–205. https://doi.org/10.1097/00004647-199802000-00011

Pfeiffer S, Leopold E, Hemmens B, et al (1997) Interference of Carboxy-PTIO with Nitric Oxide- and Peroxynitrite-Mediated Reactions. Free Radic Biol Med 22:787–794. https://doi.org/10.1016/S0891-5849(96)00407-8

Picard M, Ritchie D, Wright KJ, et al (2010) Mitochondrial functional impairment with aging is exaggerated in isolated mitochondria compared to permeabilized myofibers. Aging Cell 9:1032–1046. https://doi.org/10.1111/j.1474-9726.2010.00628.x

Picard M, Taivassalo T, Gouspillou G, Hepple RT (2011) Mitochondria: isolation, structure and function. J Physiol 589:4413–4421. https://doi.org/10.1113/jphysiol.2011.212712

Picón-Pagès P, Garcia-Buendia J, Muñoz FJ (2019) Functions and dysfunctions of nitric oxide in brain. Biochim Biophys Acta - Mol Basis Dis 1865:1949–1967. https://doi.org/10.1016/j.bbadis.2018.11.007

Pierrefiche O, Bischoff AM, Richter DW (1996) ATP-sensitive K+ channels are functional in expiratory neurones of normoxic cats. J Physiol 494:399–409. https://doi.org/10.1113/jphysiol.1996.sp021501

Piper HM, Sezer O, Schleyer M, et al (1985) Development of ischemia-induced damage in defined mitochondrial subpopulations. J Mol Cell Cardiol 17:885–896. https://doi.org/10.1016/S0022-2828(85)80102-4

Pluta RM, Dejam A, Grimes G, et al (2005) Nitrite Infusions to Prevent Delayed Cerebral Vasospasm in a Primate Model of Subarachnoid Hemorrhage. JAMA 293:1477–1484.

https://doi.org/10.1001/jama.293.12.1477

Rasmussen P, Nielsen J, Overgaard M, et al (2010) Reduced muscle activation during exercise related to brain oxygenation and metabolism in humans. J Physiol 588:1985–1995. https://doi.org/10.1113/jphysiol.2009.186767

Rassaf T, Flögel U, Drexhage C, et al (2007) Nitrite Reductase Function of Deoxymyoglobin. Circ Res 100:1749–1754. https://doi.org/10.1161/CIRCRESAHA.107.152488

Reid KH, Edmonds HL, Schurr A, et al (1988) Pitfalls in the use of brain slices. Prog Neurobiol 31:1–18. https://doi.org/10.1016/0301-0082(88)90020-2

Ren E, Curia G (2021) Synaptic Reshaping and Neuronal Outcomes in the Temporal Lobe Epilepsy. Int. J. Mol. Sci. 22

Rengasamy A, Johns RA (1996) Determination of Km for oxygen of nitric oxide synthase isoforms. J Pharmacol Exp Ther 276:30 LP – 33

Rice ME (2000) Ascorbate regulation and its neuroprotective role in the brain. Trends Neurosci 23:209–216. https://doi.org/10.1016/S0166-2236(99)01543-X

Richard MJP, Saleh TM, El Bahh B, Zidichouski JA (2010) A novel method for inducing focal ischemia in vitro. J Neurosci Methods 190:20–27. https://doi.org/10.1016/j.jneumeth.2010.04.017

Robinson DL, Hermans A, Seipel AT, Wightman RM (2008) Monitoring Rapid Chemical Communication in the Brain. Chem Rev 108:2554–2584. https://doi.org/10.1021/cr068081q

Rodrigues T, Valette J, Bouzier-Sore A-K (2013) 13C NMR spectroscopy applications to brain energy metabolism. Front Neuroenergetics 5:9. https://doi.org/10.3389/fnene.2013.00009

Ruminot I, Schmälzle J, Leyton B, et al (2019) Tight coupling of astrocyte energy metabolism to synaptic activity revealed by genetically encoded FRET nanosensors in hippocampal tissue. J Cereb Blood Flow Metab 39:513–523. https://doi.org/10.1177/0271678X17737012

Sacco RL, Kasner SE, Broderick JP, et al (2013) An Updated Definition of Stroke for the 21st Century. Stroke 44:2064–2089. https://doi.org/10.1161/STR.0b013e318296aeca

Salamone FN, Zhou M, Auerbach A (1999) A re-examination of adult mouse nicotinic acetylcholine receptor channel activation kinetics. J Physiol 514:327–341. https://doi.org/10.1111/j.1469-7793.1999.315ae.x

San Martín A, Ceballo S, Ruminot I, et al (2013) A Genetically Encoded FRET Lactate Sensor and Its Use To Detect the Warburg Effect in Single Cancer Cells. PLoS One 8:e57712

Sanderson TH, Reynolds CA, Kumar R, et al (2013) Molecular Mechanisms of Ischemia–Reperfusion

Injury in Brain: Pivotal Role of the Mitochondrial Membrane Potential in Reactive Oxygen Species Generation. Mol Neurobiol 47:9–23. https://doi.org/10.1007/s12035-012-8344-z

Santos RM, Lourenço CF, Piedade AP, et al (2008) A comparative study of carbon fiber-based microelectrodes for the measurement of nitric oxide in brain tissue. Biosens Bioelectron 24:704–9. https://doi.org/10.1016/j.bios.2008.06.034

Sarti P, Forte E, Mastronicola D, et al (2012) Cytochrome c oxidase and nitric oxide in action: Molecular mechanisms and pathophysiological implications. Biochim Biophys Acta - Bioenerg 1817:610–619. https://doi.org/10.1016/j.bbabio.2011.09.002

Scheff SW, Price DA (2006) Alzheimer's disease-related alterations in synaptic density: neocortex and hippocampus. J Alzheimers Dis 9:101–115. https://doi.org/10.3233/jad-2006-9s312

Schild L, Reiser G (2005) Oxidative stress is involved in the permeabilization of the inner membrane of brain mitochondria exposed to hypoxia/reoxygenation and low micromolar Ca2+. FEBS J 272:3593–3601. https://doi.org/10.1111/j.1742-4658.2005.04781.x

Schuh RA, Clerc P, Hwang H, et al (2011) Adaptation of microplate-based respirometry for hippocampal slices and analysis of respiratory capacity. J Neurosci Res 89:1979–1988. https://doi.org/10.1002/jnr.22650

Schultz C, Engelhardt M (2014) Anatomy of the Hippocampal Formation. In: Frontiers of Neurology and Neuroscience. pp 6–17

Schumacker PT, Chandel N, Agusti AG (1993) Oxygen conformance of cellular respiration in hepatocytes. Am J Physiol Cell Mol Physiol 265:L395–L402. https://doi.org/10.1152/ajplung.1993.265.4.L395

Schurr A (2014) Cerebral glycolysis: a century of persistent misunderstanding and misconception. Front Neurosci 8:360. https://doi.org/10.3389/fnins.2014.00360

Schurr A (2018) Glycolysis paradigm shift dictates a reevaluation of glucose and oxygen metabolic rates of activated neural tissue. Front Neurosci 12:700. https://doi.org/10.3389/fnins.2018.00700

Schurr A, Miller JJ, Payne RS, Rigor BM (1999) An Increase in Lactate Output by Brain Tissue Serves to Meet the Energy Needs of Glutamate-Activated Neurons. J Neurosci 19:34–39. https://doi.org/10.1523/JNEUROSCI.19-01-00034.1999

Schurr A, West CA, Rigor BM (1988) Lactate-supported synaptic function in the rat hippocampal slice preparation. Science (80-) 240:1326–1328. https://doi.org/10.1126/science.3375817

Schurr A, West CA, Rigor BM (1989) Electrophysiology of energy metabolism and neuronal function in the hippocampal slice preparation. J Neurosci Methods 28:7–13. https://doi.org/10.1016/0165-0270(89)90004-6

Serres S, Raffard G, Franconi J-M, Merle M (2007) Close Coupling between Astrocytic and Neuronal Metabolisms to Fulfill Anaplerotic and Energy Needs in the Rat Brain. J Cereb Blood Flow Metab 28:712–724. https://doi.org/10.1038/sj.jcbfm.9600568

Shen L, Chen C, Yang A, et al (2015) Redox proteomics identification of specifically carbonylated proteins in the hippocampi of triple transgenic Alzheimer's disease mice at its earliest pathological stage. J Proteomics 123:101–113. https://doi.org/10.1016/j.jprot.2015.04.005

Shestov AA, Liu X, Ser Z, et al (2014) Quantitative determinants of aerobic glycolysis identify flux through the enzyme GAPDH as a limiting step. Elife 3:e03342. https://doi.org/10.7554/eLife.03342

Shew WL, Bellay T, Plenz D (2010) Simultaneous multi-electrode array recording and two-photon calcium imaging of neural activity. J Neurosci Methods 192:75–82. https://doi.org/10.1016/j.jneumeth.2010.07.023

Shiva S (2013) Nitrite: A physiological store of nitric oxide and modulator of mitochondrial function. Redox Biol 1:40–44. https://doi.org/https://doi.org/10.1016/j.redox.2012.11.005

Shiva S, Huang Z, Grubina R, et al (2007a) Deoxymyoglobin Is a Nitrite Reductase That Generates Nitric Oxide and Regulates Mitochondrial Respiration. Circ Res 100:654–661. https://doi.org/10.1161/01.RES.0000260171.52224.6b

Shiva S, Sack MN, Greer JJ, et al (2007b) Nitrite augments tolerance to ischemia/reperfusion injury via the modulation of mitochondrial electron transfer. J Exp Med 204:2089 LP – 2102. https://doi.org/10.1084/jem.20070198

Silva AM, Oliveira PJ (2018) Evaluation of Respiration with Clark-Type Electrode in Isolated Mitochondria and Permeabilized Animal Cells BT - Mitochondrial Bioenergetics: Methods and Protocols. In: Palmeira CM, Moreno AJ (eds). Springer New York, New York, NY, pp 7–29

Silver IA, Erecińska M (1994) Extracellular glucose concentration in mammalian brain: continuous monitoring of changes during increased neuronal activity and upon limitation in oxygen supply in normo-, hypo-, and hyperglycemic animals. J Neurosci 14:5068–76. https://doi.org/10.1523/jneurosci.14-08-05068.1994

Singh YS, Sawarynski LE, Dabiri PD, et al (2011) Head-to-Head Comparisons of Carbon Fiber Microelectrode Coatings for Sensitive and Selective Neurotransmitter Detection by Voltammetry. Anal Chem 83:6658–6666. https://doi.org/10.1021/ac2011729

Slais K, Vorisek I, Zoremba N, et al (2008) Brain metabolism and diffusion in the rat cerebral cortex during pilocarpine-induced status epilepticus. Exp Neurol 209:145–154. https://doi.org/10.1016/j.expneurol.2007.09.008

Sokoloff L (1981) Localization of Functional Activity in the Central Nervous System by Measurement of

Glucose Utilization with Radioactive Deoxyglucose. J Cereb Blood Flow Metab 1:7–36. https://doi.org/10.1038/jcbfm.1981.4

Sokoloff L (1977) Relation between physiological function and energy metabolism in the central nervous system. J Neurochem 29:13–26. https://doi.org/10.1111/j.1471-4159.1977.tb03919.x

Sommer CJ (2017) Ischemic stroke: experimental models and reality. Acta Neuropathol 133:245–261. https://doi.org/10.1007/s00401-017-1667-0

Sotelo-Hitschfeld T, Niemeyer MI, Mächler P, et al (2015) Channel-Mediated Lactate Release by K+-Stimulated Astrocytes. J Neurosci 35:4168–4178. https://doi.org/10.1523/JNEUROSCI.5036-14.2015

Spehar-Délèze A-M, Anastasova S, Vadgama P (2021) Monitoring of Lactate in Interstitial Fluid, Saliva and Sweat by Electrochemical Biosensor: The Uncertainties of Biological Interpretation. Chemosensors 9:. https://doi.org/10.3390/chemosensors9080195

Stadlmann S, Renner K, Pollheimer J, et al (2006) Preserved coupling of oxidative phosphorylation but decreased mitochondrial respiratory capacity in IL-1β-treated human peritoneal mesothelial cells. Cell Biochem Biophys 44:179–186. https://doi.org/10.1385/CBB:44:2:179

Stepanova A, Kahl A, Konrad C, et al (2017) Reverse electron transfer results in a loss of flavin from mitochondrial complex I: Potential mechanism for brain ischemia reperfusion injury. J Cereb Blood Flow Metab 37:3649–3658. https://doi.org/10.1177/0271678X17730242

Stone D, Darley-Usmar V, Smith DR, O'Leary V (1989) Hypoxia-reoxygenation induced increase in cellular Ca2+ in myocytes and perfused hearts: the role of mitochondria. J Mol Cell Cardiol 21:963–973. https://doi.org/10.1016/0022-2828(89)90795-5

Stone EA, Sessler FM, Weimin L (1990) Glial localization of adenylate-cyclase-coupled β-adrenoreceptors in rat forebrain slices. Brain Res 530:295–300. https://doi.org/10.1016/0006-8993(90)91298-U

Swerdlow RH (2018) Mitochondria and Mitochondrial Cascades in Alzheimer's Disease. J Alzheimer's Dis 62:1403–1416. https://doi.org/10.3233/JAD-170585

Tajiri N, Dailey T, Metcalf C, et al (2013) In Vivo Animal Stroke Models. Transl Stroke Res 4:308–321. https://doi.org/10.1007/s12975-012-0241-2

Tanner GR, Lutas A, Martínez-François JR, Yellen G (2011) Single KATP Channel Opening in Response to Action Potential Firing in Mouse Dentate Granule Neurons. J Neurosci 31:8689 LP – 8696. https://doi.org/10.1523/JNEUROSCI.5951-10.2011

Taurino I, Reiss R, Richter M, et al (2013) Comparative study of three lactate oxidases from Aerococcus viridans for biosensing applications. Electrochim Acta 93:72–79.

https://doi.org/10.1016/j.electacta.2013.01.080

Taylor CP, Weber ML, Gaughan CL, et al (1999) Oxygen/Glucose Deprivation in Hippocampal Slices: Altered Intraneuronal Elemental Composition Predicts Structural and Functional Damage. J Neurosci 19:619 LP – 629. https://doi.org/10.1523/JNEUROSCI.19-02-00619.1999

Taylor CT, Moncada S (2010) Nitric Oxide, Cytochrome C Oxidase, and the Cellular Response to Hypoxia. Arterioscler Thromb Vasc Biol 30:643–647. https://doi.org/10.1161/ATVBAHA.108.181628

Terada H (1990) Uncouplers of oxidative phosphorylation. Environ Health Perspect 87:213–218. https://doi.org/10.1289/ehp.9087213

Terraneo L, Samaja M (2017) Comparative Response of Brain to Chronic Hypoxia and Hyperoxia. Int. J. Mol. Sci. 18

Teyler TJ (1980) Brain slice preparation: Hippocampus. Brain Res Bull 5:391–403. https://doi.org/10.1016/S0361-9230(80)80009-8

Thompson C, Wylie LJ, Fulford J, et al (2015) Dietary nitrate improves sprint performance and cognitive function during prolonged intermittent exercise. Eur J Appl Physiol 115:1825–1834. https://doi.org/10.1007/s00421-015-3166-0

Toledo JC, Augusto O (2012) Connecting the Chemical and Biological Properties of Nitric Oxide. Chem Res Toxicol 25:975–989. https://doi.org/10.1021/tx300042g

Tormos K V, Chandel NS (2010) Inter-connection between mitochondria and HIFs. J Cell Mol Med 14:795–804. https://doi.org/10.1111/j.1582-4934.2010.01031.x

Vaddiraju S, Legassey A, Wang Y, et al (2011) Design and Fabrication of a High-Performance Electrochemical Glucose Sensor. J Diabetes Sci Technol 5:1044–1051. https://doi.org/10.1177/193229681100500504

van Hall G, Strømstad M, Rasmussen P, et al (2009) Blood Lactate is an Important Energy Source for the Human Brain. J Cereb Blood Flow Metab 29:1121–1129. https://doi.org/10.1038/jcbfm.2009.35

Vial G, Detaille D, Guigas B (2019) Role of Mitochondria in the Mechanism(s) of Action of Metformin. Front Endocrinol (Lausanne) 10:294. https://doi.org/10.3389/fendo.2019.00294

Victor VM, Nuñez C, D'Ocón P, et al (2009) Regulation of Oxygen Distribution in Tissues by Endothelial Nitric Oxide. Circ Res 104:1178–1183. https://doi.org/10.1161/CIRCRESAHA.109.197228

Vonck J, Schäfer E (2009) Supramolecular organization of protein complexes in the mitochondrial inner membrane. Biochim Biophys Acta - Mol Cell Res 1793:117–124. https://doi.org/10.1016/j.bbamcr.2008.05.019

Wagner SR, Lanier WL (1994) Metabolism of Glucose, Glycogen, and High-energy Phosphates during Complete Cerebral Ischemia: A Comparison of Normoglycemic, Chronically Hyperglycemic Diabetic, and Acutely Hyperglycemic Nondiabetic Rats. Anesthesiology 81:1516–1526. https://doi.org/10.1097/00000542-199412000-00028

Wahono N, Qin S, Oomen P, et al (2012) Evaluation of permselective membranes for optimization of intracerebral amperometric glutamate biosensors. Biosens Bioelectron 33:260–266. https://doi.org/10.1016/j.bios.2012.01.019

Wang GL, Jiang BH, Rue EA, Semenza GL (1995) Hypoxia-inducible factor 1 is a basic-helix-loop-helix-PAS heterodimer regulated by cellular O2 tension. Proc Natl Acad Sci 92:5510 LP – 5514. https://doi.org/10.1073/pnas.92.12.5510

Wang X, Su B, Perry G, et al (2007) Insights into amyloid-β-induced mitochondrial dysfunction in Alzheimer disease. Free Radic Biol Med 43:1569–1573. https://doi.org/10.1016/j.freeradbiomed.2007.09.007

Wang Y, Hekimi S (2016) Understanding Ubiquinone. Trends Cell Biol 26:367–378. https://doi.org/10.1016/j.tcb.2015.12.007

Watts ME, Pocock R, Claudianos C (2018) Brain Energy and Oxygen Metabolism: Emerging Role in Normal Function and Disease. Front Mol Neurosci 11:216. https://doi.org/10.3389/fnmol.2018.00216

Webb AJ, Patel N, Loukogeorgakis S, et al (2008) Acute Blood Pressure Lowering, Vasoprotective, and Antiplatelet Properties of Dietary Nitrate via Bioconversion to Nitrite. Hypertension 51:784–790. https://doi.org/10.1161/HYPERTENSIONAHA.107.103523

Weltin A, Kieninger J, Urban GA (2016) Microfabricated, amperometric, enzyme-based biosensors for in vivo applications. Anal Bioanal Chem 408:4503–4521. https://doi.org/10.1007/s00216-016-9420-4

West MJ, Kawas CH, Stewart WF, et al (2004) Hippocampal neurons in pre-clinical Alzheimer's disease. Neurobiol Aging 25:1205–1212. https://doi.org/10.1016/j.neurobiolaging.2003.12.005

Wiener CM, Booth G, Semenza GL (1996) In Vivo Expression of mRNAs Encoding Hypoxia-Inducible Factor 1. Biochem Biophys Res Commun 225:485–488. https://doi.org/https://doi.org/10.1006/bbrc.1996.1199

Wilson JE (2003) Isozymes of mammalian hexokinase: structure, subcellular localization and metabolic function. J Exp Biol 206:2049–2057. https://doi.org/10.1242/jeb.00241

Wink DA, Mitchell JB (1998) Chemical biology of nitric oxide: insights into regulatory, cytotoxic, and cytoprotective mechanisms of nitric oxide. Free Radic Biol Med 25:434–456. https://doi.org/10.1016/S0891-5849(98)00092-6

Wisniewski N, Moussy F, Reichert WM (2000) Characterization of implantable biosensor membrane biofouling. Fresenius J Anal Chem 366:611–621. https://doi.org/10.1007/s002160051556

Witter MP, Amaral DG (1991) Entorhinal cortex of the monkey: V. Projections to the dentate gyrus, hippocampus, and subicular complex. J Comp Neurol 307:437–459. https://doi.org/10.1002/cne.903070308

Wyss MT, Jolivet R, Buck A, et al (2011) In Vivo Evidence for Lactate as a Neuronal Energy Source. J Neurosci 31:7477 LP – 7485. https://doi.org/10.1523/JNEUROSCI.0415-11.2011

Yager JY, Armstrong EA, Miyashita H, Wirrell EC (2002) Prolonged Neonatal Seizures Exacerbate Hypoxic-Ischemic Brain Damage: Correlation with Cerebral Energy Metabolism and Excitatory Amino Acid Release. Dev Neurosci 24:367–381. https://doi.org/10.1159/000069049

Yellen G (2018) Fueling thought: Management of glycolysis and oxidative phosphorylation in neuronal metabolism. J Cell Biol 217:2235–2246. https://doi.org/10.1083/jcb.201803152

Yorita K, Matsuoka T, Misaki H, Massey V (2000) Interaction of two arginine residues in lactate oxidase with the enzyme flavin: Conversion of FMN to 8-formyl-FMN. Proc Natl Acad Sci 97:13039 LP – 13044. https://doi.org/10.1073/pnas.250472297

Young-Collier KJ, McArdle M, Bennett JP (2012) The Dying of the Light: Mitochondrial Failure in Alzheimer's Disease. J Alzheimer's Dis 28:771–781. https://doi.org/10.3233/JAD-2011-111487

Zauner A, Bullock R, Di X, Young HF (1995) Brain Oxygen, CO2, pH, and Temperature Monitoring: Evaluation in the Feline Brain. Neurosurgery 37:1168–1177. https://doi.org/10.1227/00006123-199512000-00017

Zhang R-L, Chopp M, Chen H, Garcia JH (1994) Temporal profile of ischemic tissue damage, neutrophil response, and vascular plugging following permanent and transient (2H) middle cerebral artery occlusion in the rat. J Neurol Sci 125:3–10. https://doi.org/https://doi.org/10.1016/0022-510X(94)90234-8

Zhang Y, Chen K, Sloan SA, et al (2014) An RNA-Sequencing Transcriptome and Splicing Database of Glia, Neurons, and Vascular Cells of the Cerebral Cortex. J Neurosci 34:11929 LP – 11947. https://doi.org/10.1523/JNEUROSCI.1860-14.2014

Zhang Z, Naughton DP, Blake DR, et al (1997) Human xanthine oxidase converts nitrite ions into nitric oxide (NO). Biochem Soc Trans 25:524S-524S. https://doi.org/10.1042/bst025524s

Zhao M, Ma H, Suh M, Schwartz TH (2009) Spatiotemporal Dynamics of Perfusion and Oximetry during Ictal Discharges in the Rat Neocortex. J Neurosci 29:2814 LP – 2823. https://doi.org/10.1523/JNEUROSCI.4667-08.2009

Zhou D, Wang J, Zapala MA, et al (2008) Gene expression in mouse brain following chronic hypoxia: role of sarcospan in glial cell death. Physiol Genomics 32:370–379. https://doi.org/10.1152/physiolgenomics.00147.2007

Zilberter Y, Zilberter T, Bregestovski P (2010) Neuronal activity in vitro and the in vivo reality: the role of energy homeostasis. Trends Pharmacol Sci 31:394–401. https://doi.org/10.1016/j.tips.2010.06.005

Zimmer AD, Walbrecq G, Kozar I, et al (2016) Phosphorylation of the pyruvate dehydrogenase complex precedes HIF-1-mediated effects and pyruvate dehydrogenase kinase 1 upregulation during the first hours of hypoxic treatment in hepatocellular carcinoma cells. Hypoxia (Auckland, NZ) 4:135–145. https://doi.org/10.2147/HP.S99044

Zuend M, Saab AS, Wyss MT, et al (2020) Arousal-induced cortical activity triggers lactate release from astrocytes. Nat Metab 2:179–191. https://doi.org/10.1038/s42255-020-0170-4